

Hyperbranched Polymer Membranes for Catalytic Degradation of Phenolic Compounds in Water

Report to the
Water Research Commission

by

**SP Malinga¹, SD Mhlanga², NP Gule³, P Mathumba¹,
LE Koloti¹, DE Vlotman¹, S Dube¹**

¹University of Johannesburg

²Stellenbosch University

³University of South Africa

WRC Report No. 2488/1/18

ISBN 978-1-4312-0007-1

August 2018



Obtainable from:

Water Research Commission
Private Bag X03
Gezina, 0031

orders@wrc.org.za or download from www.wrc.org.za

DISCLAIMER

This report has been reviewed by the Water Research Commission (WRC) and approved for publication. Approval does not signify that the contents necessarily reflect the views and policies of the WRC, nor does mention of trade names or commercial products constitute endorsement or recommendation for use.

EXECUTIVE SUMMARY

Water pollution is a global challenge, and the situation has been aggravated by the introduction of harmful organic and persistent compounds into most natural water systems. Most of these compounds are stable and bio-accumulate in the environment, thus making it impossible to be removed from water systems. Traditional wastewater treatment methods have shown some limitations towards complete removal of BPA, PCBs, pesticides and organic dyes especially at trace levels. This has compelled researchers to devise more appropriate methods that can effectively remove these pollutants from water.

The specific aims of the study were as follows:

1. To synthesise and characterise HPEI bimetallic and HPEI enzyme composites.
2. To synthesise and characterise HPEI-MWCNTs composites.
3. To synthesise and characterise HPEI-MWCNTs bimetallic composites.
4. To functionalise HPEI bimetallic, HPEI enzyme and HPEI-MWCNTs bimetallic composites onto commercial membrane support.
5. To test the ability of the novel composites in the removal of organics from water (synthetic and real water samples).
6. To study fouling of the HPEI-MWCNTs-PSf membrane systems in order to establish whether the membranes systems have anti-fouling properties.

Degradation of methyl orange

Photocatalytically active polyethersulfone (PES) nanocomposite membrane embedded with hyperbranched polyethyleneimine (HPEI) and titanium dioxide (TiO₂) nanoparticles (PES/HPEI/TiO₂). This membrane was used for the photodegradation of methyl orange dye in synthetic polluted water. Fourier transform infrared (FTIR) spectroscopy, X-ray diffraction (XRD) spectroscopy and Raman spectroscopy confirmed the presence of anatase TiO₂ nanoparticles which were successfully synthesised from titanium tetrabutoxide using a sol-gel method. The use of HPEI as the template for the synthesis of TiO₂ nanoparticles produced well dispersed nano-sized particles (11 ± 2.5 nm). The HPEI was also successfully used as a dispersing agent for the synthesised TiO₂ nanoparticles to reduce particle agglomeration. The PES/HPEI/TiO₂ membranes were effective in the photodegradation of methyl orange (70.3%) at pH 2. Kinetic studies revealed that the reactions followed pseudo-first-order rate laws using Langmuir-Hinshelwood isotherms. The reaction rate for MO degradation was 11.6 × 10⁻⁶ min⁻¹ and this was accompanied by the generation of sulphate ions as degradation by-products. The modified membranes showed improved hydrophilicity (69.0° to 66.2°) as compared to the pristine PES (76.5°). This was due to the presence of -NH groups from HPEI polymer which greatly improved the hydrophilicity of the membranes. The ability of the membranes to remove dyes from water suggests that the membrane has potential for use in wastewater treatment.

Degradation of BPA

Dendritic membranes functionalised with laccase enzymes were used in the removal of BPA, correlative light and electron microscopy (CLEM) showed that the enzymes were uniformly dispersed on the nanofibres while SEM analysis revealed that the nanofibres had an average diameter of 354 ± 37 nm. The ATR-FTIR results confirmed the covalent attachment of laccase on the dendritic nanofibrous membrane through the formation of an imine bond in a Schiff-base reaction. Energy-dispersive X-ray spectroscopy (EDS) showed the presence of Cu which is the active entity in laccase enzymes. The laccase-modified membranes were hydrophilic (contact angles of 50° to 53°) and exhibited high BPA rejection of 89.7% as compared to the 52.4% demonstrated by pristine polyethersulfone (PES). The immobilised laccase showed enhanced pH and

temperature tolerance compared to free laccase. The immobilised laccase retained up to 67% of its initial activity over a pH range of 3 to 8 while the free enzymes could only retain 36%. The immobilised laccase could also maintain 68% of its initial activity over a temperature range of 20°C to 80°C, which was far greater than that of free laccase (34.8%). The immobilised laccase could retain 38.6% of its initial activity over a storage time of 28 days, while the free laccase only retained 9.7% in the same storage time. The laccase-modified membranes also maintained a constant permeate flux (7.07 ± 5.54 L/m²·h) throughout the filtration process. Recyclability studies indicated that the membranes still maintained a high BPA removal of up to 79% even after four filtration cycles. Therefore, these synthesised laccase-modified dendritic membranes were shown to have great potential for application in large-scale processes such as enzyme membrane reactors (EMRs) for water remediation.

Degradation of PCB-153

A polysulfone (PSf) composite membrane prepared by embedding hyperbranched polyethyleneimine (HPEI) polymer and Fe/Pd bimetallic system in a commercial PSf membrane support for the removal of PCB-153 from water. The morphology and physicochemical properties of the membranes were evaluated using atomic force microscopy (AFM), scanning electron microscopy (SEM) and transmission electron microscopy (TEM) coupled with energy-dispersive spectroscopy (EDS). The size of the Fe/Pd nanoparticles ranged from 44 nm to 77 nm as confirmed by AFM analysis. Moreover, AFM analysis revealed that the surface roughness of the membranes increased from 6.54 nm to 22.77 nm upon HPEI loading. The EDS mapping analysis provided evidence that the Fe and Pd nanoparticles were uniformly distributed in the membrane matrix. Hence, the Fe/Pd bimetallic system was successfully fabricated within the PSf/HPEI membrane. The catalytic activity of the PSf/HPEI-Fe/Pd membranes was evaluated against PCB-153 and GC-MS showed successful removal and degradation of the pollutant.

Degradation of TCP

Membrane modified with MWCNTs and Fe/Cu were found to be more hydrophilic ($39.27^\circ \pm 1.25$) compared to the pristine PES membranes ($55.70^\circ \pm 3.27$). Generally, the flux was found to increase with increasing operating pressure up to 300 kPa. The modified membranes exhibited a high TCP removal rate of 99% as compared to pristine PES which exhibited a TCP removal rate of 58%.

Conclusion and recommendations

The technology could be scaled up and optimised and be used as an integrated system for treatment of effluent. The scaling up of the membrane processes would require further investigation and optimisation of process design and operating variables such as membrane area, operating pressure, feed rate and composition and retentate composition. Modelling studies of such membranes systems could also be done in order to predict the scale up process from the laboratory through to full marketing production of the membranes system. Once these parameters are known via modelling it is possible to predict the membrane performance in a scaled-up setting as a function of operating pressure, processing time and membrane area.

CAPACITY BUILDING

Students

Student Name	Level of study	Status
Penny Mathumba (F)	MSc	Graduated
Lebohang Koloti (M)	MSc	Graduated
David Vlotman (M)	MSc	Submitted
Sakhile Dube (M)	MTech	To submit in July 2018

Publications

1. Penny Mathumba, AT Kuvarega, LN Dlamini, SP Malinga. Synthesis and characterisation of titanium dioxide nanoparticles prepared within hyperbranched polyethylenimine polymer template using modified sol-gel method. *Material letter*. 195, 2017, 172-177.
2. LE Koloti, NP Gule, OA Arotiba, SP Malinga. Laccase immobilised dendritic nanofibrous membranes as a novel approach towards the removal of bisphenol-A. *Environmental Technology*. 39, 2018, 392-404.
3. DE Vlotman, T Ndlovu, JC Ngila, SP Malinga. Hyperbranched polymer integrated membrane for the removal of Arsenic (III) in water. 2017. DOI: 10.22079/JMSR.2017.67560.1148
4. LE Koloti, NP Gule, OA Arotiba, SP Malinga. Recent Applications of Laccase Modified Membranes in the Removal of Bisphenol A and Other Organic Pollutants. *Emerging Trends in Chemical Sciences*, Springer Nature Publishers. 2017, 285-312.

CONFERENCE PRESENTATIONS

DE Vlotman, T Ndlovu, JC Ngila, SP Malinga. Bimetallic immobilized hyperbranched polymer embedded on a polysulfone membrane for removing organic pollutants in water. Oral presentation. UJ Postgraduate Inter-Faculty Symposium, Bunting Road Campus, University of Johannesburg, 27 October 2017.

1. DE Vlotman, T Ndlovu, JC Ngila, SP Malinga. Bimetallic immobilized hyperbranched polymer embedded on a polysulfone membrane for removing organic pollutants in water. Oral presentation. 9th International Conference of the African Materials Research Society, Gaborone, Botswana, 11th-14th December 2017.
2. ST Dube, R Motloali, S.P. Malinga. Hyperbranched polyethyleneimine-multi-walled carbon nanotubes (HPEI/MWCNTs) polyethersulfone (PES) membrane incorporated with Fe-Cu bimetallic nanoparticles for water treatment. Oral presentation. 9th International Conference of the African Materials Research Society, Gaborone, Botswana, 11th-14th December 2017
3. DE. Vlotman, T Ndlovu, JC Ngila, SP Malinga. Catalytic membrane embedded with hyperbranched polyethyleneimine polymer and Fe/Pd bimetallic system for water remediation. 3RD International conference on desalination using membrane technology Palacio de Congresos de Canarias, Las Palmas, Gran Canaria, Spain. *Poster Presentation*. 2-5 April 2017
4. DE Vlotman, T Ndlovu, JC Ngila, SP Malinga. Hyperbranched polymer integrated membrane for the removal of arsenic in drinking water. 17th Waternet/WARFSA/GWP-SA Integrated Water Resources Management symposium. Gaborone International Convention Centre, Botswana. *Oral presentation*, 26-28th October 2016.
5. SP Malinga, LE Koloti, NP Gule, AO Arotiba. Biodegradation of selected organic pollutants on an enzyme modified nanocomposite membrane towards water treatment. International Conference on Pure and Applied Chemistry. Mauritius, *Oral Presentation*, 18 to 22 July 2016.
6. LE Koloti, NP Gule, AO Arotiba, SP Malinga, Biodegradation of selected organic pollutants on an enzyme modified nanocomposite membrane towards water treatment. WISA Biennial Conference, Durban, *Oral Presentation*, 15-19 May 2016.

7. P Mathumba, LN Dlamini, AT Kuvarega, SP Malinga. Nanostructured Membranes Embedded with Hyperbranched Polyethyleneimine and Titanium Dioxide Nanoparticles for Water Purification. WISA Biennial Conference, Durban, *Oral presentation*, 15-19 May 2016.
8. Koloti LE, Arotiba OA, Gule NP and Malinga SP. Biodegradation of selected organic pollutants on an enzyme modified nanofibrous membrane for water treatment. UJ Post-Graduate Cross-faculty Symposium, Oral Presentation, Johannesburg, South Africa. 14 October 2016.
9. P. Mathumba, A.T. Kuvarega, L.N. Dlamini, S.P. Malinga. Photocatalytic membranes for dye decomposition under UV light. Oral presentation, UJ Postgraduate symposium, 13 October 2015
10. Koloti LE, Arotiba OA, Gule NP and Malinga SP. Biodegradation of selected organic pollutants on an enzyme modified nanofibrous membrane for water treatment. UJ Post-Graduate Cross-faculty Symposium, Poster Presentation, Johannesburg, South Africa. 13 October 2015.

ACKNOWLEDGEMENTS

The project team wishes to thank the following people for their contributions to the project:

Reference Group	Affiliation
Dr Nonhlanhla Kalebaila	Water Research Commission
Prof Gitari	University of Venda
Prof R Krause	Rhodes University
Dr TJ Malefetse	MINTEK
Prof AK Mishra	UNISA
Ms H Madhav	ESKOM
Mr G Gericke	ESKOM
Dr K Sikhwivhilu	MINTEK
Dr V Chauke	CSIR
Prof EN Nxumalo	UNISA
Dr M Lutz	Stellenbosch University
Prof Hlanganani Tutu	WITS
Prof Ajay Mishra	UNISA

This page was deliberately left blank

TABLE OF CONTENTS

EXECUTIVE SUMMARY	iii
ACKNOWLEDGEMENTS	vii
TABLE OF CONTENTS	ix
LIST OF FIGURES	xiii
LIST OF TABLES	xvi
ACRONYMS & ABBREVIATIONS	xvii
CHAPTER 1: BACKGROUND	1
1.1 INTRODUCTION.....	1
1.2 PROJECT AIMS.....	1
1.3 REPORT LAYOUT.....	1
CHAPTER 2: LITERATURE REVIEW	3
2.1 INTRODUCTION.....	3
2.2 ORGANIC POLLUTANTS IN WATER.....	3
2.2.1 Bisphenol A.....	3
2.2.1.1 Origin and prevalence of BPA.....	3
2.2.1.2 Health effects of BPA.....	5
2.2.2 Polychlorinated biphenyls (PCBs).....	5
2.2.2.1 Occurrence of PCBs.....	5
2.2.2.2 Prevalence of PCBs in SA water systems.....	6
2.2.2.3 Health effects of PCBs.....	8
2.2.3 Pesticides.....	9
2.3 APPLICATION OF HYPERBRANCHED POLYMER SYSTEMS IN WATER TREATMENT.....	10
2.3.1 Overview.....	10
2.3.2 Hyperbranched polyester-cellulose membranes.....	10
2.3.3 Hyperbranched poly(amine-ester) functionalised multiwalled carbon nanotubes polyvinylidene fluoride (PVDF) membranes.....	11
2.3.4 Crosslinked hyperbranched polymer/PAN composite membrane.....	11
2.3.4.1 Hyperbranched polyester-polysulfone membrane.....	12
2.3.4.2 Hyperbranched polyamidoamine-polytetrafluoroethylene membranes.....	12
2.3.5 Hyperbranched polyethyleneimine-based membrane.....	13
2.3.6 Hyperbranched poly(amidoamine)/polysulfone composite membranes.....	13
2.3.7 Membranes with hyperbranched antibacterial polymer brushes.....	13
2.3.8 Hollow-fibre membranes modified with hyperbranched polyethyleneimine polymer.....	13
2.3.9 Polyethersulfone membranes modified with hyperbranched polyethyleneimine polymer.....	14
2.3.10 Hyperbranched polyethyleneimine-graphene oxide/polyethersulfone (HPEI-GO/PES) ultrafiltration membrane.....	14
2.3.11 Nanofiltration membranes based on polyvinylidene fluoride and crosslinked hyperbranched polyethyleneimine.....	14
2.3.12 Hyperbranched polymers based on other supports.....	14
2.3.12.1 Hyperbranched polyamidoamine-chitosan adsorbents.....	14

2.3.12.2	Hyperbranched polyethyleneimine-silica nanospheres	15
2.3.12.3	Alumina ceramic filters impregnated with hyperbranched polyethyleneimine	15
2.3.12.4	Hyperbranched polyester/TiO ₂ nanocomposites	15
2.3.12.5	Hyperbranched polyethyleneimine (HPEI) functionalised silver nanomaterials	15
2.3.12.6	Hyperbranched poly(ester amide)/polyaniline nanohybrid	16
2.3.12.7	Hyperbranched polyethyleneimine modified gold surface	16
2.3.12.8	Hyperbranched copolymers based on PEG-methacrylate	17
2.3.12.9	Amino-terminated hyperbranched polymer grafted onto cotton fibres	17
2.3.12.10	Magnetite-polyethyleneimine-montmorillonite hybrid material	18
2.4	SUMMARY	18

**CHAPTER 3: DEGRADATION OF METHYL ORANGE using HYPERBRANCHED
POLYETHYLENEIMINE and TITANIUM DIOXIDE (TiO₂) MEMBRANES.....19**

3.1	INTRODUCTION	19
3.2	EXPERIMENTAL METHODOLOGY	20
3.2.1	Materials	20
3.2.2	Preparation of pristine TiO ₂ nanoparticles	20
3.2.3	Preparation of TiO ₂ nanoparticles (NPs) using HPEI as the template	20
3.2.4	Synthesis of HPEI/TiO ₂ nanocomposites	20
3.2.5	Preparation of PES/HPEI/TiO ₂ photocatalytic membranes using phase inversion	21
3.2.6	Characterisation of TiO ₂ , HPEI/TiO ₂ and PES/HPEI/TiO ₂ photocatalytic membrane	22
3.2.6.1	Fourier transform infrared (FTIR) spectroscopy	22
3.2.6.2	XRD analysis	22
3.2.6.3	Raman spectroscopy analysis	22
3.2.6.4	Transmission electron microscopy analysis	22
3.2.6.5	Scanning electron microscopy (SEM)	23
3.2.6.6	Atomic force microscopy (AFM)	23
3.2.6.7	Contact angle analysis	23
3.2.6.8	Zeta potential studies	23
3.2.6.9	Water intake capacity measurements	23
3.2.6.10	Membrane flux studies	23
3.2.7	Photocatalytic degradation of methyl orange using PES/HPEI/TiO ₂ membranes	24
3.2.8	Ion chromatography analysis	24
3.2.9	Leaching studies	25
3.3	RESULTS AND DISCUSSION	25
3.3.1	Characterisation of TiO ₂ and HPEI/TiO ₂ composite	25
3.3.1.1	Raman analysis	25
3.3.1.2	XRD analysis	26
3.3.1.3	TEM analysis	26
3.3.2	Characterisation of TiO ₂ and HPEI/TiO ₂ composite	28
3.3.2.1	Fourier transform infrared (FTIR) spectroscopy	28
3.3.2.2	Scanning electron microscopy (SEM) analysis	29
3.3.2.3	Atomic force microscopy	31
3.3.2.4	Water permeation studies	33
3.3.2.5	Water permeability analysis	33
3.3.3	Photocatalytic activity of PES/HPEI/TiO ₂ membranes	34
3.3.3.1	Photodegradation of methyl orange	34
3.3.3.2	Kinetic studies for the degradation of methyl orange	36
3.3.3.3	Zeta potential analysis and mode of degradation	37
3.3.3.4	Analysis of photodegradation by-products	38
3.3.3.5	Leaching studies	38

3.4	SUMMARY.....	39
CHAPTER 4: CATALYTIC REMOVAL OF Bisphenol A from water USING HPEI/PES NANOFIBROUS MEMBRANES40		
4.1	INTRODUCTION	40
4.2	EXPERIMENTAL	40
4.2.1	Materials.....	40
4.2.2	Synthesis of HPEI/PES nanofibrous membranes.....	40
4.2.3	Determination of laccase immobilisation efficiency	41
4.2.4	Laccase activity assay	41
4.2.5	Effect of pH on activity of free and immobilised laccase.....	42
4.2.6	Effect of temperature on activity of free and immobilised laccase.....	42
4.2.7	Storage stability of free and immobilised laccase.....	42
4.2.8	Tests to evaluate separation performance of membranes	43
4.2.9	Recyclability studies of the membranes	43
4.2.10	Leaching studies	43
4.2.11	Biodegradation studies	43
4.3	RESULTS AND DISCUSSION	44
4.3.1	Immobilisation efficiency	44
4.3.2	Properties of free and immobilised enzymes	44
4.3.2.1	Effect of pH on activity of free and immobilised laccase	44
4.3.2.2	Effect on temperature on activity of free and immobilised laccase	45
4.3.2.3	Storage stability of free and immobilised laccase	46
4.3.3	ATR-FTIR analysis of synthesised membranes	47
4.3.4	SEM analysis	48
4.3.5	CLEM analysis	51
4.3.6	Application of the laccase-modified membranes in the removal of BPA from water	53
4.3.7	Biodegradation of BPA.....	55
4.3.8	Recyclability studies.....	60
4.4	SUMMARY.....	63
CHAPTER 5: DEGRADATION OF PCB-153 USING hpei-fe/pd NANOFILTRATION MEMBRANE.....64		
5.1	INTRODUCTION	64
5.2	EXPERIMENTAL	64
5.2.1	Preparation of thin-film composite PSf-supported membrane	64
5.2.2	Leaching studies	64
5.2.3	Preparation of HPEI-Fe/Pd-PSf membranes	64
5.2.4	Characterisation of HPEI-Fe/Pd-PSf membrane	66
5.2.5	GC-MS procedure	66
5.3	RESULTS AND DISCUSSION	67
5.3.1	FTIR analysis	67
5.3.2	Focused ion beam (FIB)	67
5.3.3	X-Ray diffraction (XRD)	69
5.3.4	X-Ray photoelectron spectroscopy	69
5.3.5	Water permeation and contact angle analysis.....	70
5.3.6	GC-MS analysis	72
5.3.7	Dechlorination mechanism.....	74
5.3.8	Leaching studies	77
5.4	SUMMARY.....	78

CHAPTER 6: DEGRADATION OF TRICHLOROPHENOL USING HPEI/MWCNTS/PES MEMBRANES INCORPORATED WITH FE-CU BIMETALLIC	79
6.1 INTRODUCTION	79
6.2 EXPERIMENTAL	79
6.2.1 Materials.....	79
6.2.2 Preparation of f-MWCNTs-COOH.....	79
6.2.3 Preparation of MWCNTs-COCl.....	79
6.2.4 Synthesis of HPEI-MWCNTs	79
6.2.5 Synthesis of bimetallic nanoparticles on HPEI-MWCNT nanocomposite.....	80
6.2.6 Preparation of HPEI-MWCNTs-Fe/Cu-PES ultrafiltration membranes.....	80
6.2.7 Water permeation tests.....	82
6.2.8 Membrane fouling and protein rejection	82
6.2.9 Characterisation	82
6.3 RESULTS AND DISCUSSION	83
6.3.1 FTIR analysis	83
6.3.2 Morphological studies using TEM analysis	84
6.3.3 BET analysis of pristine MWCNTs, MWCNTs-COOH, MWCNTs-COCl and HPEI-MWCNTs.....	86
6.3.4 Raman.....	87
6.3.5 SEM analysis	89
6.3.6 Contact angle analysis.....	89
6.3.7 Pure water flux (PWF) analysis.....	90
6.3.8 Catalytic reactivity of nanocomposite membranes	91
6.3.9 Fouling analysis	93
6.3.10 Leaching studies	95
6.4 SUMMARY.....	95
CHAPTER 7: CONCLUSIONS and recommendations.....	96
7.1 CONCLUSION	96
7.2 RECOMMENDATION FOR FURTHER RESEARCH.....	96
REFERENCES	97
APPENDIX A:.....	111
Table A1: Operating parameters of ICP-OES	111

LIST OF FIGURES

Figure 2.1. Schematic representation of the synthesis of BPA	3
Figure 2.2. Eskom inventory of PCB levels per PCB units (Buah-Kwofie et al., 2011)	6
Figure 2.3. Map of South Africa indicating PCB contaminated	8
Figure 2.4. Map of South Africa indicating pesticide-contaminated areas	10
Figure 2.5. Crosslinked PAN/Boltorn composite membrane (Wang et al., 2014a)	11
Figure 2.6. Synthesis of HPAMAM-grafted PTFE membranes (Yoo and Kwak, 2013)	12
Figure 2.7. Fabrication of PEI onto Au surface (Suriyanarayanan et al., 2013)	16
Figure 2.8. Synthesis of cotton fibres grafted with hyperbranched polymers (Zang et al., 2014)	17
Figure 2.9. Preparation of hybrid material magnetite-PEI-Mt (Larraza et al., 2012)	18
Figure 3.1. Preparation of titanium dioxide nanoparticles using hyperbranched polyethyleneimine as a template	21
Figure 3.2. Illustration of TiO ₂ dispersion on hyperbranched polyethyleneimine	21
Figure 3.3. UV-radiation experimental set-up for the photodegradation of methyl orange dye	24
Figure 3.4. Raman spectra of (a) pristine TiO ₂ nanoparticles, (b) 1:6 HPEI/TiO ₂ and (c) 1:9 HPEI/TiO ₂ nanocomposites.....	25
Figure 3.5. (a) XRD patterns of pristine TiO ₂ , (b) 1:6 HPEI/TiO ₂ , and (c) 1:9 HPEI/TiO ₂	26
Figure 3.6. (a) TEM micrograph of TiO ₂ without HPEI, (b) TEM micrograph of TiO ₂ using HPEI as a template, (c) mean particle size in absence of HPEI, (d) mean particle size in the presence of HPEI, (e) TEM micrograph of TiO ₂ using HPEI as a template (insert: ImageJ spot analysis), (f) SAED pattern of TiO ₂ using HPEI as a template, and (g) EDS analysis of TiO ₂ using HPEI as a template.....	28
Figure 3.7. FTIR spectra of PES and PES/HPPEI/TiO ₂ membranes	29
Figure 3.8. SEM images of surface and cross-sectional morphologies of PES (A and A'), 0.05% HPEI/TiO ₂ (B and B'), 0.10% HPEI/TiO ₂ (C and C'), 0.50% HPEI/TiO ₂ (D and D') and 1.00% HPEI/TiO ₂ membranes (E and E').....	31
Figure 3.9. AFM images of 0% (A 2D,A' 3D), 0.05% (B 2D,B' 3D), 0.10% (C 2D,C' 3D), 0.50% (D 2D, D' 3D) and 1.00% (E 2D, E' 3D) PES/HPEI/TiO ₂ membranes.....	32
Figure 3.10. The relationship between pure water flux and pressure	34
Figure 3.11. Photodegradation of methyl orange by PES/HPEI/TiO ₂ membranes using UV light.....	35
Figure 3.12. First-order kinetic plot of methyl orange initiated by UV light irradiation	36
Figure 3.13. Acidic and basic forms of methyl orange.....	37
Figure 3.14. Mechanism for the photodegradation of methyl orange dye in water	37
Figure 3.15. Generation of sulphate ions from the degradation of methyl orange using PES/HPEI/TiO ₂ photocatalytic membranes.....	38
Figure 4.1. Synthesis of HPEI/PES nanofibrous membrane using the electrospinning technique	41
Figure 4.2. Effect of laccase concentration on immobilisation efficiency	44
Figure 4.3. Effect of pH on the activity of free and immobilised laccase	45

Figure 4.4. Effect of temperature on the activity of free and immobilised laccase	46
Figure 4.5. Storage stability of free and immobilised laccase	47
Figure 4.6. ATR-FTIR spectra of: (a) commercial PES membranes; (b) aminated HPEI/PES nanofibrous membranes; (c) glutaraldehyde activated nanofibrous membranes; and (d) laccase-immobilised nanofibrous membranes	48
Figure 4.7. SEM images of surface and cross-sectional morphology of commercial PES membranes (a, b), HPEI/PES (c, d), Lac _{0.5} -HPEI/PES (e, f), Lac _{1.0} -HPEI/PES (g, h), Lac _{2.0} -HPEI/PES (i, j), and Lac _{4.0} -HPEI/PES (k, l)	51
Figure 4.8. CLEM photo-images of: (a) PES membranes; (b) HPEI/PES; (c) Lac _{0.5} -HPEI/PES; (d) Lac _{1.0} -HPEI/PES; (e), Lac _{2.0} -HPEI/PES; and (f) Lac _{4.0} -HPEI/PES	52
Figure 4.9. Removal of BPA (a) and permeate flux (b) vs. time for commercial PES membranes and laccase-modified membranes at 600 kPa and 25°C	54
Figure 4.10. The proposed mechanism for removal of BPA in a dead-end filtration system using laccase-modified dendritic membranes	55
Figure 4.11. LC-MS spectra representing the BPA biodegradation by-products generated using laccase-immobilised HPEI/PES nanofibrous membrane	58
Figure 4.12. Recyclability of the laccase-modified membranes over 4 cycles	60
Figure 4.13. Concentration of leaching laccase enzyme in permeate vs. time for first cycle (a), second cycle (b), third cycle (c) and fourth cycle (d)	62
Figure 5.1. Preparation of PSf/HPEI-Fe/Pd membranes	65
Figure 5.2. Colour change of the solution containing HPEI/PSf-Fe/Pd (A) before and (B) after reduction of the Fe/Pd bimetallic nanoparticles	65
Figure 5.3. FTIR spectrum of pristine and HPEI-Fe/Pd modified membranes	67
Figure 5.4. SEM-FIB and EDS mapping images of 8% HPEI/PSf-Fe-Pd membrane	68
Figure 5.5. XRD spectra of Fe, Pd and Fe/Pd nanoparticles	69
Figure 5.6. XPS spectra of (A) C1S, (B) N1S and (C) Fe 2p of 8% HPEI/PSf and 8% HPEI/PSf-Fe/Pd membranes	70
Figure 5.7. Membrane contact angle vs. water uptake	71
Figure 5.8. Pure water flux vs. transmembrane pressure	72
Figure 5.9. Chromatographs of (A) 0 h dechlorination and (B) 4 h dechlorination of 8% HPEI/PSf-Fe/Pd membrane	73
Figure 5.10. PCB removal as a function of time	74
Figure 5.11. Chromatograms of (A) PCB consumption as a function of time, and (B) selected ion chromatogram of PCB congeners	75
Figure 5.12. Mass spectrum of predominantly generated PCB by-products: (A) tetrachlorobiphenyl; and (B) dichlorobiphenyl	76
Figure 5.13. Proposed dechlorination reaction	76
Figure 6.1. Synthesis route for the HPEI-MWCNTs-Fe/Cu composite	81
Figure 6.2. FTIR spectrum of (a) pristine MWCNTs, (b) MWCNTs-COOH, (c) MWCNTs-COCl and (d) HPEI-MWCNTs	83

Figure 6.3. EDS mapping of MWCNTs/HPEI/Fe-Cu (A) and corresponding EDS spectrum of MWCNTs/HPEI/Fe-Cu (B)	84
Figure 6.4. TEM images, size distribution graphs and EDX of (a) pristine MWCNTs, (b) MWCNTs-COOH, (c) MWCNTs-COCl, (d) HPEI-MWCNTs and (e) HPEI-MWCNTs/FeCu	85
Figure 6.5. BET adsorption isotherm spectrum of (a) pristine MWCNTs, (b) MWCNTs-COOH, (c) MWCNTs-COCl and (d) HPEI-MWCNTs	87
Figure 6.6. Raman spectra of (a) pristine MWCNTs, (b) MWCNTs-COOH, (c) MWCNTs-COCl and (d) HPEI-MWCNTs	88
Figure 6.7. Top surface morphology of the unmodified and modified membranes (a-c); and cross-sectional morphology of the unmodified and modified membranes (d-f).....	89
Figure 6.8. Contact angle measurement of HPEI-MWCNTs-Fe/Cu-PES membrane	90
Figure 6.9. Pure water flux of modified membrane within 15 min at 25°C	91
Figure 6.10. Removal efficiency of the modified and unmodified membranes.....	91
Figure 6.11. LC-MS spectra showing 2,4,6 TCP by-products generated using HPEI-MWCNT-Fe/Cu-PES membrane.....	92
Figure 6.12. Permeate flux vs. time for HPEI-MWCNTs-Fe/Cu blended PES membranes for water containing BSA (1 000 mg/L), at applied pressure of 200 kPa, pH 7.1, and temperature at 25°C	93
Figure 6.13. Flux recovery ratio (FRR) of the HPEI-MWCNTs-Fe/Cu blended PES membranes after BSA fouling	94

LIST OF TABLES

Table 2.1. Concentrations and possible sources of PCB 153 found in South African water supplies (Bouwman et al., 2004; Vosloo, 2005).....	7
Table 3.1. Composition of casting solution for membrane preparation.....	22
Table 3.2. FTIR transmittance bands of PES membranes.....	28
Table 3.3. Zeta potential, contact angle, water uptake capacity studies, water flux and membrane roughness.....	33
Table 3.4. Photodegradation results.....	34
Table 3.5. Previous work on TiO ₂ photocatalytic membranes for dye removal.....	36
Table 3.6. TiO ₂ leaching from the PES/HPEI/TiO ₂ membranes.....	39
Table 4.1. Membrane water permeation analyses.....	58
Table 5.1. Leaching results of 8% PSf-HPEI-Fe/Pd membrane.....	77
Table 6.1. The casting solution of the fabricated membrane.....	80
Table 6.2. BET analysis.....	86
Table 6.3. I _D /I _G ratio of pristine and functionalised MWCNTs.....	88
Table 6.4. 2,4,6-TCP by-products detected by LC-MS.....	93
Table 6.5. Leaching results for the fabricated membrane.....	95

ACRONYMS & ABBREVIATIONS

AFM	atomic force microscopy
BPA	Bisphenol A
BSA	bovine serum albumin
CA	cellulose acetate
DBP	1, 3-dibromo propane
DMF	dimethylformamide
DMM	double monomer methodology
ECH	epichlorohydrin
EDX	energy-dispersive X-ray
GO	graphene oxide
HBPE	hyperbranched polyester
HPAE	hyperbranched poly(amine-ester)
HPAMAM	hyperbranched poly(amidoamine)
HPEI	hyperbranched polyethyleneimine
HYPAM	hyperbranched poly(amidoamine)
MMT	montmorillonite
MWCNTs	multiwalled carbon nanotubes
NF	nanofiltration
NMP	N-methyl-2-pyrrolidone
PAI	polyamide-imide
PAN	polyacrylonitrile
PDMAEMA	poly[2-(N, N-dimethylamino) ethyl methacrylate]
PES	polyethersulfone
PTFE	polytetrafluoroethylene
PTP	proton transfer polymerisation
PVDF	polyvinylidene fluoride
SCROP	self-condensing ring-opening polymerisation
SCVP	self-condensing vinyl polymerisation
SEM	scanning electron microscope
SMM	single monomer methodology
TEM	transmission electron microscopy
TMC	trimesoyl chloride
TPC	terephthaloyl chloride
<i>W_d</i>	dry weight
WIC	waterintake capacity
<i>W_w</i>	wet weight

This page was left blank deliberately

CHAPTER 1: BACKGROUND

1.1 INTRODUCTION

Organic compounds such as chlorinated compounds and phenolic compounds (pesticides) are widespread, mobile, and highly toxic and persistent in the environment (Su et al., 2011). Chlorophenols such as 2,4-dichlorophenol and 2,4,6-trichlorophenols are released into the environment as they are formed during the chlorination of water for disinfection, manufacturing of pesticides, pharmaceuticals and dyes (Liu et al., 2010). Bisphenol A is a toxic phenolic compound and its usage has increased dramatically in recent years (Gassara et al., 2013). Due to improper disposal and slow degradation rates this has resulted in the accumulation of chlorinated and phenolic organic compounds in the environment (Liu et al., 2010), and thus their removal from the environment using treatment methods such as the use of catalytic degradation has become a priority for water treatment industries. Hyperbranched polymers such as hyperbranched polyethyleneimine (HPEI) have a high number of internal amine functional groups, which can act as ligands to complex metal ions such as Cu, Fe, Ag and Ni for nanoparticle synthesis (Huang et al., 2008; Diallo et al., 2005). Secondly, the presence of nanocavities in the HPEI structure acts as hosts/templates for the preparation of narrow and stable nanoparticles (Huang et al., 2008). Moreover, the nanocavities can act as catalytic and adsorption sites for the degradation and removal of organic pollutants. The hyperbranched structure of the hyperbranched polyethyleneimine also provides a shell to prevent aggregation of the nanoparticles (Huang et al., 2008). Lastly, the highly branched peripheral amine functional groups of the HPEI with the bimetallic nanoparticles can be grafted with other molecules such as cyclodextrins, carbon nanotubes and membranes to prepare a new generation of multifunctional material for advanced water treatment applications. It is envisaged that such a membrane system will exhibit high catalytic activity due to the narrow particle size distribution and also it will have antifouling properties since HPEI contains hydrophilic amine groups.

1.2 PROJECT AIMS

The aims of the project were as follows:

1. To synthesise and characterise HPEI bimetallic and HPEI enzyme composites.
2. To synthesise and characterise HPEI-MWCNTs composites.
3. To synthesise and characterise HPEI-MWCNTs bimetallic composites.
4. To functionalise HPEI-bimetallic, HPEI-enzyme and HPEI-MWNTs bimetallic composites onto commercial membrane support.
5. To test the ability of the novel composites in the removal of organics from water (synthetic and real water samples).
6. To study fouling of the HPEI-MWCNTs-PSf membrane systems in order to establish whether these membrane systems have anti-fouling properties.

1.3 REPORT LAYOUT

The summary of work give a brief description of the chapters to follow.

Chapter 2 gives an extensive literature review that is pertains to the study undertaken. This chapter dwells on the different types of pollutants that are of interest. The sources, health effects and their prevalence in South

African water systems is assessed. Hyperbranched polymer systems are evaluated as an option for the removal of pollutants from water.

Synthesise, characterisation and application of hyperbranched polymers embedded with TiO_2 for the photocatalytic degradation of methyl orange from water is covered in **Chapter 3**.

In **Chapter 4** a nanofibrous membrane that consists of hyperbranched polyethyleneimine polymer and laccase enzymes is used in the biodegradation of BPA. Synthesise and characterisation of the nanofibrous membrane is discussed.

The hyperbranched polymer membranes discussed in **Chapter 5** is embedded with Fe/Pd bimetallic system. This chapter presents the synthesise and characterisation of the membranes and its application in the dechlorination of PCB-153.

Chapter 6 reviews the synthesise, characterisation and application of a hyperbranched polyethyleneimine/multiwalled carbon nanotube/Fe-Cu system embedded on a membrane via phase inversion. This membranes was used in the catalytic degradation of 2, 4, 6-trichlorophenol. Antifouling properties of the modified membranes is investigated.

This reports concludes with **Chapter 7** which highlights the achievements of the project.

CHAPTER 2: LITERATURE REVIEW

2.1 INTRODUCTION

The high content of toxic organic and inorganic pollutants found in industrial effluents as well as in agricultural runoff has a detrimental effect on both human beings and aquatic life in general. The hazardous nature of these pollutants has resulted in various water treatment methods in an effort to overcome this world-wide crisis. However, these conventional water treatment methods have demonstrated some limitations which include low efficiency and high operational cost. Therefore, more effective, low cost, environmentally friendly techniques have to be employed for complete removal of water pollutants. Among such methods, membrane-based processes have emerged as promising techniques towards removal of such pollutants from water. However, membrane fouling is the major drawback of membrane filtration processes. Hyperbranched polymer systems have not only improved the antifouling properties of the membranes but have resulted in enhancement of filtration performance of numerous composite membranes. The potential applicability of an innovative technology involving hyperbranched polymer systems is also reviewed as an option to treat these organic pollutants present in water.

2.2 ORGANIC POLLUTANTS IN WATER

In this section, the source, health effects and prevalence of selected organic pollutants (i.e. Bisphenol A, PCB-153, trichlorophenol and methyl orange) in South African water systems is presented.

2.2.1 Bisphenol A

2.2.1.1 Origin and prevalence of BPA

Bisphenol A (BPA) was first synthesised by a Russian chemist, A.P. Dianin in 1891 through condensation of phenol with acetone (**Figure 2.1**) (Michalowicz, 2014). The estrogenic effects of BPA were reported in the 1930s, but its use as a synthetic oestrogen did not become popular (Rochester et al., 2013). Later, it was discovered that BPA can be used in the production of plastics (such as polycarbonate plastics), epoxy resins and thermal papers (Michalowicz, 2014; Gassara et al., 2013; Dehghani et al., 2016). This led to the large-scale production of this monomer which was then used extensively in various consumer products such as plastic toys, dental sealants, food packaging, plastic bottles, and electronic devices (Huang et al., 2012; 2005). In 2011, the increased demand for BPA resulted in its global consumption being over 5.5 million metric tons which led to the ubiquity of this micropollutant in the environment (Flint et al., 2012).

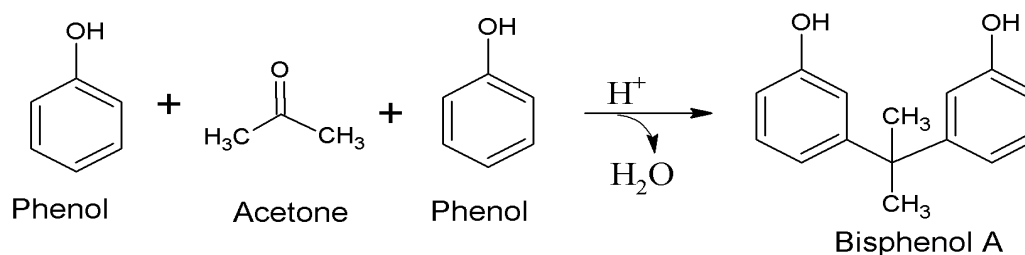


Figure 2.1. Schematic representation of the synthesis of BPA

Bisphenol A has found its way into humans, animals and plants through food and drinking water due to the extensive use of BPA-containing food packaging and plastic bottles. Scientific studies have shown that residual BPA can either diffuse out of polycarbonate packaging materials or during hydrolysis of the polymer due to alkaline conditions and the temperature of packaged food. For decades, there has been a great concern towards BPA exposure in infants since BPA was detected in their feeding bottles (Hoekstra and Simoneau, 2013). A survey conducted by Pouokam et al. (2014) revealed that feeding bottles containing BPA are being sold in countries such as Cameroon and Nigeria. The study showed that almost all the plastic bottles in Cameroonian shops did not carry the "BPA-free" sign and over 80% of feeding bottles in Nigerian shops were also not BPA-free (Pouokam et al., 2014). South Africa is the first developing country to adopt safety measures against BPA-containing commodities. The South African health ministry banned the production, importation, exportation and selling of BPA-containing bottles used by infants (Pouokam et al., 2014).

Bisphenol A has been detected in most water systems, which increases the chances of human beings and animals being exposed to BPA (Zhou et al., 2011). Traceable amounts of BPA are discharged directly into water bodies (such as marine and fresh waters) and some traces are found in nearby surroundings of plastic manufacturing industries (Huang et al., 2012). Bisphenol A leaches out into surface waters through the hydrolysis of most polycarbonate plastics and epoxy resins (Michalowicz, 2014). In Japan, BPA has been detected in landfill leachates (up to 17.2 mg/L) and in tap water (up to 0.1 µg/L). In China, BPA has been found at a concentration of 27.3 µg/L in natural surface water (Flint et al., 2012). These levels of BPA are detrimental to human health.

Traces of BPA have also been detected in developing countries in Africa. Ignatius et al. (2010) reported the presence of BPA in water at the Enugu Municipality in South East Nigeria. The study revealed BPA concentrations in tap water (0.20 ± 0.07 µg/L), well water (0.21 ± 0.07 µg/L), river water (0.18 ± 0.04 µg/L) and rain water (0.40 ± 0.16 µg/L) (Ignatius et al., 2010). The high levels of BPA were ascribed to the disposal of inadequately treated sewage effluent that contains BPA. The highest levels of BPA were found in rain water because of environmental contamination by industrial activities (Ignatius et al., 2010). A study conducted by Omoruyi et al. (2014) further revealed BPA concentrations ranging from 124.2 ng/L to 1.0008 µg/L in 31% of bottled water samples in Nigeria. Olujimi et al. (2013) detected the concentration of BPA and nonylphenol using ultra-performance liquid chromatography tandem mass spectrometry (UPLC/MS) from samples collected in Cape Flats Wastewater Treatment Works (in Strandfontein). The wastewater treatment plant in Strandfontein uses activated sludge for treating domestic, agricultural and industrial effluents. This study reported a high concentration of BPA up to 384.3 ± 131.7 µg/L in the wastewater treatment plant. Nonylphenol (another endocrine disruptive compound) was also found to reach concentrations ranging from 0.53 ± 0.15 to 9.83 ± 3.47 mg/L.

In the landfill leachates BPA was found at concentrations of between 0.022 ± 0.002 and 9.59 ± 1.48 mg/L and nonylphenol concentrations ranging from 1.04 ± 0.43 to 137.41 ± 4.73 mg/L. In the sewage sludge, BPA concentrations ranged from 0.17 ± 0.01 to 2.28 ± 0.13 µg/g, while nonylphenol levels ranged from 0.42 ± 0.02 to 8.76 ± 0.72 µg/g. The detected levels of these endocrine-disrupting phenols in the wastewater treatment plant and the landfill leachates exceeded the allowable limit of phenols (10 µg/L) in water as stated by the South African National Standards (SANS) in terms of SANS 241-1: 2015 (SANS 241-1, 2015). This high concentration of the endocrine disruptors, BPA and nonylphenol, can be a threat to nearby residents and about 30 000 migrant birds that are found around these areas. Another study conducted by De Jager et al. (2013) in South Africa revealed a detectable amount of BPA ranging from 0.0478 ng/L to 0.06798 ng/L in selected drinking water distribution points in Pretoria and Cape Town. The water samples were collected from 20 distribution points (Pretoria and Cape Town) and were analysed using gas chromatography-mass spectrometry (GC-MS). The BPA levels were found to be lower than those reported in developed countries like China where BPA concentrations in water ranging from 38.9 to 55.8 ng/L have been reported (De Jager et al., 2013).

Even though most developing countries are becoming aware of the detrimental effects of BPA on human health and wildlife, the major challenge is in linking detectable concentrations of urinary BPA to its exposure route (Baluka et al., 2016). Recently, a study conducted by Baluka et al. (2016) reported urinary BPA concentrations of 0.6 ng/L (in rural areas) and 1 µg/L (in urban areas) in young girls living in Egypt. It was concluded that the main source of BPA exposure for these girls was the consumption of canned food and storing food in plastic packages. The cans and plastics used for storing food contain high levels of BPA and this has been the only study to date in Africa that attempted to link detected urinary BPA to the sources of exposure (Baluka et al., 2016).

2.2.1.2 *Health effects of BPA*

Recent studies have shown that BPA affects the proper functioning of several hormones such as sex hormones, insulin, leptin and thyroxin which impact negatively on human and animal health (Rochester et al., 2013; Wetherill et al., 2007; Meeker et al., 2010). Exposure to BPA has been associated with immunotoxic, mutagenic and carcinogenic effects (Rochester et al., 2013; Yang et al., 2016; Doherty et al., 2010; Annamalai et al., 2015). It has also been proven that high levels of BPA in the human system can result in diabetes and obesity (Flint et al., 2012; Annamalai et al., 2015; Giulivo et al., 2016). Lang et al. (2008) established a direct relationship between BPA dosage and type-2 diabetes using data obtained from a National Health and Nutrition Examination Survey (NHANES) from individual American participants. The researchers found that higher total urinary BPA was linked to diagnosis of type-2 diabetes (Lang et al., 2008). Carwile and Michels (2014) also found that increased urinary BPA can be associated with higher chances of body mass index and obesity. Bisphenol A has shown estrogenic activity at very low doses of 0.23 pg/mL and has been found to increase the proliferation rate of breast cancer cells (Escalona et al., 2014). Bisphenol A binds to estrogen nuclear receptors responsible for regulating transcription and cell membrane receptors associated with calcium mobilization and intracellular signalling in the endocrine system (Voom Saal, 2007). Cell membrane receptors have proven to be more sensitive towards BPA resulting in observable effects even at extremely low BPA concentrations (µg/L levels) (Voom Saal, 2007).

Owing to its toxic nature and adverse effects on human health, the removal of BPA from water has become a major concern world-wide. Various conventional wastewater treatment methods have been employed in efforts to remove BPA from water, but this recalcitrant pollutant still persists in most wastewater treatment plants due to its complex aromatic structure and low biodegradability (Park et al., 2014; Erjavec et al., 2016). Hyperbranched polymers, like dendrimers, are dendritic polymers that are highly branched with globular structures that have numerous functional groups (Cai et al., 2012). These polymers have gained intense interest in various applications such as drug delivery (Kurniash et al., 2015), water treatment (Han et al., 2012), sensor materials (Orlicki et al., 2012) and solvent extraction (Seiler, 2006). These various applications are attributed to the remarkable properties of the hyperbranched polymers. Firstly, unlike dendrimers, they are easily synthesised in one-step polymerisation reactions while still retaining properties that are similar to dendrimers. The simple and inexpensive synthesis of hyperbranched polymers has earned these polymers much popularity for large-scale applications (Inoue, 2000). Secondly, the hyperbranched polymers have numerous functional groups that can be modified enhance their solubility, and improve their compatibility with other materials (Voit, 2000).

2.2.2 **Polychlorinated biphenyls (PCBs)**

2.2.2.1 *Occurrence of PCBs*

Polychlorinated biphenyls (PCBs) are a class of persistent synthetic organochlorine substances with biphenyl as the basic structural unit. Polychlorinated biphenyls consist of 209 different compounds, called congeners, found in different mixtures in commercial products. The group of chemicals known as PCBs is one of the

original 12 persistent organic pollutants (POPs) covered by the Stockholm Convention. Persistent organic pollutants (POPs) are synthetic organic compounds of anthropogenic origin which resist photolytic, chemical and biological degradation (Roos, 2011). These POP compounds include pesticides, dioxins, dibenzofurans and polychlorinated biphenyls (PCBs), of which the latter is known to be the most problematic with regards to its degradation in aqueous environments (Amdany et al., 2014). Persistent organic pollutants are insoluble in water and due to their lipophilic nature, they tend to have a high affinity to fat-rich tissues. Thus, they are prone to accumulate, persist and bio-concentrate in living organisms at higher trophic levels (Ferrante et al., 2014). The Stockholm Convention of POPs defines PCBs as aromatic compounds formed by way of hydrogen atoms on the biphenyl being replaced by up to ten chlorine atoms (Afful et al., 2013). Polychlorinated biphenyls were widely used in commercial applications in the twentieth century. Their application was mainly centred around electronics such as capacitors, insulators and transformers. These compounds also formed part of construction materials such as adhesives and paints (Guo, 2012). The widespread commercial use of PCBs was primarily due to their excellent thermal and chemical stability as well as their resistance to acids and bases.

Polychlorinated biphenyls in the environment are expected to be associated with the organic components of soils, sediments and biological tissues, or with dissolved organic carbon in aquatic systems, rather than being in solution in water (Pronczuk and Damstra, 2008). Although these compounds are typically classified as point source pollution, easy dispersal allows for movement in the soil, air, and water. Therefore, these compounds can be transported through the air and subsequently pollute water systems of countries not directly associated with PCB production

2.2.2.2 Prevalence of PCBs in SA water systems

The energy sector has been identified as the largest potential owner of PCBs oils and PCB contained equipment in South Africa. This national electricity supplier has PCB containing capacitors and transformers; however, a programme to develop PCB-free electrical systems has been put into place (Bouwman, 2003). With the aim to monitor existing PCB oils and contaminated equipment, a national standard has been implemented which is referred to as SANS 290:2007. This standard specifies highlights materials containing 51-500 mg/L as PCB-contaminated species. In terms of this standard, materials containing in excess of 500 mg/L are considered to be PCB-contaminated species. In South Africa, potential sources of PCB oils and contaminated materials have been identified and letters have been issued to identify industries requesting a status update of PCBs in their company or sector. The inventory provided by Eskom (**Figure 2.2**) for large equipment indicates that 17 086 pieces of company-owned equipment contain PCBs with a content greater than 50 mg/L. This PCB contained equipment is made up of transformers, and auxiliary equipment. **Figure 2.2** indicates that 4% of the equipment owned by Eskom was found to have PCB content greater than 500 mg/L.

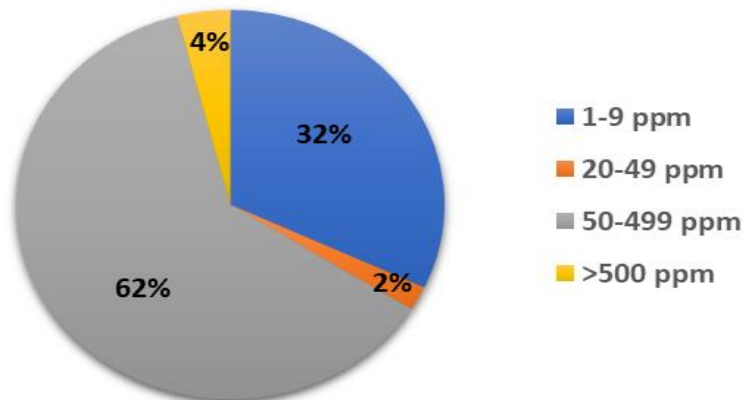


Figure 2.2. Eskom inventory of PCB levels per PCB units (Buah-Kwofie et al., 2011)

Eskom has developed a phase-out plan by which they have agreed to meet the Stockholm Convention phase-out plan (phase out of PCB equipment containing more than 50 mg/L by the year 2025) (Buah-Kwofie et al., 2011). In addition to this phase-out plan, there is also a strategy in place in terms of which the Stockholm Convention aims to dispose of all PCB-containing waste by 2028. The company is also registered to a PCB Elimination Network (PEN) where a decision was adopted to develop a network which provides information exchange on PCBs (Department of environmental affairs, 2011/2012). This implemented network therefore promotes cost-effective implementation of environmentally sound management of PCB contained and contaminated equipment. Eskom has also shipped various PCB-contaminated oils abroad for incineration (Bouwman, 2003). Unfortunately, PCBs remain in various forms in buildings created before 1979, such as PCB oils in school lighting ballast fixtures. Other applications of PCBs have been as a plasticiser in paint, flame retardants, ink solvents and plastics. Commercial PCBs were sold according to the percentage chlorine by weight. For example, in the Aroclor series, a 4-digit code is used, where biphenyls are generally indicated by 12 in the first 2 positions, whereas the last two digits indicate the chlorine percentage in the mixture. Therefore, Aroclor 1260 is a PCB containing 60% chlorine in the mixture (Ritter et al., 1995). The usage of PCBs has been phased out for a long time already, but because of the long half-life of these compounds, they are still present in the environment (Burger, 2005).

Table 2.1 shows levels and possible sources of PCB 153 found in South African water supplies (Bouwman et al., 2004; Vosloo, 2005). Van Veelen and Dhemba (2011) conducted a study in various water systems in South Africa to investigate the presence and concentration of PCBs. In this study, samples were collected in the Loskop Dam and the Olifants River. The compound PCB 118 was detected at Loskop Dam and in the Olifants River at low levels of 24.9 and 41.1 ng/kg, respectively (Van Veelen and Dhemba, 2011). Nel et al. (2015) conducted a study on the effect of PCBs on marine life in the Swartkops Estuary in South Africa. In this study, several PCBs could be quantified, i.e. PCB-101, CB-118, CB-138 and CB-153. The PCB concentrations were generally higher (83 µm/kg PCB 153 in *Argyrosomus japonicas* fish and 62 µm/kg PCB 153 in *Pomadasys commersonnii*) in the liver of fish compared to other tissues (Nel et al., 2015). The World Health Organization (WHO) allows a daily PCB intake of 6 µg/kg per day. However concentrations found in the liver of these fish exceeded these limits (Nel et al., 2015). In Mpumalanga's Olifants River, fish were found to contain 41.1 ng/kg of PCB 118 (Bouwman, 2003). Humans that consume these PCB-contaminated fish may be prone to bio-accumulation of PCBs in their tissues, which can severely affect their health. Furthermore, due to their stability, POPs may take several years to degrade (Pronczuk and Damstra, 2008). The compound PCB 153 is one of the seven non-dioxin-like indicator PCB congeners. Other indicator congeners include PCB 28, 52, 101, 118, 138 and 180. It is also one of the most detected contaminants in water supplies and revealed at high concentrations (0.5 µM) in human tissue, including adipose tissue (Ferrante et al., 2014).

Table 2.1. Concentrations and possible sources of PCB 153 found in South African water supplies (Bouwman et al., 2004; Vosloo, 2005)

River	Closest town/farm/resort	Possible sources of PCB	Concentration (µg/L)
Riet Spruit	Vanderbijlpark	Iron and steel refinery	44
Modderfontein Spruit	Modderfontein	Industrial sewage or spills	221
Swartkops Estuary	Port Elizabeth	Runoff from informal settlements or industry (Uitenhage area)	68
Hartbeespoort Dam	Oberon (North West)	Industrial	61
Crocodile River	Nelspruit	Paper mills upstream at Ngodwana	339

Amdany et al. (2014) investigated the seasonal concentration changes of PCBs in the Hartbeespoort Dam, South Africa using semi-permeable membrane devices (SPMDs) as samplers. Results obtained showed that the highest water-dissolved PCB concentration found in the dam was during summer (0.150 µg/L) then decreased as conditions became colder, with winter having the lowest concentrations detected (0.038 µg/L) (Amdany et al., 2014). The hydrophobicity of PCB compounds is affected by climate conditions, where heavy rains in winter may disrupt the strong interactions between PCBs and soil/sediment particles. This disruption leads to the remobilisation of the PCBs into the water phase, thus having lower concentrations in winter. Moreover, since the Hartbeespoort Dam receives an excess of 90% of its water from the Crocodile River, originating from Johannesburg, it is possible that a good proportion of the pollutants sampled could be of industrial origin (Amdany et al., 2014). Currently the Department of Water Affairs is carrying out a study in 17 sites along the Jukskei and Olifants River. Water sampled at Middleburg and Oxford showed that the concentration of Arochlor was 1.32 µg/L and 1.57 µg/L respectively (Personal source, 2017). A map of the prevalence of PCBs in South Africa is provided in **Figure 2.3**. Degrading POPs in contaminated water supplies has been a major challenge in the past few decades. Thus, there is an urgent need to develop newer and more effective technologies to efficiently degrade and remove PCBs from South African water systems.

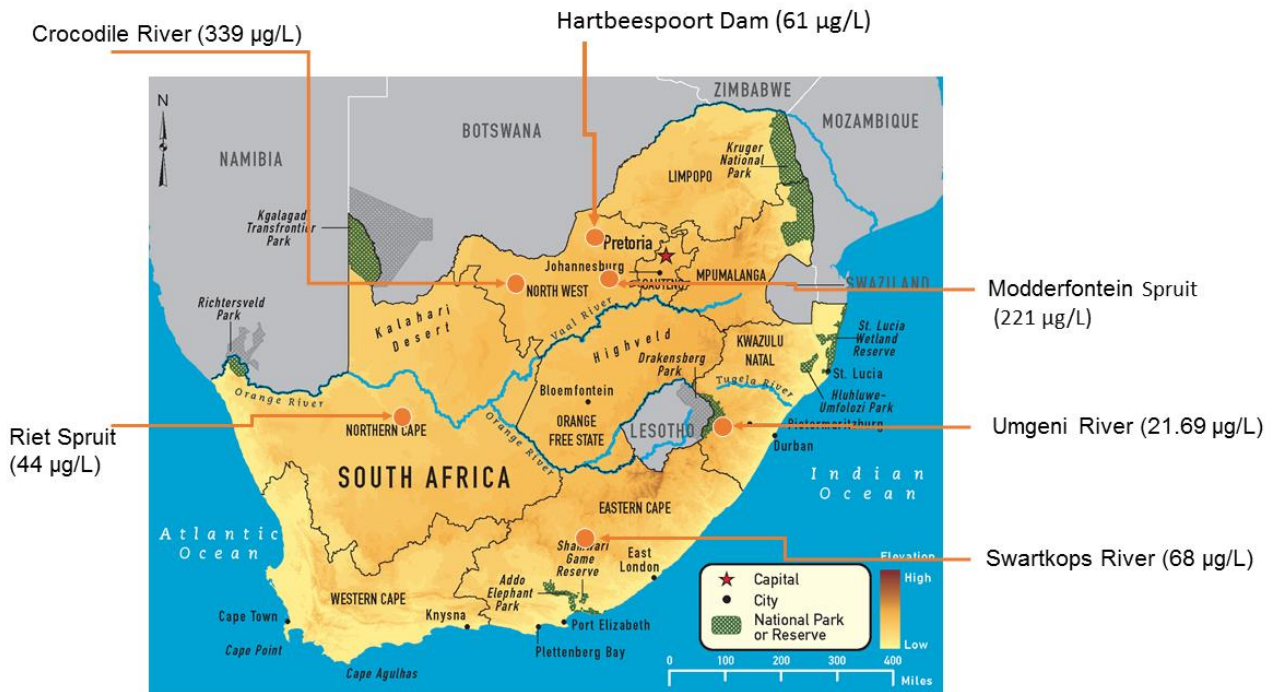


Figure 2.3. Map of South Africa indicating PCB contaminated

2.2.2.3 Health effects of PCBs

The implementation of a risk-management strategy for PCBs was successful when it was first discovered that these substances are among the most stable organic compounds known and have adverse health effects. However, PCBs have been banned worldwide since 1980s due to their pronounced toxicity effects on human health (Shang et al., 2016). Polychlorinated biphenyls typically occur in the environment in extremely low concentrations (µg/L), but they still pose a significant threat to human and wildlife health. Prolonged intake of PCBs was shown to increase the risk of being diagnosed with cancer as well as negatively impacting the developmental and reproductive systems in human beings. In addition, they are also endocrine disruptors and can interfere in the functioning of both the central and peripheral nervous systems as well as the immune system (Pieters and Focant, 2014). Furthermore, these compounds accumulate in lipid-rich tissues due to their

hydrophobic character. Hence, the adipose tissue constitutes one of the most important internal reservoirs for PCBs (Müllerová and Kopecký, 2007). As signatories of the Stockholm Convention, South Africa agreed to reduce and eliminate the release of PCBs for the preservation of human health and the environment. The objectives of the Stockholm Convention state that PCB materials containing a total concentration of 50 mg/L are to be identified and removed by 2025 (Department of Environmental affairs, 2011).

2.2.3 Pesticides

Nevertheless, South Africa is one of the developing countries which is still facing a crisis in having access to uncontaminated freshwater due to contamination by pesticides and other chlorinated compounds. In South Africa, very few data are available on environmental pollution of rural water sources by pesticides. However, a few studies have been conducted in wastewater streams. These water systems have been found to contain pesticides such as dichlorodiphenyltrichloroethane (DDT), hexachlorobenzene (HCB) and pentachlorobenzene (PCB). Pesticides are chemical substances that are used to destroy or control pests. They can be classified into three different groups, i.e. fungicides, insecticides, and herbicides (weed killers). They are normally found in wastewater streams. Due to their environmental pollution impact, there is a great need to treat water contaminated by pesticides in order to avoid economic and health issues (El-Shahawi et al., 2010). Schulz and Peall (2001) revealed that the main sources of pesticides are the agricultural uses which is the main source of water contamination by pesticides. Pesticides such as hexachlorobenzene are normally man-made synthetic organic compounds, but they also occur in plant derivatives or naturally occurring inorganic minerals. Pesticides are common in treated wastewater and local waterways and have been found at levels that can harm aquatic life (El-Shahawi et al., 2010, Köck-Schulmeyer et al., 2013). It is very difficult to remove these compounds from the aquatic environment due to their chemical structure and physicochemical properties. Sibali et al. (2008) investigated the levels of organochlorine pesticide compounds from Jukskei River catchment area in Gauteng, South Africa. The pesticide levels observed in this catchment were found to be much higher than the water criteria values recommended by USEPA and DWAF for the protection of the aquatic environment. It is noticeable that many of these pesticides arise from agricultural activities, used to destroy pests. Hexachlorobenzene was detected in samples collected in the Vaal River ranging from 0.9-296 ng/g. These levels are above the allowable limits for South Africa (0.1-0.5 µg/L) (SANS 241-1, 2015). Studies conducted in eThekweni, KwaZulu-Natal (South Africa) revealed high concentrations of pesticides such as dichlorodiphenyltrichloroethane (DDT), hexachlorobenzene (HCB) and pentachlorobenzene (PCB) in sediments in river estuaries and canals (Newman et al., 2015). The concentration levels of hexachlorobenzene were found to be 5.37 ng/g, 4.68 ng/g and 7.3 ng/g in Isipingo, Umgeni and Mhlathuze River beds, respectively. Hexachlorobenzene has also been detected in the Vaal River at levels ranging from 0.9 to 296 ng/g. In the Eastern Cape (Umtata Dam and Umtata River), Fatoki and Awofolu (2012) detected levels which ranged from 5.5 ng/L to 160 ng/L of HCBs in water samples collected from groundwater, marine, surface and drinking water. Dalvie et al. (2003) investigated pesticide contamination of groundwater and surface water in three agriculturally intensive areas in the Western Cape. In this study, the Hex River was found to contain pesticides such as endosulfan which were detected at levels of about 0.1 µg/L. Endosulfan was found to be widespread in groundwater, surface water, and drinking water. The map given in **Figure 2.4** indicates the main pesticide-contaminated areas in South Africa.

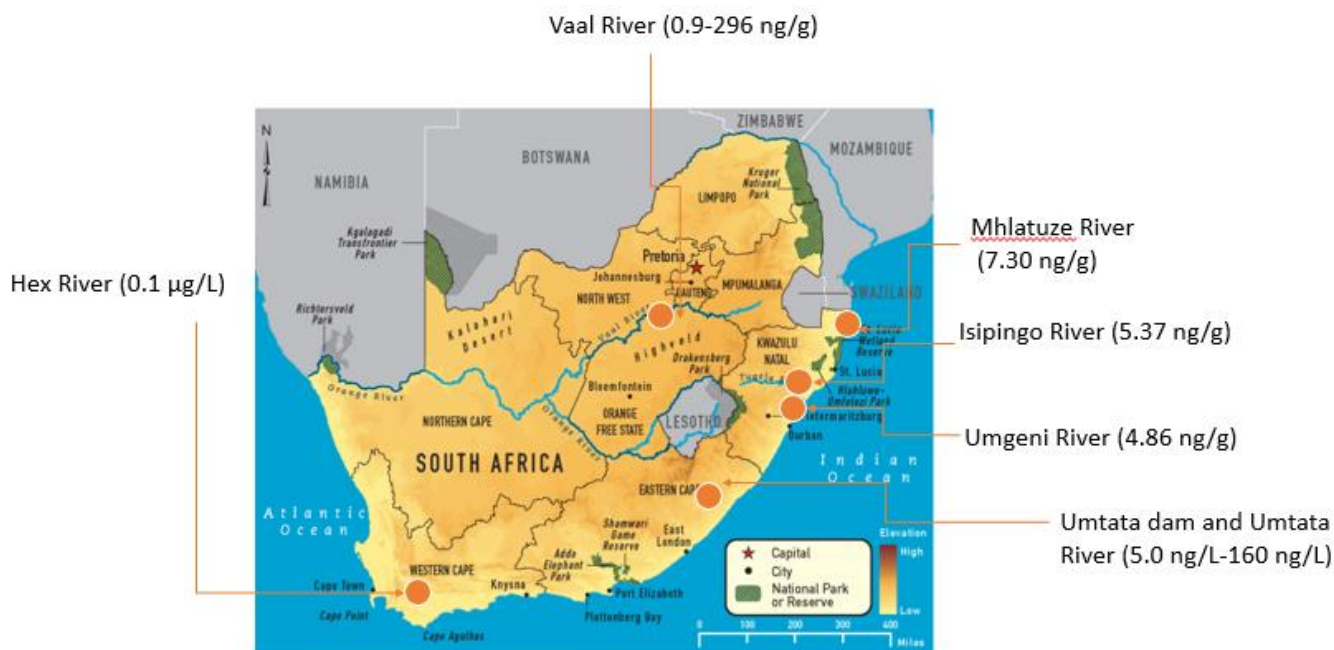


Figure 2.4. Map of South Africa indicating pesticide-contaminated areas

2.3 APPLICATION OF HYPERBRANCHED POLYMER SYSTEMS IN WATER TREATMENT

2.3.1 Overview

Hyperbranched polymers are synthesised through two preparation techniques, namely the single-monomer methodology (SMM) and the double-monomer methodology (DMM). The single-monomer methodology is the common technique and it involves polymerisation of AB_n monomers to produce hyperbranched molecules. This technique involves four specific reaction mechanism routes which are: (a) Polycondensation of AB_n monomers; (b) self-condensing vinyl polymerization (SCVP); (c) self-condensing ring-opening polymerisation (SCROP); and (d) proton transfer polymerization (PTP). The double-monomer methodology involves the direct polymerisation of two types of monomers or a monomer pair to produce hyperbranched polymer systems. This technique is classified into two categories which are: (a) 'A₂ + B₃' methodology; and (b) couple-monomer methodology (Gao and Yan, 2004). However, these polymers have been used extensively in other fields of study except in water treatment. Recently the use of hyperbranched polymers in water treatment has also drawn attention of most researchers. In the following section we review different hyperbranched polymer systems that have been synthesised in different supports, used as templates or blended with polymers to form membranes for water treatment.

2.3.2 Hyperbranched polyester-cellulose membranes

Mahdavi and Shahalizade (2015) modified cellulose acetate (CA) membranes by using generation 3 and 4 aliphatic hyperbranched polyester (HBPE). The properties of these membranes were then compared to the pure CA membranes. The results indicated that the surface hydrophilicity of the CA membrane blended with HBPE was much higher than that of the pure CA membrane. The contact angle of blended membranes reached 26.7° as compared to 65.8° for pure CA membranes. As the HBPE content was increased the HBPE modified membranes also showed high pure water flux from 24.6 to 37.6 L·m⁻²·h⁻¹.

2.3.3 Hyperbranched poly(amine-ester) functionalised multiwalled carbon nanotubes polyvinylidene fluoride (PVDF) membranes

In this study hyperbranched poly(amine-ester) (HPAE) functionalised with multiwalled carbon nanotubes (MWCNTs) were prepared by first oxidising MWCNTs to introduce carboxylic acid functional groups. The oxidised MWCNTs were then reacted with the HPAE via an acid base reaction to form HPAE-MWCNTs (Zhao et al., 2012). The HPAE-MWCNTs were then blended with PVDF polymer via phase inversion to produce a flat sheet membrane for potential application in biofouling. Hyperbranched polymers have been found to induce dispersion and prevent agglomeration of MWCNTs. In this investigation, Zhao and co-workers (2012) found that the HPAE-MWCNTs lowered the contact angle (from $85 \pm 1.3^\circ$ to $73 \pm 1.1^\circ$). Moreover, as the HPAE-MWCNTs content was increased in the casting solution the protein adsorption decreased from 70 mg/cm^2 to 20 mg/cm^2 . The inhibition in adsorption of the protein was due to the formation of hydrogen bonds between the hydrophilic groups of HPAE and water molecules, thus forming a hydrated film. The hydrated film introduces steric repulsion of the protein (Zhao et al., 2012).

2.3.4 Crosslinked hyperbranched polymer/PAN composite membrane

Hyperbranched polymer (Boltorn W3000) was crosslinked with polyacrylonitrile (PAN) polymer using one step self-assembly method to produce a PAN/Boltorn composite membrane (Figure 2.5). After incorporation of the amphiphilic hyperbranched polymer the contact angle increased from 85° to 34° . Consequently the flux was reduced from $750 \text{ L}\cdot\text{m}^{-2}\cdot\text{h}^{-1}$ to $62.3 \text{ L}\cdot\text{m}^{-2}\cdot\text{h}^{-1}$ after crosslinking due to the formation of a dense structure on the membrane (Wang et al., 2014a). The PAN/Boltorn membrane showed excellent performance for the removal of methylene blue (up to 97%) under different operation pressures. This finding thus demonstrated the capability of the membranes in the removal of dyes from water.

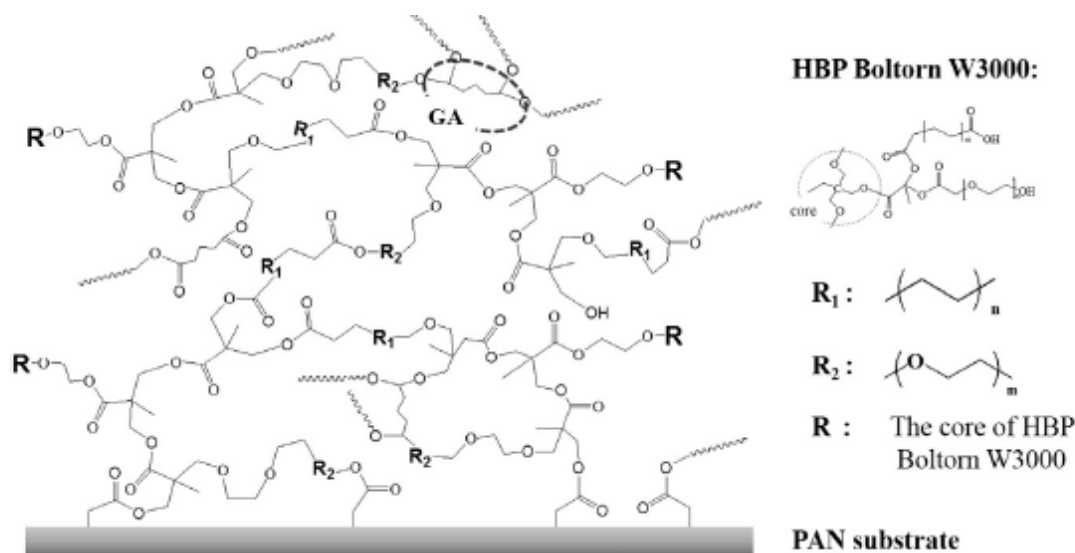


Figure 2.5. Crosslinked PAN/Boltorn composite membrane (Wang et al., 2014a)

2.3.4.1 Hyperbranched polyester-polysulfone membrane

Wei et al. (2008) prepared a new type of nanofiltration membrane based on crosslinked hydroxyl-ended hyperbranched polyester (HPE) using ultrafiltration polysulfone as a porous support. The HPE was reacted with trimesoyl chloride (TMC) to form a thin-film composite via interfacial polymerisation method. The results showed that the crosslinked hyperbranched polyester produced a uniform active ultra-thin layer on the surface of the polysulfone membrane support. The prepared nanofiltration membrane showed improved water permeability and high rejection towards salts. Permeation experiments were conducted for four inorganic salts, i.e. NaCl, Na₂SO₄, MgCl₂ and MgSO₄. The rejection and flux for Na₂SO₄ reached 85.4% and 79.1 L·m⁻²·h⁻¹, respectively. The high rejection of the salts was attributed to the structure of the HPE and the membrane charge. In another similar study, Wei et al. (2013) also investigated the influence of hyperbranched polyester on structure and properties of synthesized nanofiltration (NF) membranes. In this study hyperbranched polyester polymers with different number of hydroxyl end groups were used [i.e. H20 (G2), H30 (G3) and H40 (G4)]. The membranes were analysed for pure water flux, hydrophilicity and rejection towards cationic and anionic dyes. The NF-G2 membrane showed unstable pure water flux because of the loose structure of G2 hyperbranched polyester polymer. However, the NF-G3 and NF-G4 membranes had stable flux and this was attributed to the more spherical and rigid structure for G3 and G4 hyperbranched polymers (Wei et al., 2013). On the other hand, surface hydrophilicity was found to increase from 59.7 ± 2° for NF-G2 to 66 ± 1.5° for NF-G4. This is because G2 hyperbranched polyester is linear and open. The G3 and G4 hyperbranched polyester modified membranes have a spherical structure and hydrophilic moieties migrate to the inside of the polymer during drying (Wei et al., 2013). The modified membranes were found to be effective in the rejection of reactive brilliant blue X-BR. The rejection mechanism was found to be mainly due to steric hindrance and electrostatic action. The authors concluded that the NF membranes were suitable for the removal of anionic dyes in wastewater.

2.3.4.2 Hyperbranched polyamidoamine-polytetrafluoroethylene membranes

Yoo and Kwak (2013) prepared hyperbranched poly(amidoamine) (HPAMAM)-grafted polytetrafluoroethylene (PTFE) microfiltration membranes for the removal of Cu²⁺ ions from aqueous solution. The PTFE was first aminated with hydrazine and followed by chemical coupling with HPAMAM (**Figure 2.6**). After modification of the membranes, the flux increased to 635 ± 9 L m⁻² h⁻¹ due to the presence of hydrophilic HPAMAM. The membrane was further immersed into a 50 mL solution containing 50 mg/L Cu²⁺. The concentration of the solution was reduced to 14.2 mg/L (1.42 g/m² adsorption capacity).

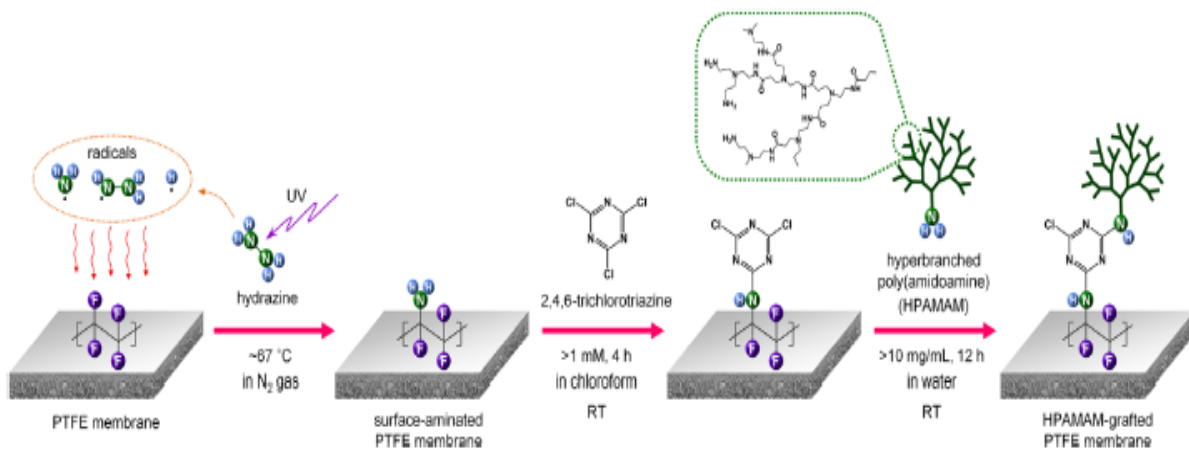


Figure 2.6. Synthesis of HPAMAM-grafted PTFE membranes (Yoo and Kwak, 2013)

2.3.5 Hyperbranched polyethyleneimine-based membrane

Sun et al. (2014) developed a hollow-fibre nanofiltration membrane by crosslinking hyperbranched polyethyleneimine (PEI) with polyamide-imide (PAI) for the rejection of a pharmaceutical drug, ciprofloxacin. The carbonyl groups of the imide polymer chain were reacted with the amine of the PEI to form amide groups which resulted in a positively charged hollow-fibre membrane. The membrane modified with PEI-60K had a smaller pore size (0.40 nm), it was more hydrophilic ($68.6 \pm 1.3^\circ$), and was positively charged (25.1 mV). These membranes showed the highest rejection and permeate flux for ciprofloxacin at a pH range of 3-9. These results confirmed that size exclusion, charge repulsion and solute-membrane affinity were all important parameters for the rejection of ciprofloxacin. In another study conducted by Chiang et al. (2009), a membrane consisting of hyperbranched polyethyleneimine was reacted with either trimesoyl chloride (TMC) or terephthaloyl chloride (TPC) via interfacial polymerisation. This membrane was used in the rejection of salts. Both types of membranes (PEI/TMC and PEI/TPC) were found to be very efficient in the rejection of salts such as $MgCl_2$ and $MgSO_4$ (up to 80%). The high salt rejection was attributed to the fact that the charged amine groups of the hyperbranched polyethylene imine drift inside the pores of the membranes thus increasing their interaction with the salts (Chiang et al., 2009). The PEI/TMC ($9.5 \text{ kg}\cdot\text{m}^{-2}\cdot\text{h}^{-1}\cdot\text{bar}^{-1}$) was however found to have very high-water permeability as compared to PEI/TPC ($2.1 \text{ kg}\cdot\text{m}^{-2}\cdot\text{h}^{-1}\cdot\text{bar}^{-1}$) since the latter had the largest pore size (1.53 nm).

2.3.6 Hyperbranched poly(amidoamine)/polysulfone composite membranes

Han and co-workers (2012) prepared a hyperbranched poly(amidoamine)(HYPAM)/polysulfone composite membrane for removal of Cd(II) from water. These membranes were prepared via phase inversion method and the hyperbranched polyamidoamine was used as the chelating polymer. As the hyperbranched polymer content was increased from 1-3 wt%, the flux increased from $4.0 \text{ L}\cdot\text{m}^{-2}\cdot\text{h}^{-1}$ for the neat PSf membrane to $18.4 \text{ L}\cdot\text{m}^{-2}\cdot\text{h}^{-1}$ for the 5 wt% HYPAM modified membrane. Inductively coupled plasma atomic emission spectroscopy showed that the removal efficiency for Cd (II) was 51%. This removal was due to the complexation of the Cd(II) metal ion on the amine groups of the hyperbranched poly(amidoamine) polymer.

2.3.7 Membranes with hyperbranched antibacterial polymer brushes

Polyvinylidene fluoride (PVDF) was grafted to poly[2-(N, N-dimethylamino) ethyl methacrylate] (PDMAEMA) side chains to form PVDF-g-PDMAEMA copolymer. This copolymer was further reacted with an alkyne which made it further susceptible to functionalisation to azido-terminated hyperbranched polyethyleneimine polymer (PEI- N_3). This membrane (PVDF-g-P[QDEMAEMA-click-QPEI]) was then tested for its ability to reduce bacteria (i.e. Gram-positive *Escherichia coli* and *Staphylococcus epidermidis*) under continuous flow conditions. Scanning electron micrographs revealed that the PEI-based membrane killed the bacteria upon contact with the membrane surface. The membrane surface was cleaner revealing that the bacterial cells were destroyed upon contact with the membrane. According to Cai and co-workers (2012), the PEI contained a high density of quaternary ammonium cations which interact with the cytoplasmic membrane of the microorganism resulting in membrane disruption.

2.3.8 Hollow-fibre membranes modified with hyperbranched polyethyleneimine polymer

A co-polyamide, P-84, was crosslinked with PEI to produce a hollow fibre for the rejection of Pb^{2+} , $MgCl_2$ and glucose (Gao et al., 2014). The rejection mechanisms for these solutes were found to be highly dependent on the mean effective pore size (r_p) of the fabricated hollow-fibre membrane. Gao et al. (2014) observed that Donnan exclusion also played a role in the rejection of Pb^{2+} and $MgCl_2$ when the $r_p > 0.34 \text{ nm}$ whilst size exclusion dominated when the $r_p < 0.34 \text{ nm}$. The crosslinked membrane showed high rejection towards $MgCl_2$ (99.06%) and $Pb(NO_3)_2$ (91.05%). Gao et al. (2014) concluded that in order to achieve maximum rejection of

lead and any other heavy metal ion using the crosslinked hollow-fibre membrane, factors such as pore size have to be manipulated.

2.3.9 Polyethersulfone membranes modified with hyperbranched polyethyleneimine polymer

Fang et al. (2015) fabricated PES/PEI flat sheet membranes by adding different PEI concentrations to the casting solution. This study was carried out to deduce the effect of PEI on the PES membrane. The addition of the HPEI was found to affect the morphology of the PES/UF membrane. The SEM analysis revealed that an increase in the PEI content led to the formation of finger-like structures within the membrane structure. It was also demonstrated that when the content of the PEI was increased to 0.3 wt% the water flux reached $359 \text{ L}\cdot\text{m}^{-2}\cdot\text{h}^{-1}$ which was 35.9 times higher than that of the pristine PES. Bovine serum albumin rejection increased from 96.3% to 97.1% for membranes modified with 0.6 wt% and 0.9 wt% PEI content, respectively.

2.3.10 Hyperbranched polyethyleneimine-graphene oxide/polyethersulfone (HPEI-GO/PES) ultrafiltration membrane

Yu et al. (2013) prepared graphene oxide (GO) nano sheets which were modified with hyperbranched polyethyleneimine (HPEI) polymers in order to enhance compatibility between the GO and the polymer macromolecule. This hybrid membrane was evaluated for anti-biofouling properties, anti-protein adsorption, pure water flux and hydrophilicity. Bovine serum albumin (BSA) was used as a model protein to evaluate the anti-protein capabilities of the membranes. The results showed that the protein adsorption for PES pristine membrane was $61.11 \mu\text{g}/\text{cm}^2$ and this decreased to $25.89 \mu\text{g}/\text{cm}^2$ as the content of HPEI-GO was increased. The membranes' ability to resist protein adsorption was due to the addition of hydrophilic groups of the HPEI-GO in the hybrid. The SEM analysis of *E. coli* grown on the membrane surface of neat PES membranes showed that the bacterial cells were intact and rod shaped. However, TEM analysis revealed that *E. coli* grown on hybrid membranes had lost their cellular integrity.

2.3.11 Nanofiltration membranes based on polyvinylidene fluoride and crosslinked hyperbranched polyethyleneimine

Park et al. (2012) developed a nanofibrous membrane which consisted of crosslinked HPEI supported on a commercial polyvinylidene fluoride (PVDF) membrane. Different cross-linkers were also investigated in this study [i.e. trimesoyl chloride (TMC), 1, 3-dibromo propane (DBP), and epichlorohydrin (ECH)] and their effects on membrane performance were investigated. Rejection performance of the membranes against four salts (NaCl , MgCl_2 , Na_2SO_4 , and MgSO_4) was carried out. It was found that the membrane crosslinked with PEI/TMC had a high flux of $30 \text{ L}\cdot\text{m}^{-2}\cdot\text{h}^{-1}$. Membranes crosslinked with TMC ($38.6 \pm 1.4^\circ$), DBP ($54.9 \pm 0.5^\circ$) and ECH ($50.2 \pm 1.3^\circ$) generally had lower contact angles compared to pure PVDF support ($130.2 \pm 0.9^\circ$). High rejection towards MgCl_2 (88%) and NaCl (65%) at pH = 6 was observed for membranes crosslinked with PEI/TMC.

2.3.12 Hyperbranched polymers based on other supports

2.3.12.1 Hyperbranched polyamidoamine-chitosan adsorbents

Hyperbranched polymers can also be blended with other compatible polymers to form adsorbents that can effectively remove heavy metals from water. Ma et al. (2009) investigated the adsorption behaviour of Hg (II) on chitosan functionalised by amino-terminated hyperbranched polyamidoamine polymer. Chitosan was used in this study since it is biocompatible, hydrophilic and non-toxic. However, this polymer tends to agglomerate and forms a gel and thus it becomes difficult to use it in water treatment applications. Therefore, hyperbranched polyethyleneimine polymer was introduced to enhance the properties of chitosan and to introduce novel

functionalities (Ma et al., 2009). In this study different generations of the chitosan-HPEI polymer were investigated in the adsorption of Hg (II) under various pH conditions. Results showed that the adsorption of mercury was found to decrease with an increase in the generation number of the fabricated polymer. The Langmuir adsorption isotherm was found to fit the data better than the Freundlich isotherm thus it was concluded that the adsorption occurred via a monolayer adsorption. The adsorption rate was also found to increase with an increase in temperature over a temperature range of 5-35°C.

2.3.12.2 *Hyperbranched polyethyleneimine-silica nanospheres*

Arkas and Tsiourvas (2009) synthesised organic/inorganic hybrid nanospheres based on hyperbranched polyethyleneimine encapsulated into silica. These silica nanospheres were used for the sorption of toxic metal ions (Pb^{2+} , Cd^{2+} , Hg^{2+} , and $\text{Cr}_2\text{O}_7^{2-}$) and polycyclic aromatic hydrocarbons (pyrene and phenanthrene) from water. The sorption rate for the metals ions using the HPEI-silica nanoparticles was found to be higher for Pb^{2+} followed by Hg^{2+} and lastly Cd^{2+} . This gave evidence that even though the HPEI was encapsulated within the silica it still maintained its chelating properties towards the metal ions. Moreover this system was found to absorb pyrene and phenanthrene efficiently. The removal of the organics was due to a charge-transfer complex between polycyclic aromatic hydrocarbons and tertiary amino groups from the hyperbranched polyethyleneimine.

2.3.12.3 *Alumina ceramic filters impregnated with hyperbranched polyethyleneimine*

Tsetsekou et al. (2008) also conducted a study on the optimisation of hybrid hyperbranched polymer/ceramics filters for the efficient absorption of polyaromatic hydrocarbons from water. Alumina ceramic filters with different pore sizes were impregnated with alkylated hyperbranched polyethyleneimine (PEI-15). In this study polycyclic aromatic organic pollutants such as phenanthrene and β -naphthol were used as model pollutants and experiments were carried out in a dead-end filtration set up. A slight increase in the impregnation percentage of PEI (0.4% to 0.6%) was found to show improvement in pollutant retention. Overall, the modified hybrid ceramic filters absorbed 98% of the phenanthrene and 55% of the water-soluble β -naphthol.

2.3.12.4 *Hyperbranched polyester/TiO₂ nanocomposites*

Ghaem et al. (2014) synthesised HPES-OH/TiO₂ by using *in situ* and *ex situ* methods. Chemical oxygen demand (COD) was used to evaluate the photocatalytic properties of the nanocomposites towards mineralisation of wastewater (Ghaem et al., 2014). The results of this study revealed that the treatment of the wastewater using UV light did not have an effect on the COD levels. However, it was observed that the percentage COD removal of 32%, 62%, 70% and 69% was recorded for pure HPES-OH, pure TiO₂-nanowires, *in situ* HPES-OH/TiO₂ and *ex situ* HPES-OH/TiO₂, respectively. The high percentage COD removal was attained since TiO₂ prepared using the *in situ* method produced well defined TiO₂ nanoparticles. It was also observed that for these nanocomposites smaller crystalline sizes of TiO₂ were obtained since during the synthesis process there is possible electrostatic interaction between the hydroxyl ends of the hyperbranched polyester and the TiO₂.

2.3.12.5 *Hyperbranched polyethyleneimine (HPEI) functionalised silver nanomaterials*

In this study, HPEI was exploited for its ability to prepare stable, narrow and well dispersed Ag nanoparticles (Li, 2014). Moreover, HPEI was used as a reducing agent and a relatively greener synthetic approach was followed. Hyperbranched polyethyleneimine (HPEI) consists of primary, secondary and tertiary amines. The nitrogen atom will lose an electron from the various amine groups. These electrons will be transferred to Ag^+ and to produce Ag^0 . The TEM analysis showed that the Ag nanoparticles were spherical in shape, well dispersed and stable over a period of one month. Li and co-workers (2014) further tested the HPEI/Ag nanomaterial against different bacterial strains and compared this with existing antibiotics. The HPEI/Ag was

found to have antibacterial activity for all strains tested. However, the antibacterial activity was enhanced for bacteria such as *S. epidermidis* and *C. albicans*. This was attributed to the fact that HPEI-Ag is positively charged and these nanoparticles interact with the negatively charged bacteria via electrostatic interactions. When these interactions occur, the cell wall of the bacteria ruptures, resulting in cell death. Moreover, more Ag ions may also penetrate into the cells (Li et al., 2014). This system would have a potential application in water contaminated by various bacterial strains.

2.3.12.6 Hyperbranched poly(ester amide)/polyaniline nanohybrid

Hyperbranched poly(ester amide) (HBPEA) was attached to montmorillonite (i.e. 1, 2.5 and 5 wt%) to form an organic-inorganic antimicrobial nanohybrid. The HBPEA was loaded at varying concentrations via *ex situ* polymerisation (Pramanik et al., 2014). The nanohybrid showed improved physico-chemical and mechanical properties. The zone of inhibition of the antibacterial test increased with an increase in nanohybrid content. The HBPEA/polyaniline nanohybrid showed pronounced activity towards *B. subtilis*, *S. aureus* as compared to *E. coli* and *P. aeruginosa*. Due to their antimicrobial properties the nanohybrid materials could find potential application in water for the removal of bacteria such as *E. coli*.

2.3.12.7 Hyperbranched polyethyleneimine modified gold surface

In this study PEI was immobilised on a gold-coated quartz surface by self-assembly as shown in **Figure 2.7**. The gold surface was functionalised with -COOH groups and further activated with 1-Ethyl-3-(3-dimethylaminopropyl)-carbodiimide (EDC)/N-hydroxysuccinimide (NHS) to ensure attachment of PEI with the gold surface via amide bonds (Suriyanarayanan et al., 2013). This resulted in composite PEI brush-like structures which are flexible and provide steric hindrance under certain conditions. These PEI brushes were then exposed to different molecular weight protein to investigate their anti-fouling properties. Experimental analysis revealed that the brushes resisted protein absorption to less than 0.08 $\mu\text{g}/\text{cm}^2$. These polymer brushes would be suitable in membrane application processes.

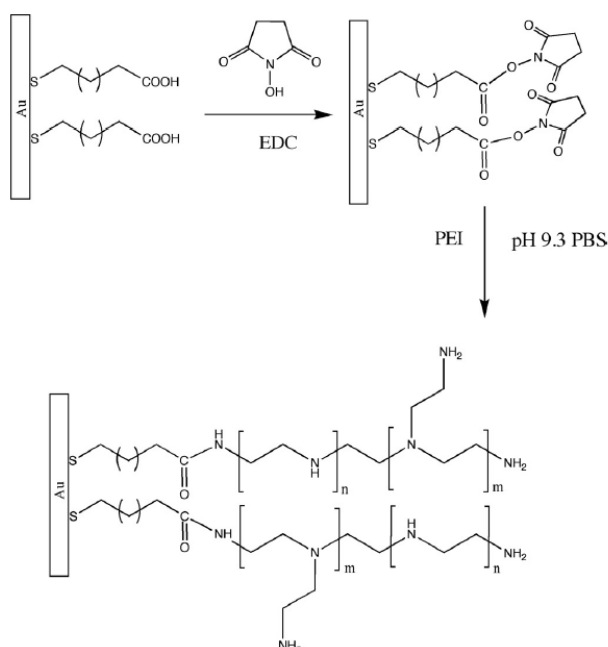


Figure 2.7. Fabrication of PEI onto Au surface (Suriyanarayanan et al., 2013)

2.3.12.8 Hyperbranched copolymers based on PEG-methacrylate

Hyperbranched poly(oligoethylene glycol) copolymers were synthesised by co-polymerisation method and these polymers were characterised using size exclusion chromatography (Luzon, 2014). The main aim of the work was to use the hyperbranched copolymers for their effective removal of Cr (VI) from water. The hyperbranched polymers were found to be effective in the removal of chromium at high temperatures. Adsorption was found to increase from 1.2 to 40.4 mg/g and this was attributed to the fact that at high temperature the hyperbranched polymers aggregate and form a porous structure. This porous structure contains numerous nanocavities which can trap metal ions. These results demonstrated that the hyperbranched copolymers are effective adsorbents for Cr (VI) and have great potential in environmental applications.

2.3.12.9 Amino-terminated hyperbranched polymer grafted onto cotton fibres

Zang and co-workers (2014) synthesised hyperbranched polymer-cotton fibres as shown in **Figure 2.8**. These cotton fibres were first pretreated to introduce -COOH into the backbone of the fibres and this was followed by attaching the amine terminated hyperbranched polymers. The adsorption properties of the hyperbranched polymer-grafted cotton fibres were studied by varying heavy metal ion (Cu^{2+} and Pb^{2+}), contact time and heavy metal ion concentration (Zang et al., 2014). As the mass of the adsorbent was increased from 0.2-1.6 g, the adsorption of Cu^{2+} and Pb^{2+} increased to 73.5 wt% and 71.2 wt.% respectively. The analysis also revealed that as the contact time increased the amount of Cu^{2+} and Pb^{2+} adsorbed was about 16.1 mg/g and 13.4 mg/g respectively. The amino groups present in the hyperbranched polymers are known to be responsible for chelation of heavy metals.

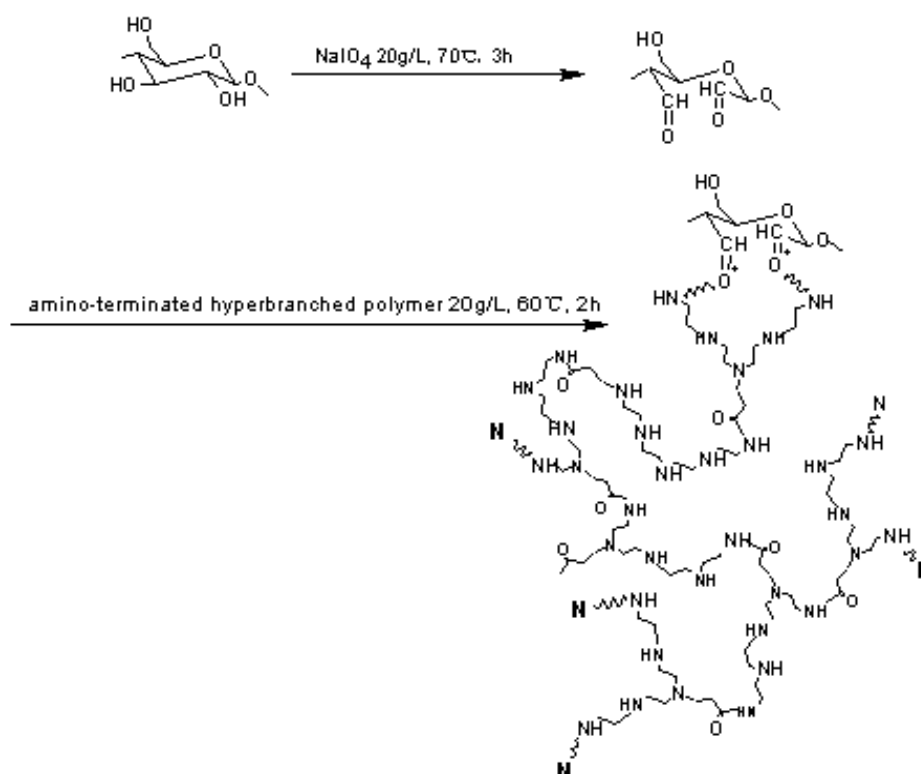


Figure 2.8. Synthesis of cotton fibres grafted with hyperbranched polymers (Zang et al., 2014)

2.3.12.10 Magnetite-polyethyleneimine-montmorillonite hybrid material

Larraza et al. (2014) prepared a hybrid material consisting of montmorillonite (MMT), Fe₃O₄ and hyperbranched polyethyleneimine (PEI) with different molecular weights. Mono-cation sodium clay was first prepared and subsequently the surface on Fe₃O₄ was coated with PEI. The coated PEI was anchored into the MMT as shown in Figure 2.9. The resulting hybrid material was used in the removal of Cr(VI) from water. The combination of MMT, PEI and Fe₃O₄ nanoparticles was found to result in high Cr(VI) removal efficiencies over a wide pH range. Moreover, the hybrid material was found to be chemically stable at all the pH ranges due to the fact that the nanoparticles were coated by PEI and MMT sheets (Figure 2.9).

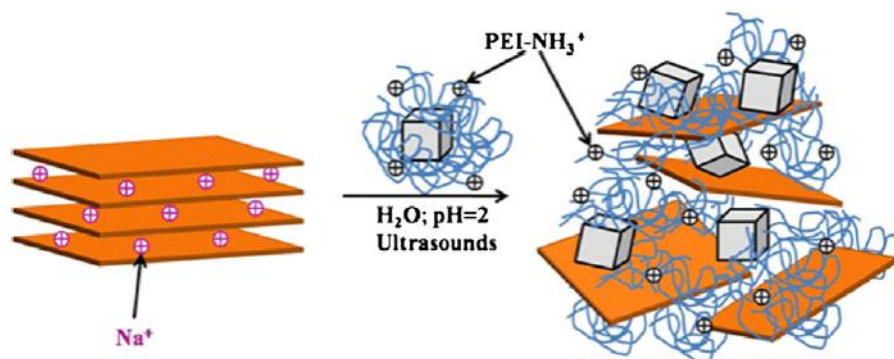


Figure 2.9. Preparation of hybrid material magnetite-PEI-Mt (Larraza et al., 2012)

2.4 SUMMARY

The literature discussed in this section highlights the sources, routes of exposure of BPA, PCB-153 and some common pesticides in South African water systems. This chapter also highlights some proposed removal technologies by using HPEI systems either embedded on a membrane or supported on other materials for water treatment. However, the studies reviewed show that not much has been done on the use of HPEI as a template for the preparation of catalysts for the degradation of phenolic compounds in water. Thus, this work dwell on the use of hyperbranched polymer membranes for the catalytic degradation of phenolic compounds.

CHAPTER 3: DEGRADATION OF METHYL ORANGE USING HYPERBRANCHED POLYETHYLENEIMINE AND TITANIUM DIOXIDE (TiO₂) MEMBRANES

3.1 INTRODUCTION

Compared to many other semiconductors, TiO₂ has proven to be most suitable for common environmental applications such as solar cells, water treatment and air purification (Mobarakabad et al., 2015; Aghighi and Haghghat, 2015). In water treatment, TiO₂ may be used as a photocatalyst due to its non-toxicity, chemical stability and its ability to possess relatively high photocatalytic activity. Titanium dioxide (TiO₂) nanoparticles can be applied at ambient temperature and pressure, without addition of chemical species (Pandey et al., 2015). However, TiO₂ nanoparticles are usually prone to agglomeration due to their magnetic nature (Kang et al., 2015; Elahi et al., 2015). Agglomeration causes a reduction in the surface area and thus reducing the reactivity of the nanoparticles. The method of preparation for nanomaterials plays an important role in controlling the shape and properties of nanoparticles (Suttioponparnit, 2011). TiO₂ has been prepared using techniques such as; hydrothermal, aerogel, chemical vapour deposition and sol-gel methods (Chen, 2009; Emregul, 2013; Chen and Mao, 2007; Belayachi et al., 2015). Sol-gel methods stand out as the most preferred methods for metal-oxide preparation since they enable mixing at an atomic level and most importantly result in small particles which are easily sinterable (Amri et al., 2014). Although this is the leading method for preparation of metal oxides, nanomaterials produced from this technique still suffer from agglomeration (Ramesh et al., 2015). Therefore, in this study hyperbranched polyethyleneimine was used as the template for the preparation of TiO₂ nanoparticles to limit agglomeration.

Azo dyes (e.g. methyl orange and methyl blue) constitute about 70% of the dyes used in the textile industry. The water discharged from textile industries is highly coloured and contains compounds that are complex in nature. Coloured water prevents the penetration of light into rivers and lakes, thus affecting the process of photosynthesis which has a negative impact on the natural flora and fauna. Moreover, the improper discharge of untreated coloured dye effluent into the environment has resulted in numerous public protests. Methyl orange has been reported to be toxic and mutagenic to animals. Moreover, most of these dyes are also not effectively removed by the use of conventional biological treatment processes since they are non-biodegradable.

Photocatalytic membranes offer the advantage of chemical decomposition and physical sieves for unwanted pollutants (Molinari et al., 2002). Research on photocatalytic membranes is an emerging field and preliminary results have shown that they are effective and efficient for water purification (Tahiri Alaoui, 2009; Chin et al., 2006). This study was focused on crafting a membrane system which is composed of titanium dioxide nanoparticles, polyethersulfone and hyperbranched polyethyleneimine for the removal of dyes from synthetic dye-polluted water. The selection of the materials was based on the fact that titanium dioxide is reported to exhibit good photocatalytic properties as compared to other semiconductor catalysts (Chen, 2009; Pandey et al., 2015). The hyperbranched polymer has been selected for use as a template and dispersing agent for the synthesis of titanium dioxide nanoparticles. Hyperbranched polyethyleneimine has cavities which act as host/templates for nanoparticle synthesis and thus producing nanoparticles which are well dispersed with uniform particle size. These nanoparticles are held together by electrostatic attractions between the nitrogen groups (Yuan et al., 2013). Moreover, these nanocavities can act as catalytic and adsorption sites for degradation and removal of organic pollutants. The amine groups on the peripheral region of HPEI bring about the antifouling properties of the material (Huang et al., 2012; Yu et al., 2013). Lastly the structure of HPEI provides a shell to prevent aggregation of nanoparticles (Malinga, 2013). The introduction of polyethersulfone into the system is to induce membrane properties such as the hydrothermal and mechanical stability and to

control leaching of the titanium dioxide catalyst (Li et al., 2006; Shen et al., 2011). In this chapter the synthesis of the PES/HPEI/TiO₂ membranes is demonstrated. Characterisation and application of the membranes in the removal of methyl orange (MO) from synthetic solutions will also be reported.

3.2 EXPERIMENTAL METHODOLOGY

3.2.1 Materials

Titanium (IV) *tert*-butoxide (TNB, reagent grade, Sigma-Aldrich Chemical Co., Ltd., USA) was used as the titania precursor. Formic acid (95%, reagent grade) was purchased from Sigma-Aldrich and used as the oxidising agent for TNB₄. Butanol (99.4%, ACS reagent, purchased from Sigma Aldrich) was used as an organic solvent in the preparation of titania nanoparticles. Hyperbranched polyethyleneimine (HPEI) (Lupasol WF, MW: 25 kDa) was supplied by Caltech (California, USA) and used as received. Polyethersulfone (PES) (MW 3000 P, India) was provided by Solvay. All other chemicals and reagents were used as received.

3.2.2 Preparation of pristine TiO₂ nanoparticles

Titanium (IV) *tert*-butoxide (TNB) was hydrolysed through the esterification reaction between formic acid and butanol. All the synthetic experiments were performed at room temperature. The TNB (20 mL) was dissolved in butanol (42 mL) and then mixed with formic acid (10 mL) while stirring. A white precipitate was formed and this was stirred for 4 h and further aged for another 2 h. The resulting solution was dried at 80°C overnight and calcined in air in a furnace at a ramp rate of 10°C/min, from 25°C to 500°C for 3 hours (Zhu, 2005).

3.2.3 Preparation of TiO₂ nanoparticles (NPs) using HPEI as the template

Titanium dioxide nanoparticles were prepared using HPEI as the template following the method reported by Dlamini et al. (2011) with a few modifications (**Figure 3.1**). Titanium *tert*-butoxide (20 mL) and 0.517 g of HPEI (0.0207 mmol) were dissolved in *n*-butanol (42 mL) and stirred continuously for 30 min at room temperature. Formic acid (10 mL) was then added to the mixture to obtain a yellowish precipitate. The resulting precipitate was stirred for 2 h and further aged for 2 h. Thereafter, the sample was dried at 80°C overnight to remove the solvent (Dlamini, 2011). The sample was then ground to a fine powder and calcined using a furnace at a ramp rate of 10°C/min, from 25°C to 500°C for 3 h to completely decompose the HPEI polymer as reported by Scott et al. (2005).

3.2.4 Synthesis of HPEI/TiO₂ nanocomposites

Hyperbranched polyethyleneimine (9.83 mmol) was dissolved in deionised water (5 mL). The HPEI mixture was then mixed with TiO₂ and dissolved in water to attain varying ratios of HPEI:TiO₂ (1:6 and 1:9). The solutions were then stirred for 2 h and consequently sonicated for another 2 h. The resulting slurry was then heated on a hot plate for 5 h at 60°C to remove the solvent and then dried in an oven for 2 h at 90°C to remove excess moisture. Synthesis of HPEI/TiO₂ nanocomposites is represented in **Figure 3.2**.

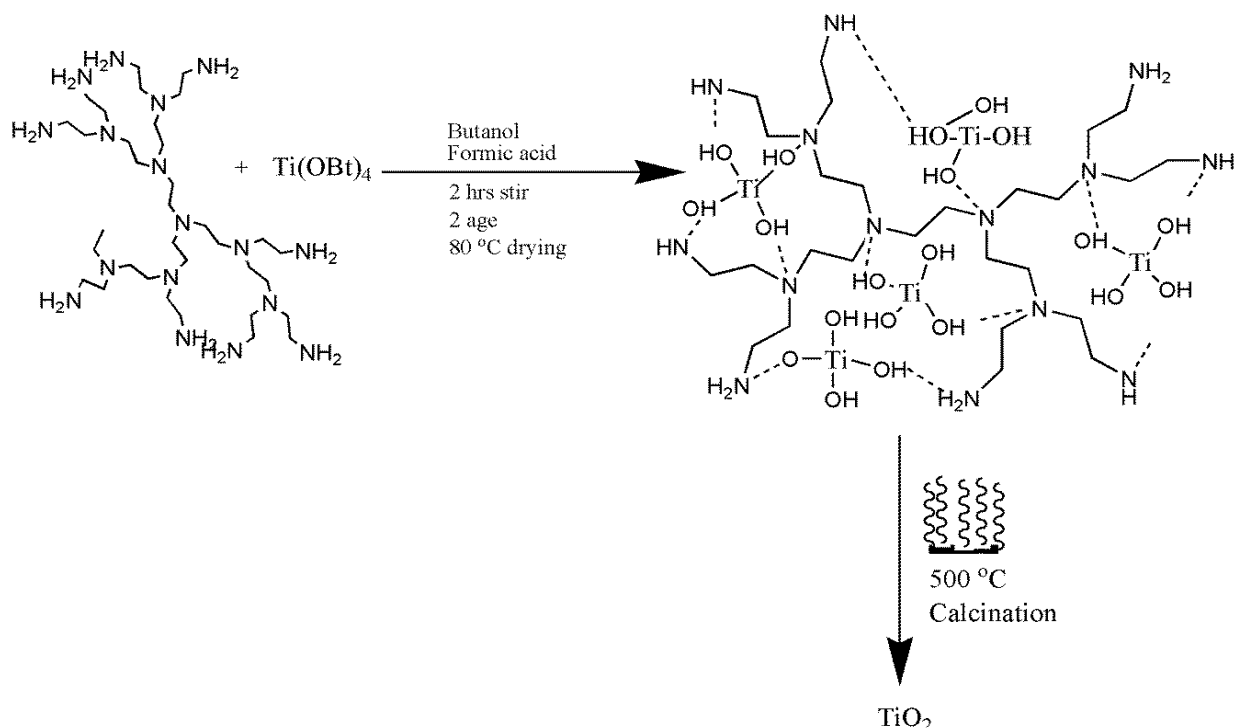


Figure 3.1. Preparation of titanium dioxide nanoparticles using hyperbranched polyethyleneimine as a template

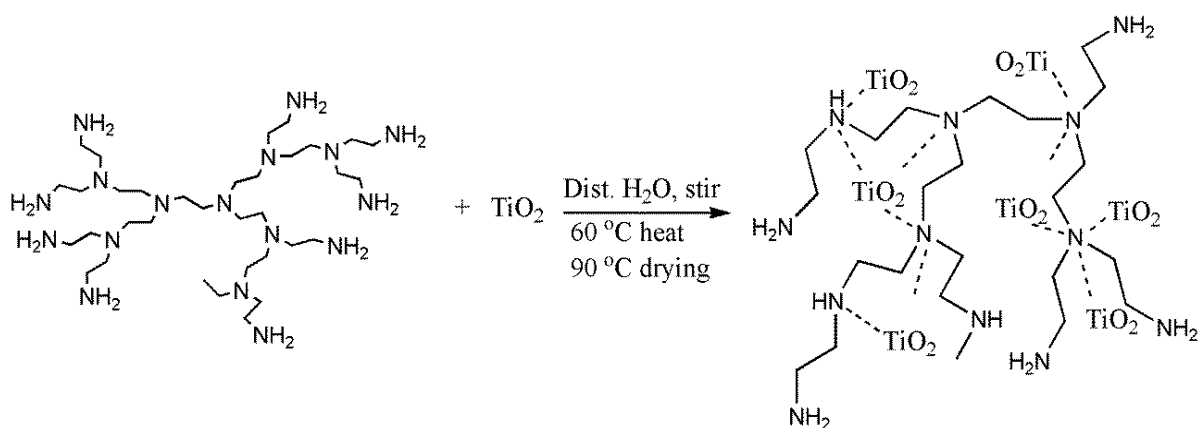


Figure 3.2. Illustration of TiO₂ dispersion on hyperbranched polyethyleneimine

3.2.5 Preparation of PES/HPEI/TiO₂ photocatalytic membranes using phase inversion

Flat sheet membranes were prepared by using the phase inversion method. The PES powder was dissolved in *N*-methyl-pyrrolidone (NMP) solvent and stirred for 2 h. Thereafter HPEI/TiO₂ nanocomposites of a ratio 1:6 were added to the NMP solvent under continuous stirring to attain varying concentrations (0.05%, 0.10%, 0.50% and 1.00%) of PES polymer (**Table 3.1**). The resulting solution was stirred overnight at a temperature of 80°C. The casting solution was further degassed using nitrogen gas to remove air bubbles formed during the reaction. A casting knife set at a height of 200 μm was used to cast the membranes on a glass plate. The casting solution was poured on the edge of the glass plate and the solution was spread on the glass plate

using the casting knife. The glass plate was immediately placed into a non-solvent bath containing deionised water at 4°C for 30 min. The membranes were dried at room temperature.

Table 3.1. Composition of casting solution for membrane preparation

PES (wt%)	HPEI/TiO ₂ (wt%)	NMP (wt%)
16	0.00	84.00
16	0.01	83.99
16	0.10	83.90
16	0.50	83.50
16	1.00	83.00

3.2.6 Characterisation of TiO₂, HPEI/TiO₂ and PES/HPEI/TiO₂ photocatalytic membrane

3.2.6.1 Fourier transform infrared (FTIR) spectroscopy

The prepared PES/HPEI/TiO₂ membranes were analysed using a PerkinElmer Spectrum 100 FTIR spectrometer against an air background. The samples were placed on the ATR and analysed in the range of 400 cm⁻¹ to 4 000 cm⁻¹, averaging 32 scans with a spectral resolution of 4 cm⁻¹.

3.2.6.2 XRD analysis

The XRD measurements were carried out at room temperature using a Philips diffractometer equipped with Cu K α radiation (0.1540 nm) polychromatic beam. The power source was set at 40 kV and 40 mA. Diffraction patterns were recorded at a scan rate of 5°/min over the range of 5° ≤ 2 θ ≤ 90°. Diffraction data were analysed using Philips X'Pert software (data collector program). The average crystal size, d , was determined by Equation (3.1):

$$d = \frac{0.89 \lambda}{\beta \cos \theta} \quad (3.1)$$

for a given phase, θ , at an X-ray wavelength, λ , of 0.1540 nm and FWHM (full width at half maximum, β).

3.2.6.3 Raman spectroscopy analysis

The Raman spectra were obtained with a PerkinElmer RamanMicro 200 Spectrometer (Spectrum software), using an output laser power of 50%. Prior to analysis, the samples were ground to a fine powder, and then placed on a glass plate. The spectra were recorded over a range of 50 to 3 270 cm⁻¹ using an operating spectral resolution of 2.0 cm⁻¹. The spectra were averaged with 20 scans, at an exposure time of 4s.

3.2.6.4 Transmission electron microscopy analysis

Transmission electron microscopy (TEM JEOL, JEM-2010, Japan) at an accelerating voltage of 200 kV was used to examine the particle size and distribution of TiO₂ and HPEI/TiO₂. The TEM specimens were prepared by placing a few drops of TiO₂ and HPEI/TiO₂ (both dispersed in ethanol) solutions on a carbon coated copper grid.

3.2.6.5 Scanning electron microscopy (SEM)

Scanning electron microscopy was used to study the surface morphology and cross-sectional images of the membrane. The membrane samples were mounted on a carbon tape and coated with carbon for surface morphology analysis. For cross-sectional image analysis the membrane samples were frozen in liquid nitrogen, fractured and coated with gold. Scanning electron microscopy (SEM) images were analysed at an accelerating voltage of 2 kV using a TESCAN Vega TC instrument (VEGA 3 TESCAN software), equipped with an X-ray detector for energy-dispersive X-ray (EDX) analysis operated at 5 kV.

3.2.6.6 Atomic force microscopy (AFM)

The surface morphology and the roughness (R_q) of the membranes were measured using a Veeco Dimension 3100 atomic force microscope (AFM) equipped with NanoScope V530r3sr3 software. Prior to analysis, the samples were mounted on a carbon tape and coated with carbon for better images.

3.2.6.7 Contact angle analysis

Contact angle measurements were conducted using the sessile drop method on a Data Physics Optical instrument (SCA 20 software) using water as a probe. This was done to carry out membrane hydrophilicity and hydrophobicity studies. About 10 measurements were conducted per sample at room temperature.

3.2.6.8 Zeta potential studies

The membrane gel solutions were analysed for the surface charge using Malvern Zetasizer Nano Series at neutral pH.

3.2.6.9 Water intake capacity measurements

The extent of water absorption by membranes was determined through sorption experiments. These experiments are helpful to determine the interaction of the membranes with the liquid penetrates (Chan et al., 2015). The samples of 25 cm² membrane pieces were weighed on an analytical balance (± 0.1 mg) and soaked in distilled water for 24 h. Thereafter, the membranes were sandwiched between papers and weighed to give the wet weight (W_w). The membranes were thereafter dried again at 60°C for 24 h in an oven to obtain the dry weight (W_d) of the membranes. The water intake capacity (WIC) was calculated using Equation (3.2):

$$WIC (\%) = \frac{W_w - W_d}{W_w} \times 100\% \quad (3.2)$$

where W_w and W_d are the weights of wet and dry membranes, respectively. All analysis were conducted in replicates.

3.2.6.10 Membrane flux studies

Membrane flux studies were conducted on a Sterlitech corporation CF042 SS316 S/N JC164 207613 instrument. The membranes were then compacted for 12 h at 250 Pa for stabilisation of flux before analysis. Four different pressures were used for the pure water flux studies, namely 50 Pa, 100 Pa, 150 Pa and 200 Pa. The flux was calculated using Equation (3.3):

$$J_w = \frac{V}{t \times A} \quad (3.3)$$

where J_w ($L \cdot m^{-2} \cdot h^{-1}$) is the pure water flux, V is the volume of the permeate (m^3), t is the permeation time (h) and A is the effective membrane surface area ($0.0036 m^2$). All analysis were conducted in replicates.

3.2.7 Photocatalytic degradation of methyl orange using PES/HPEI/TiO₂ membranes

Photocatalytic tests were performed using batch experiments as illustrated in **Figure 3.3**. Photocatalytic degradation of methyl orange dye was conducted by cutting the membranes into small pieces with an area of $25 cm^2$. The membranes were then individually immersed into 500 mL beakers covered with parafilm, containing methyl orange dye (10 mg/L, 250 mL) solutions and equilibrated for 30 minutes in the dark while stirring. The UV source for the excitation of titanium dioxide was set at a wavelength of 365 nm. Aliquots (5 mL) of the samples were collected at 10 min intervals for a maximum period of 2 h using a syringe. The photocatalytic studies were conducted at different pH values (i.e. pH =2, 5, 7, 9 and 12) and these were adjusted using 0.1 M NaOH and 0.1 M HCl. The degradation of MO dye was monitored by measuring the absorbance at $\lambda = 464 nm$, as a function of irradiation time, using a UV-Vis spectrophotometer (Shimadzu UV-2450) and these analysis were done in replicates. The photocatalytic degradation was calculated using Equation (3.4):

$$\% \text{ removal} = \left(1 - \frac{C_t}{C_0}\right) \times 100\% \quad (3.4)$$

where C_0 and C_t are the initial and final concentrations of the dyes at $t = 0$ min and $t = t$ min, respectively.

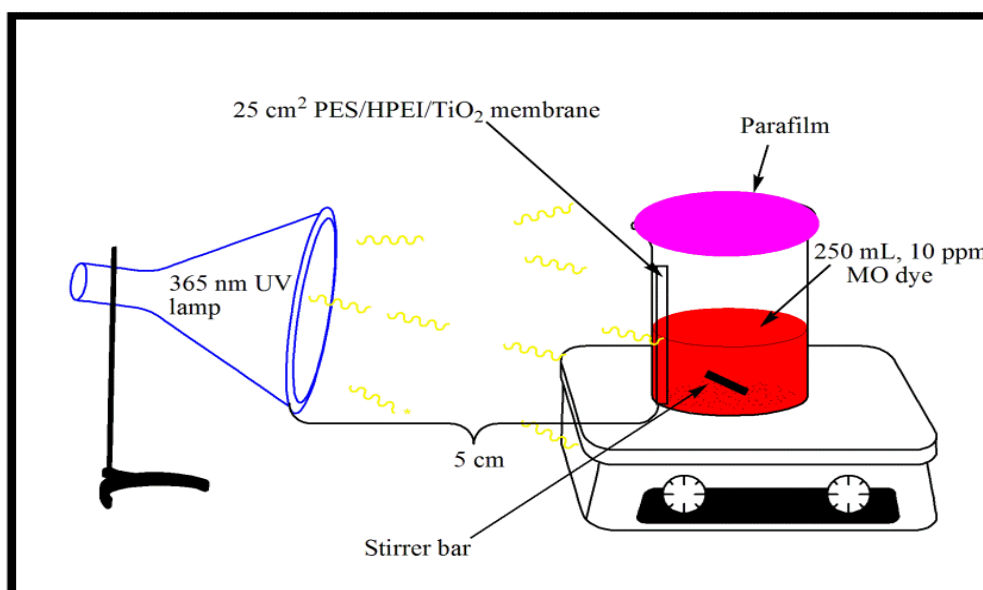


Figure 3.3. UV-radiation experimental set-up for the photodegradation of methyl orange dye

3.2.8 Ion chromatography analysis

The resulting degradation by-products of methyl orange, i.e. SO_4^{2-} ions, were measured using ion chromatography (Dionex ICS-2000 ion chromatography system equipped with a Dionex IonPac AS18 column (250 mm length) and conductivity detector). The eluent solution was 30.00 mM KOH. The pump pressure was set at 11238 kPa, column heater at $30^\circ C$ and the run time was 11 min/sample.

3.2.9 Leaching studies

Leaching studies of the membranes were conducted by using sample aliquots collected at 10 min intervals over a period of 2 h. Quantification of the leached TiO_2 (in the form of Ti^{4+}) from the PES/HPEI/ TiO_2 membranes was carried out using a ICP-OES spectrometer (iCAP 6500 Duo, Thermo Scientific, UK) equipped with a charge injection device (CID) detector. The samples were introduced with a concentric nebuliser and a cyclonic spray chamber. The operating parameters of the instrument are presented in Appendix A (**Table A1**).

3.3 RESULTS AND DISCUSSION

3.3.1 Characterisation of TiO_2 and HPEI/ TiO_2 composite

3.3.1.1 Raman analysis

The Raman spectra (**Figure 3.4**) of pristine TiO_2 and HPEI/ TiO_2 materials show very strong bands at 144 cm^{-1} (E_g), 397 cm^{-1} (B_{1g}), 520 cm^{-1} ($A_{1g} + B_{1g}$) and 639 cm^{-1} (E_g) all assigned to anatase TiO_2 (Shen, 2015). Alemany et al. (2000) conducted a study on the characterisation of titanium dioxide and observed peaks at 638 cm^{-1} (E_g), 516 cm^{-1} ($A_{1g} + B_{1g}$), 397 cm^{-1} (B_{1g}) and 144 cm^{-1} (E_g) for anatase TiO_2 , similar to the peaks obtained in this study (Alemany, 2000). The amorphous nature of HPEI makes it impossible to detect HPEI peaks on Raman spectroscopy. However, the presence of HPEI did not affect the structure of TiO_2 as all the Raman bands were exclusively assigned to anatase. These results concur with XRD observations, confirming that the TiO_2 was indeed the anatase polymorph.

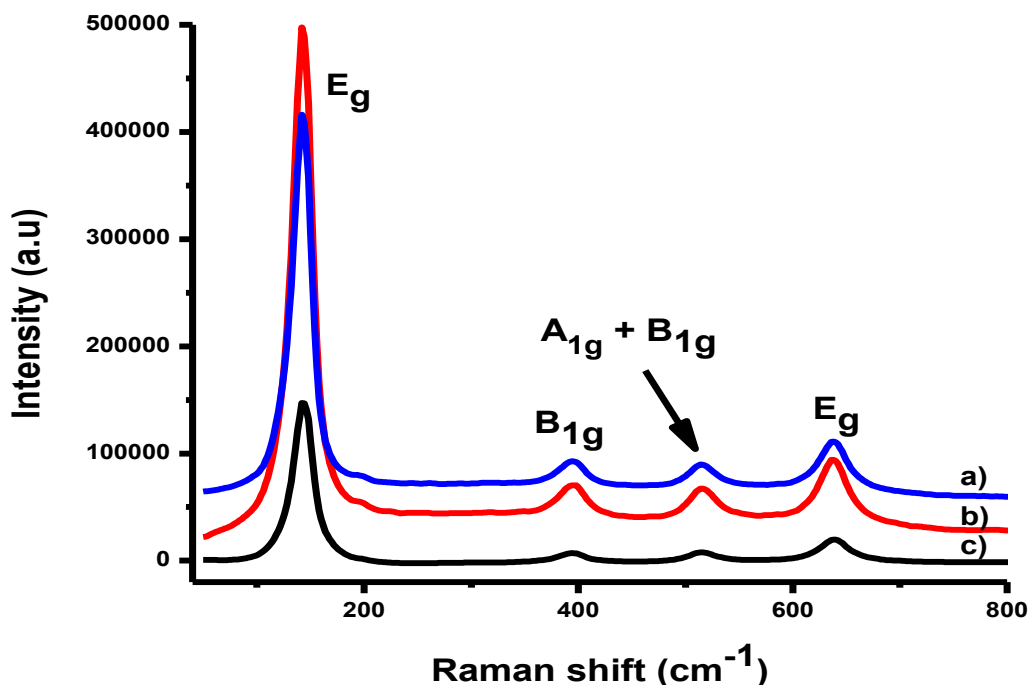


Figure 3.4. Raman spectra of (a) pristine TiO_2 nanoparticles, (b) 1:6 HPEI/ TiO_2 and (c) 1:9 HPEI/ TiO_2 nanocomposites

3.3.1.2 XRD analysis

The XRD patterns of pristine TiO_2 and HPEI/ TiO_2 nanocomposites are shown in **Figure 3.5**. Intense peaks at $2\theta = 25.3^\circ, 37.8^\circ, 48.1^\circ, 53.9^\circ, 55.1^\circ, 62.7^\circ, 68.8^\circ, 70.3^\circ$ and 74.0° , correspond to the crystal planes of TiO_2 anatase (101), (004), (200), (105), (211), (204), (116) and (220), respectively, using JCPDS card: 00-021-1272. All the patterns and planes can be exclusively assigned to anatase, a polymorph of TiO_2 , which is reported to be photocatalytically superior to the other forms of TiO_2 (Leyva-Porras, 2015 and Zhang, 2000). By applying the Scherrer equation for (101) reflection, the average particle sizes were calculated to be: 12.00 nm (pristine TiO_2), 13.30 nm (1:6 HPEI/ TiO_2) and 18.40 nm (1:9 HPEI/ TiO_2), all corresponding to the d-spacing of 0.35 nm. The sharpness of the peaks relates to the crystallinity and the particle size of the nanoparticles. (Cao, 2015). Therefore, the sharp peaks observed on the XRD spectra imply that the prepared materials were crystalline and that the presence of HPEI on TiO_2 nanoparticles did not affect the crystal structure of TiO_2 . Data from the Scherrer equation show an increase in crystallite size upon dispersion of the nanoparticles on the hyperbranched polymer.

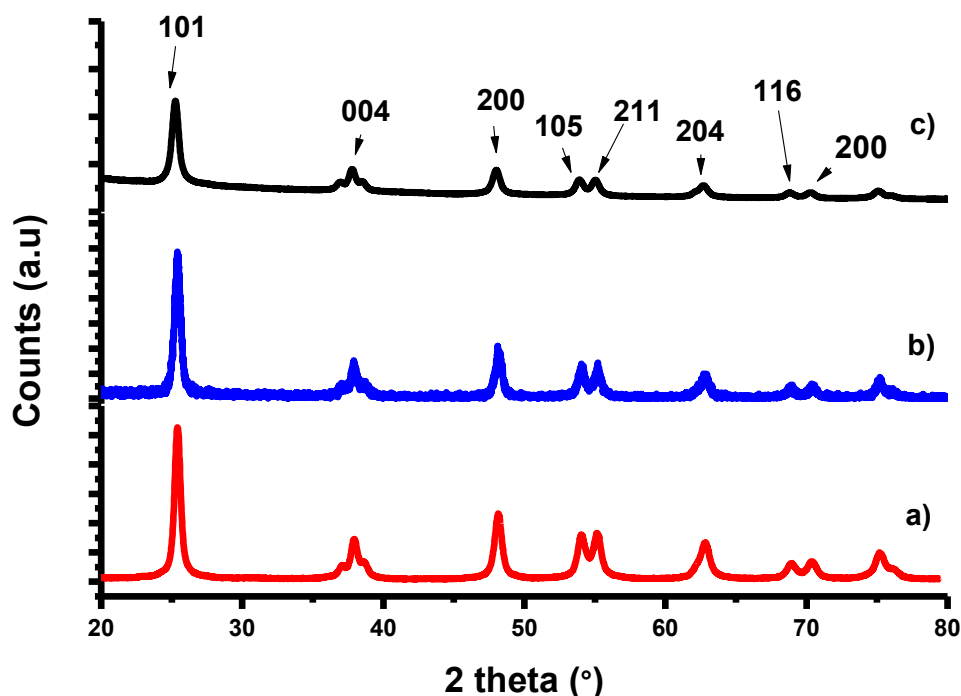
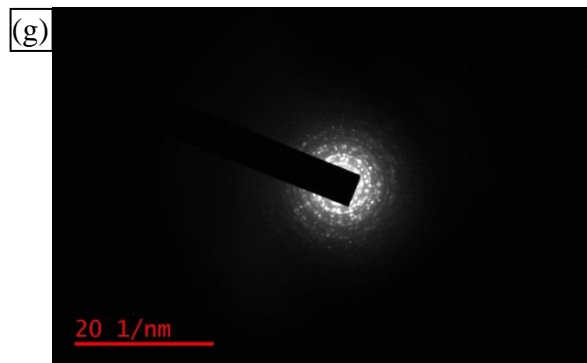
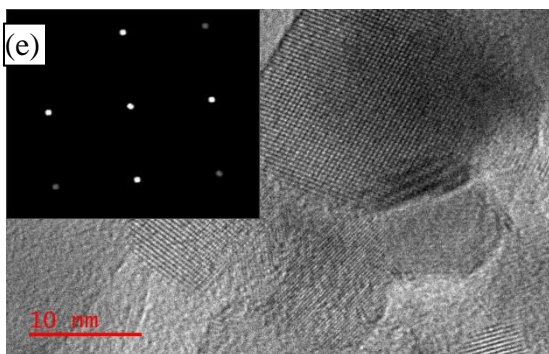
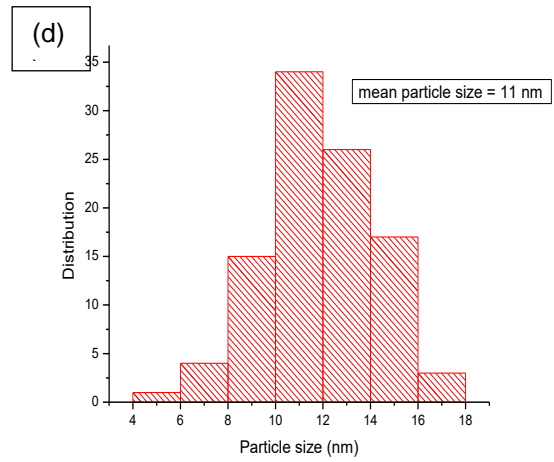
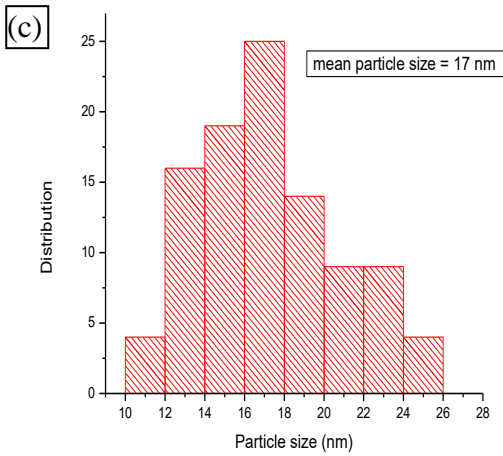
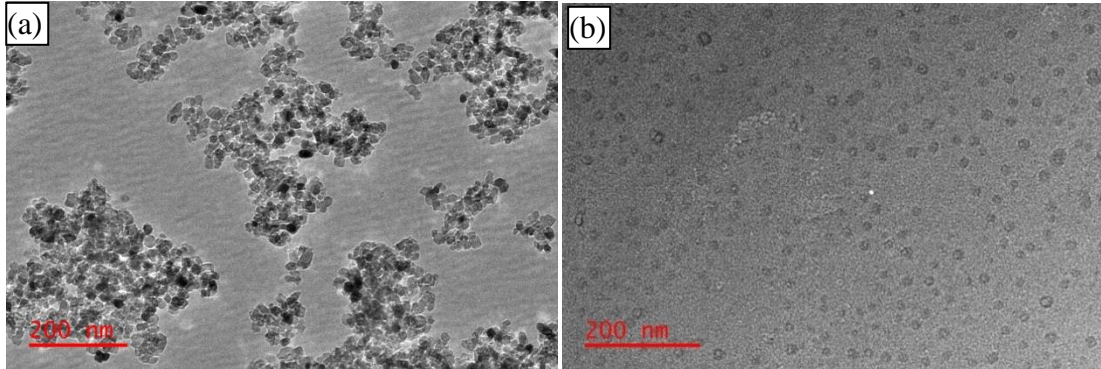


Figure 3.5. (a) XRD patterns of pristine TiO_2 , (b) 1:6 HPEI/ TiO_2 , and (c) 1:9 HPEI/ TiO_2

3.3.1.3 TEM analysis

The TEM images of the synthesised materials and the size distributions measured using the ImageJ program are shown in **Figure 3.6**. The nanoparticles prepared in the absence of HPEI showed aggregates, an indication of their agglomeration (**Figure 3.6(a)**). The average particle size was 17 nm (**Figure 3.6(c)**). The TiO_2 nanoparticles prepared using HPEI as a template were spherical and well dispersed (**Figure 3.6(b)**) with an average particle size of 11 nm (**Figure 3.6(d)**). The size distribution was narrower compared to the particles synthesised without HPEI. The use of HPEI for templated synthesis of TiO_2 nanoparticles therefore has a huge impact on the size and morphology of the resulting nanoparticles. **Figure 3.6(e)** shows the TEM image of crystalline TiO_2 nanoparticles with unidirectional fringes having lattice spacing (0.25 nm). These were analysed

with ImageJ software fast Fourier transform (FFT) to yield the spots corresponding to (001) anatase, as depicted in the insert of **Figure 3.6(e)**. Analysis of the selected area electron diffraction (SAED) patterns can be used to determine the crystallinity of a material (Beltran-Huarac, 2014). The SAED pattern illustrated in **Figure 3.6(f)** further illustrates that crystalline TiO_2 were produced when HPEI was used as a template. **Figure 3.6(g)** illustrates EDS analysis of TiO_2 using HPEI as a template.



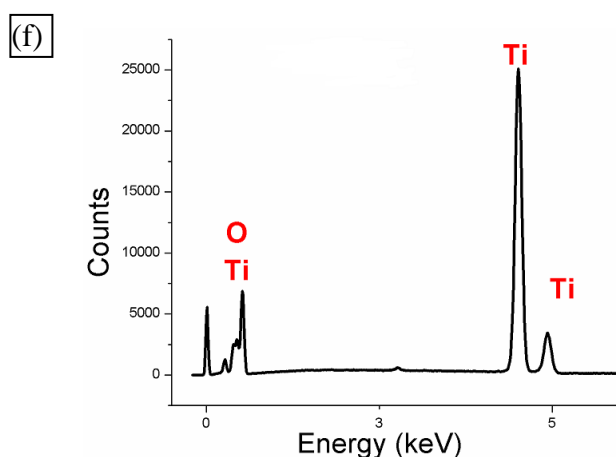


Figure 3.6. (a) TEM micrograph of TiO₂ without HPEI, (b) TEM micrograph of TiO₂ using HPEI as a template, (c) mean particle size in absence of HPEI, (d) mean particle size in the presence of HPEI, (e) TEM micrograph of TiO₂ using HPEI as a template (insert: ImageJ spot analysis), (f) SAED pattern of TiO₂ using HPEI as a template, and (g) EDS analysis of TiO₂ using HPEI as a template

3.3.2 Characterisation of TiO₂ and HPEI/TiO₂ composite

3.3.2.1 Fourier transform infrared (FTIR) spectroscopy

Structural modification of PES with HPEI/TiO₂ was determined using FTIR analysis. The FTIR functional groups and respective absorption peaks detected for the pristine PES are illustrated in **Table 3.2**. Qu et al. (2012) observed peaks at 1 580 cm⁻¹, 1 488 cm⁻¹ and 1 244 cm⁻¹ for C₆H₆ stretch, C-C stretch and aromatic ether stretch, respectively, for pristine PES membranes.

Table 3.2. FTIR transmittance bands of PES membranes

PES spectra	Wave number (cm ⁻¹)
S=O symmetric stretch	1 150, 1 307
C-SO ₂ -C asymmetric stretch	1 322
C-O asymmetric stretch	1 244, 1 260-1 000
C ₆ H ₆ ring stretch	1 587-1 489

However, blending of PES polymer with HPEI/TiO₂ nanocomposites introduced new functionalities on the nanocomposite as shown by the appearance of new peaks on the spectra. The -NH and -OH functional groups appear at 1 671 cm⁻¹ and 3 092 cm⁻¹, respectively, in all the blended membranes (**Figure 3.7**). These peaks are attributed to the presence of amine groups from HPEI and OH groups from Ti-OH vibrations. These observations confirmed the successful blending of HPEI/TiO₂ with PES to form PES/HPEI/TiO₂ membranes.

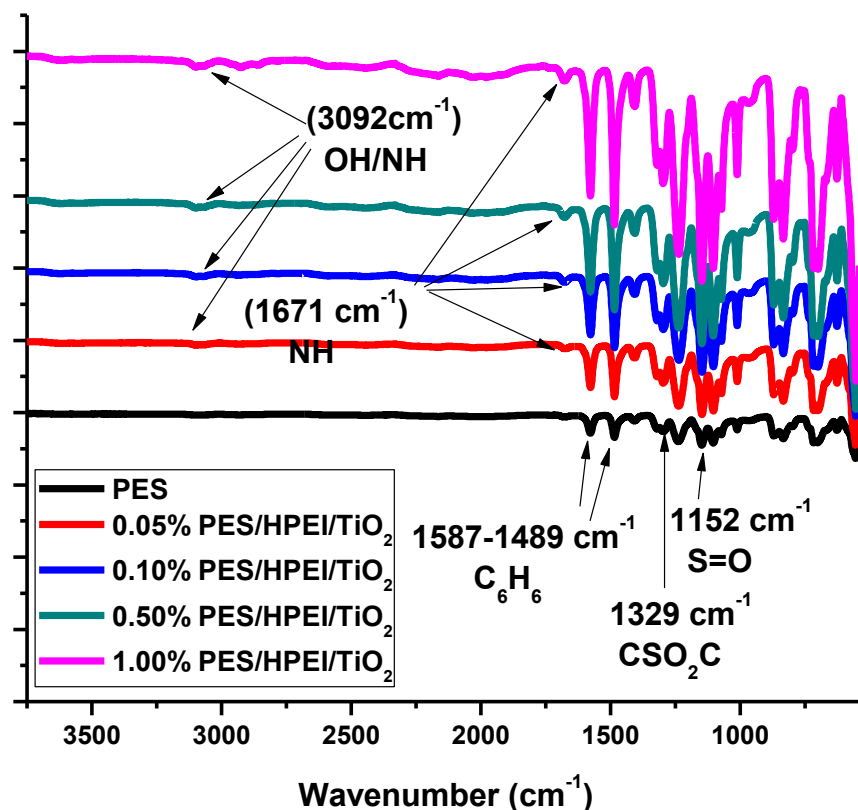
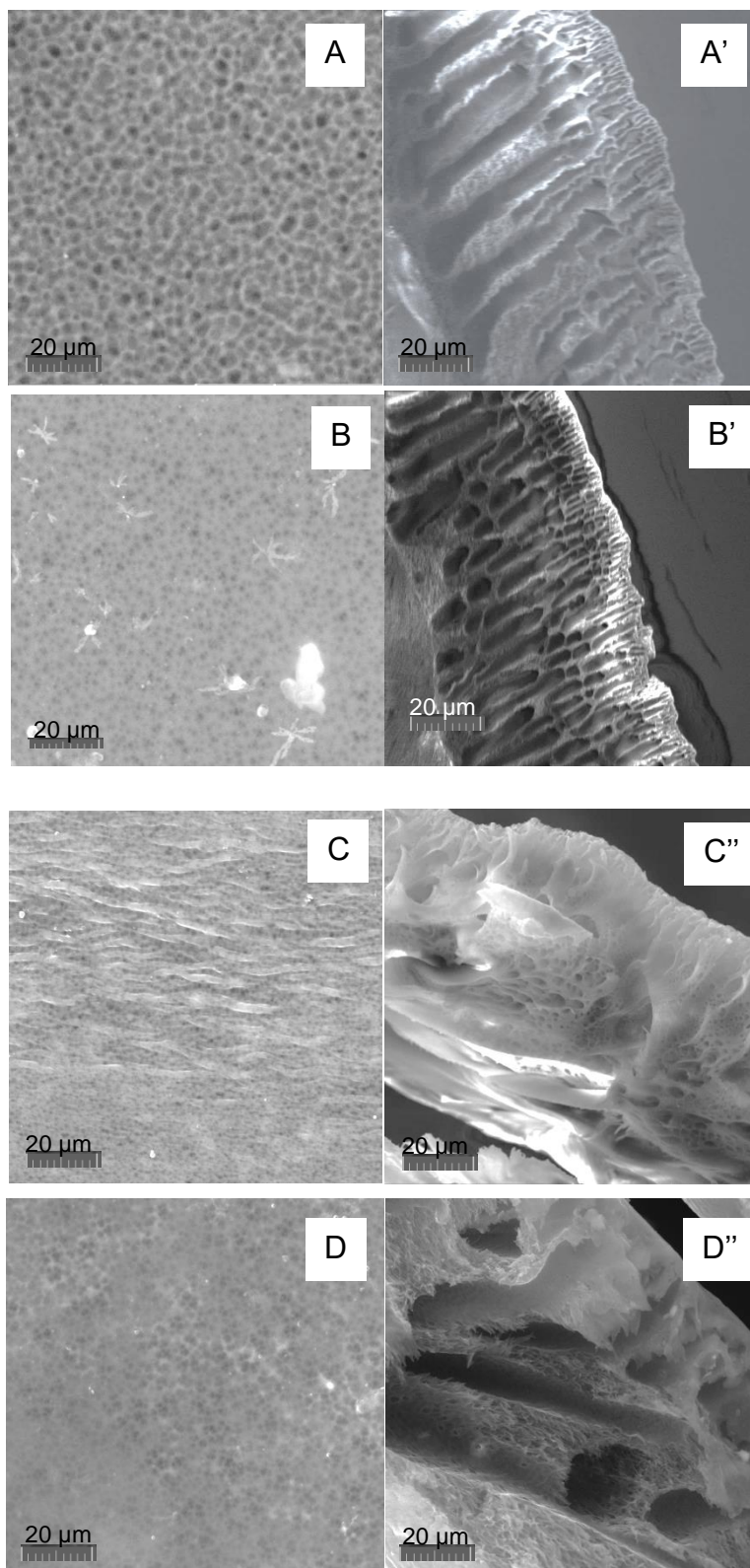


Figure 3.7. FTIR spectra of PES and PES/HPEI/TiO₂ membranes

3.3.2.2 Scanning electron microscopy (SEM) analysis

The morphology of membrane surfaces and cross-sections plays a crucial role in identifying the role of membranes in the mechanism of selectivity and permeability. **Figure 3.8** shows SEM images of the surface and cross-sectional morphologies of PES/HPEI/TiO₂ membranes. The SEM images of surface morphologies of the membranes are shown in **Figures 3.6A-E**. The pristine PES surface exhibited a highly porous surface. Upon addition of HPEI/TiO₂ (0.05 to 1%) the pores were observed to become smaller in size. This might be due to the accumulation of the HPEI/TiO₂ nanocomposite particles on the pores, thus blocking some of the pores and making them smaller. The cross-sectional SEM images of the membranes are shown in **Figure 3.8A'-E'**. The pure PES membrane showed a uniform, finger-like structure with a thin skin layer. However, the blended membranes exhibited a sponge-like structure with a dense skin layer as opposed to the pure PES membrane. Studies show that the presence of TiO₂ nanoparticles in membranes induces the formation of macrovoids. Nucleation/agglomeration of the TiO₂ nanoparticles is said to suppress the formation of macrovoids (Low et al., 2015). However, in this study, the presence of HPEI prevented the agglomeration of the nanoparticles and thus favouring the formation of macrovoids. As the composition of HPEI/TiO₂ was increased, the macrovoids in the sponge-like membrane became more pronounced (**Figure 3.8B'-E'**). This is because during the coagulation process there is instantaneous liquid-liquid de-mixing. The presence of hydrophilic HPEI polymer in the casting solution increases the affinity of the casting solution and precipitant. This therefore results in instantaneous de-mixing accompanied by macrovoid formation. As the HPEI component is increased, the de-mixing becomes stronger and larger macrovoids are formed. In this study poly(vinylidene fluoride) membranes modified with hyperbranched-star-polymers were observed to have large macrovoids with an increase in hyperbranched polymer content.



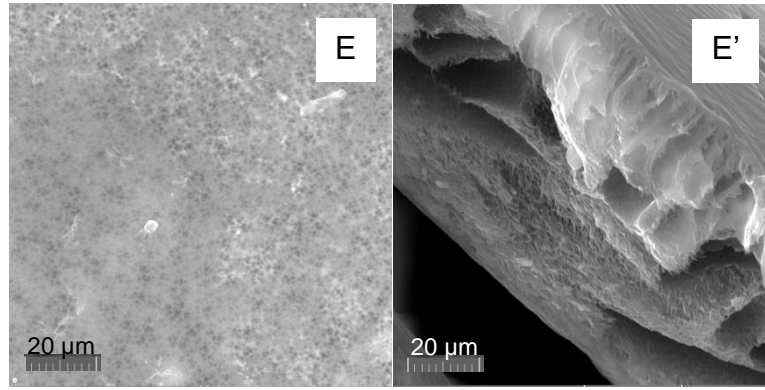
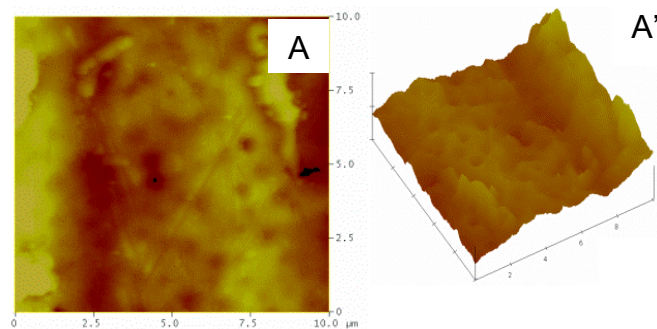


Figure 3.8. SEM images of surface and cross-sectional morphologies of PES (A and A'), 0.05% HPEI/TiO₂ (B and B'), 0.10% HPEI/TiO₂ (C and C'), 0.50% HPEI/TiO₂ (D and D') and 1.00% HPEI/TiO₂ membranes (E and E')

3.3.2.3 Atomic force microscopy

In this study, AFM analyses were carried out in 2-dimensional (2D) and 3-dimensional (3D) mode (**Figure 3.9**) at 4 μm scan to further investigate changes in surface morphology of the PES and PES/HPEI/TiO₂ membranes. The 3D AFM images, illustrated in **Figure 3.9B'-E** possess a ridge-valley like structure. In these images, the brightest area represents the highest points or ridges of the membrane surface and dark regions indicate the valleys for membrane pores. From this, it can be observed that the surface properties of the PES membranes were improved by means of blending it with HPEI/TiO₂. It can be observed that for pure PES membrane, (**Figure 3.9A'**), the surface contains large ridges and as the concentration of HPEI/TiO₂ increased the ridges decreased in size, indicating a reduction in pore size of the blend membranes. The reduction in pore size of the membranes is caused by the migration and accumulation of the HPEI/TiO₂ nanocomposites to the surface of the pores. The roughness as illustrated in **Table 3.3** decreased from 40 nm for pristine PES to 18.9 nm for 1.00% PES/HPEI/TiO₂. According to Lee et al. (2007) a rougher surface reduces permeation resistance because of increased surface area of the membranes thus having an effect on permeability of the membrane. These results are in agreement with water permeability values that were observed for pristine PES and the modified membranes (**Figure 3.7**). Membranes with a high surface roughness showed high water permeability values.



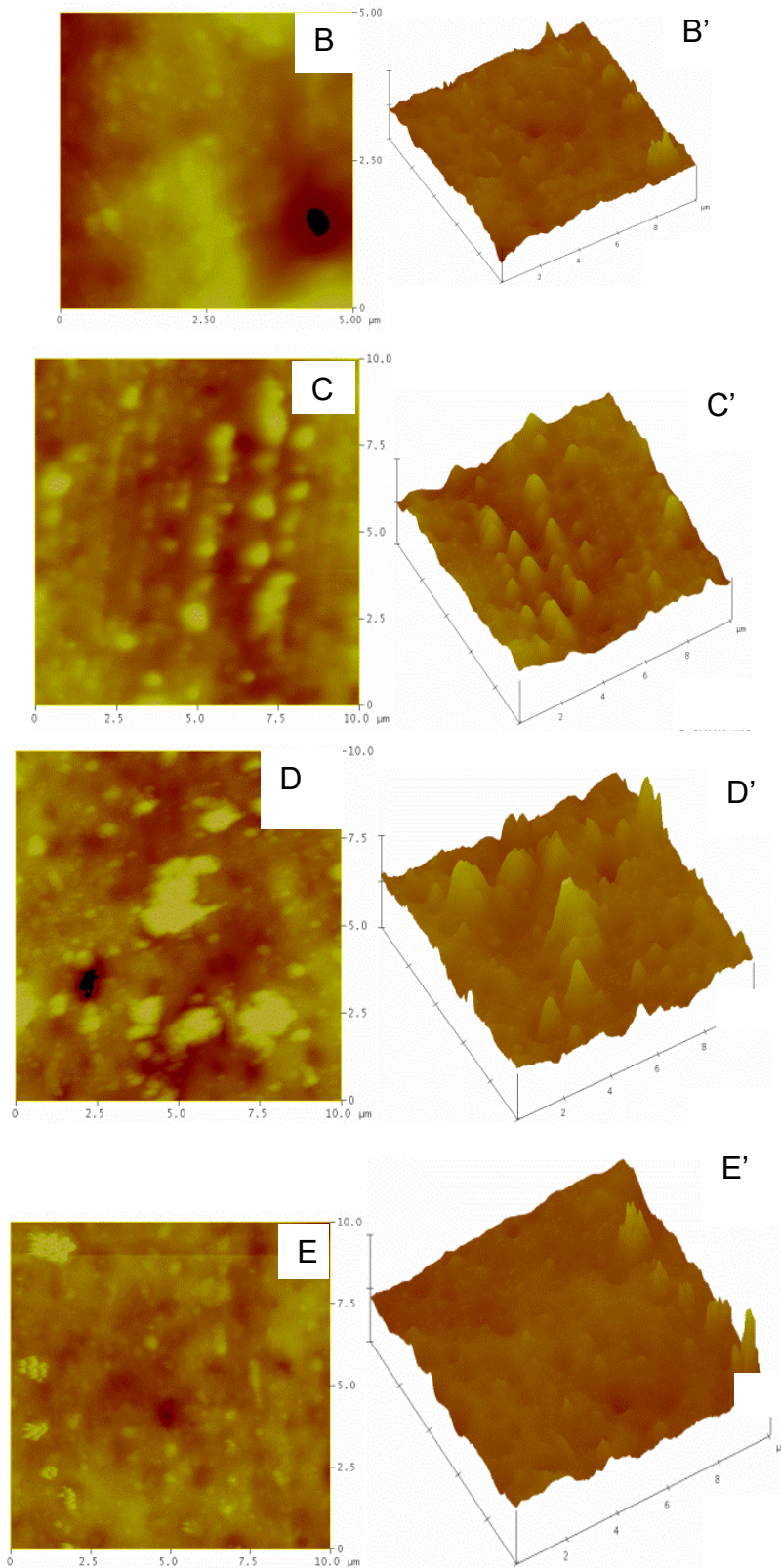


Figure 3.9. AFM images of 0% (A 2D,A` 3D), 0.05% (B 2D,B` 3D), 0.10% (C 2D,C' 3D), 0.50% (D 2D, D' .3D) and 1.00% (E 2D, E' 3D) PES/HPEI/TiO₂ membranes

3.3.2.4 *Water permeation studies*

The contact angle measurements were performed using the sessile drop method to evaluate the hydrophilicity of the membrane. Hydrophilicity is an important characteristic since it affects flux and can also impact on fouling properties of a membrane. As shown in **Table 3.3**, the contact angle decreased with an increase in HPEI/TiO₂ loadings from 0.05% to 0.1%. The presence of hydrophilic TiO₂ and HPEI enhances the hydrophilicity of the membranes, due to the NH₂ groups from HPEI. However, at 1.00% loading of HPEI/TiO₂, the contact angle increased to 66.2°. This increase may be due to the migration of hydrophobic cavities of the HPEI polymer to the surface of the membrane during the drying process (Malinga, 2013). According to Safapour et al. (2015), at high nanomaterial loading there is also possible aggregation of nanoparticles and this would result in high contact angles. However, the contact angle of all the modified membranes was lower than that of the pristine PES membrane.

Table 3.3. Zeta potential, contact angle, water uptake capacity studies, water flux and membrane roughness

PES/HPEI/TiO ₂ membrane (%)	Zeta potential (mV)	Contact angle (°)	Water uptake capacity (%)	Membrane roughness (nm)	Water flux (L/m ² ·h)
0.00	-22.00	76.5	8.32	40.3	90
0.05	-20.46	69.0	26.67	37.5	60
0.10	-18.52	65.3	38.82	28.0	45
0.50	-13.03	62.8	41.86	34.3	30
1.00	-11.42	66.2	35.28	18.9	18

3.3.2.5 *Water permeability analysis*

Figure 3.10 shows the effect of pressure on pure water flux. The flux increased with an increase in operating pressure up to 200 Pa. The pure water permeability was measured at 4 different applied pressures and a good linear relationship between the water permeability and applied pressure was observed ($R^2 \approx 0.98$). The PES membrane showed the highest water permeability of $49.5 \times 10^{-2} \text{ L} \cdot \text{m}^{-2} \cdot \text{h}^{-1} \cdot \text{Pa}^{-1}$ as compared to 0.05% ($30 \times 10^{-2} \text{ L} \cdot \text{m}^{-2} \cdot \text{h}^{-1} \cdot \text{Pa}^{-1}$), 0.10% ($22.5 \times 10^{-2} \text{ L} \cdot \text{m}^{-2} \cdot \text{h}^{-1} \cdot \text{Pa}^{-1}$), 0.50% ($15 \times 10^{-2} \text{ L} \cdot \text{m}^{-2} \cdot \text{h}^{-1} \cdot \text{Pa}^{-1}$), and 1.00% PES/HPEI/TiO₂ ($9 \times 10^{-2} \text{ L} \cdot \text{m}^{-2} \cdot \text{h}^{-1} \cdot \text{Pa}^{-1}$). The low water permeability of the modified membranes could be due to blending of PES membrane with HPEI/TiO₂ nanocomposite. The nanocomposites often block the surface pores of the membranes. This creates a dense membrane surface layer, thus resulting in high resistance of water passing through the membrane reducing the permeability.

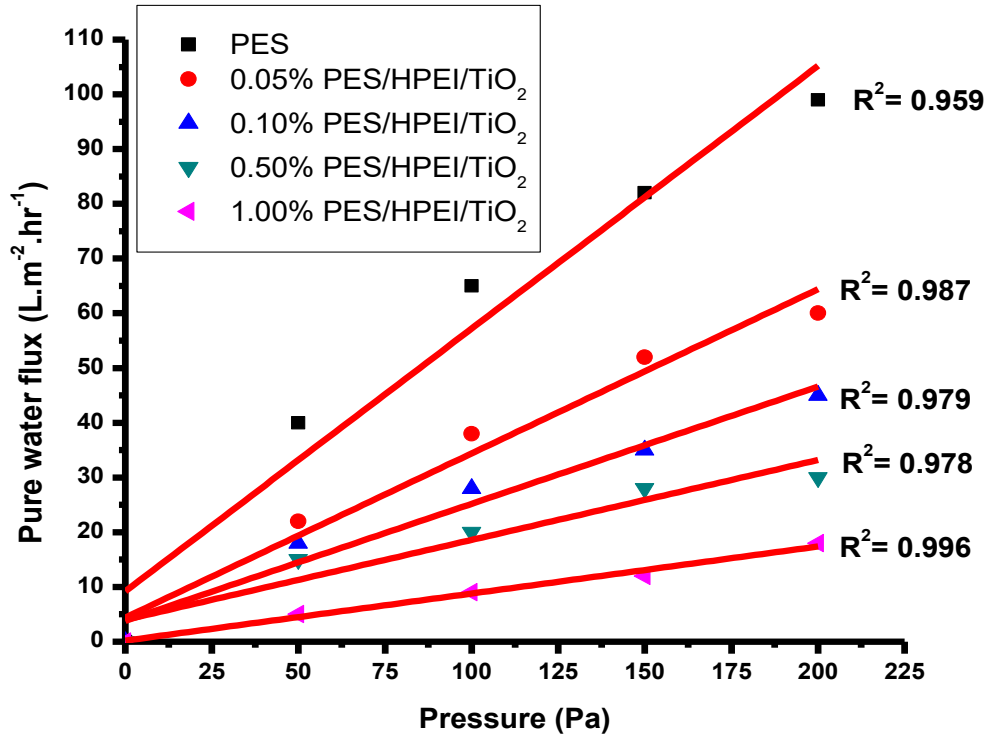


Figure 3.10. The relationship between pure water flux and pressure

3.3.3 Photocatalytic activity of PES/HPEI/TiO₂ membranes

3.3.3.1 Photodegradation of methyl orange

The PES/HPEI/TiO₂ membranes at different HPEI/TiO₂ percentage loadings (0.00, 0.05, 0.10, 0.50 and 1.00% HPEI/TiO₂) were evaluated for their ability to photodegrade methyl orange dye (10 mg/L) at different pH conditions under ultraviolet light radiation (**Figure 3.11**). It was observed that the neat PES membrane exhibited very low degradation rates (4.26, 4.04, 3.13, 3.09 and 3.03% at pH 2, 5, 7, 9 and 12, respectively), since the polymer is not photocatalytically active. Photocatalytic activity was induced in the membranes upon the introduction of HPEI/TiO₂ (**Figure 3.11** and **Table 3.4**).

Table 3.4. Photodegradation results

Membrane	% removal				
	pH 2	pH 5	pH 7	pH 9	pH 12
PES	4.26	4.04	3.13	3.09	3.03
0.05%	24.50	18.30	18.00	10.20	9.18
0.10%	55.00	42.90	39.80	38.80	35.70
0.50%	70.30	67.30	61.20	59.20	57.10
1.00%	59.20	54.10	50.00	46.90	43.90

However, the percentage removal of MO increased upon introduction of HPEI/TiO₂ nanocomposites on the PES membranes, which then reached the highest removal of 70.3% at 0.50% HPEI/TiO₂ loading. It was observed that this membrane (0.50% PES/HPEI/TiO₂) was able to achieve removal of MO in a wide pH range, i.e. from pH 2 (70.3%) to 12 (57.10%). Faster degradation rates were observed in the first 5 min of the reactions for all modified membranes (**Figure 3.11**). The rate then decreased with time up to 80 min. This might be an indication that the reactive sites on the membranes become saturated or blocked with time and thus resulting in a decrease in the photocatalytic activity. Lin et al. (2012) also observed that the degradation rate of methyl orange by PANI/TiO₂ membrane was fast at the beginning of the reaction. However, the rate decreased towards the end of the reaction due to the formation of intermediate compounds. These intermediate compounds tend to block the pores of the membranes thus limiting the adsorption of the pollutants.

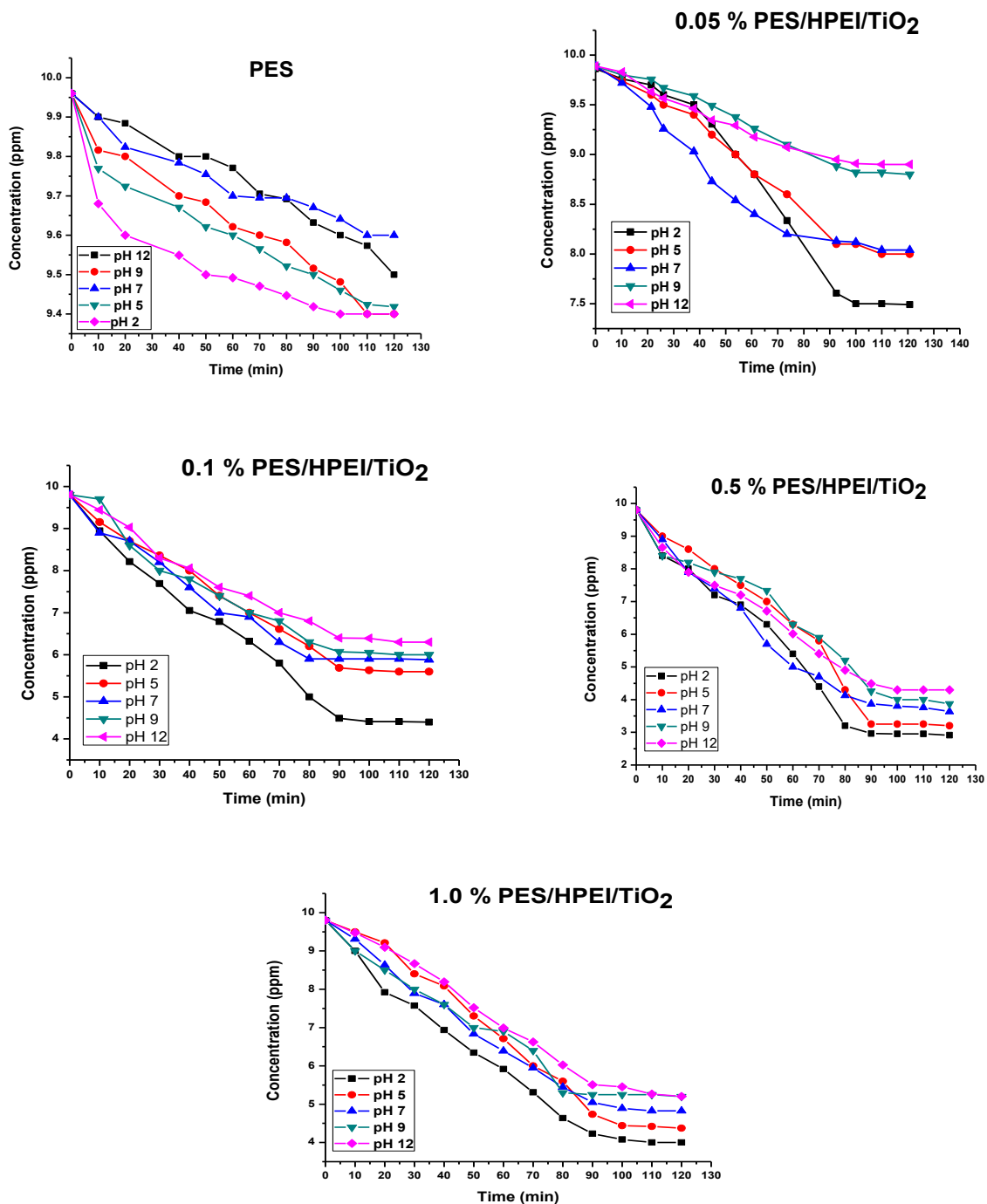


Figure 3.11. Photodegradation of methyl orange by PES/HPEI/TiO₂ membranes using UV light

Data recorded in previous studies where membranes have been used in the removal of dyes are given in **Table 3.5**. In these studies, it can be observed that a high degradation percentage was obtained over a longer period of time, i.e. >4 hours.

Table 3.5. Previous work on TiO₂ photocatalytic membranes for dye removal

Membrane	Dye	Degradation %	Time (h)	Reference
PES/TiO ₂	Methylene Blue	70%	4	Fischer et al., 2014
PSf-S-TiO ₂	Methylene Blue	90.4%	6	Pereira et al., 2015
PVDF/TiO ₂	Reactive Black 5	97.9%	5	Cruz et al., 2013

3.3.3.2 Kinetic studies for the degradation of methyl orange

The kinetics of methyl orange degradation at pH 2 for all the membrane samples was modelled using the pseudo-first-order reaction (Equation (3.4)) and the plot is shown in **Figure 3.10**.

$$-\ln \frac{C}{C_0} = kt \quad (3.4)$$

where k is the reaction constant, C_0 and C are the initial and final concentrations of methyl orange, respectively.

The rate constants for the degradation of methyl orange were found to be 0.011 min⁻¹, 0.0088 min⁻¹, 0.00513 min⁻¹, 0.00283 min⁻¹, and 0.000319 for 0.50% PES/HPEI/TiO₂, 1.0% PES/HPEI/TiO₂, 0.1% PES/HPEI/TiO₂, 0.05% PES/HPEI/TiO₂ and pristine PES membrane, respectively.

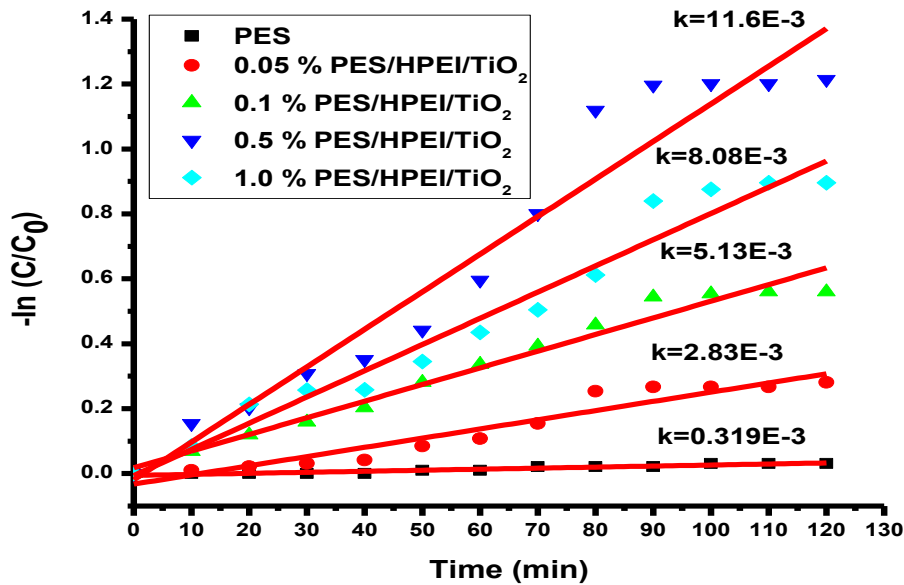


Figure 3.12. First-order kinetic plot of methyl orange initiated by UV light irradiation

3.3.3.3 Zeta potential analysis and mode of degradation

Table 3.3 illustrates the zeta potential values of the pristine PES polymers and modified polymer solution. It can be observed that the PES polymer is negatively charged. Upon blending the polymer with the positively charged HPEI/TiO₂ nanocomposites the charge was found to decrease. Methyl orange (MO) is an anionic dye and is therefore negatively charged under alkaline conditions, while under acidic pH mediums, the dye surface is positively charged (Figure 3.13). The observed negative charges of the membrane (**Table 3.3**) imply that the membranes have a greater affinity for positively charged species. Thus, based on this observation, methyl orange degradation was the lowest at pH 12 as compared to other pH mediums. It can therefore be assumed that there was an increase in repulsive forces between the negatively charged dye and the negatively charged membrane surface.

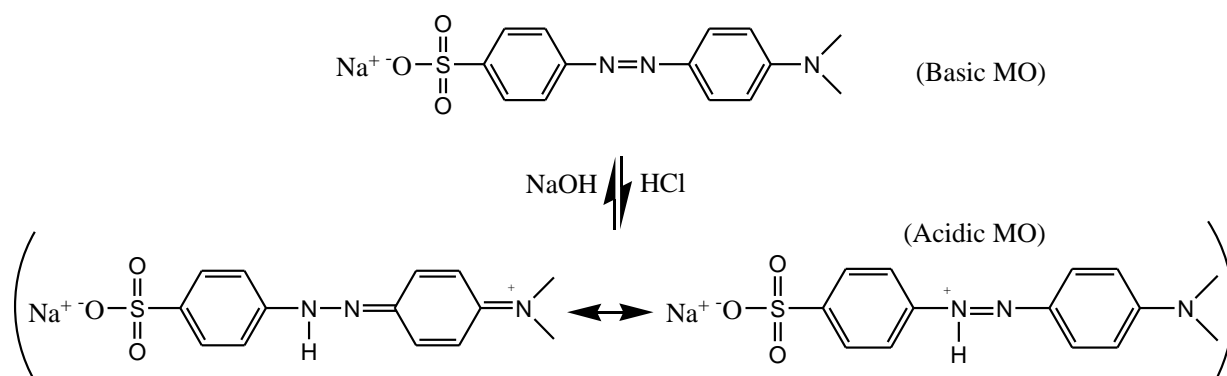


Figure 3.13. Acidic and basic forms of methyl orange

As shown in **Figure 3.14**, the attachment of the positively charged methyl orange dye on the surface of the PES/HPEI/TiO₂ membrane induced electrophilic attacks from the valence band holes in the TiO₂ photocatalyst. Single-electron transfer (SET) may also occur. The positively charged dye was then attacked by the hydroxyl radicals ($\cdot\text{OH}$). The nucleophilic attack induced degradation of the dye in the presence of UV light irradiation and the by-products were then monitored using ion chromatography.

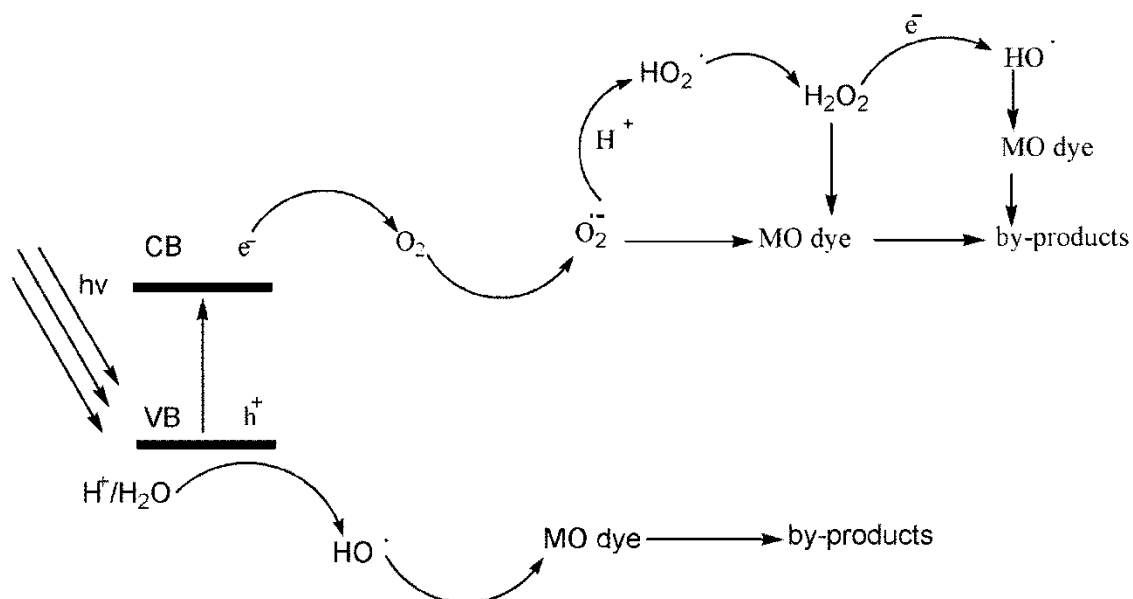


Figure 3.14. Mechanism for the photodegradation of methyl orange dye in water

3.3.3.4 Analysis of photodegradation by-products

The degradation of MO was confirmed by the liberation of SO_4^{2-} ions using ion chromatography (IC). The sulphite ion can be oxidised to sulphate, a more stable (+6) oxidation state of sulphur and hence it was more reasonable to measure than the sulphite ion. Previous studies have revealed that sulphates adsorb irreversibly on TiO_2 surfaces, and this might have accounted for the low amounts of sulphate ions detected (Liao, 2013; Sonawe, 2004; Dlamini, 2011). However, Dlamini et al. (2011) reported that the irreversible adsorption of sulphate on titania does not affect the photoactivity of metal oxides.

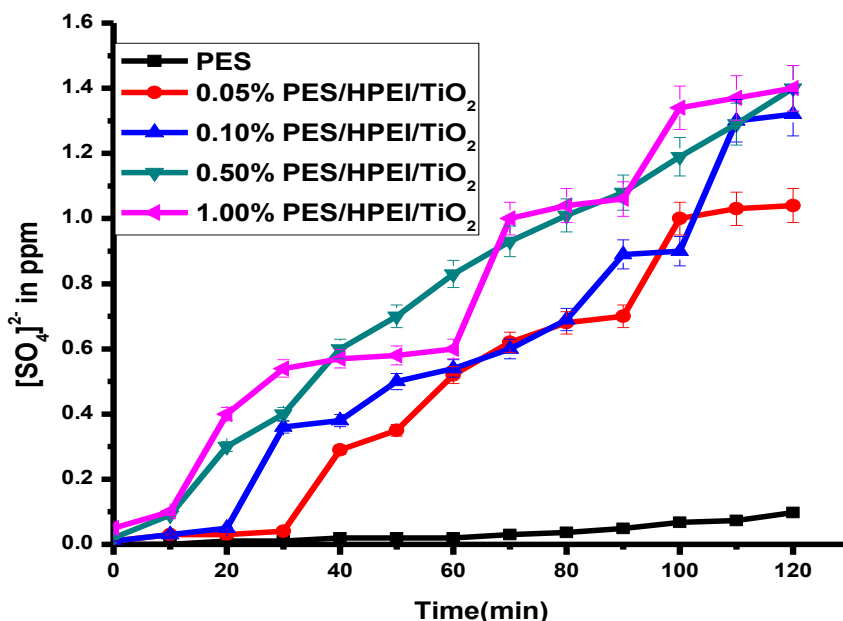


Figure 3.15. Generation of sulphate ions from the degradation of methyl orange using PES/HPEI/TiO₂ photocatalytic membranes

3.3.3.5 Leaching studies

The extent of TiO_2 leaching from the PES/HPEI/ TiO_2 membrane was assessed using ICP-OES. In this study it was found that the maximum concentration of leached TiO_2 nanoparticles was 0.047 mg/L. However, the National Institute for Occupational Safety and Health (NIOSH) recommends that fine TiO_2 particle exposure should be set at 2.4 mg/L whilst ultrafine particle exposure should be 0.3 mg/L (NIOSH, 2011). However, the concentrations obtained in this study were below the reported limits.

Table 3.6. TiO₂ leaching from the PES/HPEI/TiO₂ membranes

Time (min)	Ti ⁴⁺ concentration inmg/L	
	0.05% PES/HPEI/TiO ₂	0.50%PES/HPEI/TiO ₂
0	0.000	0.043
10	0.000	0.043
20	0.001	0.044
30	0.003	0.044
40	0.003	0.045
50	0.003	0.045
60	0.040	0.046
70	0.040	0.046
80	0.042	0.047
90	0.042	0.047
100	0.042	0.047
110	0.042	0.047
120	0.042	0.047

3.4 SUMMARY

TiO₂ nanoparticles were successfully prepared using hyperbranched polyethyleneimine as the template in a modified sol-gel method. Spectroscopy analysis (RS, FTIR, XRD, TEM and TGA) revealed that the TiO₂ nanoparticles were predominantly in the anatase phase. Moreover, HPEI played a major role in the production of small crystalline and well dispersed TiO₂ nanoparticles. The incorporation of the bare TiO₂ into HPEI further maintained their dispersion due to the strong coordination/interaction of TiO₂ via the amine groups of the HPEI polymer. The photodegradation of methyl orange (MO) was confirmed by means of UV-Vis using various loadings of PES/HPEI/TiO₂ membranes. The PES/HPEI/TiO₂ (0.5%) membrane exhibited the highest removal (57.1% to 70.3%) for all tested pH values (2-12). Thus, these membranes could be applicable in the photocatalytic degradation of dyes in highly acidic, neutral and alkaline wastewater. The PES/HPEI/TiO₂ membranes were found to be hydrophilic and had improved water intake capacity as compared to pristine PES membrane. Leaching studies revealed that the leaching of TiO₂ into the water samples was very low when compared to the exposure limit of TiO₂ (2.4 mg/L). These results suggest that strong metal/HPEI interactions exist.

CHAPTER 4: CATALYTIC REMOVAL OF BISPHENOL A FROM WATER USING HPEI/PES NANOFIBROUS MEMBRANES

4.1 INTRODUCTION

The pristine PES membrane, electrospun HPEI/PES membrane and the laccase-modified HPEI/PES nanofibrous membranes were used for the removal of BPA from a synthetic solution using a dead-end filtration cell. Water permeation properties of the laccase-immobilised dendritic nanofibrous membrane were also investigated. Membrane separation performance tests, biodegradation efficiency and recyclability of the prepared membranes are discussed in this section. The BPA degradation by-products were monitored using liquid chromatography-mass spectrometry (LC-MS). The stability of immobilised laccase was also monitored by the enzyme activity assay using syringaldazine as a substrate. The effect of pH and temperature on the relative activity of the free and immobilised enzymes was evaluated in this section. Storage stability of the free and immobilised enzymes was also assessed over 28 days. The aim of this work was thus to synthesise the HPEI/PES nanofibrous membranes and then to covalently bond them to laccase enzymes. Further work was done on the application of the laccase-modified membrane for the removal of Bisphenol A from water.

4.2 EXPERIMENTAL

4.2.1 Materials

Polyethersulfone (PES) (MW = 3 000) was purchased from India, hyperbranched polyethyleneimine HPEI (MW = 25 000) was purchased from India, and PES commercial membrane supports (MW = 35 000, pore size = 0.1 μm) were purchased from MICRODYN-NADIR. Dimethylformamide (DMF) and *n*-methyl-2-pyrrolidone (NMP) were purchased from Sigma Aldrich and were used as received.

4.2.2 Synthesis of HPEI/PES nanofibrous membranes

The HPEI/PES nanofibrous membranes were synthesised using a modified method by Diallo and co-authors (2012) as illustrated in **Figure 4.1**. Varying concentrations and ratios of HPEI and PES polymer solutions (22%:2%, 21%:2%, 20%:2%, 19%:2% (m/v)) were dissolved in various solvents such as dimethylformamide (DMF), *N*-methyl-2-pyrrolidone (NMP) and a binary solution of DMF and NMP (1:1 w/w). The resulting solution was stirred for 24 h to obtain a homogeneous solution. The prepared solution was then electrospun at a constant voltage of 16 kV, flow rate of 0.7 mL/h and spinneret-collector distance of 7.5 cm. The electrospinning procedure was conducted on a commercial membrane (as a collector) at a relative humidity of 20% and temperature of 26°C. The synthesised HPEI/PES nanofibrous membranes were then heated at 70°C for 12 h to encourage radical reaction between the sulfone groups on the PES commercial membrane and those in the electrospun nanofibres. The effects of polymer concentration and solvent properties on the fibre morphology were then monitored using SEM coupled with EDS.

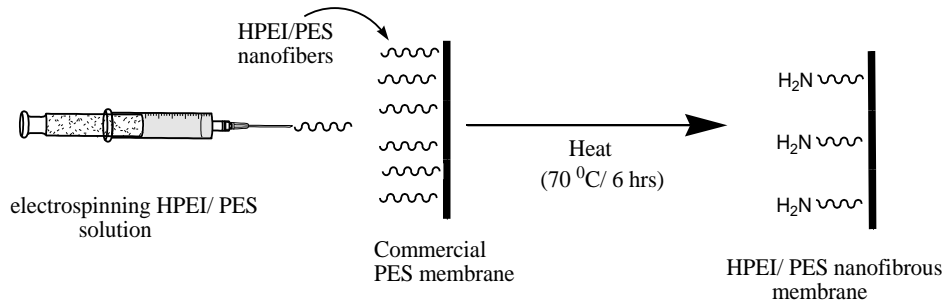


Figure 4.1. Synthesis of HPEI/PES nanofibrous membrane using the electrospinning technique

4.2.3 Determination of laccase immobilisation efficiency

The laccase content in the supernatant laccase solutions and washings was determined by the Bradford method, using UV-Vis spectroscopy (Xu et al., 2013). Bovine serum albumin (BSA), complexed with Coomassie brilliant blue dye G-250, was used to construct a calibration curve using a maximum wavelength (λ_{\max}) of 585 nm. The amount of immobilised laccase, M_i , was determined using Equation (4.1):

$$M_i (g) = M_0 - M_f - M_w \quad (4.1)$$

where M_0 , M_f and M_w is the amount of laccase initially added, the amount of laccase in the supernatant liquid, and the amount of laccase in the washing buffer, respectively.

The immobilisation efficiency (E) was calculated using Equation (4.2):

$$E (\%) = \frac{M_i}{M_0} \times 100 \quad (4.2)$$

The laccase loading on the electrospun membranes (L) was determined using Equation (4.3):

$$L (mg g^{-1}) = \frac{M_i}{M} \quad (4.3)$$

where M is the amount of HPEI/PES membranes.

4.2.4 Laccase activity assay

In this study, syringaldazine was used as a substrate to monitor the activity of immobilised laccase. Three pieces of laccase-modified membranes (1 cm x 1 cm) were cut, weighed and used for laccase activity studies. The absorbance of the reaction mixture containing 0.4 mM syringaldazine in 50 mM potassium phosphate buffer solution was measured using a UV-Vis spectrometer at λ_{\max} of 530 nm. The aliquots were withdrawn from the reaction solution at reaction interval of 5 min and the absorbance was measured. One activity unit was defined as the amount of enzyme that oxidised 1 μ mol of syringaldazine per min. The activity of the immobilised laccase was calculated using Equation (4.4) (Chen et al., 2015):

$$\text{Activity of immobilized laccase}(Ug^{-1}) = \frac{kV_{\text{Total}} \times 10^6}{M_{\text{Lac}} \times \epsilon} \quad (4.4)$$

where k is the slope of the plot of absorbance changes versus reaction time, V_{Total} is the total volume of the reaction medium (0.02 L), M_{Lac} is the mass of the laccase modified membrane (g), and ϵ is the extension coefficient of syringaldazine ($65 \text{ mM}^{-1}\text{cm}^{-1}$).

$$\text{specific activity}(Umg^{-1} \text{ protein}) = \frac{\text{Activity immobilized laccase}(Ug^{-1})}{\text{Protein loading}(mgg^{-1})} \quad (4.5)$$

$$\text{Relative activity}(Umg^{-1} \text{ protein}) = \frac{\text{Specific activity of laccase}}{\text{Initial activity of laccase in standard conditions}} \times 100\%$$

The initial activity of laccase was obtained at pH 6.5, at 30°C, in a 3 mL reaction volume using syringaldazine as a substrate.

4.2.5 Effect of pH on activity of free and immobilised laccase

The effect of pH on the activity of free and immobilised laccase was monitored over a pH range of 3 to 8 using phosphate buffer solutions. Three pieces of membrane (1 cm x 1 cm) were weighed, rinsed thoroughly with deionised water and immersed in the syringaldazine reaction mixture. Aliquots were withdrawn from the reaction mixture after intervals of 5 min for 15 min and filtered before measuring the absorbance at 530 nm using UV-Vis spectroscopy. A plot of the absorbance values at λ_{max} of 530 nm against reaction time was drawn and its gradient was determined in order to obtain k . The relative activity was expressed as a percentage of the obtained activity over the maximum activity of laccase at standard conditions (pH 6.5 and 30°C using syringaldazine as substrate).

4.2.6 Effect of temperature on activity of free and immobilised laccase

The same method as described in **Section 4.2.3** was also used to monitor the effect of temperature on the activity of free and immobilised laccase. The reaction mixture was set at the optimum pH obtained in the previous section after evaluation of the pH effect. Relative activity of the free and immobilised laccase was monitored over a temperature range of 20°C to 80°C using a hot water bath. The experiment was done in triplicates using a fresh laccase-immobilised membrane each time.

4.2.7 Storage stability of free and immobilised laccase

The prepared membranes were stored at 4°C in a phosphate buffer solution (pH 6.5) for 28 days. The relative activity of the stored membranes was also monitored as outlined in **Section 4.2.3**. The experiment was conducted using the reaction mixture at optimum pH and temperature obtained in the previous experiments (**Sections 4.2.3 and 4.2.4**). A fresh membrane was used in each experimental trial.

4.2.8 Tests to evaluate separation performance of membranes

To evaluate the efficiency of the membranes in terms of BPA rejection, the BPA feed (100 µg/L) was passed through the membranes at a constant pressure of 600 kPa. The permeate flux and rejection were monitored every 20 min over 240 min. The permeate was analysed using UV-Vis spectroscopy at λ_{\max} of 276 nm. The percentage rejection of BPA was calculated using Equation (4.6):

$$R (\%) = 1 - \left(\frac{C_p}{C_f} \right) \times 100 \quad (4.6)$$

where C_p and C_f are the concentrations of BPA (µg/L) in the permeate and feed, respectively.

The percentage rejection of BPA by deactivated laccase-modified nanofibrous membrane was also conducted. The laccase-modified membranes were deactivated by boiling the membranes in deionised water.

4.2.9 Recyclability studies of the membranes

The rejection capabilities of the PES membranes, electrospun HPEI/PES nanofibrous membranes, and the laccase-modified membranes were assessed over 4 cycles. After each cycle the membranes were rinsed thoroughly with deionised water to remove the trapped BPA (Zhang et al., 2006). A fresh solution of BPA (100 µg/L) was used in each filtration cycle under a constant pressure of 600 kPa at 25°C. The BPA concentration after each cycle was determined using UV-Vis spectroscopy.

4.2.10 Leaching studies

The amount of laccase enzymes that leached out over four filtration cycles (over 240 min) was determined using the Bradford method. The calibration curve was constructed using bovine serum albumin and Coomassie brilliant blue dye at λ_{\max} of 585 nm using UV-Vis spectroscopy.

4.2.11 Biodegradation studies

The permeate solutions obtained as described in **Section 4.2.1** were also used to determine the present by-products formed during the biodegradation of BPA by the immobilised laccase in the dead-end filtration set up. The by-products formed were detected using LC-MS spectrometry. A Waters Synapt G2-Si quadrupole time-of-flight mass spectrometer was used for LC-MS analysis; it provides high resolution UPLC-MS/MS performance and was fitted with photodiode array detector. Separation was achieved on a Waters BEH C18, 2.1x100 mm column with 1.7 µm particles. A gradient was applied using 0.1% formic acid (solvent A) and acetonitrile containing 0.1% formic acid (solvent B). The gradient started at 100% solvent A for 1 min and changed to 28% solvent B over 22 min in a linear way. It then went to 40% solvent B over 50 s and a wash step of 1.5 min at 100% solvent B, followed by re-equilibration to initial conditions for 4 min. The flow rate was 0.3 mL/min and the column were kept at 55°C. The injection volume was 2 µL. Data were acquired in MS^E mode which consisted of a low collision energy scan (6 V) from m/z 150 to 1 500 and a high collision energy scan from m/z 40 to 1 500. The high collision energy scan was done using a collision energy ramp of 30-60 V. The photodiode array detector was set to scan from 220-600 nm. The mass spectrometer was optimised for best sensitivity; a cone voltage of 15 V, desolvation gas was nitrogen at 650 L/h and desolvation temperature was 275°C. The instrument was operated with an electrospray ionisation probe in the negative mode. Sodium formate was used for calibration and leucine encephalin was infused in the background as lock mass for accurate mass determinations.

4.3 RESULTS AND DISCUSSION

4.3.1 Immobilisation efficiency

The immobilisation efficiency for Lac_{0.5}-HPEI/PES, Lac_{1.0}-HPEI/PES, Lac_{2.0}-HPEI/PES and Lac_{4.0}-HPEI/PES was 87.2%, 93.3%, 98.4% and 97.6%, respectively (**Figure 4.2**). The high loading efficiencies can be attributed to the abundant terminal amine groups present in the HPEI polymer. These amine groups are capable of covalently binding a large number of laccase enzyme molecules. These results are comparable to studies conducted by Khoobi et al. (2015) where lipase enzymes were covalently attached onto polyethyleneimine modified super-paramagnetic Fe₃O₄ nanoparticles through a glutaraldehyde cross-linker. In this study, enzyme immobilisation of up to 84 ± 2.5% was achieved. The improved enzyme loading can be ascribed to the highly branched cationic polyethyleneimine polymer with high density of NH₂ functional groups acting as anchoring sites for enzymes (Woo et al., 2015). Moreover, at pH 6.5, laccase enzymes are negatively charged and polyethyleneimine is positively charged. Thus, electrostatic interactions occur, further resulting in increased enzyme-polymer interactions which result in enhanced loading efficiency (Khoobi et al., 2015).

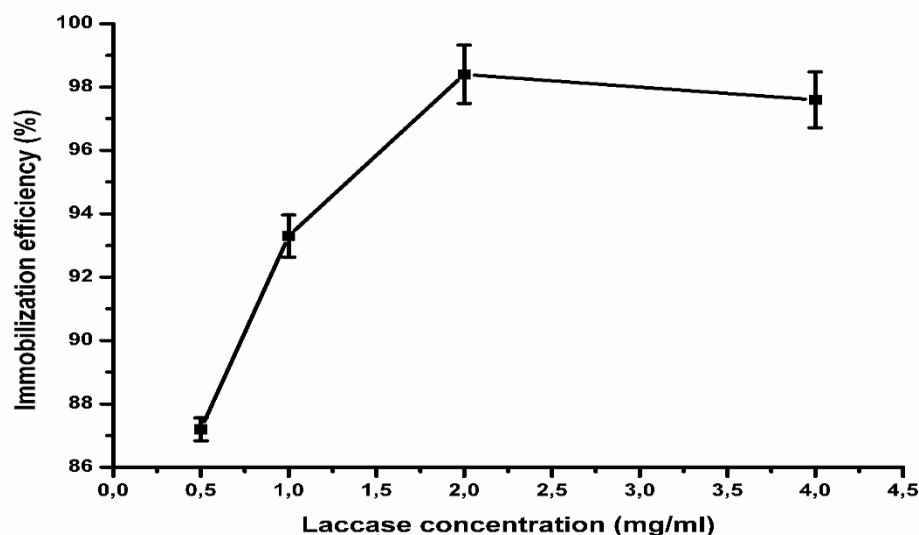


Figure 4.2. Effect of laccase concentration on immobilisation efficiency

4.3.2 Properties of free and immobilised enzymes

4.3.2.1 Effect of pH on activity of free and immobilised laccase

Various biocatalytic processes including water bioremediation require enzymes with high tolerance to extreme micro-environmental conditions such as pH and temperature. **Figure 4.3** shows the effect of pH on the catalytic activity of the free and immobilised laccase enzymes. The optimum pH of the free and immobilised enzymes was found to be pH 4. At this optimum pH, the activity of the free enzymes was 78.4% while the activities of the immobilised enzymes were Lac_{0.5}-HPEI/PES (76.3%), Lac_{1.0}-HPEI/PES (76.7%), Lac_{2.0}-HPEI/PES (78.8%) and Lac_{2.0}-HPEI/PES (78.9%). Xu et al. (2013) also reported the optimum pH of 4 for free laccase and laccase immobilised on chitosan (polyvinyl alcohol) nanofibrous membrane. The optimum pH of laccase can be dependent on the type of substrate used. When phenolic substrates such as syringaldazine are used, the optimum activity at pH 4 is normally exhibited (Chen et al., 2015). At lower pH (pH 3), free laccase lost 35.3% of its activity while the immobilised laccase lost about 24.2%. The activity of free laccase was also reduced by 65% while that of immobilised laccase decreased by 33% (for Lac_{4.0}-HPEI/PES). These results indicate the

increased tolerance of immobilised laccase over a wide pH range. The improved pH stability of the immobilised enzymes using laccase-modified polyacrylonitrile nanofibrous membrane has also been reported by Xu et al. (2013). This improved resistance to pH for immobilised laccase indicates that the HPEI/PES nanofibrous membrane support had low charge density which could not affect the ideal structure of immobilised laccase. Moreover, the stable covalent bonds attaching laccase on the dendritic membrane support may also restrict the immobilised laccase from undergoing structural changes that would inhibit their catalytic performance at extreme pH levels (Zhu et al., 2015).

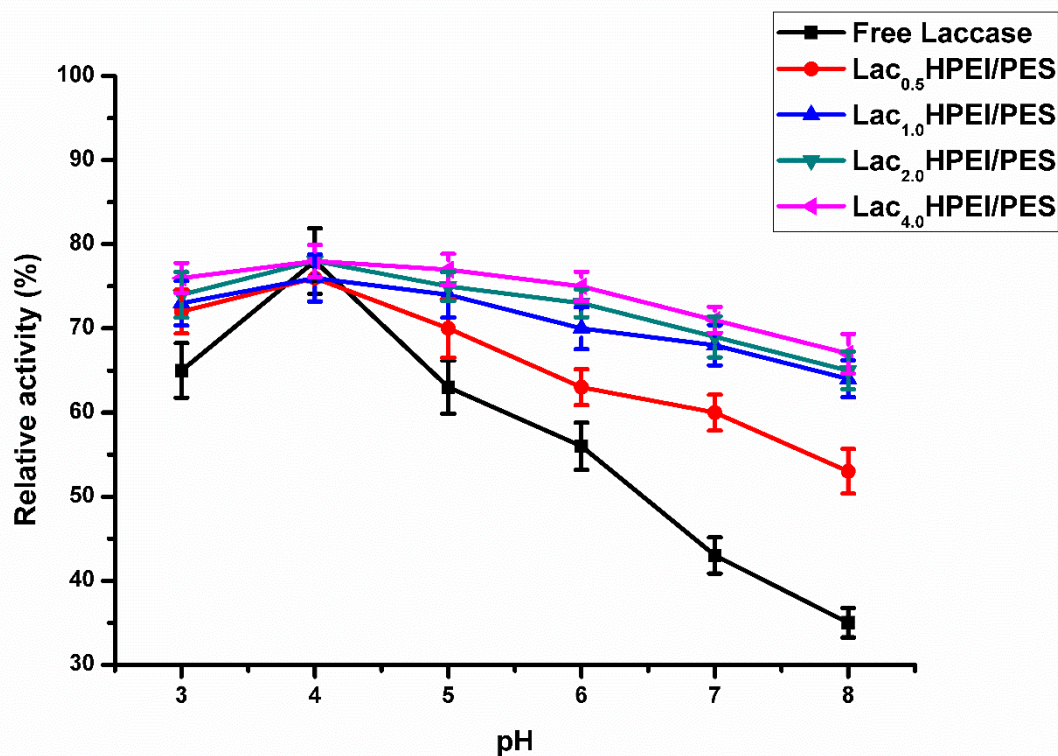


Figure 4.3. Effect of pH on the activity of free and immobilised laccase

4.3.2.2 Effect on temperature on activity of free and immobilised laccase

Figure 4.4 shows the effect of temperature on the relative activity of free laccase and immobilised laccase. As depicted in Figure 4.4, the relative activity of the free and immobilised laccase increased from 20°C to the optimum temperature of 40°C, after which it starts to decrease. The activity of the free laccase at the optimum temperature (40°C) was 81.3% and that of immobilised laccase was Lac_{0.5}-HPEI/PES (79.4%), Lac_{1.0}-HPEI/PES (83.6%), Lac_{2.0}-HPEI/PES (86.7%), and Lac_{4.0}-HPEI/PES (88.4%). The free laccase exhibited a significant decline in its initial activity of approximately 66.4% while immobilised laccase was shown to have a decline of about 31.8% (for Lac_{4.0}-HPEI/PES). This thermal response has also been reported by Xu et al. (2013) when laccase was covalently attached on chitosan (polyvinyl alcohol) and polyacrylonitrile nanofibrous membranes. It was also observed that the immobilised laccase could retain most of its relative activity even at a higher temperature as compared to the free enzymes. The improved thermal stability of the immobilised laccase was ascribed to the stable covalent bonds which conserve the proper conformation for the binding of the substrate (Majeau et al., 2010; Zhang et al., 2012).

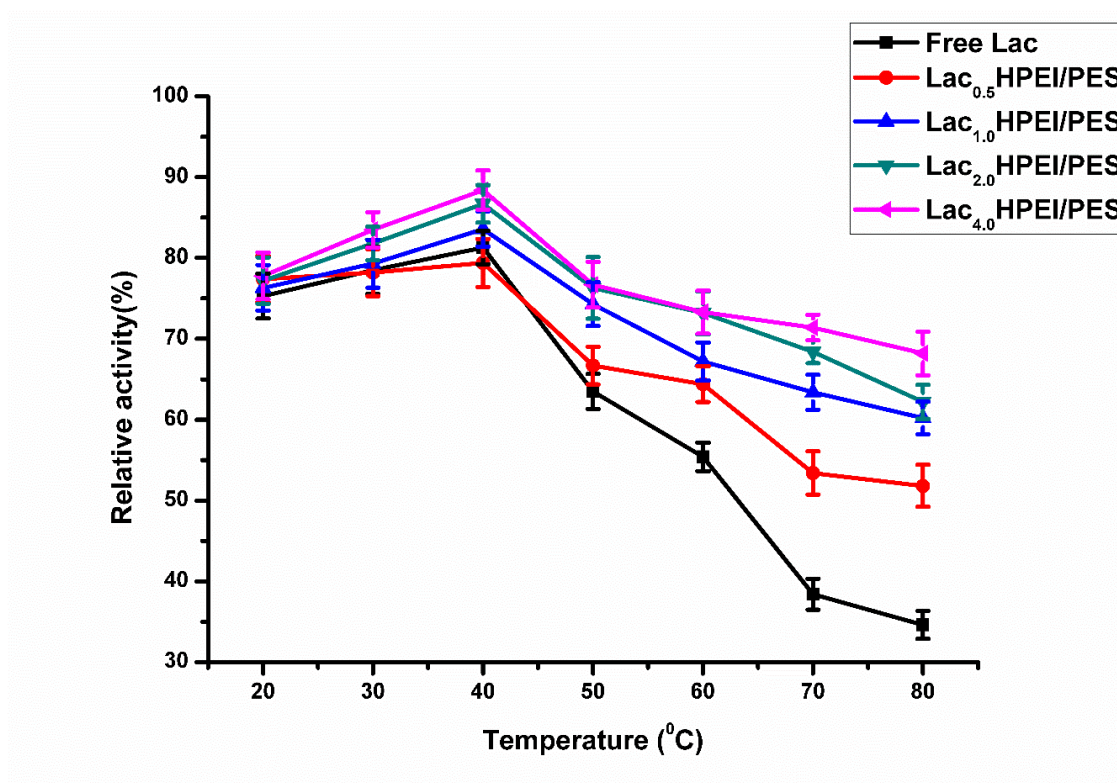


Figure 4.4. Effect of temperature on the activity of free and immobilised laccase

4.3.2.3 Storage stability of free and immobilised laccase

Figure 4.5 illustrates the storage stability of the free and immobilised laccase over 28 days. The relative activity of the free laccase decreased faster than that of the immobilised laccase. The free laccase could only retain 8.8% of its activity in 28 days while the immobilised laccase retained LaC_{0.5}-HPEI/PES (20.1 days), LaC_{1.0}-HPEI/PES (24.3 days), LaC_{2.0}-HPEI/PES (40.6 days), and LaC_{4.0}-HPEI/PES (39.6 days). The enhanced storage stability of the immobilised laccase was attributed to the stable covalent bonding which restricted the structural denaturation of the enzyme (Forde et al., 2010). This can also be ascribed to the biocompatible matrix of the HPEI/PES nanofibrous membrane which assists in preserving the native conformation of the laccase enzyme (Dai et al., 2011). It is worth noting that LaC_{4.0}-HPEI/PES lost its activity faster than LaC_{2.0}-HPEI/PES which may be due to the lateral interactions experienced in LaC_{4.0}-HPEI/PES caused by aggregation of the enzymes on the nanofibres of LaC_{4.0}-HPEI/PES which results in the distortion of the enzyme conformation (Wan et al., 2008).

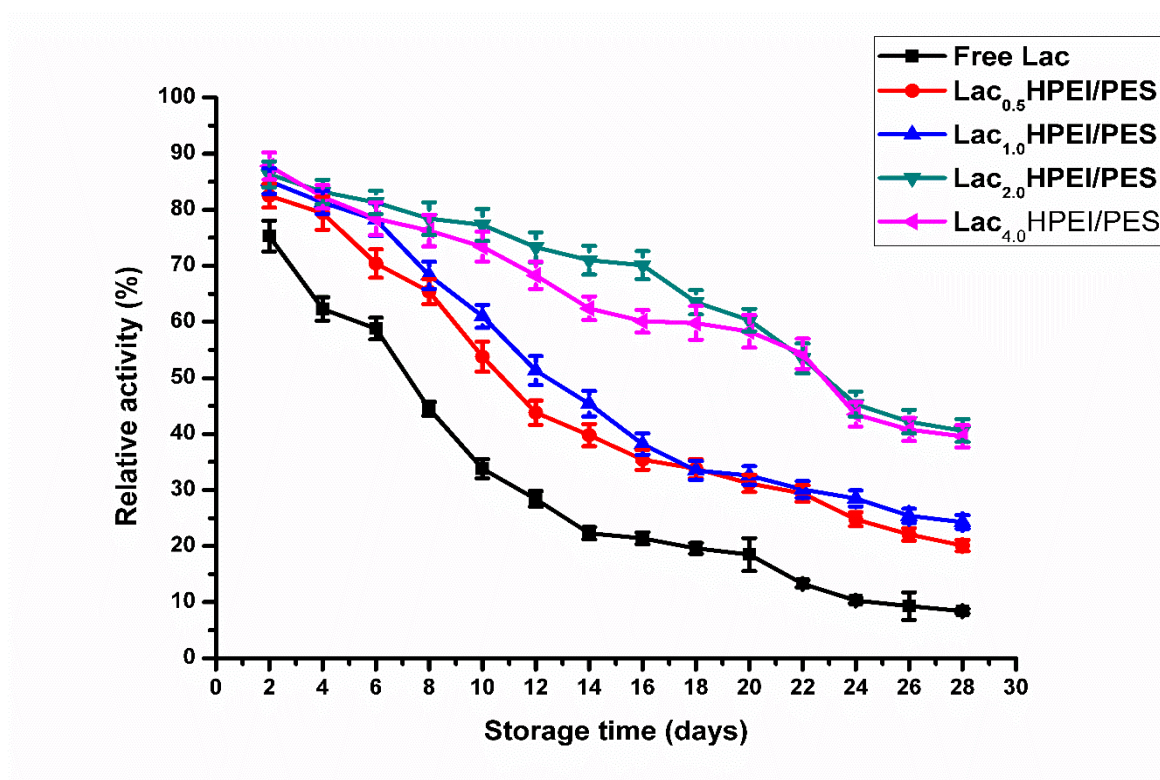


Figure 4.5. Storage stability of free and immobilised laccase

4.3.3 ATR-FTIR analysis of synthesised membranes

Figure 4.6 shows the FTIR analysis of pristine PES membranes, aminated PES/HPEI nanofibrous membranes, glutaraldehyde activated nanofibrous membranes, and laccase-immobilised membranes (Lac-HPEI/PES). The characteristic peaks for pristine PES membranes (Figure 4.6a) such as aromatic C-H stretches (3094 and 3065 cm^{-1}), benzene ring stretches (1572 and 1487 cm^{-1}), and the S=O bands (1303 and 1146 cm^{-1}) can be observed (Belfer, 2000). Figure 4.6b shows the appearance of a new peak at 1660 cm^{-1} is attributed to the N-H band, which confirms the attachment of HPEI on the nanofibrous membranes. After the activation of the HPEI/PES nanofibrous membranes with glutaraldehyde (Figure 4.6c), the N-H peak shifted to 1665 cm^{-1} and a new absorption band attributed to C=O (from glutaraldehyde) appeared at 1737 cm^{-1} . The C=O peak shifted to 1736 cm^{-1} upon laccase immobilisation on the activated membranes (Figure 4.6d). Moreover, a new broad peak attributed to the C=N band, was detected at 1658 cm^{-1} , thus confirming the covalent attachment of laccase enzymes on the activated HPEI/PES membranes. The covalent attachment of laccase enzyme and HPEI occurs via a Schiff base reaction between the carbonyl groups in glutaraldehyde chains and the amine groups in the lysine residue of laccase enzyme (Landarani-Isfahani, 2015)

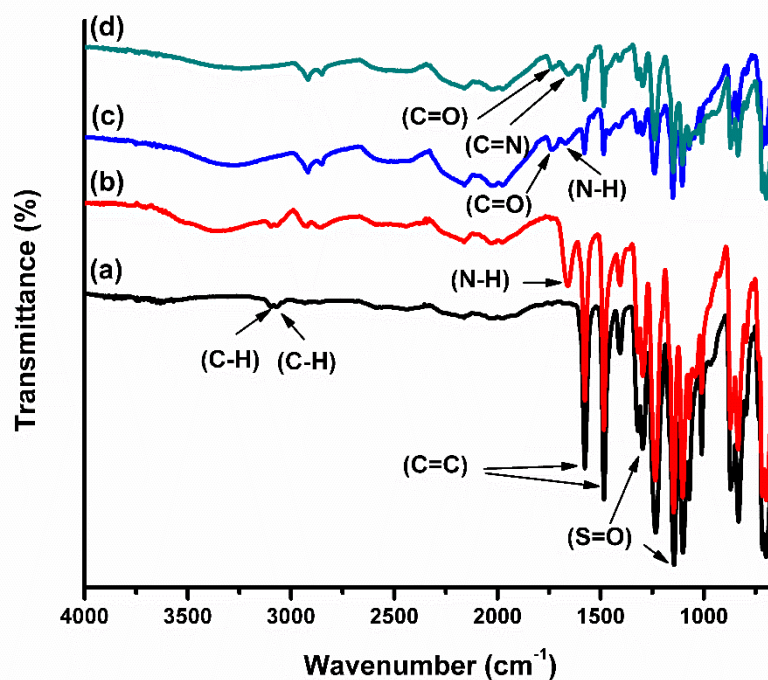
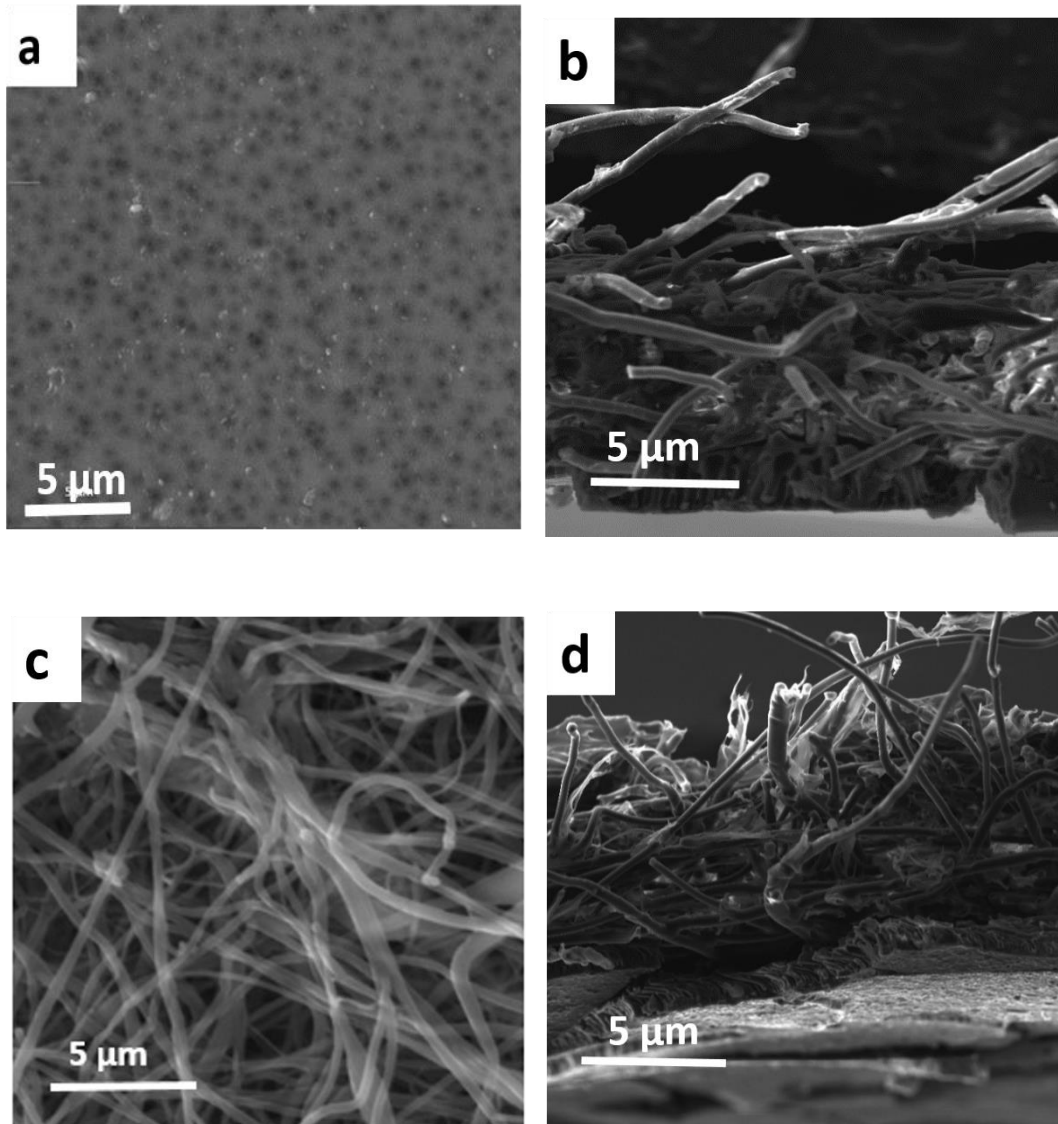


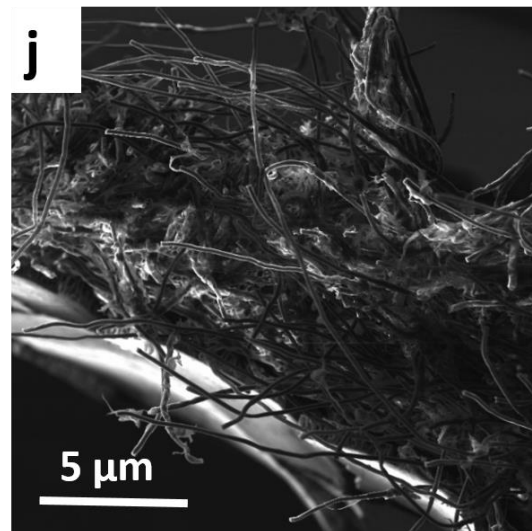
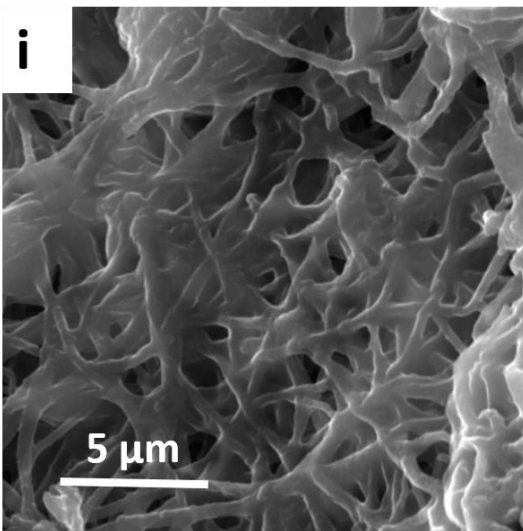
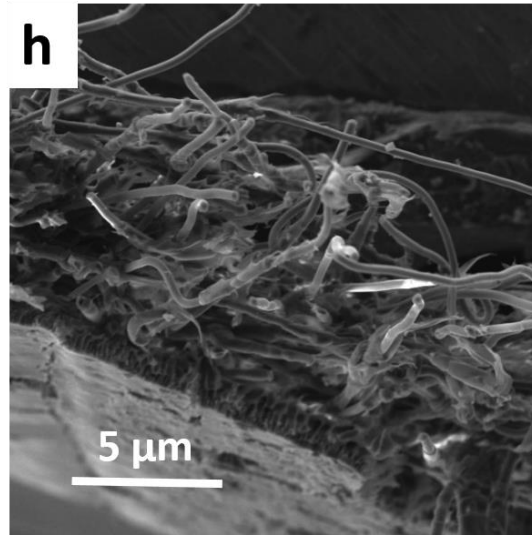
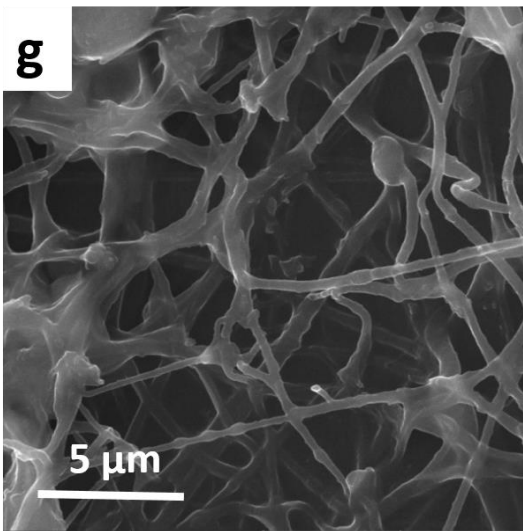
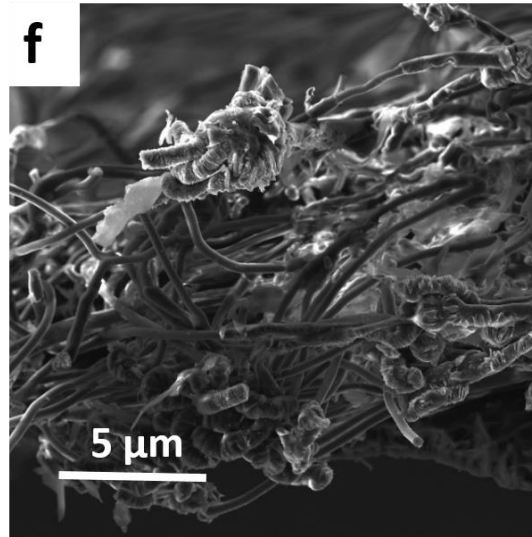
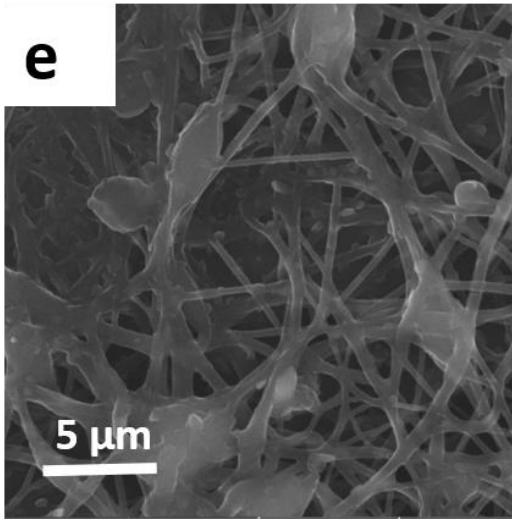
Figure 4.6. ATR-FTIR spectra of: (a) commercial PES membranes; (b) aminated HPEI/PES nanofibrous membranes; (c) glutaraldehyde activated nanofibrous membranes; and (d) laccase-immobilised nanofibrous membranes

4.3.4 SEM analysis

Figure 4.7a shows the porous morphology of the commercial PES membranes prior to electrospinning. The SEM image and histogram of the HPEI/PES nanofibrous membranes show a uniform well dispersed porous interconnected network of fibres with an average fibre diameter of 234 ± 32 nm (**Figure 4.7c** and **Figure S1(a)** listed in the supplementary results in the Appendix). The observed average fibre diameter of the HPEI/PES nanofibrous membranes was less than that of the electrospun cellulose acetate/polyethyleneimine (CA/PEI) nanofibres reported by Hou et al. (2016). In this study, CA/PEI nanofibres were electrospun using varying PEI concentrations with acetone/water as the solvent. The fibre diameter of the electrospun nanofibres was found to increase with an increase in the PEI concentration. The increase in PEI content resulted in an increased viscosity of the polymer solution. Thus, fibres with large diameters were formed due to sufficient molecular chain entanglements resulting from the high viscosity of the polymer solution (Hou et al., 2016). Park et al. (2012) also found that the use of binary solvents (n-methyl-2-pyrrolidone/dimethylformamide) could result in an increase in electrospun fibre diameter. The density and viscosity of n-methyl-2-pyrrolidone are higher than those of dimethylformamide, and result in an increase in fibre diameter due to increased viscosity of the polymer solution even at constant polymer concentration [5]. In this study, a binary solvent system was used in preparation of HPEI/PES nanofibres. **Figures 4.7b, d and f** show the cross-sectional morphology of the pristine PES, the nanofibrous HPEI/PES and the laccase-modified nanofibrous membranes. There was an observed increase in membrane thickness upon electrospinning of the HPEI/PES nanofibres on the parent PES membrane. The membrane thickness further increased upon laccase immobilisation as can be observed in **Figures 4.7f, h, j, and l**. This increase was ascribed to the formation of an additional layer of nanofibrous mat on the PES support membrane upon electrospinning as well as the swelling of the nanofibres when the enzymes were bound on their backbone.

After the amination and activation of glutaraldehyde, the HPEI/PES fibre diameter did not change significantly. The EDS analysis of the nanofibrous membranes revealed the presence of oxygen (0.53 keV) and sulphur (2.31 keV) which are characteristic of PES (**Figure S1a**) (Erjavec, 2016). The nitrogen peak at 0.27 keV also gave evidence of the presence of the HPEI polymer in the electrospun nanofibrous membranes (**Figure S1b**). The laccase-immobilised nanofibrous membranes showed aggregates of the laccase enzymes on the electrospun nanofibres (**Figure 4.7e-k**). This observation confirmed the attachment of the laccase on the surface of the HPEI/PES nanofibrous membranes. After enzyme immobilisation, the fibre diameter increased from 354 ± 37 nm (Lac0.5-HPEI/PES) to 356 ± 80 nm (Lac4.0-HPEI/PES) which could be attributed to the swelling behaviour of fibres during enzyme loading (Brena et al., 2013). From the EDS analysis, copper was observed at 0.52 keV which indicated the presence of laccase enzymes on the activated membranes (**Figure S1c**). Laccase is an oxidoreductase that contains copper atoms in its catalytic centre. The thickness of the prepared membranes which was estimated using ImageJ software, showed an increase in the overall membrane thickness upon electrospinning and laccase immobilisation. The membrane thickness of pristine PES was 283 ± 14 μ m and increased to 337 ± 7 μ m for HPEI/PES nanofibrous membranes. The Lac_{1.0}-HPEI/PES membrane showed a slight decrease in membrane thickness. A possible explanation to this trend could not be found. The laccase immobilised membranes further showed an increase in thickness up to 400 ± 50 μ m. Increased thickness of the laccase-modified membranes' surface can be attributed to the swelling behaviour of the enzyme-modified nanofibres, thus occupying a larger volume.





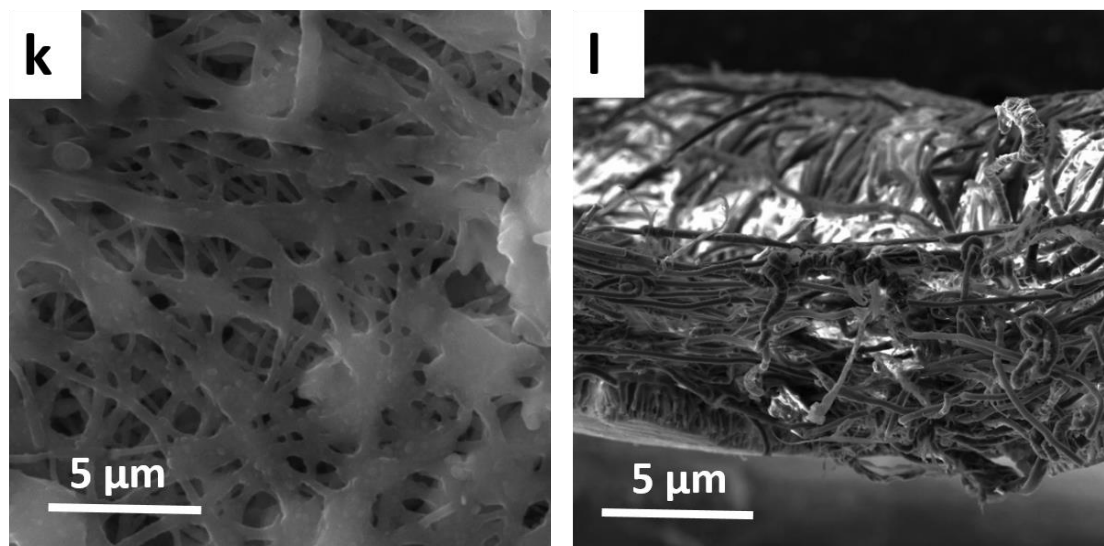


Figure 4.7. SEM images of surface and cross-sectional morphology of commercial PES membranes (a, b), HPEI/PES (c, d), Lac_{0.5}-HPEI/PES (e, f), Lac_{1.0}-HPEI/PES (g, h), Lac_{2.0}-HPEI/PES (i, j), and Lac_{4.0}-HPEI/PES (k, l)

4.3.5 CLEM analysis

The CLEM photo-images of the neat PES membrane and electrospun HPEI/PES nanofibrous membrane did not show any fluorescence emission upon excitation which confirmed the absence of any laccase enzymes on the membranes (**Figure 4.8a and b**). However, the laccase modified membranes emitted green fluorescence upon excitation and showed evenly dispersed aggregates of laccase enzymes coating the surface of the interconnected nanofibres (**Figure 4.8c-f**). These observations are similar to those reported by Dai and co-authors (2016) when observing laccase-carrying multiwalled carbon nanotubes nanofibrous membranes under laser scanning confocal microscopy (LSCM) (Zhu, 2014; Hou, 2014).

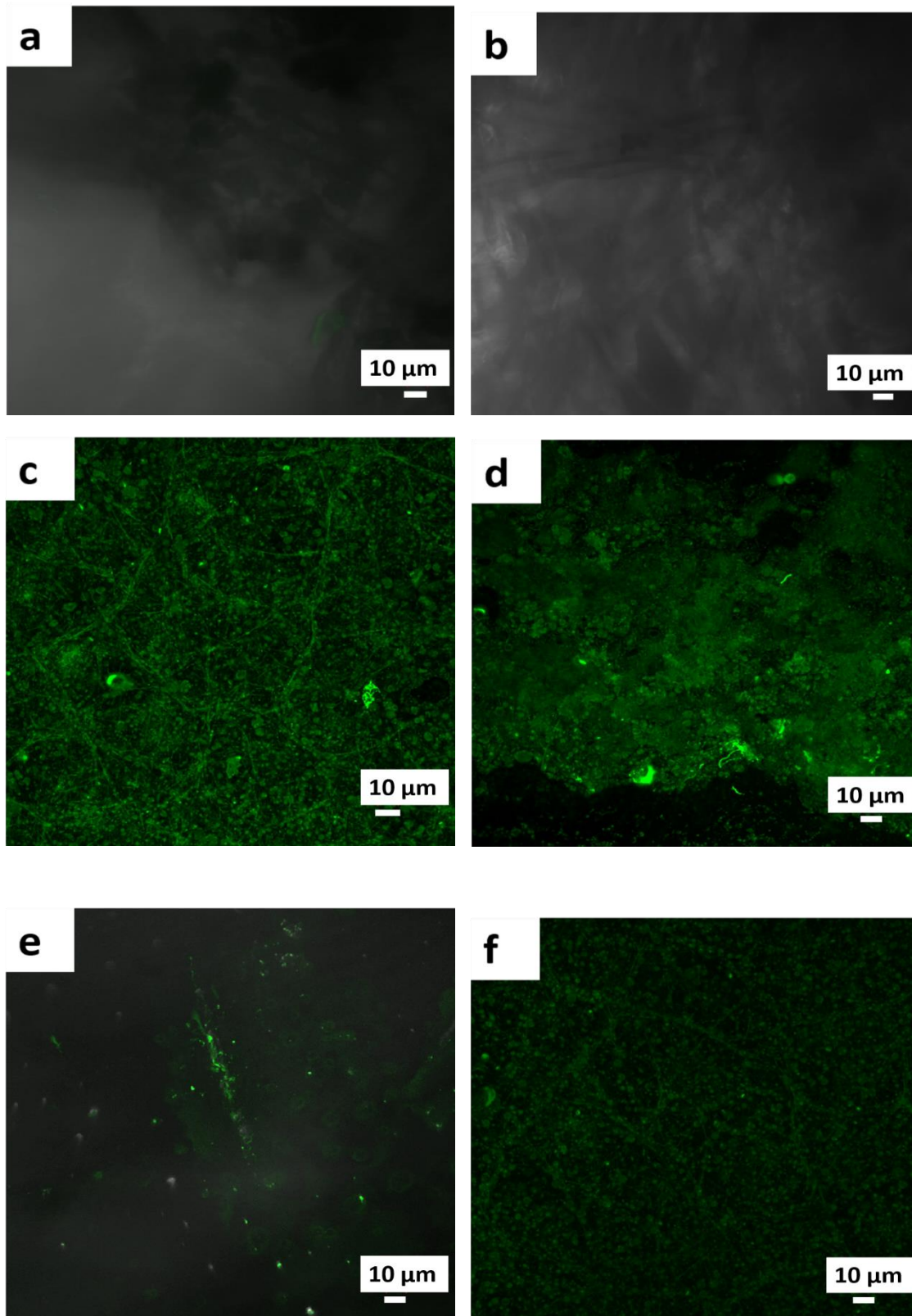


Figure 4.8. CLEM photo-images of: (a) PES membranes; (b) HPEI/PES; (c) Lac_{0.5}-HPEI/PES; (d) Lac_{1.0}-HPEI/PES; (e), Lac_{2.0}-HPEI/PES; and (f) Lac_{4.0}-HPEI/PES

4.3.6 Application of the laccase-modified membranes in the removal of BPA from water

Figures 4.9a and 4.9b demonstrate the removal of BPA and the permeate flux using the pristine PES, HPEI/PES and laccase-modified membranes. The commercial PES membranes had the lowest BPA rejection of 52.4% as compared to the HPEI/PES nanofibrous membranes (66.7%), Lac_{0.5}-HPEI/PES membranes (83.4%), Lac_{1.0}-HPEI/PES membranes (84.6%), Lac_{2.0}-HPEI/PES membranes (85.4%) and Lac_{4.0}-HPEI/PES membranes (89.7%), respectively (**Figure 4.9a**). The three key membrane removal mechanisms could be ascribed to the presence of hydrophobic nanocavities in the HPEI polymer, possible coordination-type bonding (ion-dipole) between the oxygen atom in the phenol group of BPAs and the cationic HPEI polymer, and hydrogen bonding between the pollutant and the HPEI polymer. The modified membranes, i.e. HPEI/PES and Lac-HPEI/PES, contain hydrophobic HPEI polymer nanocavities, which can efficiently adsorb and encapsulate hydrophobic molecules such as BPA. In a study conducted by Arkas et al. (2005), hyperbranched polymers were alkylated to form molecular nanosponges that could encapsulate polycyclic aromatic hydrocarbons from water. The hyperbranched polymers were alkylated to form the insoluble nanosponges. Pyrene, fluoranthene and phenanthrene were encapsulated in the cavities of HPEI, hyperbranched polyglycerol and hyperbranched polyesteramides (Arkas et al., 2005). The alkylated hyperbranched polyethyleneimine achieved an adsorption efficiency of 90% for pyrene in 2 h, 75% for fluoranthene in 3 h and 65% for phenanthrene in 3 h. This enhanced removal efficiency was attributed to the flexible chains of hyperbranched polyethylenimine that result in adaptable cavities which can be adjusted to fit the size and shape of the pollutant (Arkas et al., 2005).

The BPA adsorption on the HPEI nanofibrous network system could also be enhanced by the coordination of the oxygen atoms of BPA with the cationic HPEI polymer. The oxygen atom in the phenol group of BPAs can donate electrons and the positively charged HPEI acts as electron acceptor in this coordination-type bonding. This phenomenon was discussed by Dong et al. (2010) where BPA was adsorbed on surfactant (hexadecyltrimethylammonium) (HDTMA) modified zeolite. Adsorption of BPA on the modified zeolite was ascribed to interaction of oxygen atoms from BPA with the positively charged heads of HDTMA (Dong et al., 2010). The same mechanism was suggested by Böhm et al. (2011) for encapsulation of dichloro-1,4-dihydroxyanthraquinone (AQ-OH) into HPEI polymer nanocavities. The encapsulation of AQ-OH into the HPEI was promoted by the interaction between the phenolate groups of AQ-OH and the protonated amine groups of the HPEI polymer (Böhm et al., 2011). The proposed mechanism for the removal of BPA using laccase-modified membranes is shown in **Figure 4.10**. During the pollutant removal process, it is envisaged that the BPA diffuses from the bulk water and is adsorbed within internal hydrophobic HPEI cavities in the nanofibrous part of the membranes according to the mechanisms discussed above. The overall removal of BPA can be ascribed to the adsorption of BPA on the dendritic nanofibrous membrane and the possible degradation of BPA by the immobilised laccase. The biodegradation of BPA was confirmed by LC-MS analysis by determining the generated by-products. The water molecules free from BPA (with a size of 0.0002 μm) will easily pass through the pores of the PES support membranes (with a pore size of 0.02 μm). The deactivated laccase-modified membranes exhibited lower BPA removal mainly due to the reduced internal surface area caused by the swelling behaviour of the nanofibres upon laccase immobilisation. The water molecules free from BPA (with a size of 0.0002 μm) easily pass through the pores of the PES support membranes (with a pore size of 0.02 μm).

The permeate flux (**Figure 4.9b**) of the laccase-modified membranes ($7.07 \pm 5.54 \text{ L/m}^2\cdot\text{h}$) was lower than that of the commercial PES membranes ($63.15 \pm 5.56 \text{ L/m}^2\cdot\text{h}$). The permeate flux for the laccase-modified membranes was found to be dependent on the pore size of the membranes. As the pore sizes are reduced there is more resistance to water flowing through the membranes matrix. Moreover, the reduction in the permeate flux can be attributed to the thickness of the selective membrane(s) layer. In this study the modified membranes exhibited a thicker layer than the pristine PES membrane. A thick membrane layer has been found to cause a reduction in permeate flux (Liu et al., 2013).

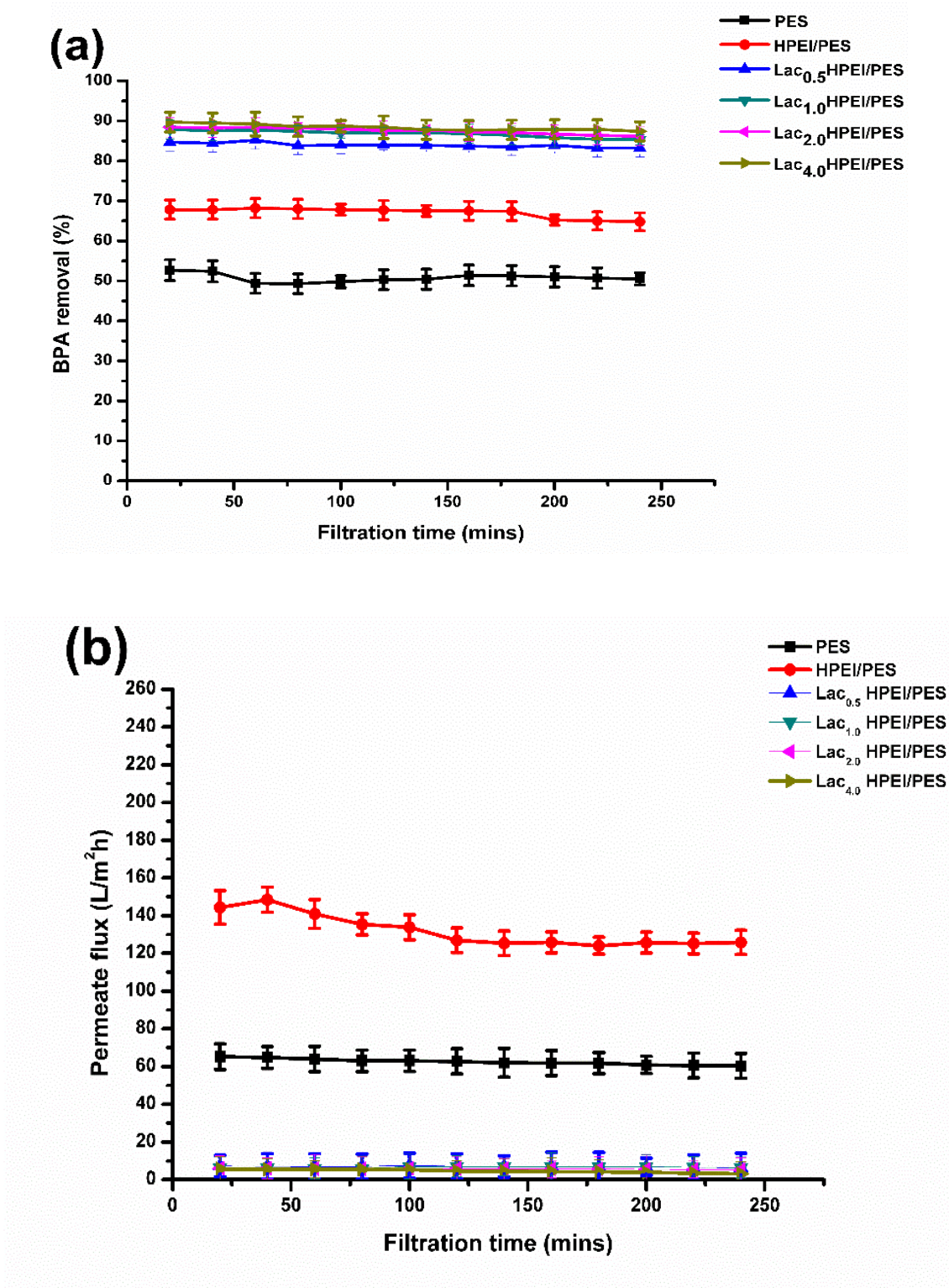


Figure 4.9. Removal of BPA (a) and permeate flux (b) vs. time for commercial PES membranes and laccase-modified membranes at 600 kPa and 25°C

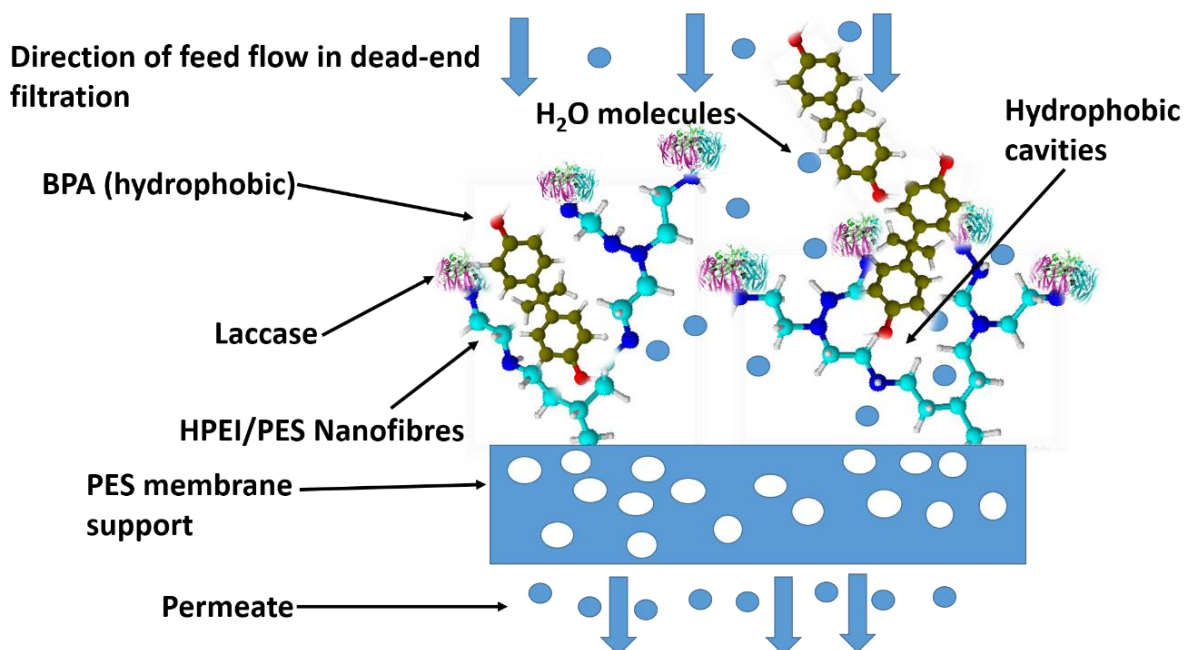


Figure 4.10. The proposed mechanism for removal of BPA in a dead-end filtration system using laccase-modified dendritic membranes

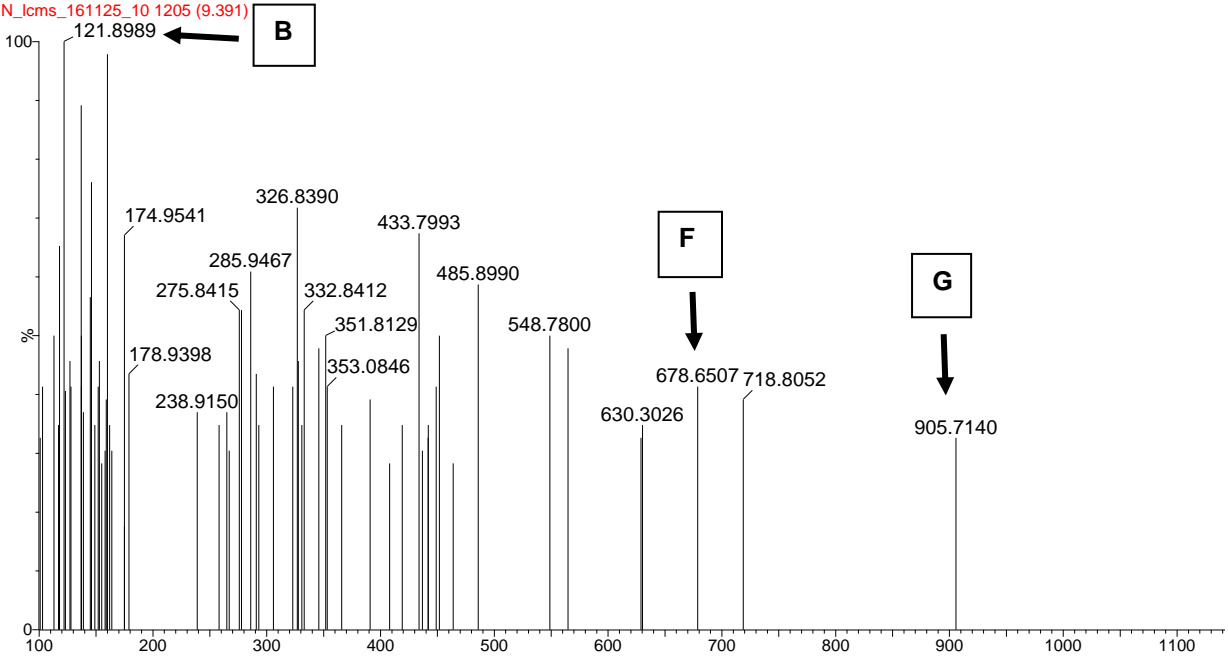
4.3.7 Biodegradation of BPA

Successful biodegradation of BPA by the synthesised laccase-immobilised HPEI/PES membranes was confirmed by detection of present by-products in the permeate over a filtration time of 240 min using LC-MS. The detected BPA degradation by-products were 4-isopropylphenol (**A**: $m/z = 137.00$), 4-hydroxybenzaldehyde (**B**: $m/z = 121.9$), 2,2-bis(4-hydroxyphenyl) propanoic acid (**C**: $m/z = 258.0$), 4,4-dihydroxy- α -methylstibene (**D**: $m/z = 194.9$), BPA dimer (**E**: $m/z = 452.9$), BPA trimer (**F**: $m/z = 678.7$) and BPA tetramer (**G**: $m/z = 905.7$) as shown in **Figure 4.11** and **Table 4.1**. Most of the detected by-products were detected after a filtration time of 220 min using the Lac_{1.0}-HPEI/PES membrane. However, 4,4-dihydroxy- α -methylstibene was also detected after a filtration time of 200 min using the Lac_{4.0}-HPEI/PES membrane. Peng et al. (2015) also detected 2,2-bis(4-hydroxyphenyl) propanoic acid and 4-dihydroxy- α -methylstibene when biodegrading BPA using microorganisms from a river sediment (comprising mainly of *Pseudomonas knackmussii* and other similar strains). Bechambi et al. (2015) degraded BPA using C-doped zinc oxide under UV light in the presence of hydrogen peroxide and reported 4-isopropylphenyl and 4-hydroxybenzaldehyde as some of the intermediates formed during photodegradation. Formation of 4-isopropylphenol during degradation of BPA has also been reported by Du et al. (2016) when a mesoporous sulphur-modified iron oxide was used. Prins et al. (2015) detected BPA dimers, trimers and tetramers using LC-MS when biodegrading BPA using fungal and bacterial laccase. In most studies it has been noted that there is an increase in toxicity of BPA due to the generation of more toxic intermediates. However further degradation of these intermediates results in the gradual decrease in toxicity (Han et al., 2015; Lu et al., 2013). Toxicity tests would have to be conducted in this study in order to analyse the effect of the BPA by-products against bacteria such as *Vibrio fischeri*.

<< Hyperbranched polymer membranes for catalytic degradation >>

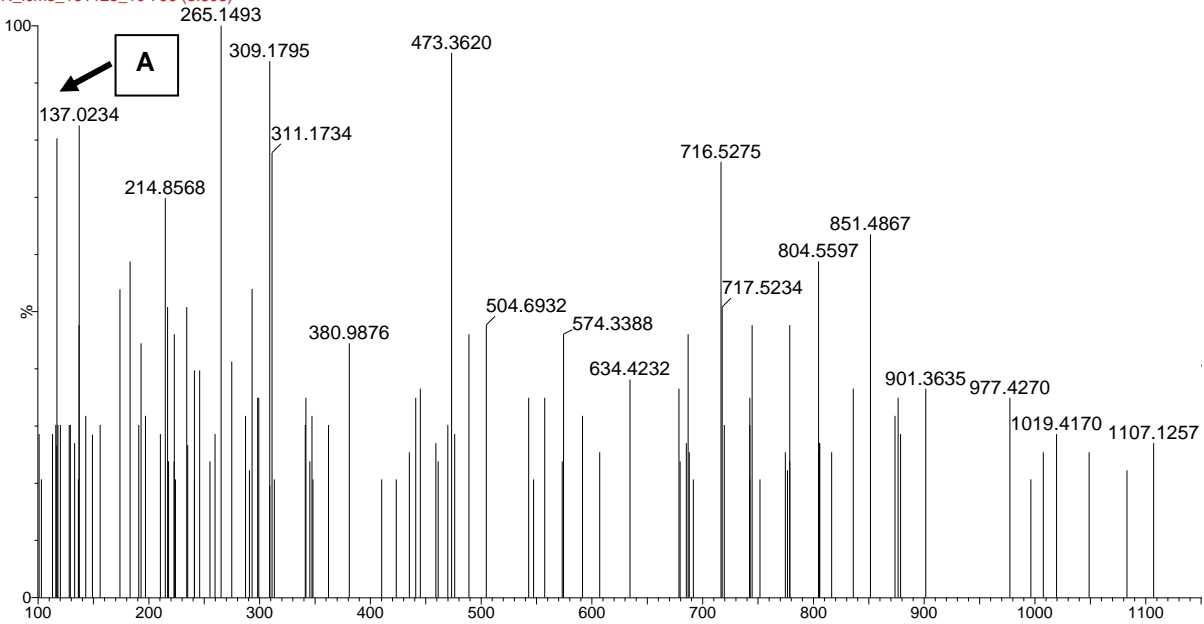
Lac 1.0 220min

N_lcsm_161125_10 1205 (9.391)



Lac 1.0 220min

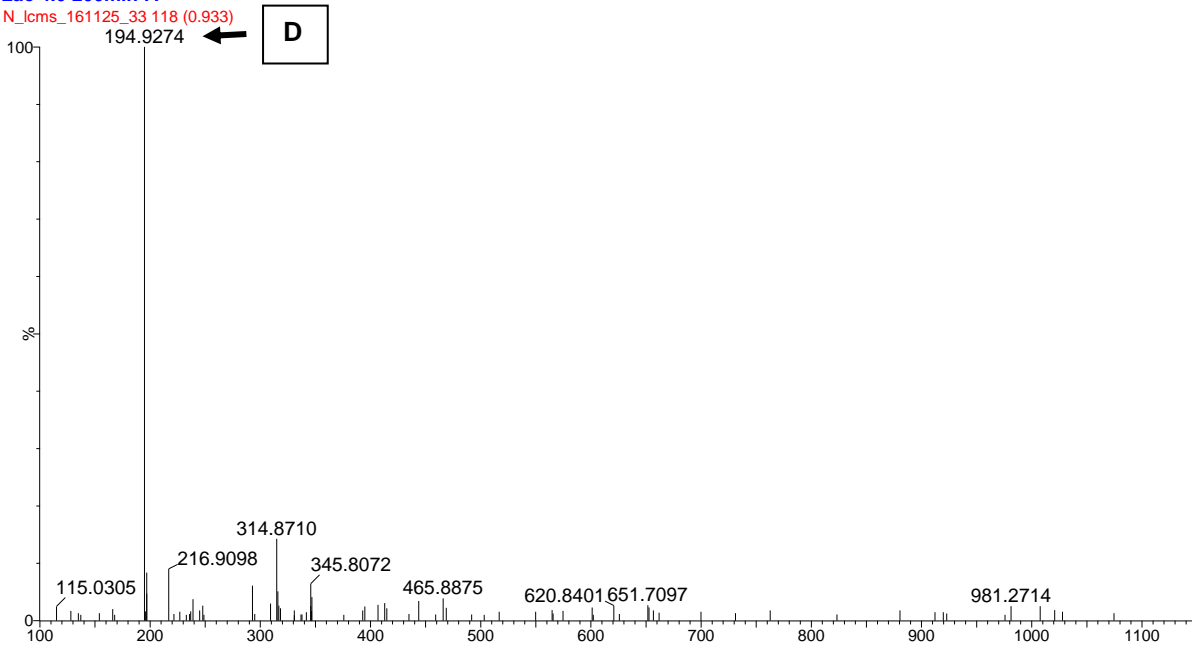
N_lcsm_161125_10 756 (5.898)



<< Hyperbranched polymer membranes for catalytic degradation >>

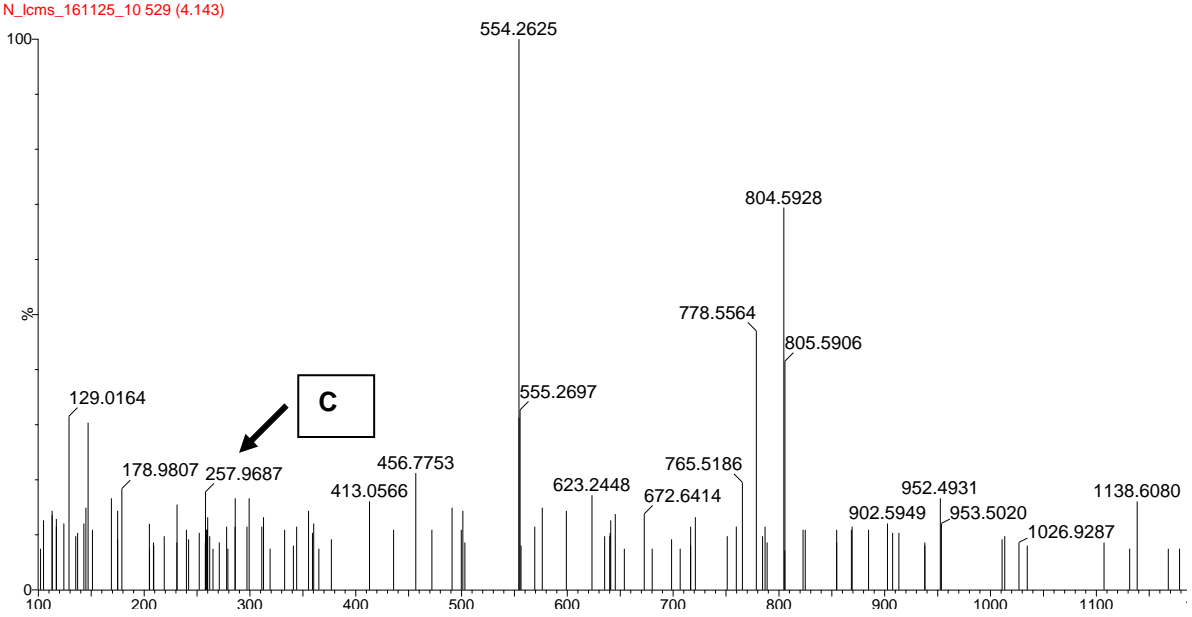
Lac 4.0 200min-A

N_lcsm_161125_33 118 (0.933)



Lac 1.0 220min

N_lcsm_161125_10 529 (4.143)



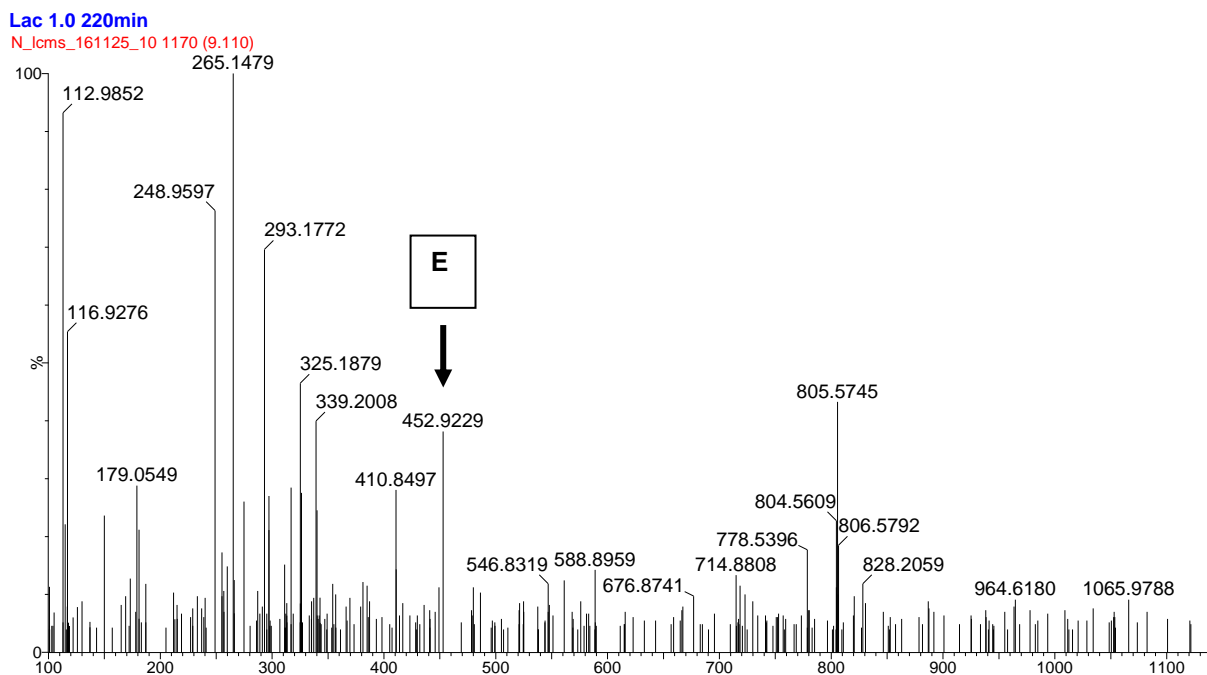
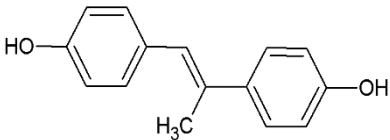
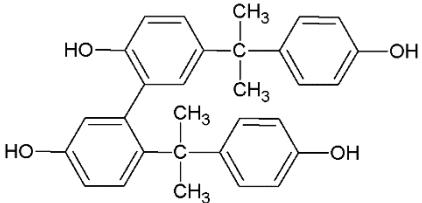
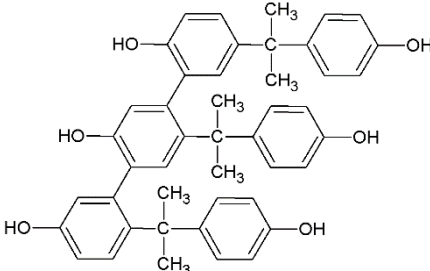
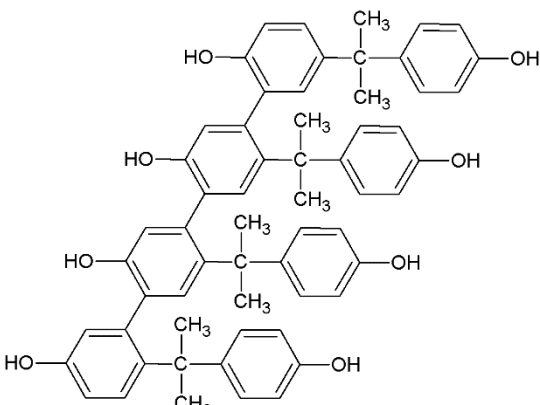


Figure 4.11. LC-MS spectra representing the BPA biodegradation by-products generated using laccase-immobilised HPEI/PES nanofibrous membrane

Table 4.1. Membrane water permeation analyses

By-product	Chemical structure	(m/z)	References
A		137	Bechambi et al., 2015; Du et al., 2016
B		122	Peng et al., 2015
C		258	Peng et al., 2015

D		194	Peng et al., 2015
E		453	Prins et al., 2015
F		679	Prins et al., 2015
G		905	Prins et al., 2015

4.3.8 Recyclability studies

The laccase-modified membranes and pristine PES membranes were reused for four cycles to determine their recyclability. The BPA removal efficiency of the laccase-modified membranes generally ranged from 73% to 79% for the four filtration cycles whilst the efficiency of the pristine PES membranes ranged from 45% to 54% (Figure 4.12). These results demonstrate that covalent bonding of the enzymes onto the modified membranes mitigates leaching out of the immobilised enzymes. Leaching studies (Figure 4.12) revealed that laccase leaching during the recyclability studies was very low. These results further affirmed the strong interaction between HPEI and laccase enzyme via a covalent bond. Studies conducted by Sahoo et al. (2015) also ascribed the long-term stability or reusability of carbonic anhydrase covalently immobilised on graphene oxide modified polylactic acid nanofibrous membranes to reduced enzyme leaching due to stable covalent bonds formed between the enzymes and the support. Moreover, the hydrophobic-hydrophobic interactions responsible for BPA adsorption can easily be reversed by washing the modified membranes with water, thus leaving the hydrophobic micro-voids in the HPEI/PES nanofibres available for repeat adsorption.

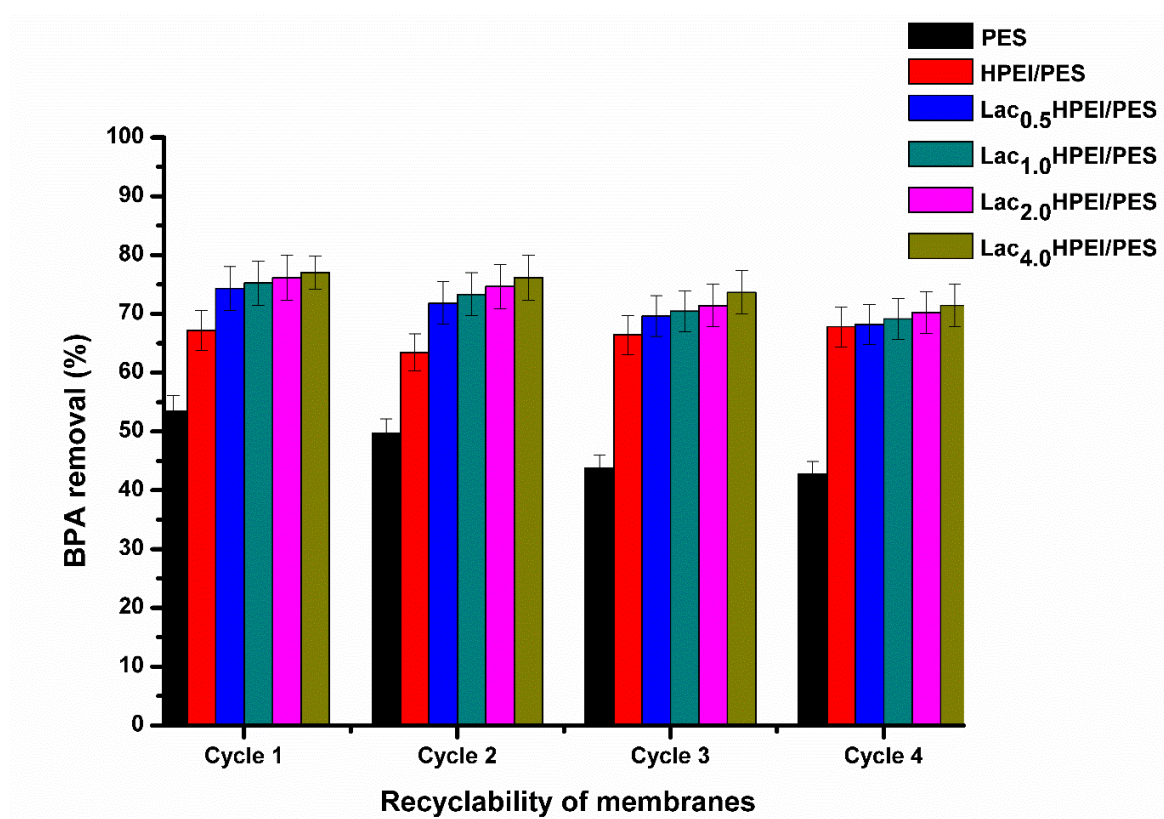
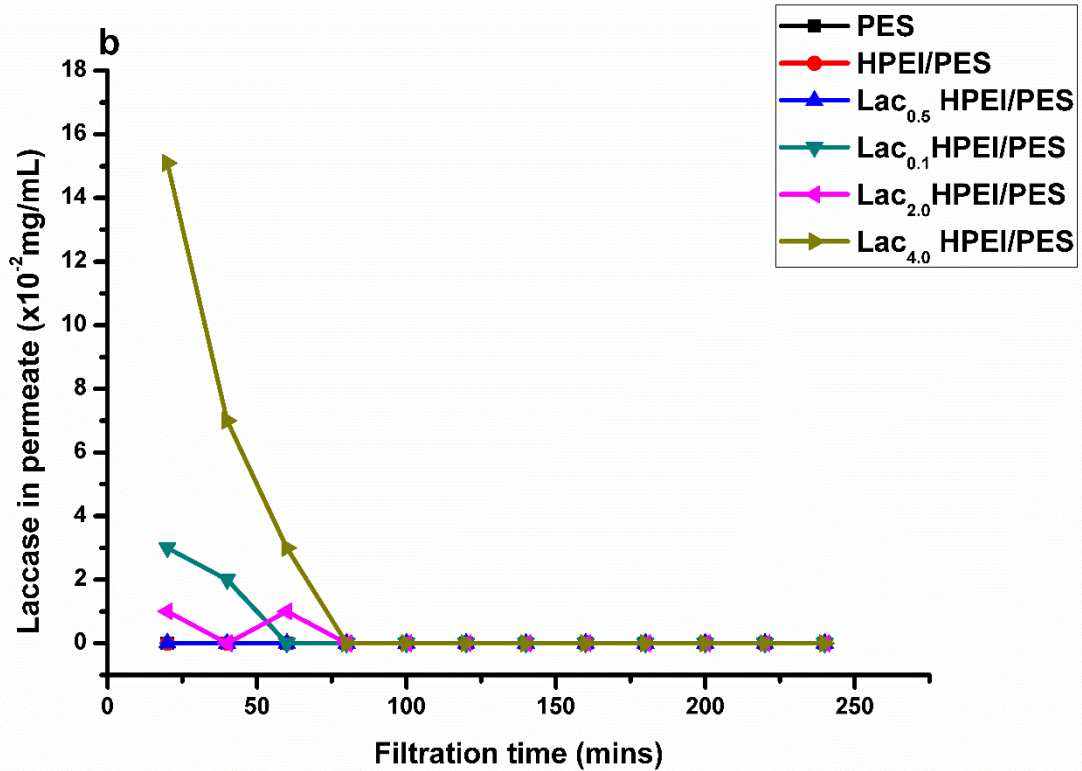
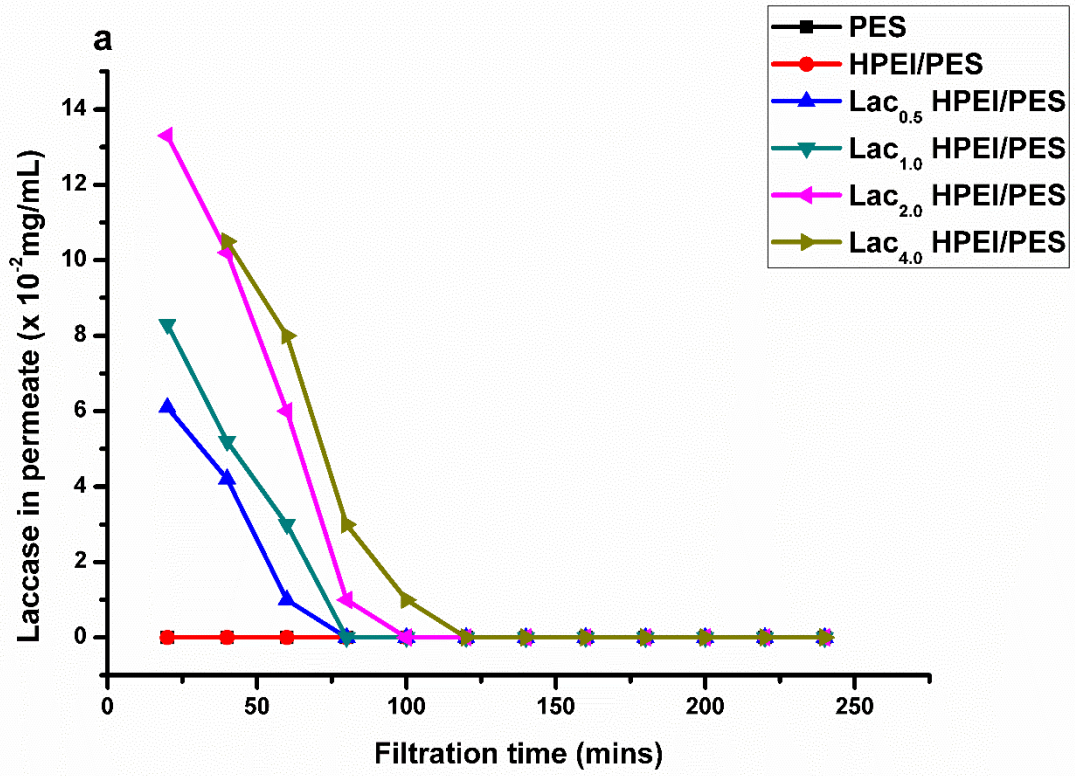


Figure 4.12. Recyclability of the laccase-modified membranes over 4 cycles



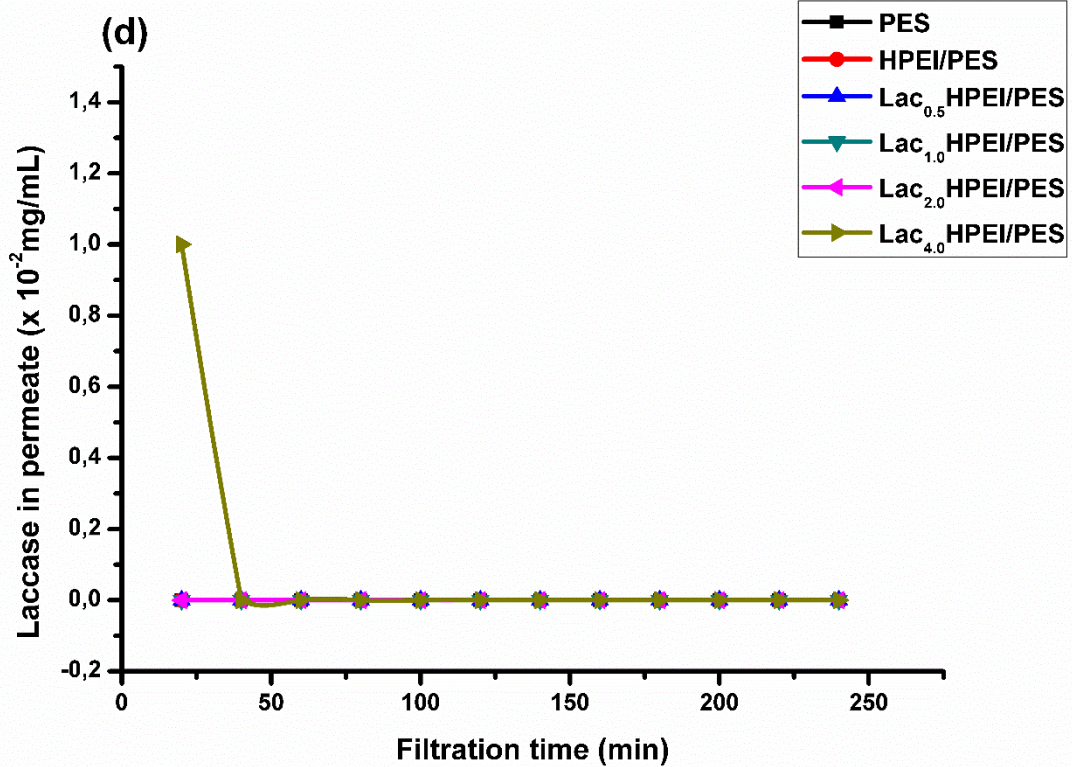
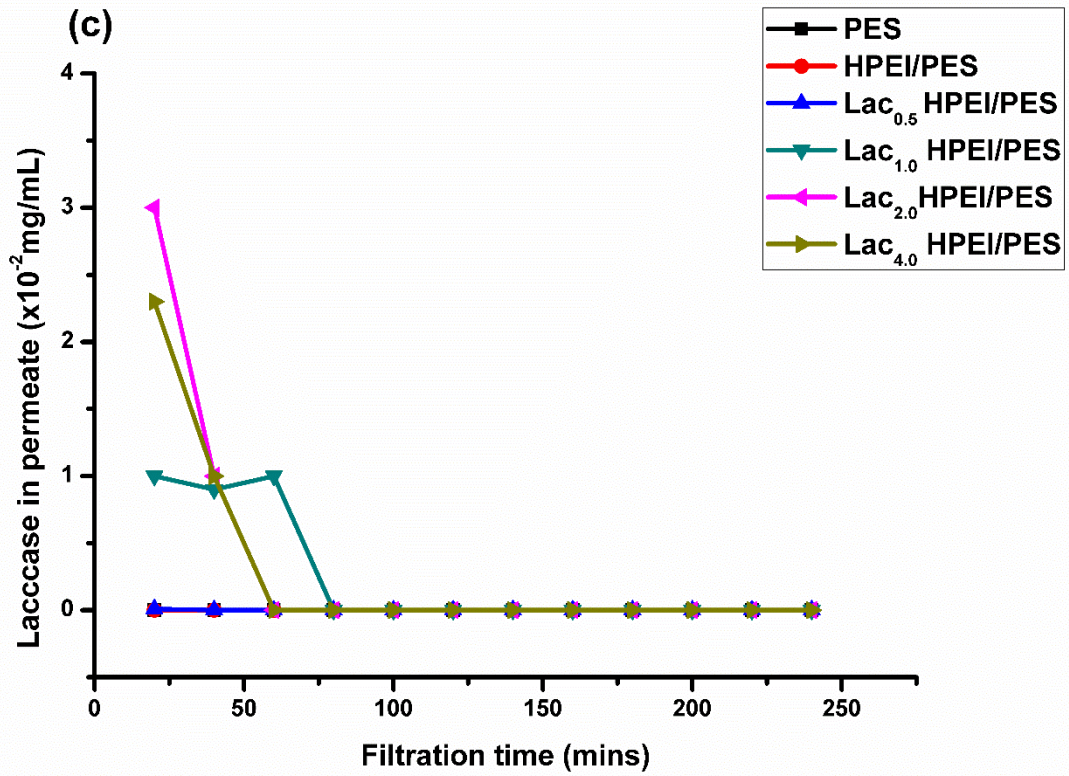


Figure 4.13. Concentration of leaching laccase enzyme in permeate vs. time for first cycle (a), second cycle (b), third cycle (c) and fourth cycle (d)

4.4 SUMMARY

HPEI/PES electrospun nanofibrous membranes containing immobilised laccase enzymes were successfully synthesised in this study and fully characterised. These nanofibrous membranes were used for the removal of BPA from water. The prepared nanofibrous membranes had laccase loading efficiency of 98.3% with improved tensile strength of 28.2 ± 3.0 MPa. The high loading efficiency was due to the abundant peripheral amine functional groups in HPEI that act as coupling agents in covalent attachment of laccase enzymes on the electrospun HPEI/PES nanofibrous membranes. These laccase-modified nanofibrous membranes showed BPA removal of up to 89.6%. This can be attributed to the hydrophobic-hydrophobic interactions between the nanocavities in the HPEI polymer and the BPA molecules, as well as the hydrogen bonding between BPA and amino groups in HPEI which resulted in improved adsorption of the pollutant on the prepared membranes. Electrostatic interactions between the oxygen atoms in the BPA and the cationic HPEI also enhanced BPA removal efficiency. The enhanced removal efficiency of the BPA using the laccase-modified dendritic can be attributed to the synergistic effect of both high adsorption efficiency (according to the proposed mechanisms) and enhanced degradation performance of the immobilised laccase. The immobilised laccase exhibited high activity of about 88.4% under optimum conditions (pH 4 at 40°C). The immobilised laccase showed higher resistance to pH and temperature than free laccase. The laccase-modified membranes showed a high removal efficiency of BPA even after four repeated filtration cycles thus confirming the stability of laccase on the membranes support. Leaching studies showed negligible detachment of immobilised enzymes over four filtration cycles, which is due to the stable carbodiimide bonds used to attach laccase enzymes onto the HPEI/PES nanofibrous membranes. The LC-MS results revealed the formation of 4-isopropylphenol, 4-hydroxybenzaldehyde, 2,2-bis(4-hydroxyphenyl) propanoic acid, 4,4-dihydroxy- α -methylstibene, BPA dimer, BPA trimer and BPA tetramer as BPA degradation by-products. This study contributes to the field of membrane improvement by biomolecules (enzymes) and the laccase-immobilised dendritic nanofibrous membranes were shown to have great potential for use in large-scale applications such as enzyme membrane reactors for the removal of most emerging micropollutants (EMPs).

CHAPTER 5: DEGRADATION OF PCB-153 USING HPEI- FE/PD NANOFILTRATION MEMBRANE

5.1 INTRODUCTION

This chapter deals with the synthesis, characterisation and application of HPEI/FePd membranes. Techniques such as FTIR, SEM, AFM, XRD and XPS were employed in the characterisation of the membranes. The removal and degradation by-products of PCB-153 were monitored by the use of GC-MS.

5.2 EXPERIMENTAL

5.2.1 Preparation of thin-film composite PSf-supported membrane

These membranes were prepared using the interfacial polymerisation method. Aqueous solutions were prepared by dissolving hyperbranched polyethyleneimine (HPEI), (2, 4%, 6, 8% w/v) in a water/ethanol (90/10) mixture. The PSf commercial membranes were then immersed in the aqueous solutions for 24 h at room temperature. After immersion in the aqueous phase, the bimetallic metals (adjusted to pH 5) were incorporated into the modified membrane and the solution was then left to stand for a further 24 h. The membranes were then immersed in trimesoyl chloride (TMC) solution (1.0% w/v) in *n*-hexane. The membrane surface was rolled with a soft rubber roller to eliminate any bubbles formed during the soaking process. The membranes were further dried at 80°C for 15 min for further crosslinking to occur.

5.2.2 Leaching studies

The amount of absorbed Fe and Pd in the ion-exchange process was determined by mass balance after the metal complexation process, where the ratio of concentration before and after leaching was documented. The amounts of zero-valent iron (ZVI) and coated Pd in the membranes were measured by digesting Fe/Pd immobilised membranes in dilute nitric acid (25%) for 2, 8, 12 and 24 h. During digestion, the membranes were continuously stirred on a shaker at a speed of 120 rpm (batch analysis). The same procedure was implemented when digesting the membranes in distilled water; however, since they were not being forced out of the membrane as in the case of HNO₃, these digestion periods were done in daily intervals (day 1 to day 4). Thereafter, 15 mL of the samples at each time interval was taken and analysed on the ICP-OES instrument.

5.2.3 Preparation of HPEI-Fe/Pd-PSf membranes

The bimetallic nanoparticles were prepared using experimental modifications to Smuleac et al. (2010). The complete process for the preparation can be seen in **Figure 5.1**. Briefly, a solution of FeCl₂·4H₂O (500 mL, 200 mg/L) was prepared. Secondly, K₂PdCl₄ (250 mL, 50 mg/L) was prepared in a volumetric flask containing ethanol/distilled water (90/10; v/v) solution. Due to the high reactivity of Fe nanoparticles, 90 vol% ethanol was used to reduce possible iron corrosion and side-reactions (Xu and Bhattacharyya, 2007). The pH was adjusted to pH 5 to drive the iron and palladium metals towards the core of HPEI, enabling their encapsulation (Zhu et al., 2015). The HPEI modified membrane were immersed in the Fe²⁺/Pd²⁺ solutions and mechanically stirred for 24 h. A freshly prepared sodium borohydride (NaBH₄ 0.1 M in 100 mL distilled water) solution was added drop-wise into the HPEI/PSf-Fe²⁺/Pd²⁺ mixture at a rate of 1-2 drops per second with mechanical stirring under a N₂ environment. Sodium borohydride (NaBH₄) was used to simultaneously reduce the iron and palladium

metals to metal ions (Fe^0/Pd^0). Upon reduction, a visual colour change on the membranes from white to black was observed (Figure 5.2).

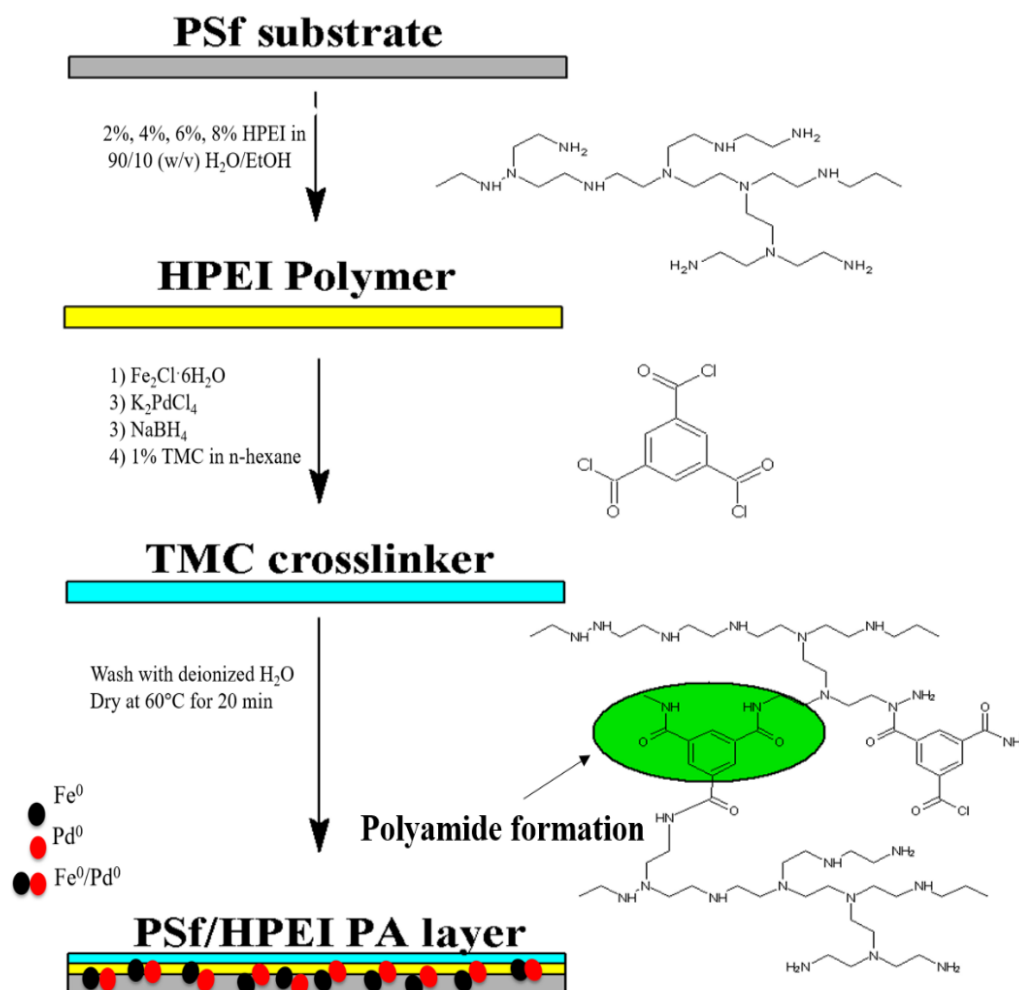


Figure 5.1. Preparation of PSf/HPEI-Fe/Pd membranes

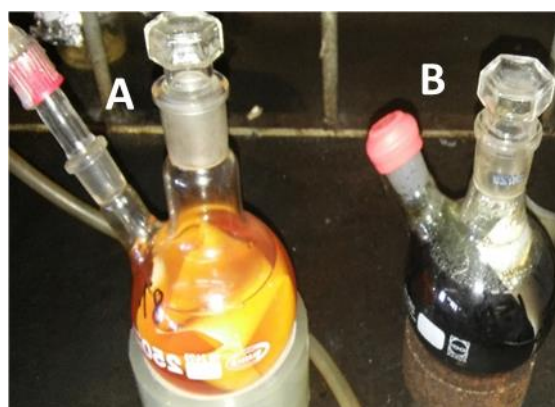


Figure 5.2. Colour change of the solution containing HPEI/PSf-Fe/Pd (A) before and (B) after reduction of the Fe/Pd bimetallic nanoparticles.

5.2.4 Characterisation of HPEI-Fe/Pd-PSf membrane

The structural changes were observed using Fourier transform-infrared-attenuated total reflectance mode (FTIR-ATR) (PerkinElmer Spectrum 100). The contact angle measurements were recorded at room temperature using a DataPhysics Optical Contact Angle (OCA) 15 EC equipped with video capture. A series of 5-10 measurements were conducted at different sites per sample and all measurements were recorded at room temperature, after which the average was used as the final contact angle measurement. The concentration of the metal ions in solution was measured using inductively coupled plasma optical emission spectrometry (ICP-OES), Thermo Scientific (iCAP 6500 duo). The surface morphologies and cross-section of pristine PSf and modified membranes was observed using FEI Nova NanoLab 600 SEM. Following surface imaging of the region of interest, a lamella was lifted out of the membrane sample and its thickness gradually reduced using FIB. The specimen was then imaged via scanning electron microscopy (SEM) in the FIB-SEM. Following this treatment, the Fe/Pd nanoparticles inside the membrane pores could then be directly observed (Wan et al., 2017). A Rigaku Ultima IV XRD spectrometer (Rigaku Corporation, Japan) was used to investigate the phases of the nanoparticles (Ndlwana et al., 2013). The membranes were fitted into aluminium holders. The anode material used on this instrument was copper (K α) which generated 40 KV X-rays at 40 mA towards the sample placed on a spinning stage. The scan speed and step width used for analysis was 1 $^\circ$ /min and 0.01 $^\circ$, respectively. The SPECS PHOIBOS 150 hemispherical energy analyser and a monochromatised aluminium (K α) photon source (hv=1486.71 eV) were used for X-ray photoelectron spectroscopy (XPS). The overall energy was set to 0.5 eV for all the spectra shown.

5.2.5 GC-MS procedure

Solid phase extraction has been used to extract, clean, and enrich/pre-concentrate the analytes in water samples using Restek™ Bonded Reversed Phase Resprep SPE Cartridges C18; Volume 6 mL/250 mg. The SPE cartridges were conditioned with 10 mL of methanol, ultrapure water and n-hexane, respectively. The water samples (10 mL) containing the target analytes were loaded onto the SPE cartridge followed by washing with 10 mL of deionised water. The SPE disks were then subjected to air drying for 10 min to remove excess water/solvent before eluting the analyte compounds with n-hexane (3 \times 5 mL). The extracted solution was finally evaporated and reconstituted to a volume of ca. 2 mL using nitrogen gas prior to GC-MS analysis (Madikizela et al., 2014). The concentration of PCB 153 was measured by gas chromatography coupled with mass spectrometry GC-MS (Agilent 7890) equipped with a Restek RXi 5Sil MS column (30m \times 0.25 mm ID \times 0.25 μ m). Helium was used as carrier gas at constant flow of 1 mL/min. One microlitre (1 μ L) of the PCB extract was injected in splitless mode into the column. The oven temperature programme was as follows: 60 $^\circ$ C (5 min), 20 $^\circ$ C \cdot min $^{-1}$ to 200 $^\circ$ C (1 min), 10 $^\circ$ C \cdot min $^{-1}$ to 305 $^\circ$ C (5 min). The purge time and purge flow was 90 seconds and 20 mL \cdot min $^{-1}$, respectively. The ion source was operated at 250 $^\circ$ C. The electron energy was -70 eV. The data acquisition rate was 10 spectra/s, covering a mass range of 35-600 m/z. The 2,2',4,4',5,5'-hexachlorobiphenyl (PCB 153) stock solutions were diluted in n-hexane to cover a calibration range of 1, 5, 10, 15, 20 and 25 mg/L. For each experimental sample vial, 1 mL of the sample was spiked with 50 μ L of PCB 180 which was used as an internal standard. Prior to the GC-MS analyses, the sample vials were vortexed for 5 min to ensure that a homogeneous solution was obtained. Finally, the sample vials were transferred to the GC auto-sampler for analysis. The data processing was carried out on LECO GC-TOFMS ChromaTOF software. This software deals with noise and instrumental fluctuations, deconvolution of overlapping peaks, and identifying deconvoluted peaks based on mass spectral matching (Hilton et al., 2010).

5.3 RESULTS AND DISCUSSION

5.3.1 FTIR analysis

Structural modification of the membranes was confirmed using FTIR-ATR analysis, illustrated in **Figure 5.3**. Adsorption bands for polysulfone which showed peaks at $1\ 550\ \text{cm}^{-1}$ and $2\ 843\ \text{cm}^{-1}$ were ascribed to $-\text{SO}_2$ stretching and $-\text{CH}$ stretching, respectively. Additionally, bands were observed at $1\ 576\ \text{cm}^{-1}$, $1\ 641\ \text{cm}^{-1}$ and $1\ 722\ \text{cm}^{-1}$, corresponding to an amide-II (primary NH_2) band of the amide groups ($-\text{CONH}-$), amide-I ($-\text{C}=\text{O}$) stretching, and $\text{C}=\text{O}$ stretching of the carboxylic acid ($-\text{COOH}$) which resulted from the hydrolysis of the acyl chloride ($-\text{COCl}$) from TMC, respectively (Xiang et al., 2014). Two new adsorption bands were identified at $3\ 124\ \text{cm}^{-1}$, corresponding to NH_2 stretching, and $3\ 350\ \text{cm}^{-1}$ which was attributed to primary amine stretching from HPEI and hydroxyl functional groups from COOH (Masuelli, 2013). It is evident that the latter becomes more pronounced as the loading of HPEI increases. Therefore, from the obtained results, it was clear that interfacial polymerisation between HPEI and TMC was indeed successful.

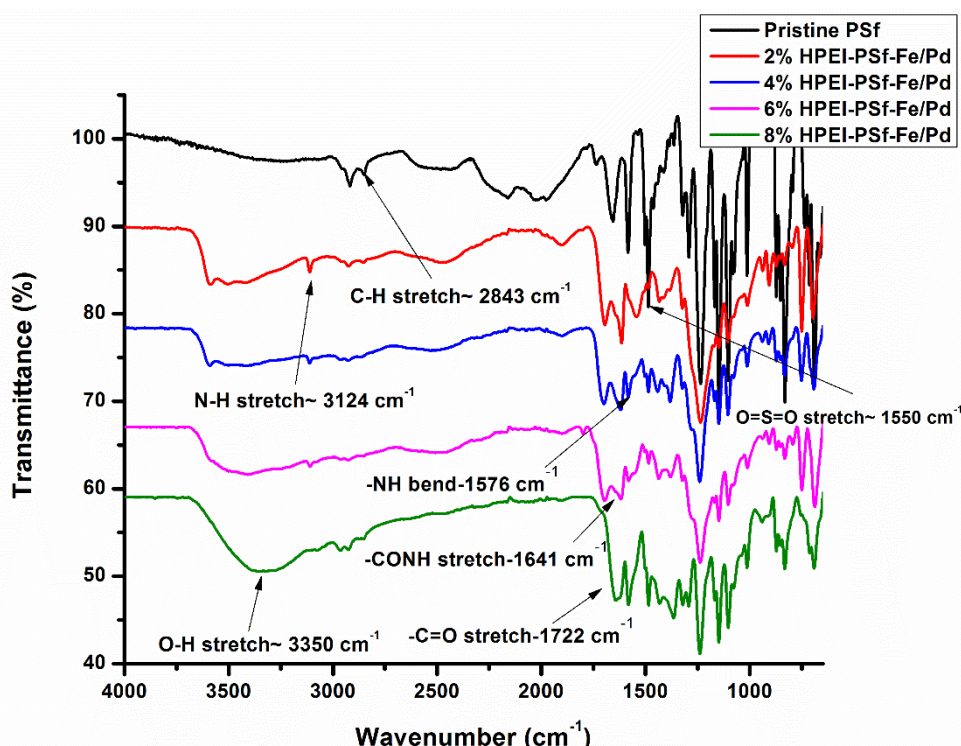


Figure 5.3. FTIR spectrum of pristine and HPEI-Fe/Pd modified membranes

5.3.2 Focused ion beam (FIB)

The cross-section lamella of the bimetallic immobilized membrane was assessed using SEM-FIB, (**Figure 5.4**). The identification of nanoparticles was measured at a depth of $40\ \mu\text{m}$ and a width of $13.67\ \mu\text{m}$ in the membrane. In **Figure 5.4** the membranes lamella was lifted under the membrane surface and the corresponding EDS and EDS mapping images are shown. From the EDS spectra, it was existence of palladium and iron evident. The peak observed at $K\alpha = 9.241$ corresponds to gallium which was used as the ion source to slice the membrane into its lamella. An observation was made which confirmed the nanoparticles were not only on the surface of the membranes but also inside the membrane network. These findings were also reported by Wan *et al.* (2017), where SEM-FIB successfully characterized Fe/Pd bimetallic system in a polyacrylic acid functionalized PVDF membrane (Wan *et al.*, 2017). Typically, nanoparticle agglomeration is caused by inter-particle interactions such as Van der Waals forces. Fe^0 as a magnetic metal can result in more

intense agglomeration due to the strong magnetic interactions (Xu, 2007). This aggregation leads to the decrease in mobility and reactivity of these nanoparticles (Lu *et al.*, 2016). EDS mapping furthermore complemented the presence and uniform dispersion of iron and palladium in the membrane. Minimal nanoparticle agglomeration was observed in these images. The reason for the observed uniform dispersion may be attributed to properties of these selected HPEI polymer. Firstly, it contains a high number of internal amine functional groups, effectively acting as ligands which can complex to Fe and Pd. HPEI possess nanocavities within its structure which act as a template for the preparation of narrow and stable nanoparticles (Wan and 2017). Furthermore, the quaspherical structure of HPEI provides a shell to prevent aggregation of the nanoparticles (Malinga, 2013). It was therefore clear from **Figure 5.4 (B-D)** that iron and palladium were the major constituents in the material, denoting successful synthesis of the metallic particles.

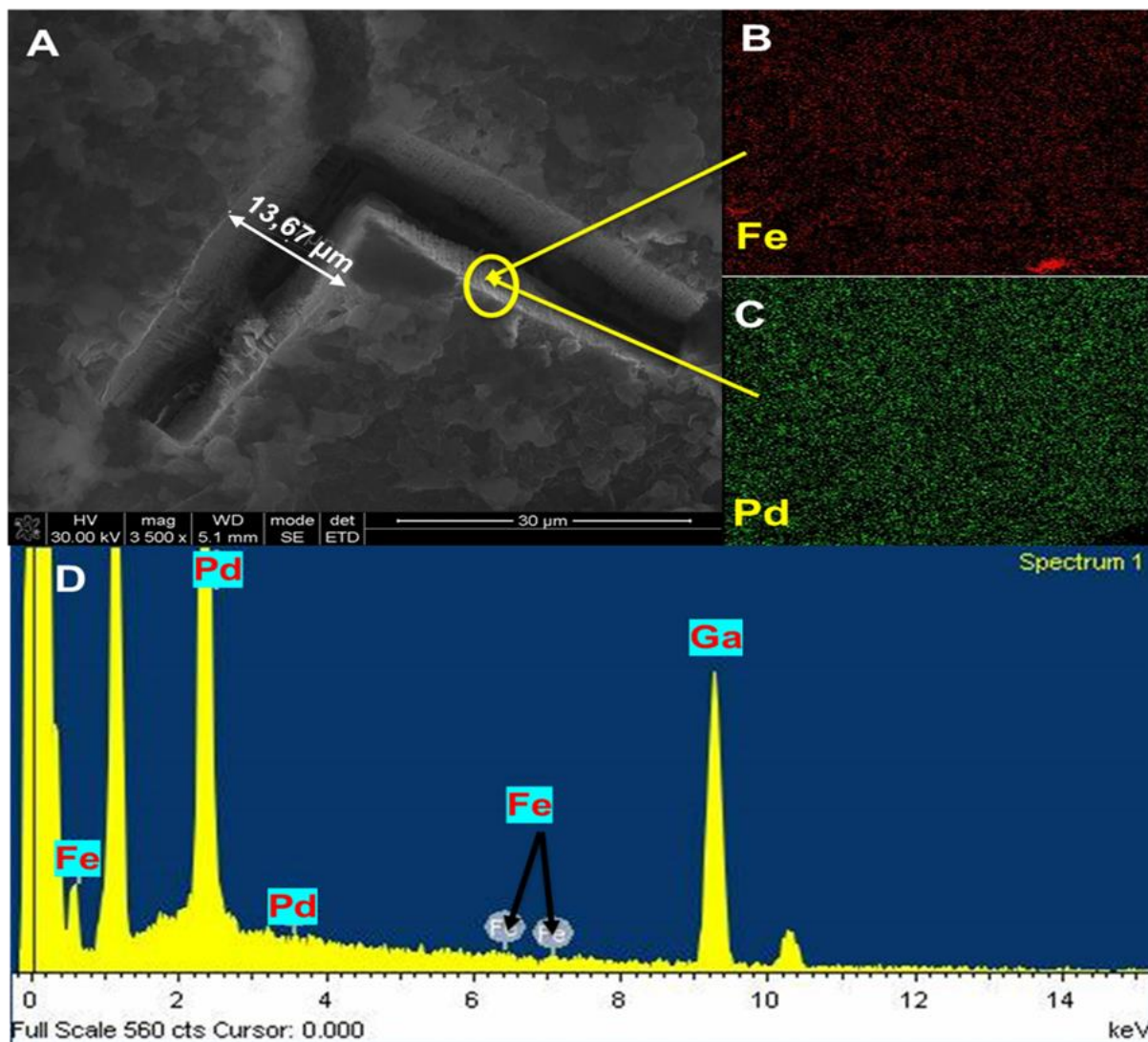


Figure 5.4. SEM-FIB and EDS mapping images of 8% HPEI/PSf-Fe-Pd membrane

5.3.3 X-Ray diffraction (XRD)

The XRD patterns of pristine and HPEI-Fe/Pd modified membranes are shown in **Figure 5.5**. From XRD the confirmation of zero-valent iron (Fe^0) was seen at 2θ values of 44.8° (110) and 64.78° (200) according to data from literature (Smuleac et al., 2010; Ndlwana et al., 2012; Wang et al., 2014b). The XRD pattern of Pd^0 contains characteristic peaks at 38.1° (111) and 46.6° (200) (Venkatachalam et al., 2008). This technique can mainly be used as a qualitative analysis tool to quantify changes in the structure of the materials especially polymeric membrane materials. Since HPEI acts as a protective layer to the nanoparticles, it does not only prevent nanoparticle agglomeration but also the exposure to air. This protective layer effectively shields the nanoparticles from the X-ray source, leading to a decrease in the peak intensity. Thus, XRD could confirm the bimetallic phase of Fe and Pd with respect to their individual XRD 2θ values.

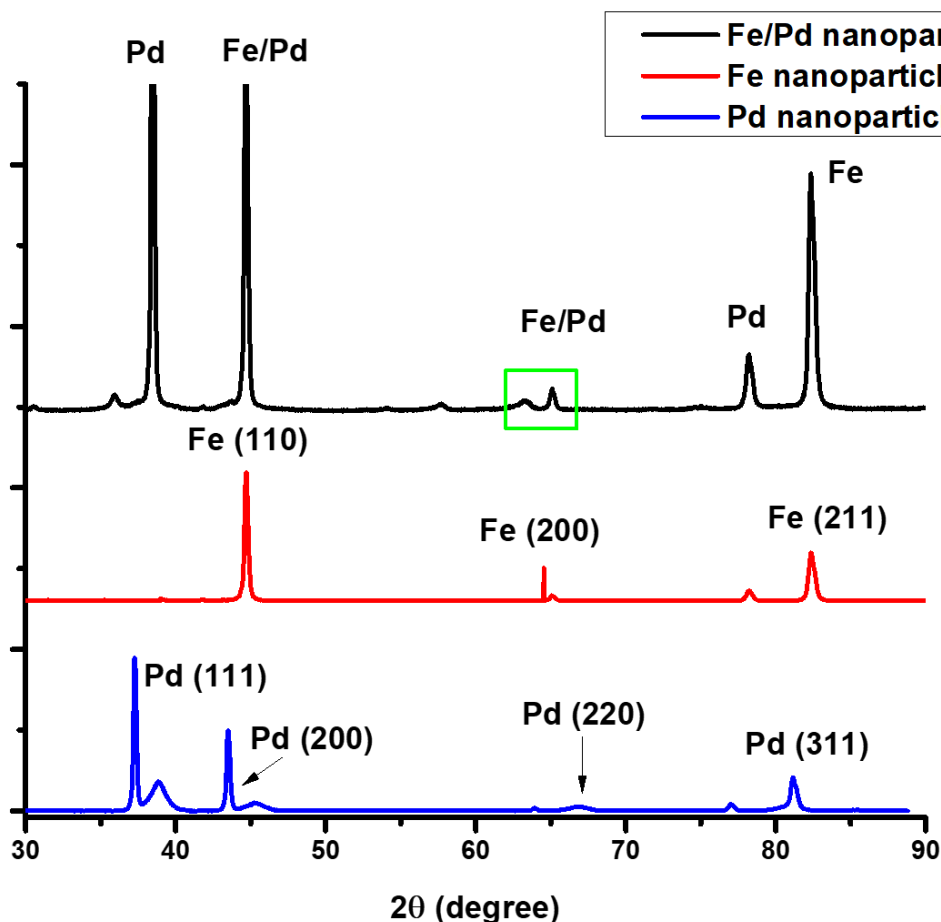


Figure 5.5. XRD spectra of Fe, Pd and Fe/Pd nanoparticles

5.3.4 X-Ray photoelectron spectroscopy

XPS analyses was used to investigate the surface chemical compositions of the Fe/Pd nanoparticle immobilized membranes. The deconvoluted XPS spectra is presented in **Figure 5.6**. The C1s core-level spectrum of HPEI/PSf-Pd/Fe NPs [**Figure 5.6 (A)**] is fitted to two peaks at 284.4 and 286.3 eV, corresponding to the C-C and C-O species, respectively (Biesinger *et al.*, 2011). These carbon peaks arose from the sp^3 C-H and COOH functional groups present in the membranes. The XPS spectrum of N1s is seen in **Figure 5.6 (B)**. This spectrum confirms the presence of a polyamide (CONH) functional group on the membrane. The XPS survey on the region of Fe 2p is presented in **Figure 5.6 (C)**. The Fe 2p photoelectron peaks at 710.9 eV, 718.3 eV, and 724.8 eV are assigned to Fe 2p_{3/2}, Fe 2p_{3/2}, and Fe 2p_{1/2}, respectively (Huang *et al.*, 2017). These peaks are evidence of Fe in its oxidized form (FeO) (Lin *et al.*, 2010). The photoelectron peak observed

at 707.1 eV for Fe 2p_{3/2} confirms the presence of Fe⁰. These peaks were clearly absent in the membrane without nanoparticles. Two peaks with binding energies of Pd 3p_{3/2} = 340.6 and Pd 3p_{5/2} = 335.9 eV which correspond to Pd⁰ was expected but could unfortunately not be identified. The unsuccessful identification of palladium in the membrane matrix was possibly due to the low amount of Pd (25% of Fe loading) in the bimetallic system. The absence of Pd could also be due to the formation of oxides on the membrane surface (Du *et al.*, 2013).

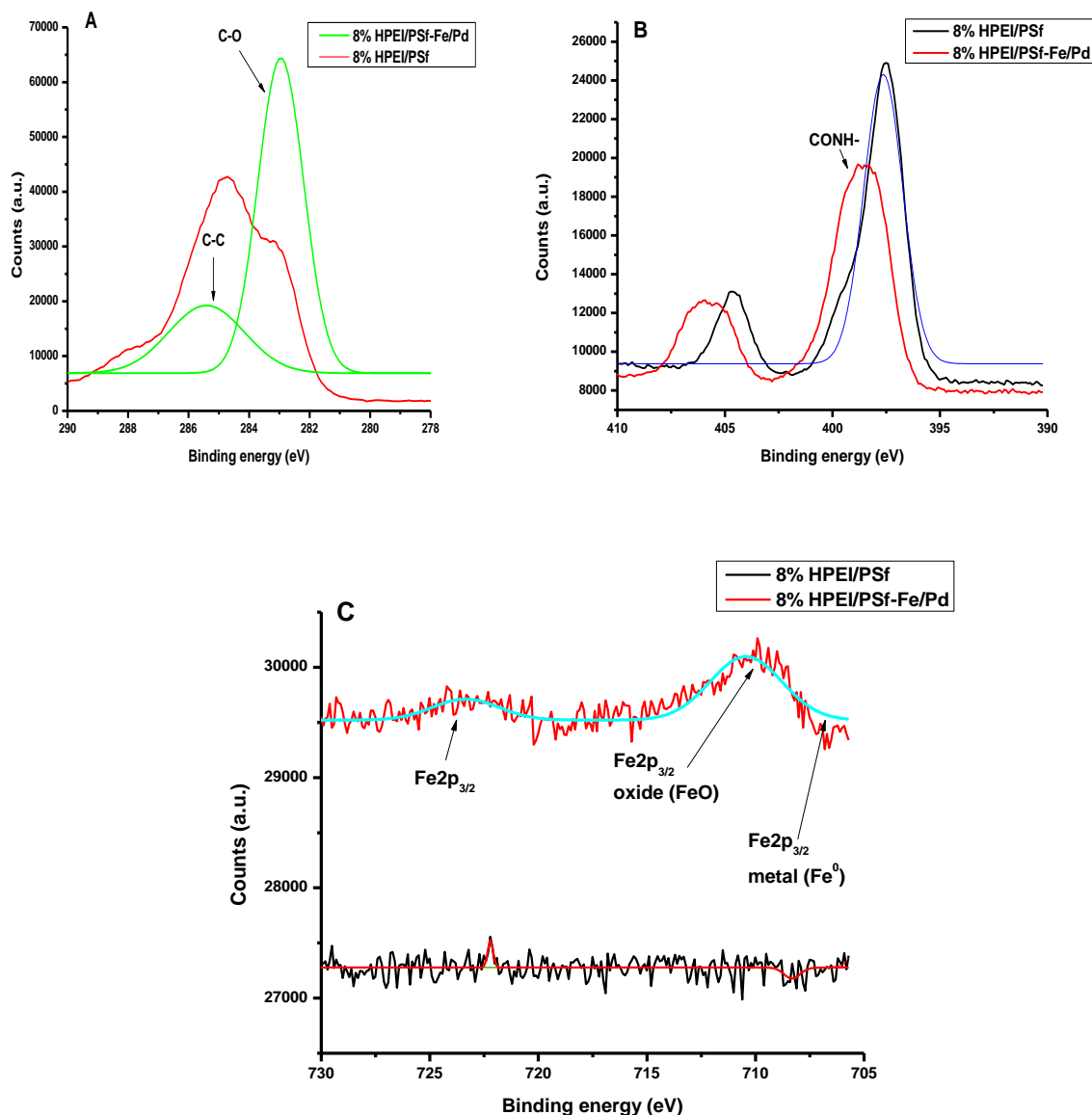


Figure 5.6. XPS spectra of (A) C1S, (B) N1S and (C) Fe 2p of 8% HPEI/PSf and 8% HPEI/PSf-Fe/Pd membranes

5.3.5 Water permeation and contact angle analysis

Contact angle and water uptake measurements were conducted for the various membranes, as shown in **Figure 5.7**. Contact angle measurements provide crucial information on the hydrophilicity of the membranes. The pristine membrane showed the highest contact angle (73°) whereas all the modified membranes had contact angles well below that of the bare PSf membrane. As illustrated in **Figure 5.7**, the hydrophilicity increases (decrease in contact angle) upon modification of HPEI due to the copious amounts of amine functional groups on the surface of the HPEI modified membrane. This decrease in contact angle (CA) can be ascribed to an increase in the effective surface area of HPEI, allowing water molecules to interact with terminal

amine functional groups. Furthermore, the HPEI modified membranes provide high polarity to the membrane surface that attracts polar molecules such as water. Thus, modification introduced more sites for hydrogen bonding to occur. The contact angle further decreases to a minimum of 25.3° for the 6% HPEI-PSf-Fe/Pd membranes; this is in good agreement with FTIR analysis (**Figure 5.7**) where NH₂ and COOH bands were observed. Water uptake capacity measurements of the membranes coincided with contact angle results. The water uptake of the membranes ranged from 39.8% for the pristine PSf membrane, to 91% for the 8% HPEI-PSf-Fe/Pd membrane. This trend can be explained by the unreacted acyl chloride functional groups from TMC which can form carboxylic acid (COOH) groups once reacted with moisture as shown in the FTIR spectrum. Thus, from **Figure 5.7** it was clear that the presence of NH₂ and -COOH functional groups not only enhances hydrophilicity but also improves water uptake of the membranes (Obaid et al., 2015).

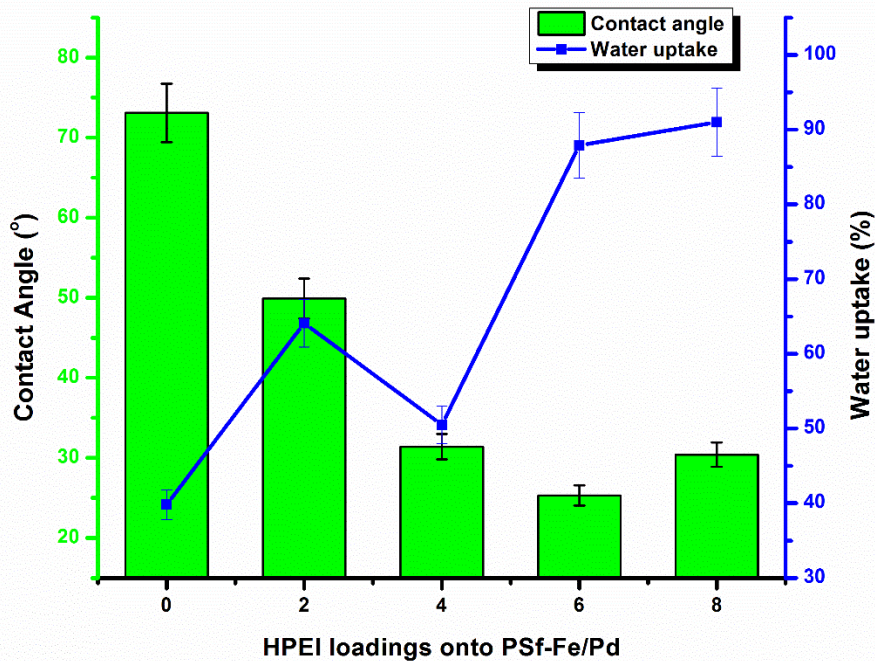


Figure 5.7 Membrane contact angle vs. water uptake

Figure 5.8 illustrates the pure water flux of the pristine and modified membranes. It could be deduced that the pure water flux clearly increases proportionally with pressure. At a transmembrane pressure of 600 kPa, the pure water flux of the pristine PSf membrane was 888.3 L·m⁻²·h⁻¹. The pure water flux for the modified membranes ranged from 195.5 L·m⁻²·h⁻¹ for the 2% HPEI/PSf-Fe/Pd which displayed the lowest water flux to 1 294.3 L·m⁻²·h⁻¹ for the 4% HPEI/PSf-Fe/Pd modified membrane. The observation made from this analysis was that at extreme loadings (i.e. 2% and 8% HPEI/PSf-Fe/Pd) the water flux was the lowest in comparison to the pristine and other intermediate loadings (4% and 6% HPEI/PSf-Fe/Pd). During the membrane drying process, HPEI can be insolubilised (Wu et al., 2014). The HPEI not only covers the surface of the PSf substrate but also diffuses into the pores that are large enough to accommodate the macromolecules, resulting in a denser and thicker top layer which subsequently reduces the water flux of the membranes. Conversely, at the intermediate HPEI loadings, the HPEI molecules present in the pores can migrate to the interface via a concentration gradient (Wu et al., 2014).

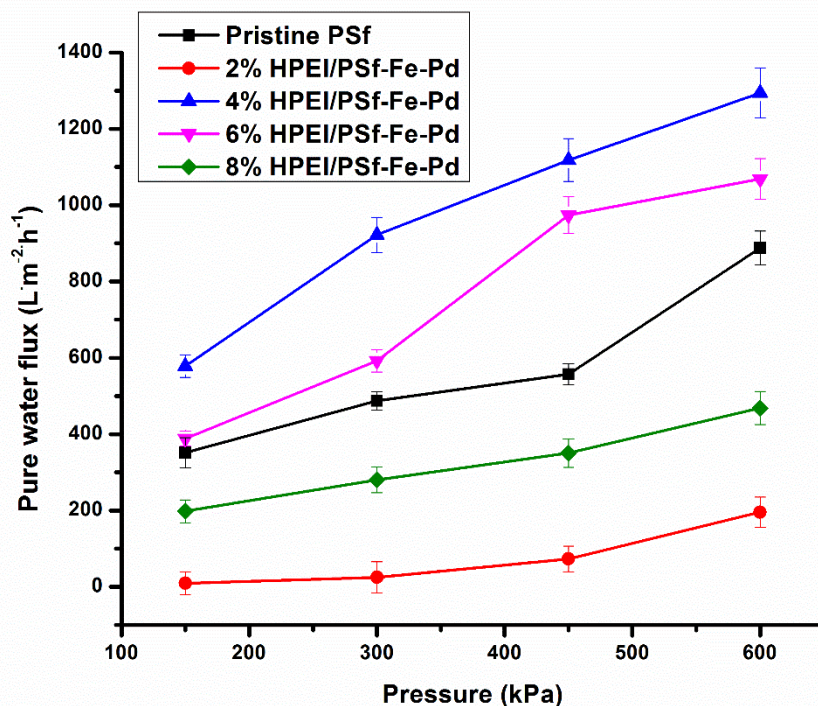


Figure 5.8. Pure water flux vs. transmembrane pressure

5.3.6 GC-MS analysis

The application of the HPEI/PSf-Fe/Pd membranes for the removal of PCB 153 was assessed in a batch study. At various time intervals, PCB 153 samples were collected and extracted via SPE before being analysed on GC-MS. A calibration curve was constructed using PCB 153 standards and the obtained correlation coefficient was $R^2 = 0.99$. The concentration of the membrane treated samples was acquired as a function of time using the equation of the calibration curve and PCB 180 was used as an internal standard for the GC-MS analysis. **Figure 5.9** illustrates the chromatograms for the dechlorination reactions at time 0 h and 24 h for the 8% HPEI/PSf-Fe/Pd membrane. From **Figure 5.9 (A)**, the characteristic peak for PCB 153 can be seen, whereas, after 4 h (**Figure 5.9 (B)**) various peaks were observed corresponding to PCB 101, PCB 29, PCB 153 and PCB 180 (internal standard) (Afful et al., 2013). Based on the retention times of the PCBs, it was confirmed that the dechlorination reaction of PCB 153 with the bimetallic immobilised membrane was successful.

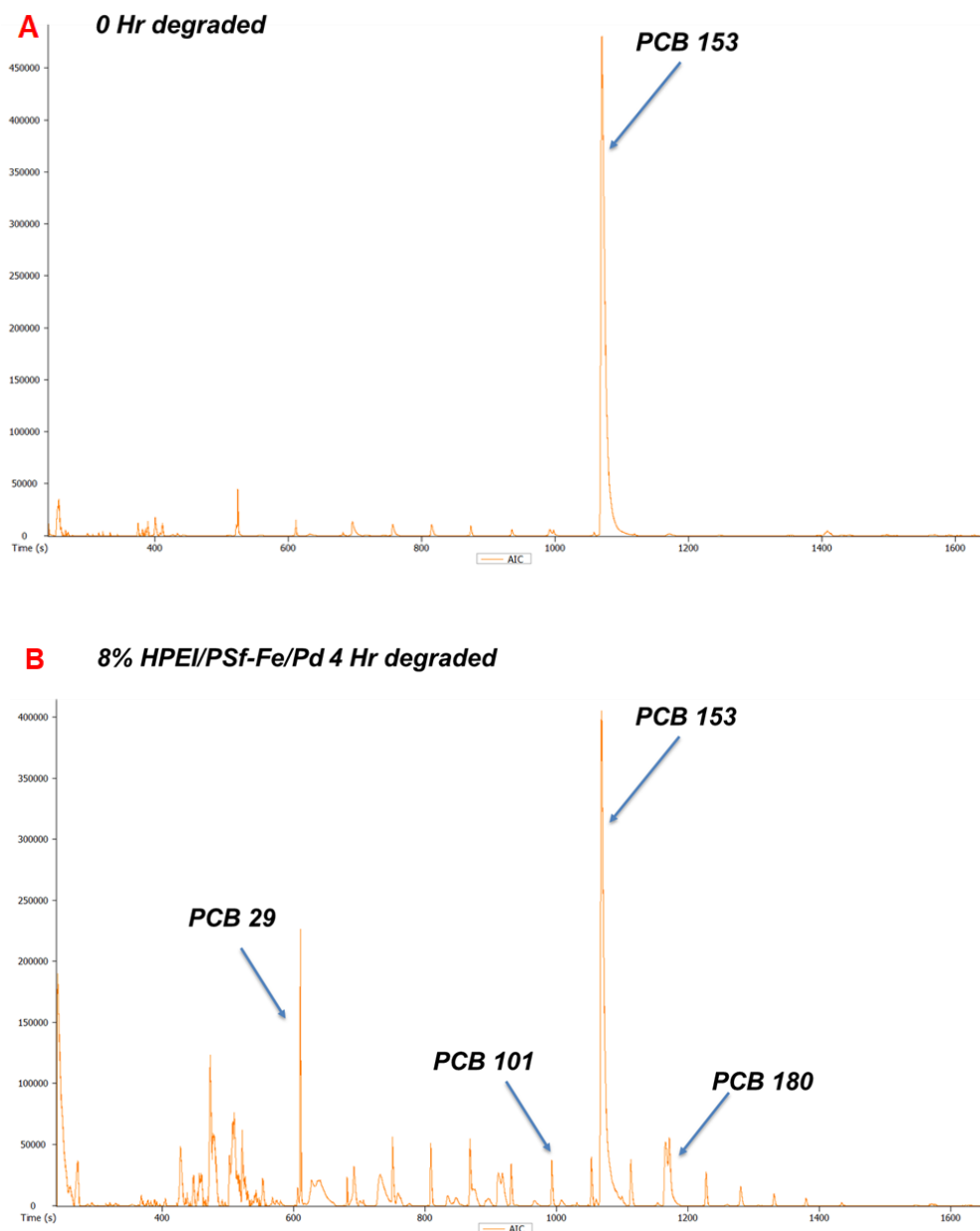


Figure 5.9. Chromatograms of (A) 0 h dechlorination and (B) 4 h dechlorination of 8% HPEI/PSf-Fe/Pd membrane

The dechlorination of PCB 153 is illustrated in **Figure 5.10**. A general trend observed for the dechlorination reaction was that the catalytic activity of the Fe/Pd nanoparticles increased with increasing treatment time. However, the 8% HPEI/PSf-Fe/Pd membrane displayed the highest PCB removal (93.3% removal) within 4 h of treatment. The removal of PCB 153 within 4 h followed the sequence: 8% HPEI/PSf-Fe/Pd > 4% HPEI/PSf-Fe/Pd > 6% HPEI/PSf-Fe/Pd > 2% HPEI/PSf-Fe/Pd. This observation was attributed to the size and distribution of the nanoparticles in the respective membranes as confirmed by AFM particle size and distribution analysis. A similar finding was reported by Zhou et al. (2016), where a phosphorus-doped mesoporous carbon embedded with Fe/Pd nanoparticles successfully dechlorinated 2,4-dichlorophenol to less harmful phenol (Zhou et al., 2016). In addition, the hydrophobic core of HPEI is well located to capture hydrophobic PCB compounds, whereas the interior and exterior branches can be tailored by metal and/or ionic pollutants through electrostatic and/or hydrogen bonding (Das et al., 2017), thus contributing to the successful dechlorination of PCB 153.

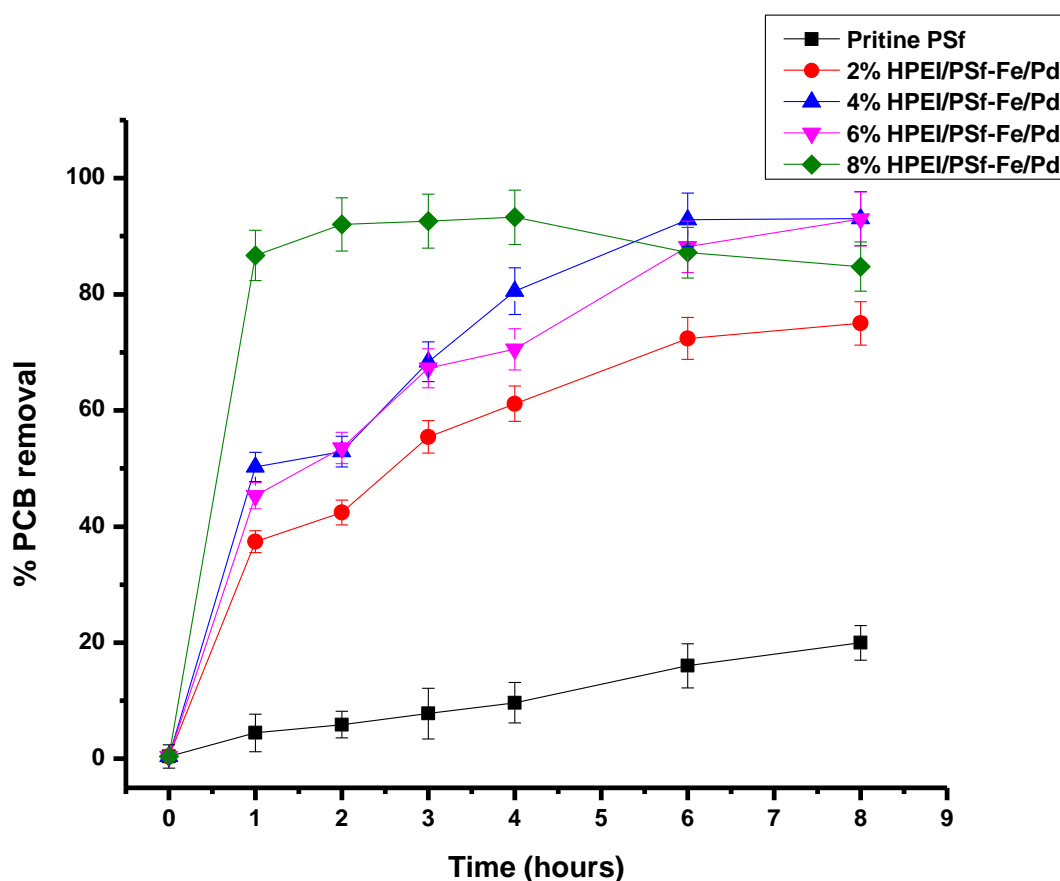


Figure 5.10. PCB removal as a function of time

Studies have shown that the addition of dispersant-supported nanoparticles to a membrane can significantly increase the dechlorination rate and efficiency of the water remediation process. Du et al. (2013) immobilised Fe⁰/Pd⁰ bimetallic nanoparticles in a nylon 6,6/polyethylene glycol (PEG) membrane via co-complexation reduction of the metals. This membrane successfully dechlorinated 85% of pentachlorophenol within 45 min. However, the authors found it difficult to avoid the formation of iron oxides during the dechlorination reactions. The formation of iron oxides impeded the contact of Fe/Pd with pentachlorophenol, effectively reducing the catalytic activity of the bimetallic system (Du et al., 2013). The negative reduction potential of divalent iron ($E^0 = -0.44$ V) and positive standard reduction potential of divalent palladium ($E^0 = 0.91$ V) makes it suitable for the removal of chlorine atoms from the chlorinated organic compounds (Yoo et al., 2007). The effective removal of PCB 153 in the Fe/Pd system is due to their high reduction potential ($E^0 = +0.5$ to 1.5 V) (Wang et al., 2014b). In this bimetallic system, palladium collects H₂ generated during the iron corrosion reaction and decomposes it into atomic H, which can then be used to replace chlorine atoms in PCB compounds (Venkatachalam et al., 2008).

5.3.7 Dechlorination mechanism

The effect of treatment time and predominant PCB by-products can be seen in **Figure 5.11 (A)**. In this figure, the dechlorination activity of the nanoparticles shows optimum removal in the first 4 h of treatment. As shown in **Figure 5.11(B)**, the most prominent PCB congeners after treatment with Fe/Pd membranes were tetrachlorobiphenyl (PCB 52; 290 m/z) and dichlorobiphenyl (PCB 29; 220 m/z) illustrating that these PCBs are preferably generated during the degradation of PCB 153 (360 m/z) (Nikonova and Gorshkov, 2011; Wang and He, 2013)

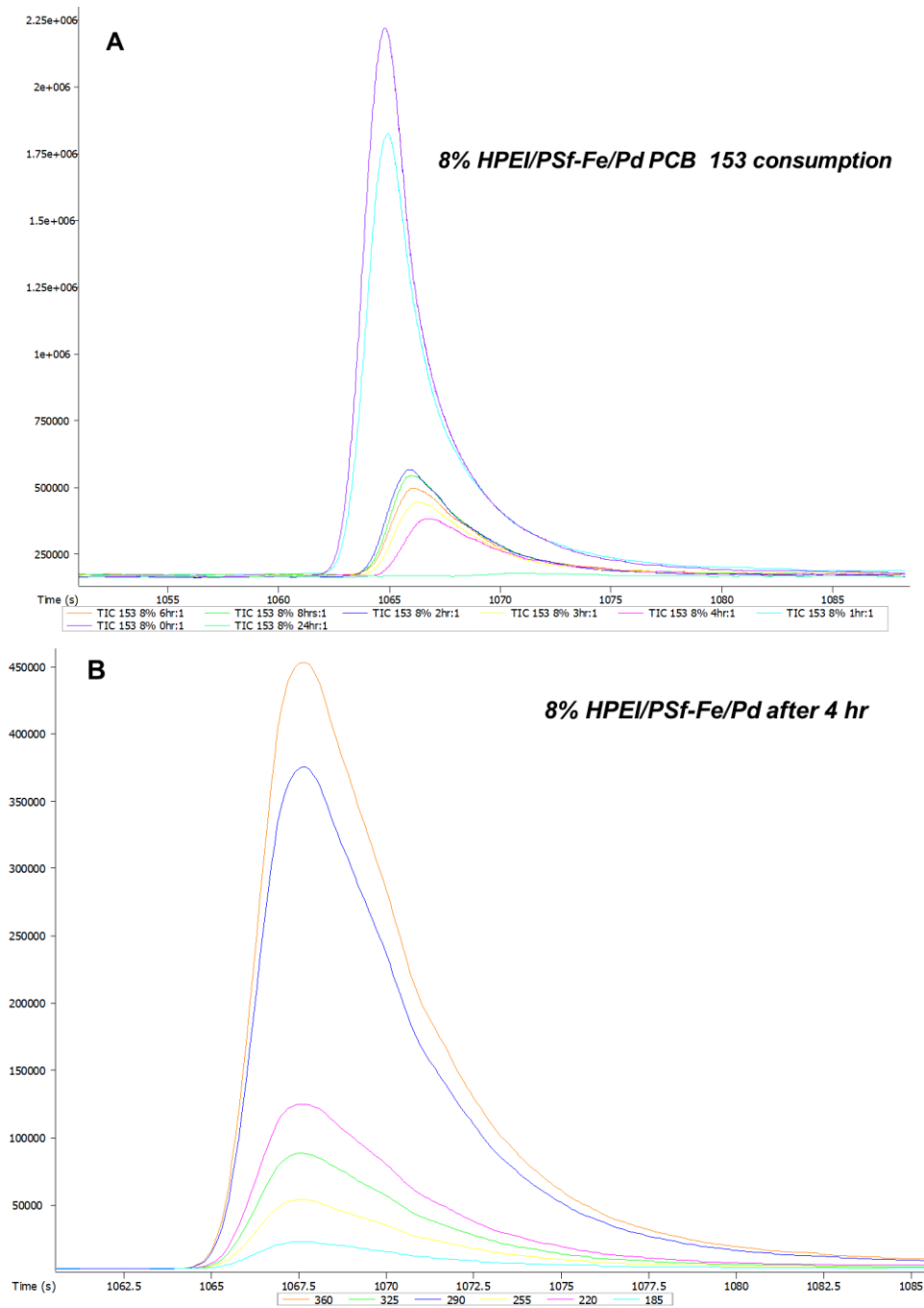


Figure 5.11. Chromatograms of (A) PCB consumption as a function of time, and (B) selected ion chromatogram of PCB congeners

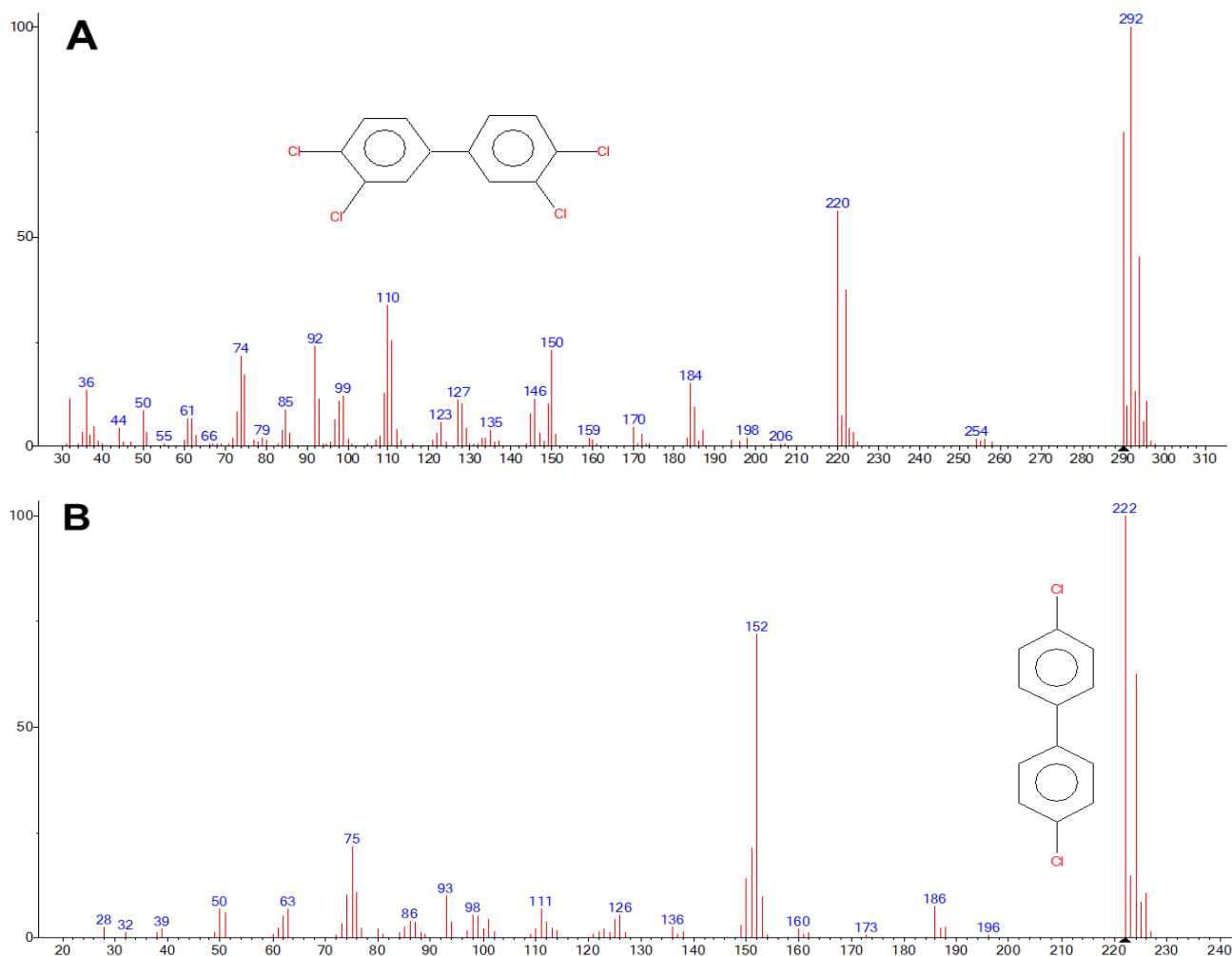


Figure 5.12. Mass spectrum of predominantly generated PCB by-products: (A) tetrachlorobiphenyl; and (B) dichlorobiphenyl

A proposed dechlorination reaction mechanism is shown in **Figure 5.13**. As iron corrodes, protons from water are reduced to adsorbed H atoms and to molecular hydrogen at the catalytic Pd surface. Thereafter, the PCB is adsorbed onto the surface of the Fe/Pd particles where the C-Cl bond is broken, and the chlorine atom is replaced by hydrogen.

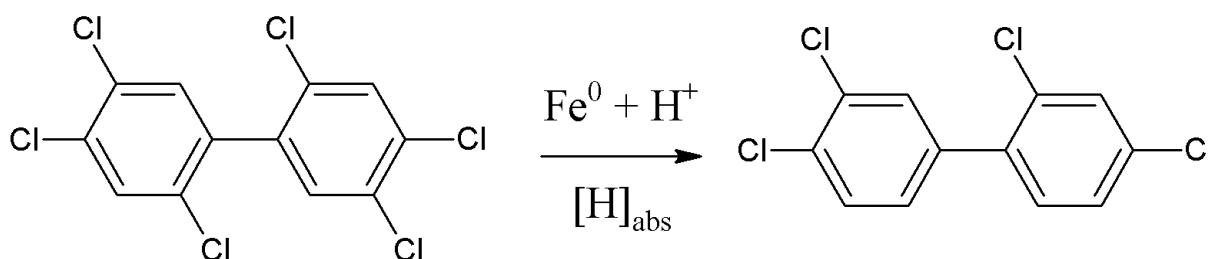


Figure 5.13. Proposed dechlorination reaction

5.3.8 Leaching studies

Inductively coupled plasma optical emission spectroscopy (ICP-OES, VARIAN) was used to measure the concentration of metal ions in solution. The amount of absorbed Fe and Pd in the ion exchange process was determined by mass balance after the metal complexation process (Wan et al., 2017). The amounts of zero-valent iron (ZVI) and coated Pd in the membranes were measured by digesting Fe/Pd immobilised membranes in dilute nitric acid (25%). From the obtained results, it was confirmed that the ratio of iron to palladium (Fe:Pd) in the membrane was roughly 4:1. Furthermore, the obtained conformation of the bimetallic nanoparticles was a core-shell structure. According to the South African Water Quality Guidelines, SANS allows an iron daily intake of 200 µg/L whereas palladium intake can be 5 mg/L (DWAF, 1996). In **Table 5.1** it can be observed that the leaching of the Fe and Pd bimetallic system was very low.

Table 5.1. Leaching results of 8% PSf-HPEI-Fe/Pd membrane

Leaching conditions	Metals	Day 1 (% leached)	Day 2 (% leached)	Day 3 (% leached)	Day 4 (% leached)
Water	Fe	0.0015	0.0009	0.0019	0.0005
	Pd	0.0093	0.0091	0.0086	0.0081
Leaching conditions	Metals	2 hours (% leached)	8 hours (% leached)	12 hours (% leached)	24 hours (% leached)
Nitric acid (25% HNO ₃)	Fe	0.0058	0.0044	0.0042	0.0033
	Pd	0.25	0.21	0.15	0.14

The original concentration of Fe on the membranes was 200 mg/L whereas that of Pd was 50 ppm. During the first two hours of batch studies, the leaching of these metals was the highest for the 4% HPEI loaded membrane (0.04 mg/L for Fe and 0.134 mg/L for Pd). However, as the time of digestion in nitric acid increased, the leaching of the metals subsequently decreased. After 24 hours of digestion in HNO₃, less than 0.03 ppm of iron was leached out of the membranes. In addition, less than 0.11 mg/L of palladium was leached out of all membranes. The general high leaching of the metals in the first two hours could be attributed to unreacted Fe and Pd nanoparticles which agglomerated on the surface of the formed composite hence it was easy to be leached out from the membrane. The interaction mechanisms consisted of ion exchange, chelation and electrostatic binding in the composite membranes. The leaching of Pd content is assumed to be the result of the interaction between Fe and the exposed functional groups (-COOH and -NH₂). Due to the strong magnetisation of Fe⁰, it has intense interactions with Pd⁰ resulting in strong Van de Waals interactive forces between the two metals. However, due to the core-shell conformation, we hypothesise that the palladium was more easily leached out than the iron. Seteni et al., 2014 obtained similar results in their study where Fe and Ni displayed minimal leaching. In their study, the authors argued that the leaching of the secondary metal (Ni) was caused by unreacted Fe⁰ on the surface of the membrane which resulted in the leaching of Ni (Seteni et al., 2014). A general trend was observed for the batch studies done in water. In these results the membranes showed minimal metal leaching after a period of four days. All membranes displayed iron leaching of <0.0075mg/L. Correspondingly, less than 0.445 mg/L palladium was leached out of the membranes. The leaching of palladium, which was higher than that of iron once again, could be ascribed to the core-shell bimetallic conformation. However, when compared to the South African Water Quality Guidelines, these obtained leaching concentrations of the metals are well below the stated limits. Therefore, the immobilisation of Fe/Pd onto the HPEI modified membranes showed negligible leaching, thereby concluding successful embedding within and on the surface of the membranes.

5.4 SUMMARY

Results obtained in this study confirmed that interfacial polymerization between HPEI and TMC was successful. This was verified by FTIR spectroscopy. SEM-EDS and FIB confirmed the successful immobilization of the bimetallic nanoparticles in and on the membrane surface. Contact angle results indicated an increase in hydrophilicity of the membranes as the degree of HPEI increased. SEM-EDS mapping displayed homogenous and good dispersion of the nanoparticles on the membranes surface. XRD and XPS analyses confirmed the presence of iron and palladium in their zero-valent state. AFM data illustrated a change in surface morphology as well as surface roughness ranging from 6.5 nm to 28.2 nm with bulk particle sizes ranging from 44.7 to 127.4 nm upon HPEI loading. Metal leaching studies showed that the leaching of both metals was minimal. These leached out concentrations of both Fe and Pd metals were well below the allowable limited. The dechlorination efficiency of the bimetallic immobilized membranes showed optimum performance within 4 hours of treatment with an average removal of 92%. The predominant dechlorinated by-products were tetra- and dichlorobiphenyls.

CHAPTER 6: DEGRADATION OF TRICHLOROPHENOL USING HPEI/MWCNTs/PES MEMBRANES INCORPORATED WITH FE-CU BIMETALLIC

6.1 INTRODUCTION

The main aim of this study was to synthesise, characterise and apply the HPEI/MWCNTs/Fe-Cu/PES membrane for the removal of organic pollutants from water.

6.2 EXPERIMENTAL

6.2.1 Materials

Commercial multiwalled carbon nanotubes (MWCNTs) were purchased from Sigma Aldrich. The diameter and the length ranged between 10-20 nm and 3-6 μm , respectively. Sulphuric acid (98%), nitric acid (65%), N,N-dimethylformamide (AR), thionyl chloride (AR), hyperbranched polyethyleneimine (average $M_w = 25\ 000$ g/mol), potassium bromide (AR) and dialysis tubing, average flat width of 32 mm, were also obtained from Sigma Aldrich.

6.2.2 Preparation of f-MWCNTs-COOH

In order to remove the impurities of raw multiwalled carbon nanotubes (such as the metallic catalyst particles and amorphous carbon) and graft functional groups onto the surface of MWCNTs, the MWCNTs were treated with sulphuric acid and nitric acid. The MWCNTs (1.0 g) (**Figure 6.1a**) were refluxed for 12 h at 70°C in an acid mixture of $\text{H}_2\text{SO}_4:\text{HNO}_3$ (3:1) (Motchelaho et al., 2011). The purified and functionalised MWCNTs (f-MWCNTs) were filtered and washed with distilled water until the pH was neutral. The product was washed with acetone before drying in an oven at 100°C for 12 h.

6.2.3 Preparation of MWCNTs-COCl

In order to prepare MWCNTs-COCl, 1 g of MWCNTs-COOH (**Figure 6.1b**) was added to thionyl chloride (20 mL) and DMF (10 mL). The mixture was refluxed under constant stirring for 24 h. The black product was filtered and dried at 100°C for 6 h. The final weight of the acyl derivative yielded (0.88 g, 88%) from the initial weight of MWCNTs-COOH.

6.2.4 Synthesis of HPEI-MWCNTs

Attachment of MWCNTs-COCl onto HPEI (**Figure 6.1c**) was carried out according to a method reported by Shen et al. (2009). The prepared MWCNTs-COCl (1.0 g) was added to a solution containing HPEI. The HPEI (0.2 mmol) was dissolved in distilled water (20 mL). Then, 10 mL of N,N-dimethylformamide and 200 μL of triethylamine (TEA) were introduced into a reaction mixture. The overall solution was refluxed and heated to 60°C for 48 h. The excess DMF and by-products were removed from the mixture by dialysis against water (Shen et al., 2009).

6.2.5 Synthesis of bimetallic nanoparticles on HPEI-MWCNT nanocomposite

The nanoparticles deposited onto the HPEI-MWCNTs were prepared using the solvothermal polyol method. First, HPEI-MWCNTs (0.1 g) were added to an ethylene glycol solution and transferred into an autoclave. Thereafter, a solution of iron(III) chloride (0.4 g), and copper(II) sulphate (0.1 g) was prepared. The metal solution was bubbled with nitrogen for an hour to prevent the oxidation of Fe(III) before the reaction occurred. The mixture was heated at 150°C for 6 h and the resultant HPEI-MWCNTs-Fe/Cu composite was purified by centrifuging and rinsing with ethanol. The product was dried at 80°C for 12 h under nitrogen to prevent the oxidation of Fe(III). The overall reaction scheme for the decoration of HPEI-MWCNTs with Fe or Cu nanoparticles is shown in **Figure 6.1d**.

6.2.6 Preparation of HPEI-MWCNTs-Fe/Cu-PES ultrafiltration membranes

The membrane sheet of HPEI-MWCNTs-Fe/Cu-PES membranes was prepared via phase inversion by the induced immersion precipitation technique. The polyethersulfone (PES) and polyvinylpyrrolidone (PVP) powder were mixed in N-methylpyrrolidone (NMP) solvent for 1 h using an overhead stirrer (150 rpm). The precise amount of HPEI-MWCNTs-Fe/Cu was added to the NMP solvent solution under constant stirring by varying the concentration (0.1 wt% and 0.5 wt%) of PES polymer as shown in **Table 6.1**. The prepared composite membrane was stirred for the period of 24 h at 25°C. The overall polymer was again sonicated for 10 min to remove air bubbles. Thereafter, the polymer solution was poured on a glass plate and the membrane was cast using a casting knife at a thickness of 200 µm. The glass plate was immersed in deionised water at 25°C. The resulting polymer film was separated from the glass plate within 30 seconds. The prepared membranes were rinsed and stored in fresh deionised water for 24 h. This was done to remove any residual solvents in the membrane matrix during the phase-inversion process. The membrane was then placed between two filter paper sheets for a period of 24 h at room temperature until it was dry.

Table 6.1. The casting solution of the fabricated membrane

PES (wt%)	HPEI-MWCNTs-Fe/Cu (wt%)	PVP (wt%)	NMP (wt%)
16	0.00	2	82
16	0.10	2	81.9
16	0.50	2	81.5

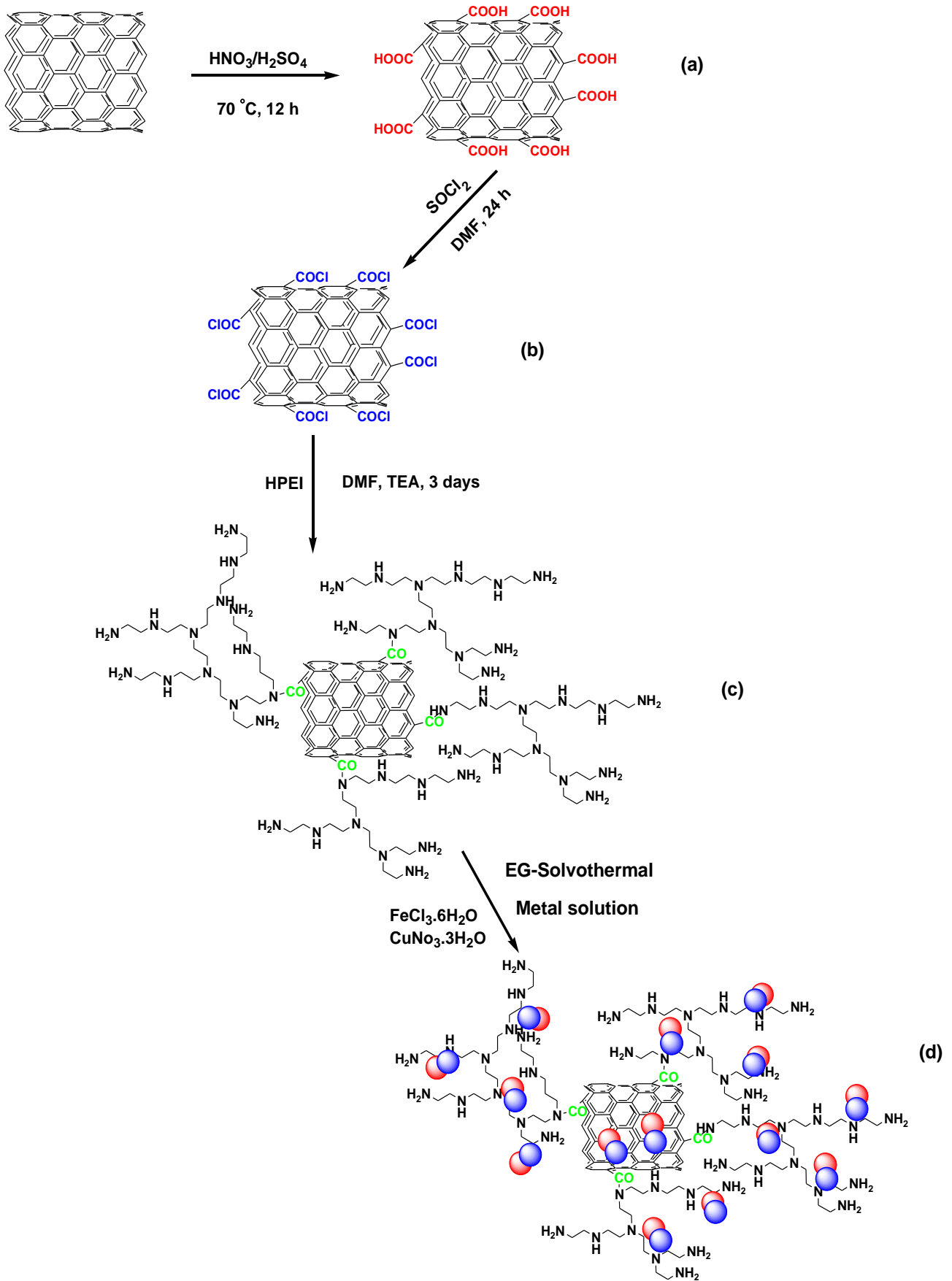


Figure 6.1. Synthesis route for the HPEI-MWCNTs-Fe/Cu composite

6.2.7 Water permeation tests

The membranes were filled up and stabilised with deionised water at a relative pressure (kPa) for 30 min. The permeation test was obtained at a constant water flux using a dead-end filtration cell. Four different pressures were used to measure pure water flux, namely 100 kPa, 150 kPa, 200 kPa, 250 kPa and 300 kPa. The pure water flux (J) was monitored and was calculated as shown in the Equation 6.1:

$$J = \frac{V}{At} \quad 6.1$$

where V is the volume of permeate (L), A is the membrane's effective area (0.00126 m²) and t is the filtration time (h) to collect the permeate volume.

To evaluate the membrane's capability for removal of 2,4,6-trichlorophenol, 2,4,6-TCP (25 µg/L) was passed through the membranes at a constant pressure of 200 kPa. The permeate flux was monitored every 15 min. The permeate was also analysed using liquid chromatography-mass spectroscopy (LC-MS) and the percentage rejection of TCP was calculated using Equation 6.2:

$$R(\%) = 1 - \left(\frac{C_p}{C_f}\right) \times 100 \quad 6.2$$

where C_p and C_f are the concentrations of TCP (µg/L) in the permeate and feed, respectively.

The filtration permeate tests were performed in triplicate.

6.2.8 Membrane fouling and protein rejection

The antifouling property of membrane was evaluated using BSA solution (1 000 mg/L) at 200 kPa according to Vatanpour et al., 2011. The pH of the BSA solution was measured and maintained at 7.2. The permeation experiment was conducted for a period of 180 min under dead-end cell filtration. The water flux was monitored for 60 min (J_{w1}) and the membranes were exposed to BSA solution for 60 min and flux was recorded. The membranes were subsequently washed using deionised water for 30 min and the flux (J_{w2}) was evaluated again for another 60 min. The fouling-resistance ability of the fabricated membranes was evaluated by calculating the flux recovery ratio (FRR) using Equation 6.3:

$$\% FRR = \frac{J_{w2}}{J_{w1}} \times 100 \quad 6.3$$

6.2.9 Characterisation

In order to characterise the membranes, transmission electron micrographs were generated using a JOEL transmission electron microscope (TEM) coupled with EDX model 2010 operated at 200 kV. These measurements were used to study the morphological changes of MWCNTs, MWCNTs-COOH, MWCNTs-COCl and HPEI-MWCNTs. Pristine MWCNTs, MWCNTs-COOH, MWCNTs-COCl and HPEI-MWCNTs were prepared by ultrasonic dispersion of the sample in ethanol. Two drops of each were dropped onto a carbon-coated copper grid. The diameter distributions of MWCNTs were obtained by using ImageJ software. The diameters of about 100 MWCNTs were measured per micrograph. Fourier transform infrared (FTIR) spectroscopy (PerkinElmer Spectrum 100, USA) was used to confirm the presence of functional groups after acidification of the raw MWCNTs and acylation of MWCNTs-COOH. A small quantity of pristine MWCNTs, MWCNTs-COOH and MWCNTs-COCl was mixed with oven-dried potassium bromide in a porcelain mortar. The mixture was then pressed into a small pellet using a mechanical press. Scanning electron microscopy (SEM) images were analysed at an accelerating voltage of 20 kV using a TESCAN Vega TC instrument (VEGA 3 TESCAN software), equipped with an X-ray detector for energy-dispersive X-ray (EDX) analysis operated at 5 kV in order to determine the presence of elements of functionalised multiwalled carbon nanotubes. The cross-section and the surface morphologies of the membrane were observed. The membrane samples were dipped in liquid nitrogen for 5 min, frozen and then broken into two pieces. The dried samples were coated with carbon for introducing the electric conductivity.

The Brunauer-Emmett-Teller (BET) technique was used to determine the specific surface area, specific pore volume and the pore size, and the BET analysis was carried out using a Micromeritics ASAP 2020 and porosity analyser. A sample weight ranging from 200-300 mg was degassed at 110°C for 14 h under vacuum. Nitrogen gas was used as a probe gas. Raman spectra were obtained from the WITec project 2.10 Raman microscope and the laser beam was focused onto the sample using 50X magnification lenses. Membrane hydrophilicity and hydrophobicity were determined by measuring the contact angle and this was conducted using the sessile drop method on a DataPhysics Optical instrument (SCA 20 software) using water as a probe. To minimise the experimental error, the contact angle was measured at about 10 random locations for each membrane surface while maintaining room temperature and the average data were reported. The concentration of by-products of the selected pollutant was measured using a liquid chromatography-mass spectrometer (Shimadzu LCMS-8030 (triple quadrupole)) equipped with a Shimadzu LC-30AD Nexera High Performance Liquid Chromatograph, a Shimadzu SIL-30 AC Nexera Autosampler, and a Shimadzu CTO-20 AC Prominence Column Oven. A C18 column (Shimadzu 2 μm , 2.1 mm \times 100 mm) was used in the analysis. The concentration of the metal ions in solution was measured using inductively coupled plasma optical emission spectrometry (ICP-OES), Thermo Scientific (iCAP 6500 duo).

6.3 RESULTS AND DISCUSSION

6.3.1 FTIR analysis

The FTIR spectra of the pristine MWCNTs, MWCNTs-COOH and MWCNTs-COCl are indicated in **Figure 6.2**. The spectrum of pristine MWCNTs shows the characteristic peaks sp^2 and sp^3 which are attributed to $-\text{CH}_3$ stretch (2906 cm^{-1}) and $-\text{CH}_2$ stretch (2846 cm^{-1}). However, after the oxidation process additional peaks are observed which indicated that MWCNTs-COOH was successfully synthesised. A C=O stretch at 1712 cm^{-1} , O-H stretch at 3423 cm^{-1} and C=C stretch at 1602 cm^{-1} confirmed the modification of MWCNTs to MWCNTs-COOH. Vatanpour et al. (2011) observed C=O and O-H peaks at 1680 cm^{-1} and 3300-3600 cm^{-1} , respectively, for the oxidised MWCNTs. After the reaction of MWCNTs-COOH with SOCl_2 , the C=O bond shifted from 1712 to 1711 cm^{-1} . The IR bands at 3412 cm^{-1} , and at 1678 cm^{-1} were attributed to $-\text{OH}$ and $-\text{C}=\text{C}-$. A new bond was formed at 1680 cm^{-1} and this confirmed the presence of an amide bond, thus confirming the reaction between MWCNTs-COCl with the terminal $-\text{NH}_2$ groups of the HPEI.

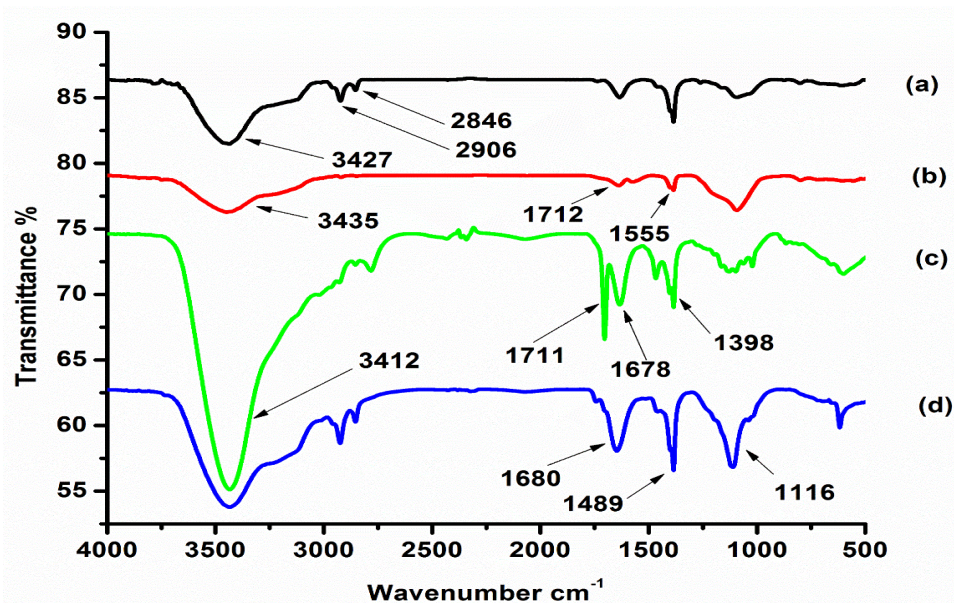


Figure 6.2. FTIR spectrum of (a) pristine MWCNTs, (b) MWCNTs-COOH, (c) MWCNTs-COCl and (d) HPEI-MWCNTs

6.3.2 Morphological studies using TEM analysis

The TEM images of MWCNTs and MWCNTs-COOH are shown in **Figure 6.4**. It is clear that the pristine MWCNTs contained impurities which are amorphous carbon and residual metal as shown in TEM **Figure 6.4(a)**, i.e. black dots on the tips of the pristine MWCNTs. These residual metals were subsequently removed after treatment with HNO_3 and H_2SO_4 . The TEM images in **Figure 6.4(b)** further confirmed that impurities were removed after acid treatment resulting in the clear tubular structure of MWCNTs. The modified MWCNTs showed a good structural integrity. This can be observed from the clear tubular nature of the MWCNTs after acidification and acylation. The size distribution histogram clearly showed the reduction of the diameter down to $10.02 \text{ nm} \pm 1.64$ with a tubular structure. **Figure 6.4(d)** shows that the MWCNTs-HPEI composite was grafted with HPEI. This is shown by the significant change in morphology of the MWCNTs after embedding HPEI. However, no aggregation of MWCNTs was observed in the images, which further suggests that the HPEI was uniformly grafted onto MWCNTs. **Figure 6.4(d')** shows EDX analysis of MWCNTs-COCl which confirms the presence of chlorine confirming the formation of an acyl chloride. The Fe-Cu bimetallic nanoparticles in **Figure 6.4(e)** was also observed and well dispersed in the surface of HPEI-MWCNTs. Fe-Cu bimetallic nanoparticles shows the uniformity and shape. The average diameter of nanoparticles was found to be $11.3 \text{ nm} \pm 2.1$. The EDS images in **Figure 6.4(e')** clearly show the presence of Fe and Cu in the composite of HPEI-MWCNTs.

Figure 6.3(A) shows that the Fe and Cu were uniformly distributed, thus confirming the synthesis of a bimetallic system within the MWCNTs/HPEI composites. The Fe and Cu were found to be effectively synthesised within the HPEI-MWCNTs which is indicated by the uniformly distributed metals in the composite. Thus the result corresponds with the EDS image mentioned above. The EDS spectrum in **Figure 6.3(B)** further confirms the presence of Fe-Cu bimetallic nanoparticles in the MWCNTs/HPEI system.

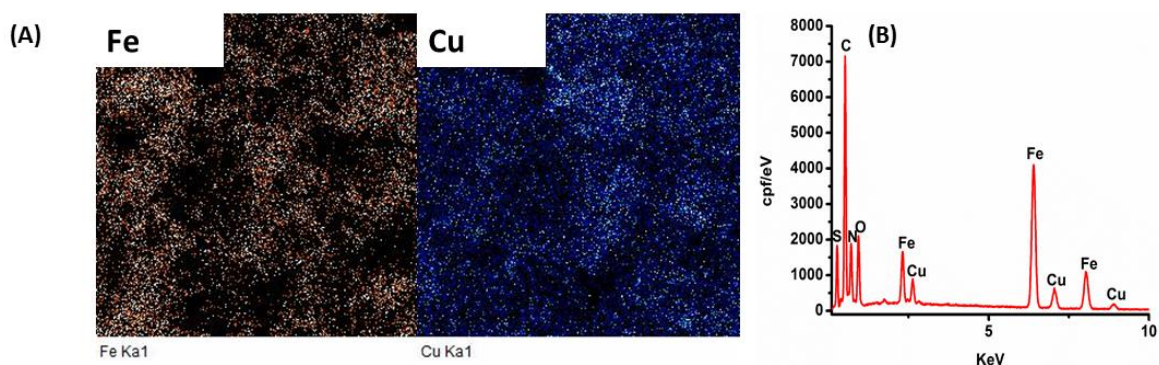


Figure 6.3. EDS mapping of MWCNTs/HPEI/Fe-Cu (A) and corresponding EDS spectrum of MWCNTs/HPEI/Fe-Cu (B)

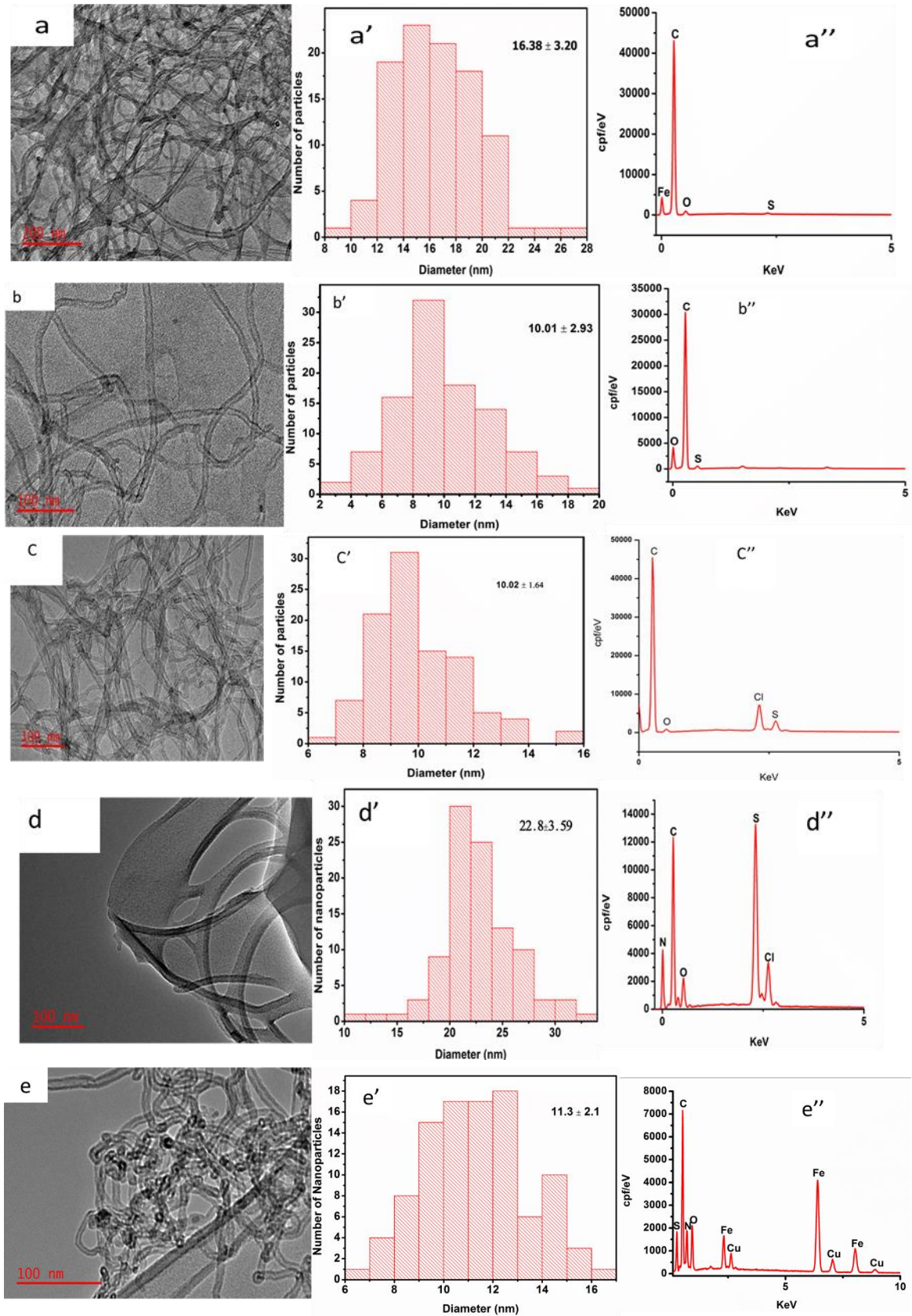


Figure 6.4. TEM images, size distribution graphs and EDX of (a) pristine MWCNTs, (b) MWCNTs-COOH, (c) MWCNTs-COCl, (d) HPEI-MWCNTs and (e) HPEI-MWCNTs/FeCu

6.3.3 BET analysis of pristine MWCNTs, MWCNTs-COOH, MWCNTs-COCl and HPEI-MWCNTs

Surface area, pore volume and pore size measurements of material were carried out using Brunauer-Emmett-Teller (BET) analysis (**Table 6.2**). It is noticeable that the surface area increased after introducing the -COOH. However, a drastic decrease in the surface area was noted for MWCNTs-COCl and HPEI-MWCNTs. This is due to the huge chlorine molecules that might be clogging tubes. Moreover, the HPEI-MWCNTs still had a low surface area because of the small amount of MWCNTs added which did not have a much significant effect on the total surface area of the nanocomposites. The BET adsorption isotherm shown in **Figure 6.5** illustrates the shapes of hysteresis loops, which are often used to identify specific pore structures. The result showed a type (V) isotherm, which is uncommon. This type of isotherm is obtained with certain porous adsorbents.

Table 6.2. BET analysis

Sample	Surface area (m ² /g)	Pore volume (cm ³ /g)	Pore size (nm)
Pristine MWCNTs	217.12	1.53	28.24
MWCNTs-COOH	250.31	2.15	33.97
MWCNTs-COCl	12.38	0.13	41.50
HPEI-MWCNTs	14.06	0.14	38.01

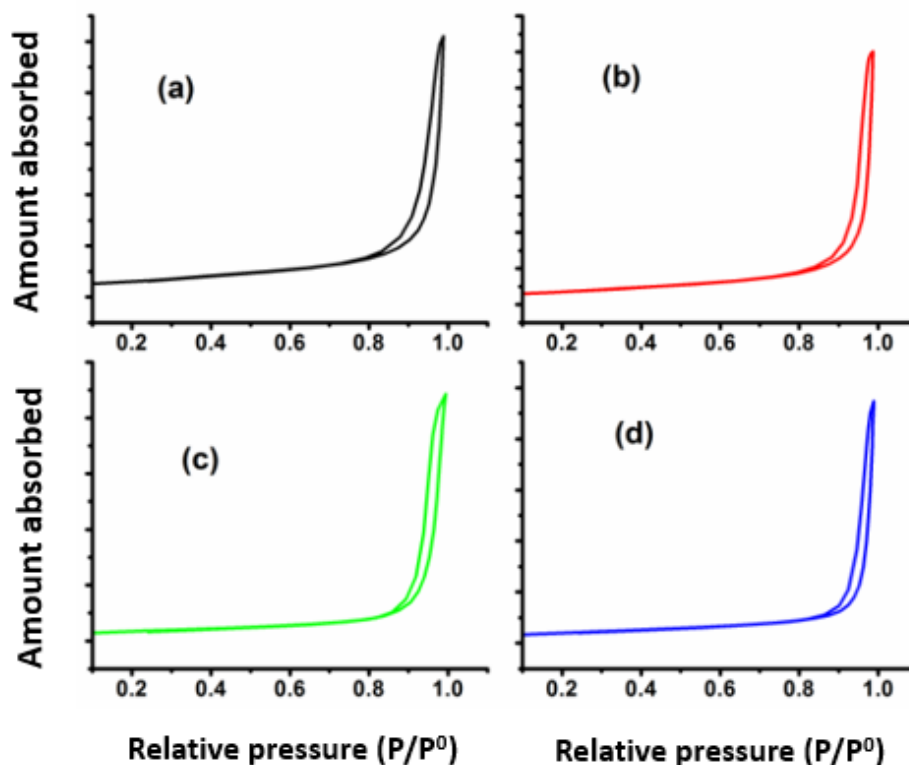


Figure 6.3. BET adsorption isotherm spectrum of (a) pristine MWCNTs, (b) MWCNTs-COOH, (c) MWCNTs-COCl and (d) HPEI-MWCNTs

6.3.4 Raman

Two major bands differentiate the Raman spectra for MWCNTs. Firstly, the D-band (defect band) which ranges in the region between 1 300-1 350 cm^{-1} ; secondly, the G-band (tangential in-plane stretching vibration of carbon-carbon bond) that can be found between 1 550-1 600 cm^{-1} . The intensity of the G-band shows the crystallinity and a defect-free sample, whereas the existence of defect and disordered graphite are indicated by broad bands around 1 300-1 350 cm^{-1} (Osswald et al., 2007). Moreover, the Raman spectra of pristine MWCNTs and the functionalised MWCNTs show two characteristics peaks (**Figure 6.6a-d**). One peak is detected at 1 348.14 cm^{-1} due to the D-band and the other peak is due to the G-band (1 585.20 cm^{-1}). The G-band observed in pristine-MWCNT (**Figure 6.6a**) can be ascribed to the vibration of sp^2 bonded to graphite carbon whereas the D-band lies on the defect induced in the MWCNTs due to the disruption of sp^2 -C=C- bonds. After functionalisation of the MWCNTs, the I_D/I_G ratio (**Table 6.3**) was found to increase due to the addition of functional groups on MWCNTs. This was because of the disruption of the -C=C- bond in the MWCNTs structure.

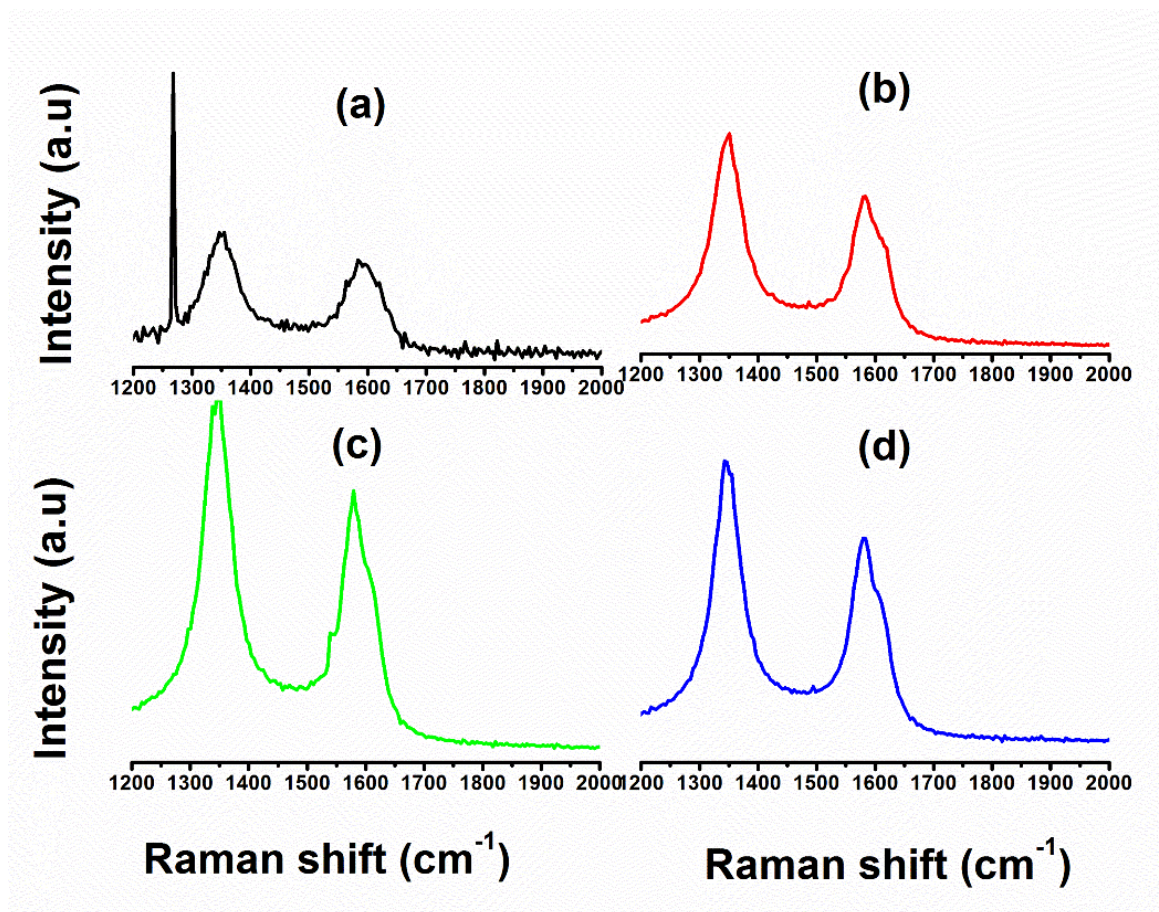


Figure 6.4. Raman spectra of (a) pristine MWCNTs, (b) MWCNTs-COOH, (c) MWCNTs-COCl and (d) HPEI-MWCNTs

Table 6.3. I_D/I_G ratio of pristine and functionalised MWCNTs

Sample	Peak position/cm ⁻¹		I_D/I_G
	D-Band	G-Band	
Pristine MWCNTs	1 348.14	1 585.2	1.07
MWCNTs-COOH	1 350.14	1 580.98	1.27
MWCNTs-COCl	1 350.14	1 578.76	1.25
HPEI-MWCNTs	1 343.92	1 578.76	1.23

6.3.5 SEM analysis

The surface morphology of the unmodified (**Figure 6.7a**) and modified membranes (**Figure 6.7b-c**) showed similar features with numerous pores evident on the surface of the membrane which revealed a porous structure. The images of the cross-sectional structure of the HPEI-MWCNT-Fe/Cu-PES membrane are given **Figures 6.7d-f** and showed finger-like microvoids supported by a spongy structure observed in flat-sheet polymer membrane fabricated using the phase-inversion method. As the HPEI-MWCNT-Fe/Cu content is increased, larger finger-like microvoids were observed. The inclusion of hydrophilic composite (HPEI-MWCNTs-Fe/Cu) accelerated the diffusion rate between the non-solvent (water) and solvent (NMP).

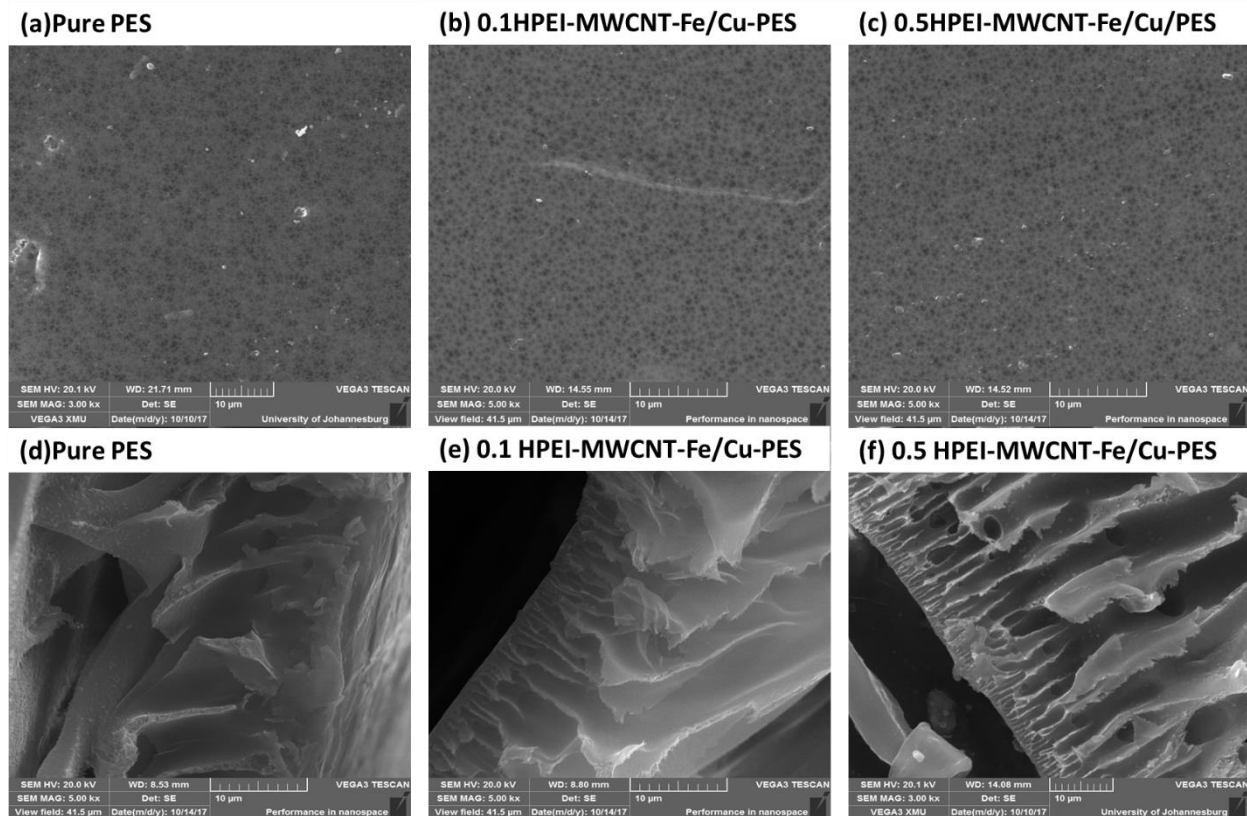


Figure 6.5. Top surface morphology of the unmodified and modified membranes (a-c); and cross-sectional morphology of the unmodified and modified membranes (d-f)

6.3.6 Contact angle analysis

The hydrophilicity and hydrophobicity of the membrane were determined by measuring the membrane contact angle as shown in **Figure 6.8**. As the HPEI-MWCNTs-Fe/Cu concentration increased from 0.1 to 0.5 wt%, the contact angle also decreased ($55.7^\circ \pm 2.9$ to $39.7^\circ \pm 2.6$). These results demonstrated that the hydrophilicity improved as the content of HPEI-MWCNTs-Fe/Cu was increased. This is because of the hydrophilic functional groups such as COOH and NH₂ on the surface of MWCNTs. These results are in agreement with those reported in the literature. In a study conducted by Wu and co-workers (2013) a lower contact angle of the ultrafiltration membrane was reported. The result showed that as HPEI-GO was increased, this effectively enhanced the hydrophilicity of the membrane (Yu et al., 2013). Xue et al. (2016) prepared poly (piperazine-amide) nanofiltration membranes modified with functionalised MWCNTs. In that study, the contact angle was found to decrease after functionalisation of MWCNTs. This was due to increased hydrophilicity of functional groups in the modified membrane.

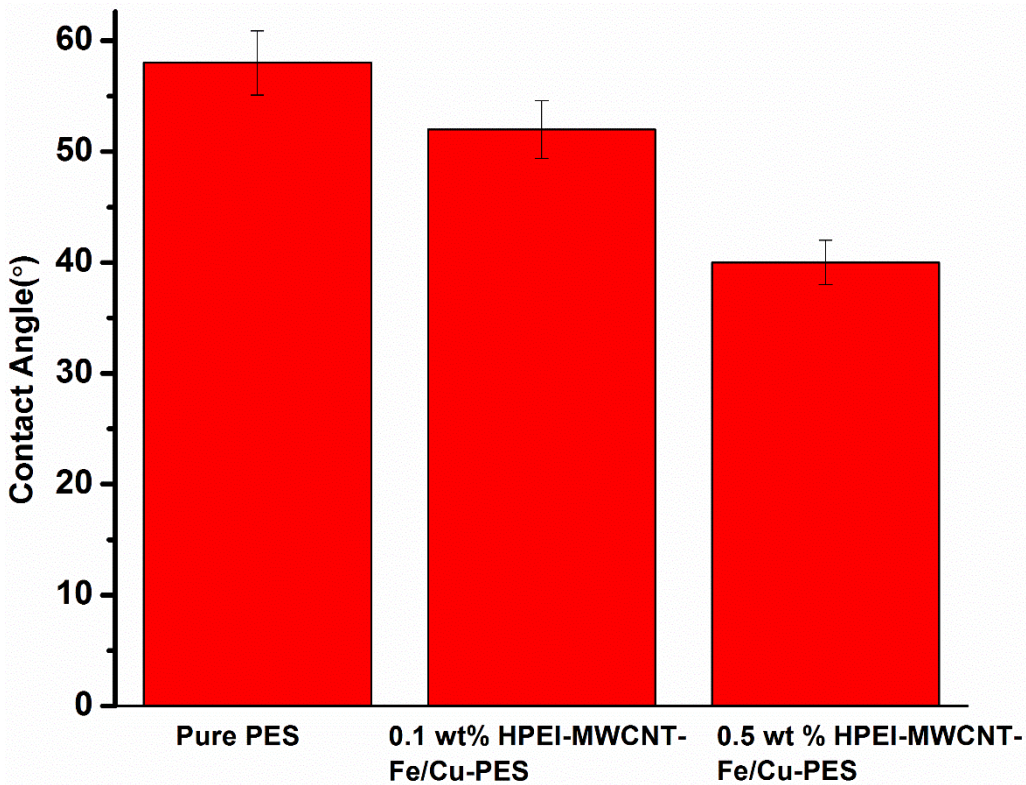


Figure 6.6. Contact angle measurement of HPEI-MWCNTs-Fe/Cu-PES membrane

6.3.7 Pure water flux (PWF) analysis

Figure 6.9 demonstrates the results of pure water flux (PWF) against pressure for the fabricated membranes. These results reveal the effect of different pressures on PWF. Generally, the flux was found to increase with an increase in operating pressure up to 300 kPa. The pure PES membrane exhibited a higher flux than the modified membranes for all measured pressure. The addition of nanocomposite in the membrane showed a decrease in PWF in comparison to the pure PES membrane (77.99 ± 1.29 L/m²·h) at 300 kPa. The low of PWF (26.3 ± 1.3665 L/m²·h) upon addition of HPEI-MWCNTs-Fe/Cu was due to the presence of bimetallic nanoparticles in the pores of the membrane. This can cause water not to flow gradually due to pore clogging and reduction of pore sizes after fabrication with nanoparticles. Ariono et al. (2017) reported the effect of polymer concentration on the flux stability of a polysulfone membrane. The membrane was prepared by blending polysulfone, dimethylacetamide with, polyethylene glycol and acetone. The results showed that there was a sharp decrease in PWF from 1 230 to 7 L/m²·h when the PSf concentration was increased from 14 to 24 wt%. Koloti et al. (2017) also observed a similar trend in the degradation of Bisphenol A by increasing the concentration of enzyme laccase on the HPEI-PES membrane. In that study, the flux decreased from 73.95 ± 6.23 L/m²·h for the pure PES to 17.01 ± 5.64 L/m²·h for the modified membranes.

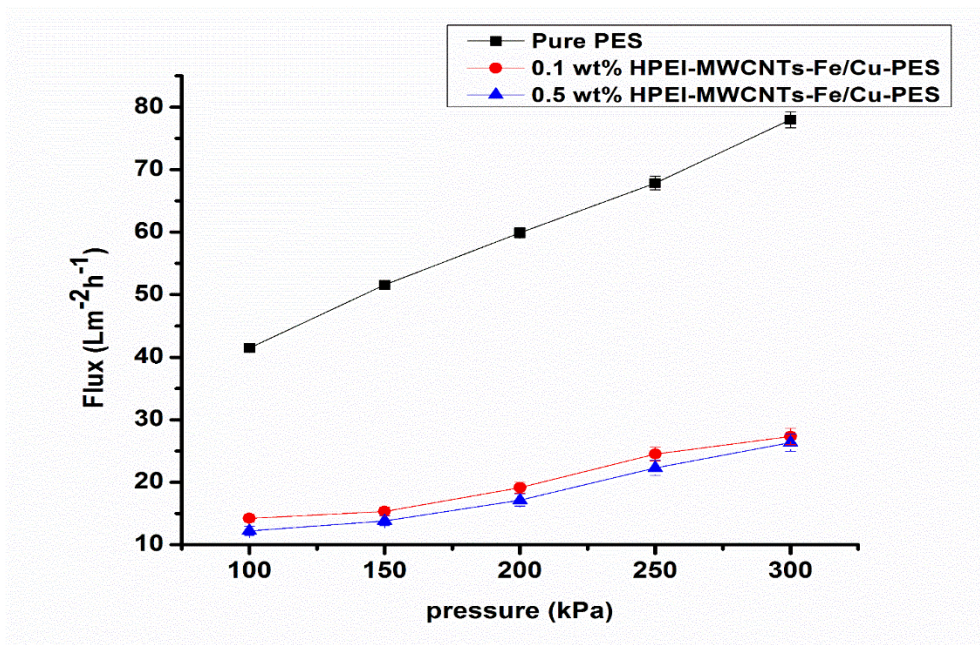


Figure 6.7. Pure water flux of modified membrane within 15 min at 25°C

6.3.8 Catalytic reactivity of nanocomposite membranes

Figure 6.10 shows the removal of 2,4,6-TCP using the modified and unmodified membranes. The modified membranes showed a higher removal rate than the pristine PES. PES also exhibited a removal efficiency of 58%, this could be due to the rejection of TCP via hydrophobic-hydrophobic interactions. The modified membranes exhibit HPEI nanocavities, which can efficiently absorb the pollutant and expose it to the Fe/Cu bimetallic catalyst for further degradation. To further confirm that catalytic degradation of TCP had occurred, the by-products of the reaction were analysed using LC-MS, and the spectra are given in Figure 6.11. The degradation by-products detected were 2, 4-dichlorophenol (A: m/z = 161), propanol (B: m/z = 60), phenol (C: m/z = 91) and propane (D: m/z = 45).

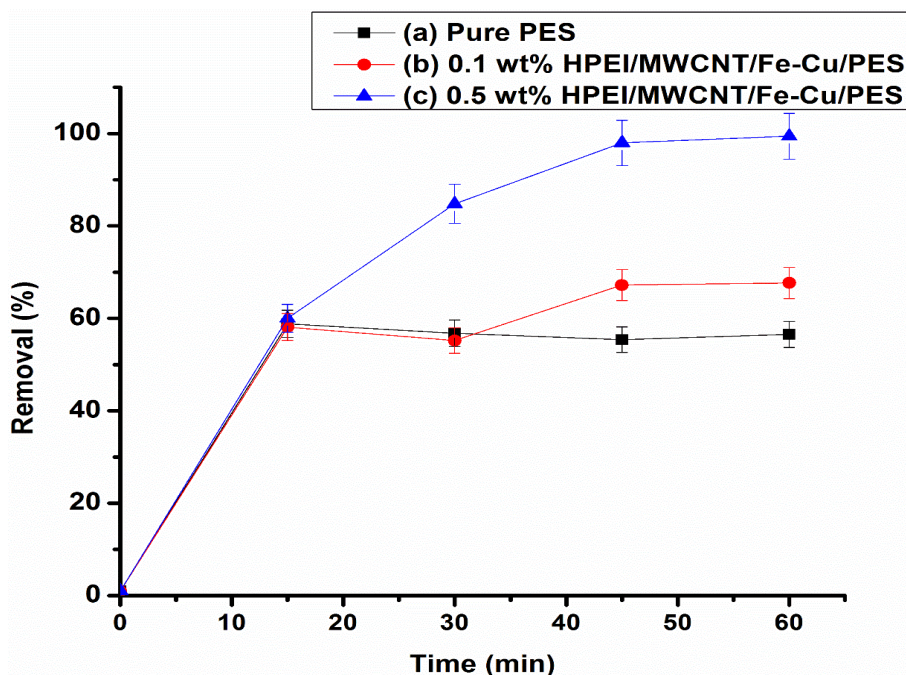


Figure 6.8. Removal efficiency of the modified and unmodified membranes

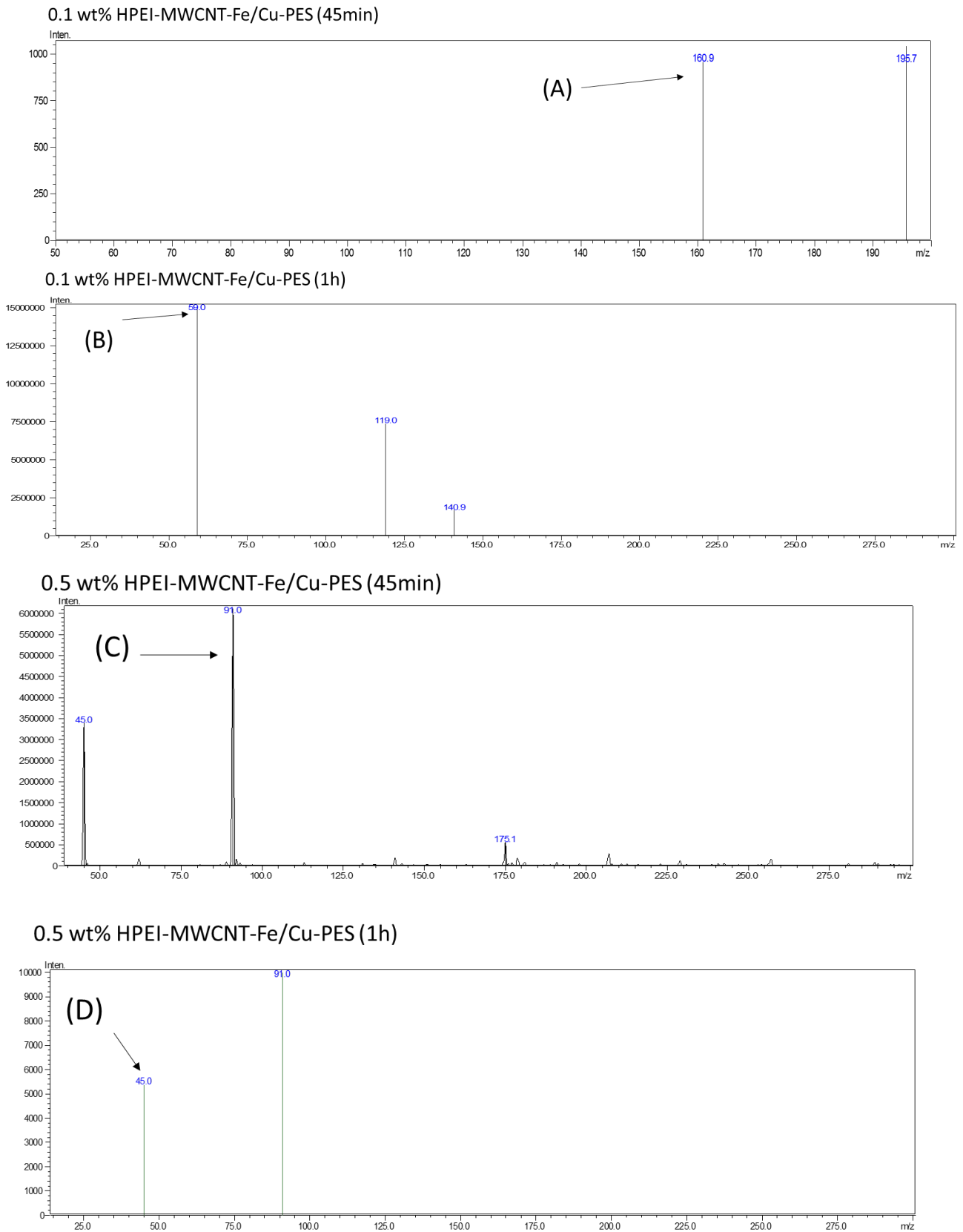
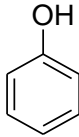
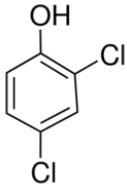


Figure 6.9. LC-MS spectra showing 2,4,6 TCP by-products generated using HPEI-MWCNT-Fe/Cu-PES membrane

Table 6.4. 2,4,6-TCP by-products detected by LC-MS

Degradation product	by-	Chemical structure	(m/z)	References
Phenol			91	Joa and Almeida, 2007
2,4-dichlorophenol			161	Elvira-Cozar and Len-Gonz, 1995
Benzene			78	Okamoto and Tomonari, 1999

6.3.9 Fouling analysis

The antifouling performance of the fabricated membrane and pure PES ultrafiltration membrane was monitored by measuring the water flux recovery after fouling with bovine serum albumin (BSA) (1 000 mg/L) as shown in **Figure 6.12**. It is known that the main problem associated with membranes is fouling, thus BSA suspension was used as the fouling agent in this study. The pure water flux was measured before and after exposure of the membrane to the BSA suspension. The PWF of the fouled membrane was examined after washing each membrane with deionised water for 60 min. As indicated in the results, the flux declined after pure water was replaced by the BSA suspension. However, the flux became constant and relatively stable during BSA filtration. Farahbakhsh et al. (2017) used raw and oxidized MWCNTs for the fabrication of reverse osmosis polyamide membranes.

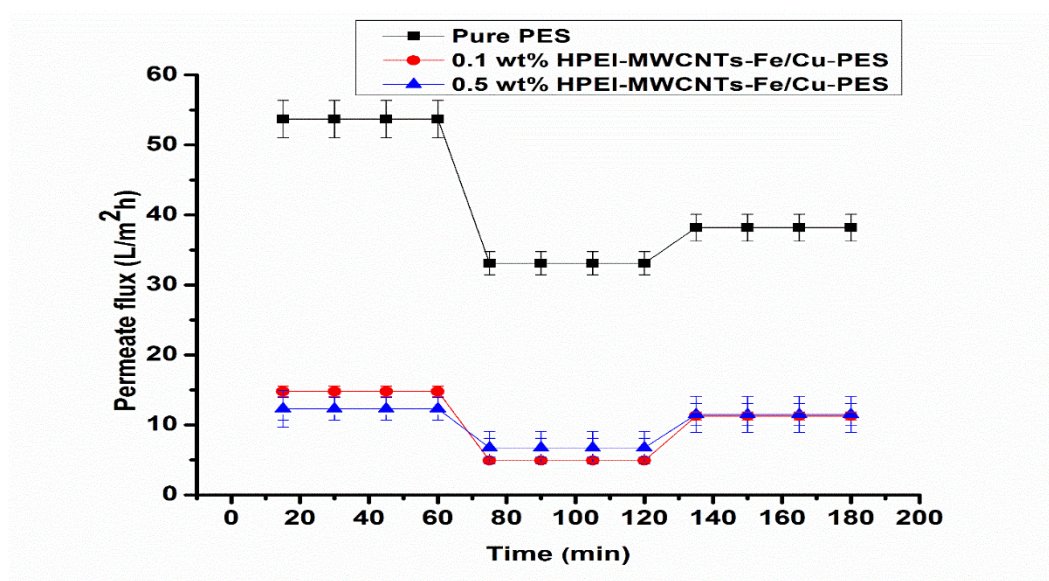


Figure 6.10. Permeate flux vs. time for HPEI-MWCNTs-Fe/Cu blended PES membranes for water containing BSA (1 000 mg/L), at applied pressure of 200 kPa, pH 7.1, and temperature at 25°C

The MWCNTs were envisaged to improve antifouling properties. In this study membranes were synthesised via interfacial polymerization method. Results exhibited a major decline after the deposition of protein in the pores of membranes. This was due to the hydrophobic nature of the BSA (Farahbakhsh et al., 2017). Boributh et al. (2009) reported a similar trend in the use of a modified PVDF membrane by chitosan solution for the reduction of protein (Boributh et al., 2009); in this study the BSA was found to decline after being introduced in the modified membrane.(Boributh et al., 2009). **Figure 6.13** shows that the flux recovery ratio (FRR) of the unmodified membrane (71.1%) was lower than those of the various modified membranes (0.1 wt% HPEI-MWCNTs-Fe/Cu-PES: 76.2% and 0.5 wt% HPEI-MWCNTs-Fe/Cu-PES: 93.4%). The higher FRR describes the better fouling properties of the prepared membranes. This could be attributed to the presence of hydrophilic groups present in the HPEI and MWCNTs structures which prohibits protein adsorption on the surface of the modified membrane (Rahimi et al., 2015). This finding suggested that the modified membranes had excellent antifouling properties due to improvement in hydrophilicity by the HPEI-MWCNTs-FeCu. Celik and co-workers (2011) synthesised MWCNTs/PES membranes via a phase inversion method. The antifouling properties of the membrane towards natural organic matter (NOM) were investigated. The blended membrane demonstrated 95% flux recovery after fouling which indicated that the modified membrane had high resistance to fouling (Celik et al., 2011). Kanagaraj et al. (2015) incorporated hyperbranched polyethyleneimine and amphiphilic triblock copolymer (Pluronic® F-127) onto an ultrafiltration membrane using a phase inversion method. The FRR of the modified membranes was observed to be 92.4% compared to that of the unmodified membrane (73.3%). This was due to the presence of the hydrophilic groups present in the PEI and Pluronic® F-127 structure (Kanagaraj et al., 2015).

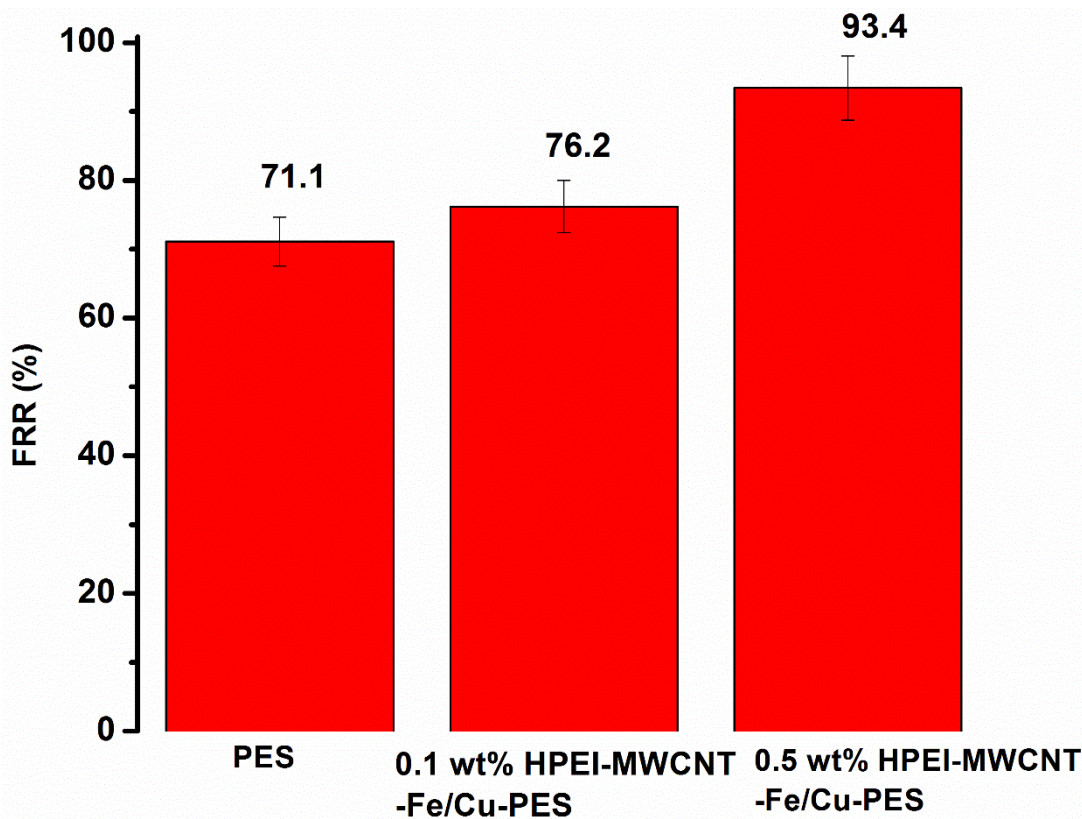


Figure 6.11. Flux recovery ratio (FRR) of the HPEI-MWCNTs-Fe/Cu blended PES membranes after BSA fouling

6.3.10 Leaching studies

The leaching of bimetallic nanoparticles from the membrane was studied using ICP-OES. In terms of the South African Water Quality Guidelines (DWAF, 1996), the allowable limit for Fe and Cu is 0.3 mg/L and 0.02 mg/L. As is shown in **Table 6.5**, the maximum amount of Fe and Cu that leached out was 0.0038 and 0.0019 mg/L. These levels are very low, thus suggesting that strong metal/HPEI interactions exist within the membrane matrix.

Table 6.5. Leaching results for the fabricated membrane

Composite membrane	Time (min)	Fe (mg/L)	Cu (mg/L)
0.1 wt% HPEI-MWCNTs-Fe/Cu-PES	15	0.0038±0.0012	0.0019±0.0024
	30	0.0017±0.0002	-0.008±0.0001
	45	0.00010±0.0002	-0.0009±0.0002
	60	0.0005 ±0.0001	-0.00013±0.0001
0.5 wt% HPEI-MWCNTs-Fe/Cu-PES	15	0.0026±0.0007	0.0009±0.0003
	30	0.0013±0.0003	0.0007±0.0022
	45	0.0001±0.0001	-0.0014±0.0002
	60	-0.001±0.0002	-0.0018±0.0001

6.4 SUMMARY

A novel HPEI-MWCNTs-Fe/Cu membrane with improved hydrophilicity and fouling properties was fabricated via phase inversion. It was found that ethylene glycol played a measured role in terms of reducing bimetallic nanoparticles to the zero-valent state. The branched cationic dendritic polymer (HPEI) was found to play a major role in assisting in the dispersion of multiwalled carbon nanotubes (MWCNTs) and chelating Fe-Cu bimetallic nanoparticles. In order to evaluate the performance of the membrane, 2,4,6-TCP was used as a model pollutant. The 2,4,6-TCP removal rate of the membranes was found to increase as the HPEI/MWCTs/Fe/Cu content was increased. The removal rate reached up to 90% for the modified membranes as compared to 60% for the pristine membrane.

CHAPTER 7: CONCLUSIONS AND RECOMMENDATIONS

7.1 CONCLUSION

In this study we were able to synthesise and functionalise membranes with different nanomaterials such as HPEI, photocatalytic nanoparticles (TiO_2), bimetallic nanoparticles (Fe/Pd and Fe/Cu). Firstly in the fabrication of enzyme modified nanofibrous membranes, the presence of the HPEI amine peripheral groups acted as a coupling agent in the attachment of the enzyme on the membrane thus improving the enzyme loading capacity. Secondly, the abundant internal and peripheral amine groups of the HPEI polymer in the HPEI/PSf-Fe/Pd membranes were found to effectively enhance the encapsulated the bimetallic nanoparticles (Fe/Pd). In another study where TiO_2 was prepared within the HPEI template, and functionalised onto a membrane. It was found that the HPEI as a template reduced agglomeration and produced catalytic TiO_2 nanoparticles which were of uniform size and were well dispersed. In the preparation of HPEI-MWCNTs-Fe/Cu/PSf membrane the presence of the branched cationic dendritic polymer (HPEI) played a role of assisting in the dispersion of multi-walled carbon nanotube (MWCNTs) and chelating Fe-Cu bimetallic nanoparticles. The results showed that the HPEI induced unique properties to the membranes thus this polymer can be considered as a promising material for membrane fabrication and modification.

These catalytic membranes were tested for the removal of various pollutants from water such as BPA, 2, 4-Trichlorophenol, methyl orange and PCB-153 from water. The PES/HPE/ TiO_2 membrane was found to exhibit the high removal rated of methyl orange for all tested pH values (2-12). Thus these membranes could be applicable in the photocatalytic degradation of dyes in highly acidic, neutral and alkaline wastewater. HPEI/PSf-Fe/Pd membrane removed 93.3% of PCB 153 within 4 hours of treatment which was accompanied by the presence of by-products such as tetrachlorobiphenyl (Ar_2Cl_4) [PCB 52] and dichlorobiphenyl (Ar_2Cl_2) [PCB 2]. Successful biodegradation of BPA using laccase immobilized HPEI/PES nanofibrous membrane was confirmed by the detection of 4-isopropylphenol, 4-hydroxybenzealdehyde, 2,2-bis(4-hydroxyphenyl) propanoic acid, 4,4-dihydroxy- α -methylstibene, BPA dimer, BPA trimer and BPA tetramer by-products using LC-MS analysis. High dechlorination efficiency towards 2,4,6-TCP was observed for the catalytic membranes and the presence of by-products such as 4-dichlorophenol, propanol, phenol and propane indicated that the membrane is feasible as a support of Fe/Ni nanoparticles. The catalytic membranes showed highly desirable properties suitable for the field of bioremediation or catalysis applications including stability, good activity and its ability to degrade phenolic based compounds. These membranes also demonstrated a high flux recover ratio after being exposed to BSA which is a fouling materials thus demonstrating that the fabricated membranes had a preferable antifouling performance.

7.2 RECOMMENDATION FOR FURTHER RESEARCH

- The technology could be scaled and used as an integrated system for the treatment of effluent. It can also be used in conjunction with other treatment methods as a polishing up step, i.e. in a treatment plant.
- Perform modelling experiments of the membranes which would assist in predicting the pressure, processing time and membrane area. This would assist in knowing the requirements or conditions of the scaling up process.
- The immobilised enzyme nanofibrous membranes has shown promising results. This technology can be further explored by using these biocatalytic materials in practical applications such as in membrane bioreactor technology. These reactors are known to have high reaction rates, the enzymes are retained and thus the system can be used several times, simple and robust.

REFERENCES

- Afful, S., Awudza, J.A.M., Twumasi, S.K., Osaе, S. (2013) Determination of indicator polychlorinated biphenyls (PCBs) by gas chromatography-electron capture detector. *Chemosphere*, 93, 1556-1560.
- Aghighi, A., Haghigat, F. (2015) Evaluation of nano-titanium dioxide (TiO₂) catalysts for ultraviolet photocatalytic oxidation air cleaning devices. *Journal of Environmental Chemical Engineering*, 3: 1622-1629.
- Alemanу, L.J., Banares, M.A., Pardo, E., Martin-Jimenez, F. & Blasco, J.M. (2000) Morphological and Structural Characterization of a Titanium Dioxide System. *Material Characterisation* 44, 271-275.
- Amdany, R., Chimuka, L., Cukrowska, E., Kukučka, P., Kohoutek, J., Vrana, B. (2014) Investigating the temporal trends in PAH, PCB and OCP concentrations in Hartbeespoort Dam, South Africa, using semipermeable membrane devices (SPMDs). *Water SA*, 40: 425-436. doi:10.4314/wsa.v40i3.5.
- Amri, A., Jiang, Z.T., Pryor, T., Yin, C-Y, Djordjevic, S. (2014) Developments in the synthesis of flat plate solar selective absorber materials via sol-gel methods: A review. *Renewable Sustainable Energy Reviews*, 36: 316-328.
- Annamalai J., Namasivayam, V. (2015) Endocrine disrupting chemicals in the atmosphere: Their effects on humans and wildlife, *Environment International*, 76,78-97
- Ariono, D., Aryanti, P.T.P., Subagjo1, S., Wenten, I.G. (2017) The effect of polymer concentration on flux stability of polysulfone membrane. *American Institute of Physics (AIP) Conference Proceedings*, 1788, 030048-1-030048-10. doi.org/10.1063/1.4968301.
- Arkas, M., Tsiourvas, D. (2009) Organic/inorganic hybrid nanospheres based on hyperbranched poly (ethylene imine) encapsulated into silica for the sorption of toxic metal ions and polycyclic aromatic hydrocarbons from water. *Journal of Hazardous Materials*, 170: 35-42.
- Arkas, M., Eleades, L. Paleos, C.M., Tsiourvas, D. (2005) Alkylated hyperbranched polymers as molecular nanospheres for the purification of water from polycyclic aromatic hydrocarbons, *Journal of Applied Polymer Science*, 97: 2299-2305.
- Wan, H., Briot, N.J., Saad, A., Ormsbee, L., Bhattacharyya, D., (2017) Pore functionalized PVDF membranes with in-situ synthesized metal nanoparticles: Material characterization, and toxic organic degradation. *Journal of Membrane Science* 530, 147-157.
- Baluka, S.A., Rumbelha, W.K. (2016) Bisphenol A and food safety: Lessons from developed to developing countries. *Food and Chemical Toxicology*, 92: 58-63.
- Bechambi, O., Sayadi, S., Najjar, W. (2015) Photocatalytic degradation of bisphenol A in the presence of C-doped ZnO: Effect of operational parameters and photodegradation mechanism. *Journal of Industrial and Engineering Chemistry*, 32: 201-210.
- Belayachi, H., Bestani, B., Benderdouche, N., Belhakem, M. (2015) The use of TiO₂ immobilized into grape marc-based activated carbon for RB-5 azo dye photocatalytic degradation. *Arabian Journal of Chemistry*, doi:10.1016/j.arabjc.2015.06.040.

Beltran-Huarac, J., Palomino, J., Resto, O., Wang, J., Jadwisieniczak, W.M., Weiner, B.R., Morell, G. (2014) Highly-crystalline γ -MnS nanosaws. *RSC Advances*, 4: 38103-38110.

Biesinger, M.C., Payne, B.P., Grosvenor, A.P., Lau, L.W.M., Gerson, A.R., Smart, R. St. C. (2011) Resolving surface chemical states in XPS analysis of first row transition metals, oxides and hydroxides: Cr, Mn, Fe, Co and Ni. *Applied Surface Science*, 257(7): 2717-2730. doi: 10.1016/j.apsusc.2010.10.051.

Böhm, I., Kreth, S.K., Ritter, H. (2011) Hyperbranched polyethylenimine bearing cyclodextrin moieties showing temperature and pH controlled dye release. *Beilstein Journal of Organic Chemistry*, 7: 1130-1134.
Bouwman, H. (2003) POPs in Southern Africa. *Environmental Chemistry*, 3: 297-320.

Bouwman, H., (2004) South Africa and the Stockholm convention on persistent organic pollutants: Science policy, *South African Journal of Science*, 100, 323-328.

Brena, B., Gonzalez-Pombo, P., Batista-Viera, F. (2013) Immobilization of enzymes: A literature survey. In: Guisan, J.M. (Ed.), *Immobilization of Enzymes and Cells*. Totowa (New Jersey): Humana Press Inc. pp. 15-31.

Buah-Kwofie, A., Yeboah, P.O., Pwamang, J. (2011) Determination of levels of polychlorinated biphenyl in transformers oil from some selected transformers in parts of the Greater Accra Region of Ghana. *Chemosphere*, 82: 103-106.

Burger, A. (2005) WRC Programme on Endocrine Disrupting Compounds (EDCs) Volume 1: Strategic Research Plan for Endocrine Disruptors in South African Water Systems. WRC Report No. KV 143/05 of this report series. Water Research Commission, Pretoria, South Africa.

Boributh, S., Chanachai, A., Jiratananon, R., (2009) Modification of PVDF membrane by chitosan solution for reducing protein fouling. *Journal of Membrane Science*, 342: 97-104.

Cai, T., Yang, W.J., Neoh, K-G., Kang, E-T. (2012) Poly(vinylidene fluoride) membranes with hyperbranched antifouling and antibacterial polymer brushes. *Industrial Engineering Chemistry Research*, 51: 15962-15973.

Cao, Y., Zhang, H., Li, F., Lu, L. & Zhang, S. (2015) Preparation and characterization of ultrafine ZrB₂-SiC composite powders by a combined sol-gel and microwave boro/carbothermal reduction method. *Ceramics International* 41, 7823-7829.

Casper, L.S., Stephens, J.S., Tassi, N., Chase, D.B., Rabolt, J. (2003) Controlling surface morphology of electrospun polystyrene fibers: Effect of humidity and molecular weight in the electrospinning process. *Macromolecules*, 37: 573-578.

Chen, X., Mao, S.S. (2007) Titanium dioxide nanomaterials: Synthesis, properties, modifications and applications. *Chemical Reviews*, 107: 2891-2959.

Chen, X. (2009) Titanium dioxide nanomaterials and their energy applications. *Chinese Journal of Catalysis*, 30: 839-851.

Chen, L., Zou, M., Hong, F.F. (2015) Evaluation of fungal laccase immobilized on natural nanostructured bacterial cellulose, *Frontiers in Microbiology*, 6:1-10.

Chiang, Y-C., Hsub, Y-Z., Ruaan, R-C., Chuang, C-J., Tung, K-L. (2009) Nanofiltration membranes synthesized from hyperbranched polyethyleneimine. *Journal of Membrane Science*, 326:19-26.

Carwile, J.L., Michels, K.B. (2011) Urinary bisphenol A and obesity: NHANES 2003-2006 *Environmental Research*, 111: 825-830.

Celik, E., Park, H., Choi, H., Choi, H. (2011) Carbon nanotube blended polyethersulfone membranes for fouling control in water treatment. *Water Research*, 45(1): 274-282. Chen, M. Chen, M., Chen, X., Wang, J. (2010) Functionalization of MWNTs with hyperbranched PEI for highly selective isolation of BSA. *Macromolecular Bioscience*, 10(8): 906-915.

Chen, X. (2009) *Titanium Dioxide Nanomaterials and Their Energy Applications*. Chinese Journal of Catalysis. 30, 839-851.

Chin, S.S., Chiang, K. & Fane, A.G. (2006) *The stability of polymeric membranes in a TiO₂ photocatalysis process*. Journal of Membrane Science **275**, 202-211.

Choi, J., Choi, S.J. & Kim, Y. (2008) Hydrodechlorination of 2, 4, 6-trichlorophenol for a permeable reactive barrier using zero-valent iron and catalyzed iron. *Korean Journal of Chemical Engineering*, 25(3): 493-500.

Cruz N.K.O, Semante G.U. & Lu S.C. (2013) Dye degradation and antifouling properties of PVDF/TiO₂ membrane prepared by sol-gel method. *Journal of Taiwan Institute of Chemical Engineers* 4: 32-54.

Dai, Y., Yin, L., Niu, J. (2011) Laccase-carrying electrospun fibrous membranes for adsorption and degradation of PAHs in shoal soils, *Environmental Science and Technology*, 45:10611-10618.

Dalvie, M.A., Cairncross, E., Solomon, A., London, L. (2003) Contamination of rural surface and ground water by endosulfan in farming areas of the Western Cape, South Africa. *Environmental Health: A Global. Access Science Source*, 2: 1-15.

Das, R., Vecitis, C.D., Schulze, A., Cao, B., Ismail, A.F., Lu, X., Chen, J. and Ramakrishna, S. (2017) Recent advances in nanomaterials for water protection and monitoring. *Chemical Society Reviews*, 46: 6946-7020.

De Jager, C., Swart, P., Truebody, B. (2013) Estrogenic activity and endocrine disrupting chemical (EDC) status in water obtained from selected distribution points in Pretoria and Cape Town. WRC Report No. KV 317/13. Water Research Commission, Pretoria, South Africa.

Dehghani, M.H., Ghadermazi, M., Bhatnagar, A., Sadighara, P., Jahed-Khaniki, G., Heibati, B., McKay, G. (2016) Adsorptive removal of endocrine disrupting bisphenol A from aqueous solution using chitosan. *Journal of Environmental Chemical Engineering*, 4: 2647-2655.

Diallo, M.S., Christie, S., Swaminathan, P., Johnson, J.H. (Jr.), Goddard, W.A. III (2005) Dendrimer enhanced ultrafiltration.1. Recovery of Cu (II) from aqueous solutions using PAMAM dendrimers with ethylene diamine core and terminal NH₂ groups. *Environmental Science and Technology*, 39: 1366-1377.

Dlamini, L.N., Krause, R.W., Kulkarni, G.U., Durbach, S.H. (2011) Photodegradation of bromophenol blue with fluorinated TiO₂ composite. *Applied Water Science*, 1: 19-24.

Doherty, L.F., Bromer, J.G., Zhou, Y., Aldad, T.S., Taylor, H.S. (2010) In utero exposure to diethylstilbestrol (DES) or bisphenol-A (BPA) increases EZH2 expression in the mammary gland: An epigenetic mechanism linking endocrine disruptors to breast cancer, *Hormones and Cancer*, 1,146-155.

Dong, Y., Wu, D., Chen, X., Lin, Y. (2010) Adsorption of bisphenol A from water by surfactant-modified zeolite. *Journal of Colloid and Interface Science*. 348: 585-590.

Du, J., Bao, J., Tong, M., Yuan, S. (2013) Dechlorination of pentachlorophenol by palladium/iron nanoparticles immobilized in a membrane synthesized by sequential and simultaneous reduction of trivalent iron and divalent palladium ions. *Environmental Engineering Science*, July 2013, 30(7): 350-356.

Du, J., Bao, J., Fu, X., Lu, C., Kim, S.H. (2016) Mesoporous sulfur-modified iron oxide as an effective Fenton-like catalyst for degradation of bisphenol A, *Applied Catalysis B: Environmental*, **184**:132-141.

DWAF (1996) South African Water Quality Guidelines: Domestic Water Use. Department of Water Affairs and Forestry (DWAF), Pretoria, South Africa.

Department of Environmental Affairs Annual Report (2011) National Implementation Plan for the Stockholm Convention of Persistent Organic Pollutants. Accessed at: https://www.environment.gov.za/sites/default/files/docs/national_implementation_plaun_organic_pollutants.pdf

Elahi, A., Irfan, M., Shakoor, A., Niaz, N.A., Mahmood, K., Qasim, M. (2015) Effect of loading titanium dioxide on structural, electrical and mechanical properties of polyaniline nanocomposites. *Journal of Alloys and Compounds*, 651: 328-332.

El-Shahawi, M.S., Hamza, A., Bashammakh, A.S., Al-Saggaf, W.T. (2010) An overview on the accumulation, distribution, transformations, toxicity and analytical methods for the monitoring of persistent organic pollutants. *Talanta* 80, 1587-1597.

Elvira-Cozar, C.P.C., Len-Gonz, L.V.P.M.E. (1995) Trace priority pollutant phenols enrichment from water by ion chromatography. *Chromatographia*, 40: 91-95.

Emregul, E., Kocabay, O., Derkus, B. (2013) A novel carboxymethylcellulose-gelatin-titanium dioxide-superoxide dismutase biosensor; electrochemical properties of carboxymethylcellulose-gelatin-titanium dioxide-superoxide dismutase. *Bioelectrochemistry*, 90: 8-17.

Environmental Protection Agency (EPA) (2012) Literature Review of Remediation Methods for PCBs in Buildings. Report No. EPA/600/R-12/034, January 2012. Report produced by Environmental Health & Engineering, Inc., Needham, Massachusetts, for Zhishi Guo, US Environmental Protection Agency (EPA), Cincinnati, USA. pp.68.

Escalona, I., de Grooth, J., Font, J., Nijmeijer, K. (2014) Removal of BPA by enzyme polymerization using NF membranes. *Journal of Membrane Science*, 468: 192-201.

Fang, X.F., Li, J., Li, X., Sun, X., Shen, J., Han, W., Wang, L. (2015) Polyethyleneimine an effective additive for polyethersulfone ultrafiltration membrane with enhanced permeability and selectivity. *Journal of Membrane Science*, 476: 216-223

Farahbakhsh, J., Delnavaz, M., Vatanpour, V. (2017) Investigation of raw and oxidized multiwalled carbon nanotubes in fabrication of reverse osmosis polyamide membranes for improvement in desalination and antifouling properties. *Desalination*, 410: 1-9.

Fatoki, O.S., Awofolu, O.R. (2004). Levels of Organochlorine Pesticide Residues in Marine-, Surface-, Ground- and Drinking Waters from the Eastern Cape Province of South Africa. *Journal of Environmental Science and Health, Part B*, 39: 101-114.

Ferrante, M.C., Amero, P., Santoro, A., Monnolo, A., Simeoli, R., Di Guida, F., Mattace Raso, G., Meli, R. (2014) Polychlorinated biphenyls (PCB 101, PCB 153 and PCB 180) alter leptin signaling and lipid metabolism in differentiated 3T3-L1 adipocytes, *Toxicology and Applied Pharmacology*, 279, 401-408.

- Fischer, K., Gläser, R. & Schulze, A. (2014) *Nanoneedle and nanotubular titanium dioxide – PES mixed matrix membrane for photocatalysis*. Applied Catalysis. B Environmental 160-161, 456-464.
- Flint, S., Markle, T., Thompson, S., Wallace, E. (2012) Bisphenol A exposure, effects, and policy: A wildlife perspective, *Journal of Environmental Management*, **104**,19-34.
- Gao, C., Yan, D. (2004) Hyperbranched polymers: from synthesis to applications. *Progress in Polymer Science*, 29: 183-275.
- Gao, J., Sun, S-P., Zhu, W-P., Chung, T-S. (2014) Polyethyleneimine (PEI) cross-linked P84 nanofiltration (NF) hollow fiber membranes for Pb²⁺ removal. *Journal of Membrane Science*, 452: 300-310.
- Gassara, F., Brar, S.K., Verma, M., Tyaga, R.D. (2013) Bisphenol A degradation in H₂O by lignolytic enzymes. *Chemosphere*, 92: 1356-1360.
- Ghaem, A.F., Badaway, A.A., Ismail, N., Tian, R.Z., Abdel Rehim, M.H., Rabia, A. (2014) Photocatalytic activity of hyperbranched polyester/TiO₂ nanocomposites. *Applied Catalyst A: General*, 472: 191-197.
- Giulivo, M., Lopez De Alda, M., Capri, E., Barceló, D. (2016) Human exposure to endocrine disrupting compounds: Their role in reproductive systems, metabolic syndrome and breast cancer. A review, *Environmental Research*, 151,251-264.
- Gupta, S., Singh, Y.K., Bhattacharya, A. (2009) Studies on permeation of bovine serum albumin (BSA) through photo-modified functionalized asymmetric membrane. *Journal of Macromolecular Science, Part A, Pure and Applied Chemistry*, 46: 90-96.
- Guo, Z., Officer, P., Prevention, A.P., Division, C., Risk, N., Agency, U.S.E.P., 2012. Literature review of remediation methods for PCBs in buildings 1-68.
- Han, N.K., Yu, W.B., Kwak, S.Y. (2012) Hyperbranched poly(amidoamine)/polysulfone composite membranes for Cd (II) removal from water. *Journal of Membrane Science*, 396: 83-91.
- Han, Q., Wang, H., Dong, W., Liu, T., Yin, Y., Fan, H. (2015) Degradation of bisphenol A by ferrate(VI) oxidation: Kinetics, products and toxicity assessment. *Chemical Engineering Journal*, 262: 34-40.
- Hilton, D.C., Jones, R.S., Sjödin, A. (2010) A method for rapid, non-targeted screening for environmental contaminants in household dust. *Journal of Chromatography A*, 1217: 6851-6856.
- Hoekstra E.J., Simoneau, C., (2013) Release of bisphenol A from polycarbonate: a review., *Critical reviews in food science and nutrition*, **53**, 386-4.
- Hou, J., Dong G., Ye, Y., Chen V. (2014) *Enzymatic degradation of bisphenol-A with immobilized laccase on TiO₂ sol-gel coated PVDF membrane*, *Journal of Membrane Science*, **469**:19-30.
- Hou, J., Xue, H., Li, L. et al. (2016) Fabrication and morphology study of electrospun cellulose acetate/polyethylenimine nanofibre. *Polymer Bulletin*, 73: 2889-2906.
- Huang, W., Kuhn, J.N., Tsung, C., Zhang, Y., Habas, S.E., Yang, P., Somorjai, G.A. (2008) Dendrimer templated synthesis of one nanometer Rh and Pt particles supported on mesoporous silica: catalytic activity for ethylene and pyrrole hydrogenation. *Nano Letter* 8: 2027-2034.

- Huang, Q., Weber, W.J. (2005) Transformation and removal of bisphenol A from aqueous phase via peroxidase-mediated oxidative coupling reactions: Efficacy, products, and pathways. *Environmental Science and Technology*, 39: 6029-6036.
- Huang, Y.Q., Wong, C.K.C., Zheng, J.S., Bouwman, H., Barra, R., Wahlstrom, B., Neretin, L., Wong, M.H. (2012) Bisphenol A (BPA) in China: A review of sources, environmental levels, and potential human health impacts. *Environment International*, 42: 91-99.
- Huang, Z.M., Zhang, Y.Z., Kotaki, M., Ramakrishna, S. (2003) A review on polymer nanofibers by electrospinning and their applications in nanocomposites. *Composite Science Technology*, 63: 2223-2253.
- Huang, W., Kuhn, J.N., Tsung, C., Zhang, Y., Habas, S.E., Yang, P., Somorjai, G.A. (2008) Dendrimer templated synthesis of one nanometer Rh and Pt particles supported on mesoporous silica: catalytic activity for ethylene and pyrrole hydrogenation. *Nano Letters*, 8: 2027-2034.
- Huang, J., Zhang, K. & Wang, K. (2012) *Fabrication of polyethersulfone-mesoporous silica nanocomposite ultrafiltration membranes with antifouling properties*. *Journal of Membrane Science*. 423-424, 362-370.
- Inoue, K. (2000) Functional dendrimers, hyperbranched and star polymers. *Progress in Polymer Science*, 25: 453-571.
- Ignatius, M.C., Francis, E.F., Neboh, E.E., Shu, E.E., Ikekpeazu, E.J. (2010) BPA and environmental estrogen in potable water sources in Enugu Municipality, south-east Nigeria, *Bulletin of Environmental Contamination and Toxicology*, 85: 534-537.
- Joa, M., Almeida, C.M.M. (2007) Experimental and statistical validation of SPME-GC – MS analysis of phenol and chlorophenols in raw and treated water. *Chemosphere*, 68: 501-510.
- Kanagaraj, P., Neelakandan, S., Nagendran, A., et al. (2015) Removal of BSA and HA contaminants from aqueous solution using amphiphilic triblock copolymer modified poly(etherimide) UF membrane and their fouling behaviors. *Industrial & Engineering Chemistry Research*, 54: 11628–11634.
- Kang, K., Jang, M., Cui, M. (2015) Enhanced sonocatalytic treatment of ibuprofen by mechanical mixing and reusable magnetic core titanium dioxide. *Chemical Engineering Journal*, 264: 522-530.
- Khoobi, M., Farshad, S., Asadgol, Z., Forootanfar, H., Sha, A., Ali, M. (2015) *Polyethyleneimine-modified superparamagnetic Fe₃O₄ nanoparticles for lipase immobilization: Characterization and application*, *Material Chemistry and Physics*, 150: 77-86.
- Kurniash, I.N., Kleilitz, J., Haag, R. (2015). Dendritic nanocarriers based on hyperbranched polymers. *Chemical Society Reviews*, 44: 4145-4164.
- Köck-Schulmeyer, M., Villagrasa, M., López, M., Alda, D., Céspedes-sánchez, R., Ventura, F., Barceló, D. (2013) Occurrence and behavior of pesticides in wastewater treatment plants and their environmental impact. *Science of the Total Environment*, 458-460: 466-476.
- Koloti, L.E., Gule, N.P., Arotiba, O.A., Malinga, S.P. (2018) Laccase-immobilized dendritic nanofibrous membranes as a novel approach towards the removal of bisphenol A. *Environmental Technology*. 39:392-404
- Lang, I.A., Galloway, T.S., Scarlett, A., Henley, W.E. Depledge, M.R., Wallace, R.D., Melzer, D. (2008) Association of urinary bisphenol A concentration with medical disorders and laboratory abnormalities in adults. *The Journal of the American Medical Association*. 300: 1303-1310.

Larrazza, I., López-González, M., Corrales, T., Marcelo, G. (2012) Hybrid materials: Magnetite-polyethyleneimine-montmorillonite, as magnetic adsorbents for Cr (VI) water treatment. *Journal of Colloid and Interface Science*, 385: 24-33.

Lee, S.Y., Kim, H.J., Patel, R., Im, S.J., Kim, J.H., Min, B.R. (2007) Silver nanoparticles immobilized on thin film composite polyamide membrane: characterization, nanofiltration, antifouling properties. *Polymers for Advanced Technologies*, 18: 562-568

Leyva-Porras, C., Toxqui-Teran, A. & Vega-Becerra, O. (2015) Low-temperature synthesis and characterization of anatase TiO₂ nanoparticles by an acid assisted sol-gel method. *Journal of Alloys and Compounds*. 647, 627-636.

Li, Z., Wang, Y., Zu, Y., Fu, Y., Li, N., Guo, N., Liu, R., Zhang, Y. (2014) Synthesis of polyethylenimine (PEI) functionalized silver nanoparticles by a hydrothermal method and their antibacterial activity study. *Materials Science and Engineering, C*, 42: 31-37.

Liao, Y., Brame, J. & Que, W. (2013) *Photocatalytic generation of multiple ROS types using low-temperature crystallized anodic TiO₂ nanotube arrays*. *Journal of Hazardous Materials* 260, 434-441.

Li, Y., Chung, T. & Kulprathipanja, S. (2006) *Dual-layer polyethersulfone (PES)/BTDA-TDI/MDI co-polyimide (P84) hollow fiber membranes with a submicron PES-zeolite beta mixed matrix dense-selective layer for gas separation*. *Journal of Membrane Science* 277, 28-37.

Lin, Y.-H., Tseng, H.-H., Wey, M.-Y., Lin, M.-D. (2010) Characteristics of two types of stabilized nano zero-valent iron and transport in porous media. *Science of the Total Environment*, 408(10): 2260-2267. doi: <https://doi.org/10.1016/j.scitotenv.2010.01.039>.

Lin, Y., Li, D. & Hu, J. (2012) *Highly efficient photocatalytic degradation of organic pollutants by PANI-modified TiO₂ composite*. *Journal of Physics and Chemistry C* 116, 5764-5772.

Li, Z., Wang, Y., Zu, Y., Fu, Y., Li, N., Guo, N., Liu, R., Zhang, Y. (2014) Synthesis of polyethylenimine (PEI) functionalized silver nanoparticles by a hydrothermal method and their antibacterial activity study. *Materials Science and Engineering C* 42: 31-37.

Liu, Y., Qu, R., Sun, C., Wang, C., Chen, H., Ji, C. (2013). Adsorption of Pb (II) from aqueous solution by silica-gel supported hyperbranched polyamidoamine dendrimers. *Journal of Hazardous Materials*, 244-245: 276-286.

Liu, L.F., Zhang, P.H., Yang, F.L. (2010) Adsorptive removal of 2,4-DCP from water by fresh or regenerated chitosan/ACF/TiO₂ membrane. *Separation Purification Technology*, 70: 354-361.

Lu, H.-J., Wang, J.-K., Ferguson, S., Wang, T., Bao, Y., Hao, H. (2016) Mechanism, synthesis and modification of nano zerovalent iron in water treatment. *Nanoscale, Royal Society of Chemistry*, 8(19): 9962-9975, doi: 10.1039/C6NR00740F.

Lu, N., Ying, L., Liu, F., Zhao, K., Yuan, X., Zhao, Y., Yuan, L., Qin, H., Zhu, J. (2013) H₃PW₁₂O₄₀/TiO₂ catalyst-induced photodegradation of bisphenol (BPA): Kinetics, toxicity and degradation pathways. *Chemosphere*. 91: 1266-1272.

Luzon, M., Corrales, T. (2014) Thermal studies and chromium removal efficiency of thermo responsive hyperbranched copolymers based on PEG-methacrylates. *Journal of Thermals Analysis and Calorimetry*, 116: 401-409.

Ma, F., Qu, R., Sun, C., Wang, C., Ji, C. (2009) Adsorption behaviour of Hg (II) on chitosan functionalized by amino-terminated hyperbranched polyamidoamine polymers. *Journal of Hazardous Materials*, 172: 792-801.

Madikizela, L.M., Muthwa, S.F., Chimuka, L. (2014) Determination of triclosan and ketoprofen in river water and wastewater by solid phase extraction and high performance liquid chromatography. *South African Journal of Chemistry*, 67: 143-150.

Mahdavi, H., Shahalizade, T. (2015) Preparation, characterization and performance study of cellulose acetate membranes modified with aliphatic hyperbranched polyester. *Journal of Membrane Science*, 473: 256-266.

Majeau, S., Brar, K., Tyagi, R.D. (2010) Bioresource Technology Laccases for removal of recalcitrant and emerging pollutants, *Bioresource Technology*, 101: 2331-2350.

Malinga, S.P. (2013) β -Cyclodextrin dendritic-polymers and nanostructured materials for water treatment. PhD Thesis, University of Johannesburg, Johannesburg, South Africa.

Masuelli, M.A. (2013) Synthesis polysulfone-acetyethanol ultrafiltration membranes. Application to oily wastewater treatment. *Journal of Materials Physics and Chemistry*, 1: 37-44.

Meeker, J.D., Calafat, A.M., Hauser, R. (2010) Urinary bisphenol A concentrations in relation to serum thyroid and reproductive hormone levels in men from an infertility clinic, *Environmental Science and Technology*, 44, 1458-1463.

Michalowicz, J. (2014) Bisphenol A – sources, toxicity and biotransformation. *Environmental Toxicology and Pharmacology*, 37: 738-758.

Mobarakabad, P., Moghadassi, A.R., Hosseini, S.M. (2015) Fabrication and characterization of poly(phenylene ether-ether sulfone) based nanofiltration membranes modified by titanium dioxide nanoparticles for water desalination. *Desalination*, 365: 227-233.

Molinari, R., Borgese, M., Drioli, E., Palmisano, L. & Schiavello, M. (2002) *Hybrid processes coupling photocatalysis and membranes for degradation of organic pollutants in water. Catalysis Today* **75**, 77-85.

Motchelaho, M.A.M., Xiong, H., Moyo, M., Jewell, L.L., Coville, N.J. (2011) Chemical effect of acid treatment on the surface of multiwalled carbon nanotubes prepared from Fe – Co supported on CaCO₃: Correlation with Fischer-Tropsch catalyst activity. *Journal of Molecular Catalysis, A, Chemical*, 335: 189-198.

Müllerová, D., Kopecký, J. (2007) White adipose tissue: Storage and effector site for environmental pollutants. *Physiological Research*, 56: 375-381.

Ndlwana, L., Ngila, J.C., Sikhwivhilu, K., Ramontjaa, J., Moutloali, R. (2013) Dechlorination of PCB77 using Fe/Pd Bimetallic Nanoparticles Immobilized Microfiltration Membranes. WaterNet/WARFSA/GWP-SA, Whitesands Hotel, Dar-es-Salaam, Tanzania, 30 October-1 November 2013.

Newman, B., Arabi, S., Weerts, S., Pieters, R., Vogt, N. (2015) Prevalence and significance of organic contaminants and metals in aquatic ecosystems in the eThekweni area of KwaZulu-Natal. WRC Report No. 1977/1/15. Water Research Commission, Pretoria, South Africa.

Nel, L., Strydom, N.A., Bouwman, H. (2015) Preliminary assessment of contaminants in the sediment and organisms of the Swartkops Estuary, South Africa. *Marine Pollution Bulletin*, 101: 878-885.

Nikonova, A.A., Gorshkov, A.G. (2011) Rapid chromatography for the determination of polychlorinated biphenyls by GC-MS in environmental monitoring, *Analytical Letters*, 44: 1290-1300.

National Institute for Occupational Safety and Health (NIOSH) (2011). Occupational Exposure to titanium dioxide. Current Intelligence bulletin 63.

Obaid, M., Fadali, O.A., Lim, B.H., Fouad, H., Barakat, N.A.M. (2015) Super-hydrophilic and highly stable in oils polyamide-polysulfone composite membrane by electrospinning. *Materials Letters*, 138: 196-199.

Okamoto, Y., Tomonari, M. (1999) Formation pathways from 2, 4, 5-Trichlorophenol (TCP) to polychlorinated dibenzo-p-dioxins (PCDDs): An ab initio study. *Journal of Physical Chemistry A*, 103: 7686-7691.

Olujimi, O.O., Fatoki, O.S., Daso, A.P. et al. (2013) Levels of nonylphenol and bisphenol in wastewater treatment plant effluent, sewage sludge and leachates around Cape Town, South Africa. In: Valdez, C.J., Maradona, E.M. (Eds.), *Handbook of Wastewater Treatment*. New York: Nova Science Publishers. pp. 705-711.

Omoruyi, M.I., Ahamioje, D., Pohjanvirta, R. (2014) Dietary exposure of Nigerians to mutagens and estrogen-like chemicals. *International Journal of Environmental Research and Public Health* 11:8347-8367

Orlicki, J.A., Wang, X., Bratcher, M.S., Jensen, R.E., Samuelson, L.A., McKnight, S.H. (2012) Modified hyperbranched Polymers for Fluorescence Sensing Applications. Available at: www.dtic.mil/cgi-bin/GetTRDoc?AD=ADA568734 (Accessed on 18/10/2015).

Osswald, S., Havel, M., Gogotsi, Y. (2007) Monitoring oxidation of multiwalled carbon nanotubes by Raman spectroscopy. *Journal of Raman Spectroscopy*, 38: 728-736.

Pandey, A., Kalal, S., Ameta, C., Ameta, R., Kumar, S., Punjabi, P.B. (2015) Synthesis, characterization and application of naïve and nano-sized titanium dioxide as a photocatalyst for degradation of methylene blue. *Journal of Saudi Chemical Society*, 19: 528-536.

Park, S-J., Cheedra, R.K., Mamadou, S., Diallo, M.S., Kim, C., Kim, I.S., Goddard III, W.A. (2012) Nanofiltration membranes based on polyvinylidene fluoride nanofibrous scaffolds and crosslinked polyethyleneimine networks. *Journal of Nanoparticle Research*, 14: 884

Park, Y., Sun, Z., Ayoko, G.A., Frost, R.L. (2014) Bisphenol A sorption by organo-montmorillonite: Implications for the removal of organic contaminants from water, *Chemosphere*, 107, 249-256.

Peng, Y.H., Chen, Y.J., Chang, Y.J., Shih, Y. (2015) Biodegradation of bisphenol A with diverse microorganisms from river sediment. *Journal of Hazardous Materials*. 286: 285-290.

Pereira V.R. & Isloor A.M. (2015) *Preparation and performance studies of polysulfone-sulfonated nanotitania (S-TiO₂) nanofiltration membrane for dye removal*. RSC Advances, 5: 53874-53885.

Pieters, R., Focant, J.F. (2014) Dioxin, furan and PCB serum levels in a South African Tswana population: Comparing the polluting effects of using different cooking and heating fuels. *Environment International* 66: 71-78.

Pouokam, G.B. Ajaezi, G.C. Mantovani, A., Orisakwe, O.E., Frazzoli, C. (2014) Use of Bisphenol A-containing baby bottles in Cameroon and Nigeria and possible risk management and mitigation measures: Community as milestone for prevention. *Science of the Total Environment*, 481: 296-302.

Pramanik, S., Bharali, P., Konwar, B.K., Karak, N. (2014) Antimicrobial hyperbranched poly (ester amide)/polyaniline nanofiber modified montmorillonite nanocomposites. *Materials Science and Engineering, C* 35: 61-69.

Prins, A. (2015) The degradation of the endocrine disrupting chemical, bisphenol-A: a comparative study between fungal and bacterial laccases. MSc Dissertation, University of the Western Cape, Cape Town, South Africa.

Pronczuk, J., Damstra, T. (2008) Persistent Organic Pollutants (POPs): Children's Health and the Environment. WHO Training Package for the Health Sector, World Health Organization, www.who.int/ceh. pp. 1-48.

Qu, P., Tang, H., Gao, Y., Zhang, L. P. & Wang, S. (2010) *Polyethersulfone composite membrane blended with cellulose fibrils*. *BioResources* 5:2323-2336.

Rahimi, Z., Zinatizadeh, A.A.L., Zinadini, S. (2015) Preparation of high antibiofouling amino functionalized MWCNTs/PES nanocomposite ultrafiltration membrane for application in membrane bioreactor. *Journal of Industrial and Engineering Chemistry*, 29: 366-374.

Ritter, L., Solomon, K.R., Forget, J., Stemeroff, M., O'Leary, C. (1995) A Review of Selected Persistent Organic Pollutants: DDT-Aldrin-Dieldrin-Endrin-Chlordane, Heptachlor-Hexachlorobenzene-Mirex-Toxaphene, Polychlorinated Biphenyls, Dioxins and Furans. Report No PCS/95.39, December 1995. This review was produced for the International Programme on Chemical Safety (IPCS) within the framework of the Inter-Organization: Programme for the Sound Management of Chemicals (IOMC).

Roos, C. (2011) Characterising the scale and significance of persistent organic pollutants in South African sediments. PhD Thesis. North-West University, Potchefstroom, South Africa.

Rochester, J.R. (2013) Bisphenol A and human health: A review of the literature. *Reproductive Toxicology*, 42: 132-155.

Ramesh, S., Natasha, A.N., Tan, C.Y. (2015) Characteristics and properties of hydroxyapatite derived by sol-gel and wet chemical precipitation methods. *Ceramics International*, 41:10434-10441.

Safarpour, M., Vatanpour, V. & Khataee, A. (2016) *Preparation and characterization of graphene oxide/TiO₂ blended PES nanofiltration membrane with improved antifouling and separation performance*. *Desalination* 39: 65-78.

Sahoo, P.C., Sambudi, N.S., Bin Park, S., Lee, J.H., Han, J.I. (2015) Immobilization of Carbonic Anhydrase on Modified Electrospun Poly(Lactic Acid) Membranes: Quest for Optimum Biocatalytic Performance, *Catalysis Letters*, 145:519-526.

SANS (2015) SANS 241-1:2015 Edition 2 South African National Standard (SANS). Drinking water. Part 1: Microbiological, physical, aesthetic and chemical determinants. South African Bureau of Standards, Pretoria, South Africa. ISBN 978-0-626-29841-8.

Schulz, R., Peall, S.K.C. (2001) Effectiveness of a constructed wetland for retention of nonpoint-source pesticide pollution in the Lourens River catchment, South Africa. *Environmental Science and Technology*, 35: 422-426.

Scott, R.W.J., Sivadinarayana, C. & Wilson, O.M. (2005) *Titania-Supported PdAu Bimetallic Catalysts Prepared from Dendrimer-Encapsulated Nanoparticle Precursors*. *Journal of American Chemical Society* 127: 1380-1381.

Seiler, M. (2006) Hyperbranched polymers: Phase behaviour and new applications in the field of chemical engineering. *Fluid Phase Equilibria*. 241:155-174.

Seteni, B., Ngila, J.C., Sikhwivhilu, K., Moutloali, R.M., Mamba, B. (2013) Dechlorination of 3, 3', 4, 4' - tetrachlorobiphenyl (PCB 77) in water, by nickel/iron nanoparticles immobilized on L-Lysine/PAA/PVDF membrane. *Physics and Chemistry of the Earth, Parts A/B/C*, 66: 60-67

Shang, X., Dong, G., Zhang, H., Zhang, L., Yu, X., Li, J., Wang, X., Yue, B., Zhao, Y., Wu, Y. (2016) Polybrominated diphenyl ethers (PBDEs) and indicator polychlorinated biphenyls (PCBs) in various marine fish from Zhoushan fishery, China. *Food Control*, 67: 240-246.

Shen, M., Wang, S.H., Shi, X., Chen, X., Huang, Q., Petersen, E.J., Pinto, R.A., Baker, J.R., Weber, W.J. (2009) Polyethyleneimine-mediated functionalization of multiwalled carbon nanotubes: Synthesis, characterization, and in vitro toxicity assay. *Journal of Physical Chemistry, C*, 113: 3150-3156.

Shen, J., Ruan, H., Wu, L. & Gao, C. (2011) *Preparation and characterization of PES-SiO₂ organic-inorganic composite ultrafiltration membrane for raw water pretreatment*. *Chemical Engineering Journal* 168: 1272-1278

Shen, P.-S., Tseng, C.-M. & Kuo, T.-C. (2015) *Microwave-assisted synthesis of titanium dioxide nanocrystalline for efficient dye-sensitized and perovskite solar cells*. *Solar Energy* 120: 345-356.

Sibali, L.L., Okwonkwo, J.O., McCrindle, R.I. (2008) Determination of selected organochlorine pesticide (OCP) compounds from the Jukskei River catchment area in Gauteng, South Africa. Available on website <http://www.wrc.org.za> 34, pp. 611-621.

Smuleac, V., Bachas, L., Bhattacharyya, D. (2010) Aqueous-phase synthesis of PAA in PVDF membrane pores for nanoparticle synthesis and dichlorobiphenyl degradation. *Journal of Membrane Science*, 346: 310-317.

Sonawane, R., Kale, B. & Dongare, M. (2004) *Preparation and photo-catalytic activity of Fe-TiO₂ thin films prepared by sol-gel dip coating*. *Materials Chemistry and Physics*. 85, 52-57.

Sun, S.P., Hatton, A.T., Chung, S-T. (2011) Hyperbranched polyethyleneimine induced cross-linking of polyamide imide nanofiltration hollow fiber membranes for effective removal of ciprofloxacin. *Environmental Science and Technology*, 45: 4003-4009.

Su, J., Lin, S., Chen, Z., Megharaj, M., Naidu, R. (2011) Dechlorination of p-chlorophenols from aqueous solution using bentonite supported Fe/Pd nanoparticles: Synthesis, characterization and kinetics. *Desalination*, 280: 167-173.

Suriyanarayanan, S., Lee, H-H., Liedberg, B., Aastrup, T., Nicholls, I.A. (2013) Protein-resistant hyperbranched polyethyleneimine brush surfaces. *Journal of Colloid and Interface Science*, 396:307-315.

Simelane, S., Ngila, J.C. & Dlamini, L.N. 2017. The effect of humic acid on the stability and aggregation kinetics of WO₃ nanoparticles. *Particulate Science and Technology*. Available at: <http://dx.doi.org/10.1080/02726351.2017.1302536>.

Tahiri Alaoui, O., Nguyen, Q.T., Mbareck, C. & Rhlalou, T. (2009) *Elaboration and study of poly(vinylidene fluoride)-anatase TiO₂ composite membranes in photocatalytic degradation of dyes*. *Applied Catalysis A General*. 358, 13-20.

Tsetsekou, A., Arkas, M., Kritikaki, A., Simonetis, S., Tsiourvas, D. (2008) Optimization of hybrid hyperbranched polymer/ceramic filters for the efficient absorption of polyaromatic hydrocarbons from water. *Journal of Membrane Science*, 311: 128-135.

Voit, B. (2000) New developments in hyperbranched polymers. *Journal of Polymer Science: Part A: Polymer Chemistry*, 38: 2505-2525.

Vatanpour, V., Madaeni, S.S., Moradian, R., Zinadini, S., Astinchap, B. (2011) Fabrication and characterization of novel antifouling nanofiltration membrane prepared from oxidized multiwalled carbon nanotube/polyethersulfone nanocomposite. *Journal of Membrane Science*, 375: 284-294.

Van Veelen, M., Dhemba, N. (2011) Development of a Reconciliation Strategy for the Olifants River Water Supply System. Water Quality Report No. P WMA 04/B50/00/8310/7. Department of Water Affairs (DWA), Pretoria, South Africa.

Venkatachalam, K., Arzuaga, X., Chopra, N., Gavalas, V.G., Xu, J., Bhattacharyya, D., Hennig, B., Bachas, L.G. (2008) Reductive dechlorination of 3,3',4,4'-tetrachlorobiphenyl (PCB77) using palladium or palladium/iron nanoparticles and assessment of the reduction in toxic potency in vascular endothelial cells. *Journal of Hazardous Materials*, 159(2-3): 483-491.

Vosloo, H., Bouwman, R. (2005) "WRC Report no. 1213/1/05.

Voom Saal F.S. et al. (2007) Chapel Hill bisphenol A expert panel consensus statement: integration of mechanisms, effects in animals and potential impact to human health at current levels of exposure. *Reproductive Toxicology* 24: 131-138.

Wan, H., Briot, N.J., Saad, A., Ormsbee, L., Bhattacharyya, D. (2017) Pore functionalized PVDF membranes with in-situ synthesized metal nanoparticles: Material characterization, and toxic organic degradation. *Journal of Membrane Science*, 530: 147-157.

Wan, L.S., Ke, B.B., Xu, Z.K. (2008) Electrospun nanofibrous membranes filled with carbon nanotubes for redox enzyme immobilization, *Enzyme and Microbial Technology*, 42: 332-339.

Wang, S., He, J. (2013) Dechlorination of commercial PCBs and other multiple halogenated compounds by a sediment-free culture containing *Dehalococcoides* and *Dehalobacter*. *Environmental Science and Technology*, 47: 10526-34.

Wang, L., Ji, S., Wang, N., Zhang, R., Zhang, G., Li, J.R. (2014a) One-step self-assembly fabrication of amphiphilic hyperbranched polymer composite membrane from aqueous emulsion for dye desalination. *Journal of Membrane Science*, 452: 143-151.

Wang, X., Li, F., Yang, J. (2014b) Polyvinyl pyrrolidone-modified Pd/Fe nanoparticles for enhanced dechlorination of 2,4-dichlorophenol', *Desalination and Water Treatment*, 52(40-42): 7925-7936.

Wei, X., Kong, X., Yang, J., Zhang, G., Chen, J., Wang, J. (2013) Structure influence of hyperbranched polyester on structure and properties of synthesized nanofiltration membranes. *Journal of Membrane Science*, 440: 67-76.

Wei, Z.X., Zhu, L.P., Deng, H.Y., Xu, Y.Y., Zhu, K.B., Huang, M.Z. (2008) New type of nanofiltration membrane based on crosslinked hyperbranched polymers. *Journal of Membrane Science*, 323: 278-287.

Wetherill, Y.B., Akingbemi, B.T., Kanno, J., McLachlan, J.A., Nadal, A., Sonnenschein, C., Watson, C.S., Zoeller, R.T., Belcher, S. (2017) In vitro molecular mechanisms of bisphenol A action, *Reproductive Toxicology*, 24,178-198.

Woo, S.H., Park, J., Min, B.R. (2015) Relationship between permeate flux and surface roughness of membranes with similar water contact angle values, *Separation and Purification Technology*, 146, pp. 187-191

Wu, D., Huang, Y., Yu, S., Lawless, D., Feng, X. (2014). Thin film composite nanofiltration membranes assembled layer-by-layer via interfacial polymerization from polyethylenimine and trimesoyl chloride. *Journal of Membrane Science*, 472, 141-153.

Xiang, T., Xie, Y., Wang, R., Wu, M., Sun, S., Zhao, C. (2014) Facile chemical modification of polysulfone membrane with improved hydrophilicity and blood compatibility. *Materials Letters*, 137: 192-195.

Xu, J., Bhattacharyya, D. (2007) Fe/Pd nanoparticle immobilization in microfiltration membrane pores: Synthesis, characterization, and application in the dechlorination of polychlorinated biphenyls. *Industrial Engineering Chemistry Research*, 46: 2348-2359.

Xu, R., Chi, C., Li, F., Zhang, B. (2013) Laccase-Polyacrylonitrile Nanofibrous Membrane : Highly Immobilized, Stable, Reusable, and effacious for 2,4,6-Trichlorophenol Removal, *Applied Materials and Interfaces*, 5:12554-12560.

Xu, S., Xu, Z., Tang, Y., Ji, C. (2016) Polypiperazine-amide nano filtration membrane modified by different functionalized multiwalled carbon nanotubes (MWCNTs). *ACS APPLIED Materials & Interfaces*, 8:19135-19144.

Yang, Q., Gao, M., Luo, Z., Yang, S. (2016) Enhanced removal of bisphenol A from aqueous solution by organo-montmorillonites modified with novel Gemini pyridinium surfactants containing long alkyl chain, *Chemical Engineering Journal*, 285, 27-38.

Yoo, H., Kwak, S.Y. (2013) Surface functionalization of PTFE membranes with hyperbranched poly (amidoamine) for the removal of Cu²⁺ ions from aqueous solution. *Journal of Membrane Science*, 448: 125-134.

Yoo, B.Y., Hernandez, S.C., Koo, B., Rheem, Y., Myung, N.V. (2007) Electrochemically fabricated zero-valent iron, iron-nickel, and iron-palladium nanowires for environmental remediation applications. *Water Science and Technology*, 55:149-156. doi: 10.2166/wst.2007.017.

Yuan, Z., Cai, N. & Du, Y. (2013) Sensitive and Selective Detection of Copper Ions with Highly Stable Polyethyleneimine-Protected Silver Nanoclusters. *Analytical Chemistry* 86: 419-426.

Yu, L., Zhang, Y., Zhang, B., Liu, J., Zhang, H., Song, C. (2013) Preparation and characterization of HPEI GO/PES ultrafiltration membrane with antifouling and antibacterial properties. *Journal of Membrane Science*, 447: 452-462.

Yu, L., Yatao, Z., Bing, Z., Jindun, L., Haoqin, Z., Chunhua, S. (2013) Preparation and characterization of HPEI-GO/PES ultra filtration membrane with antifouling and antibacterial properties. *Journal of Membrane Science*, 447: 452-462.

Yu, Z., Yu, Z., Zeng, G., Pan, Y., Lv, L., Min, H. (2015) Effect of functionalized multi-walled carbon nanotubes on the microstructure and performances of PVDF membranes. *RSC Advances*, 5: 75998-76006

Zang, C., Zhang, D., Xiong, J., Lin, H., Chen, Y. (2014) Preparation of a novel adsorbent and heavy metal ion adsorption. *Journal of Engineered Fibers and Fabrics*, 9: 165-170.

Zhang, W.F., Zhang, M.S., Yin, Z. & Chen, Q. (2000) *Photoluminescence in anatase titanium dioxide nanocrystals*. Applied Physics B: Laser and Optics. 265, 261-265.

Zhang, H., Xun, E., Wang, J., Chen, G., Cheng, T., Wang, Z., Ji, T. and Wang L. (2012) *Immobilization of laccase for oxidative coupling of trans-resveratrol and its derivatives*, International Journal of Molecular Sciences, 13, pp. 5998-6008.

Zhao, X., Ma, J., Wang, Z., Wen, G., Jiang, J., Shi, F, Sheng, L. (2012) Hyperbranched-polymer functionalized multi-walled carbon nanotubes for poly (vinylidene fluoride) membranes: From dispersion to blended fouling-control membrane. *Desalination*, 303: 29-38.

Zhou, Y., Chen, L., Lu, P., Tang, X., Lu, J. (2011) Removal of bisphenol A from aqueous solution using modified fibric peat as a novel biosorbent. *Separation and Purification Technology*, 81:184-190, 2011.

Zhou, Y., Tang, L., Yang, G., Zeng, G., Deng, Y., Huang, B., Cai, Y., Tang, J., Wang, J., Wu, Y. (2016) Phosphorus-doped ordered mesoporous carbons embedded with Pd/Fe bimetal nanoparticles for the dechlorination of 2,4-dichlorophenol. *Catalysis Science & Technology*, Royal Society of Chemistry, 6: 1930-1939.

Zhu, J.L., Liu, Y., Liu, X.Y., Liu, H.J., Chen, Y. (2015) Multi stimuli-responsive photoluminescent nanocomposite of silver nanoclusters with hyperbranched polyethylenimine derivatives. *RSC Advances*, 5: 8146-8151.

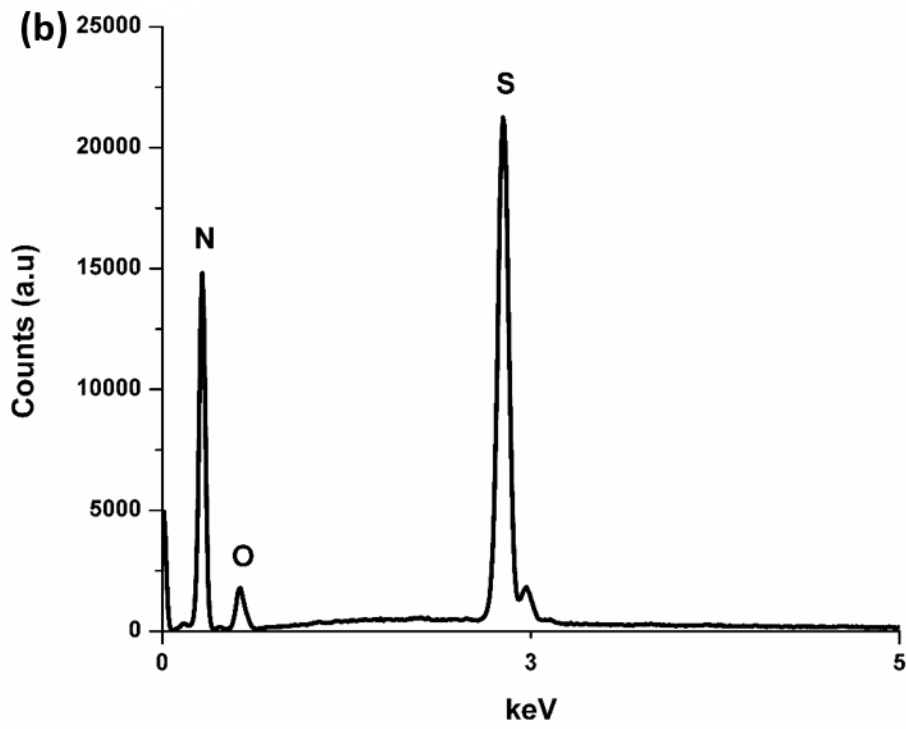
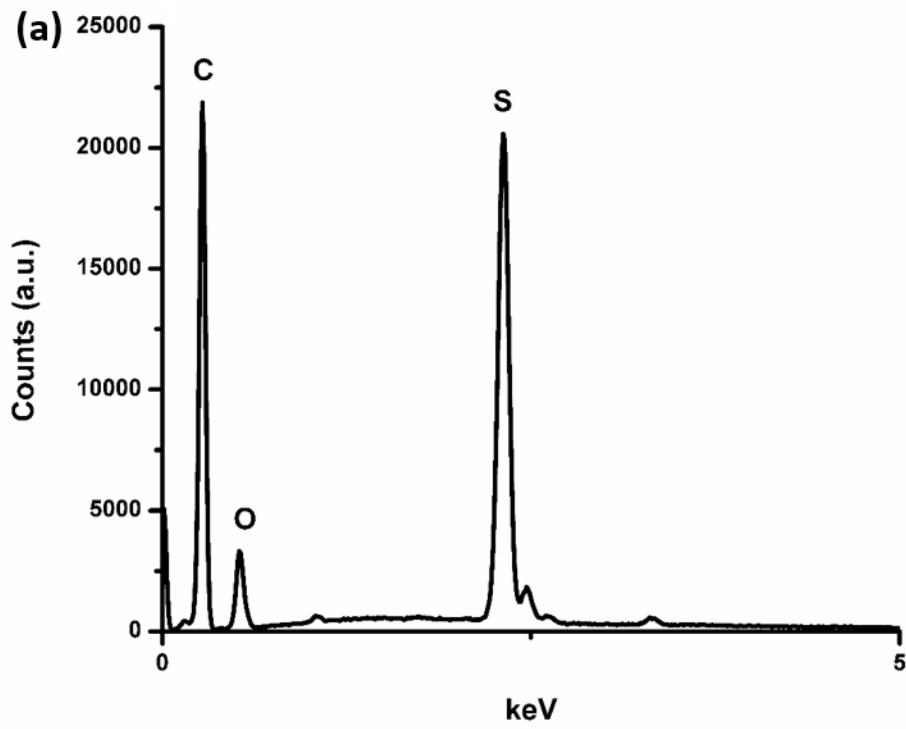
Zhu, J., Sun, G. (2012) Lipase immobilization on glutaraldehyde-activated nanofibrous membranes for improved enzyme stabilities and activities. *Reactive Functional Polymers*, 72: 839-845.

Zhu, J., Zhang, J., Chen, F., Iino, K. & Anpo, M. (2005) *High activity TiO₂ photocatalysts prepared by a modified sol-gel method: Characterization and their photocatalytic activity for the degradation of XRG and X-GL*. *Top. Catalysis*: 35, 261-268

APPENDIX A:

Table A1: Operating parameters of ICP-OES

ICP-OES parameters	Operating values
RF generator power (W)	1150
Frequency of RF generator (MHz)	40
Coolant gas flow rate (L·min ⁻¹)	12
Carrier gas flow rate (L·min ⁻¹)	0.7
Auxiliary gas (L·min ⁻¹)	1.0
Max integration times (s)	15
Pump rate (rpm)	50
Viewing configuration/touch mode	Axial
Replicate	3
Flush time (s)	30



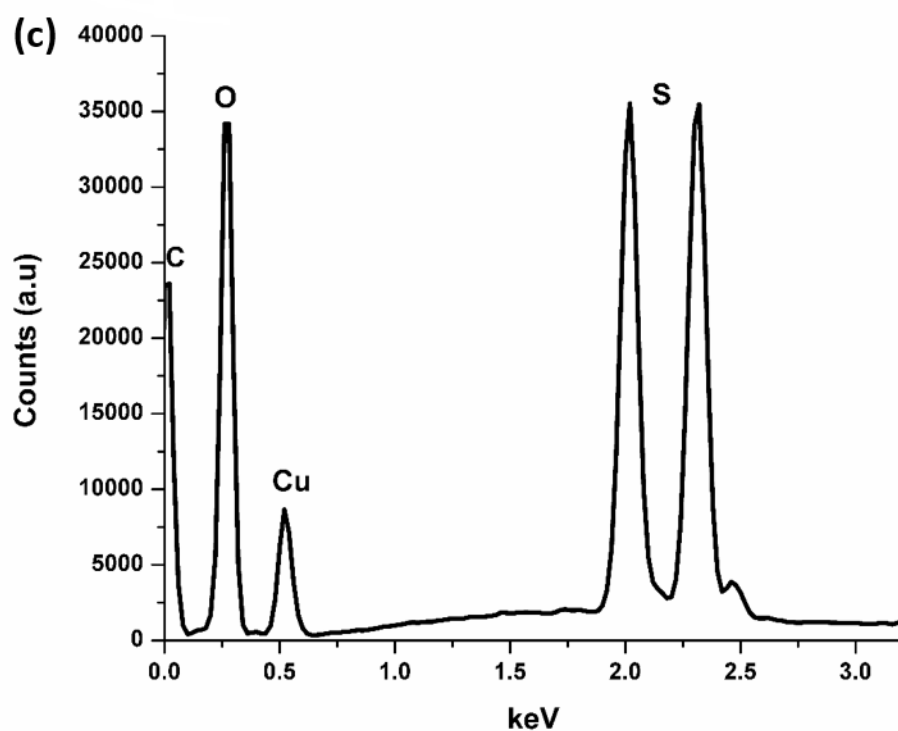


Figure S1: EDS analysis of (a) commercial PES, (b) electrospun HPEI/PES, and (c) laccase-immobilised membranes